University of Stavanger

FACULTY OF SCIENCE AND TECHNOLOGY

MASTER'S THESIS

Study program/Specialization: M.Sc. Petroleum Geoscience	Spring Semester, 2019 Open
Author: Thomas Meldahl Olsen	…… (signatures of author)

Program Coordinator:
Supervisors: Professor Carita Augustsson and Rodmar Ravnås

Title of master`s thesis:

Provenance on the Lysing-Lange megasequences on the Dønna Terrace: focus on stratigraphic variability and lateral sandbody connectivity

Credits (ECTS): 30

Keywords: Provenance Lysing-Lange U-Pb detrital zircon dating Hafnium analysis Whole-rock geochemistry Petrography Stratigraphic variability Lateral variability Regional source regions	Total Pages: 122 + supplement material/other: 29 Stavanger, 29/06/2019

Provenance on the Lysing-Lange megasequences on the Dønna Terrace: focus on stratigraphic variability and lateral sandbody connectivity

by

Thomas Meldahl Olsen

MSc. Thesis

Presented to the Department of Energy Resources

The University of Stavanger

The University of Stavanger

June 2019

Acknowledgment

First, I would like to express my gratitude to Aker BP, who sponsored my thesis and provided me with the necessary data. My sincere gratitude goes to my supervisor, Rodmar Ravnås, who provided me with a tailored master thesis and supplied the necessary data to complete it. My great appreciation goes to both supervisors Carita Augustsson and Rodmar Ravnås for providing me with constructive comments and valuable support. I would also like to extend my gratitude to Tom Andersen and Magnus Kristoffersen at UiO for guidance and sharing ideas through U-Pb and hafnium analysis, and for being available day and night through the process. I would also like to thank Caroline Ruud and Alexandra Elisabet Strandmyr Baeza for the support and guidance through the laboratory work performed at the UiS and thanks to Mona Wetrhus Minde for guidance in the SEM laboratory. I want to thank my fellow students for two fantastic years at the master program at UiS, and especially thanks to Olav Josefsen and Andrea Trollsås Liverød for motivation and support throughout the five years. Finally, I would like to thank my family and friends for your endless support and inspiration.

Abstract

The Cenomanian to Coniacian-Turonian Lange-Lysing megasequences are located on the Dønna Terrace in the Norwegian Sea. Provenance study using traditional provenance methods such as petrography, whole-rock geochemistry, and single grain U-Pb and hafnium isotope analysis, combined with stratigraphy were used to test the validity of correlation within the megasequences. Low to a high degree of weathering and recycling, a different tectonic setting between a continental island arc and passive continental margin combined with element ratios, reveals significant contrasts within the stratigraphy of the megasequences. A relation between stratigraphic variability and lower slope to the basinfloor gross depositional environment have been established by a moderate to a high degree of sediment recycling with broader age spectra from U-Pb zircon dating of 90-3300 Ma. The marginal-marine to upper slope reveals a stratigraphic consistency by none to a low degree of sediment recycling combined with a narrower age spectrum of 350-1850 Ma. Provenance development of the marginal-marine unravels a difference in reservoir quality; however, better the reservoir quality decreases with the gross depositional environment. The basinfloor to lower slope gross depositional environment show overall bad reservoir quality, however, there are variations within the sandbodies from bad to good reservoir quality pointing to stratigraphic variability. A decrease in reservoir quality has defined a lateral rationale association between the marginal-marine towards the lower slope. Four main sediment transportation directions from seven provenance regions were deduced by frequent (350-1850 Ma), and subordinate (90-300 Ma and 2000-3300 Ma) U-Pb zircon age spectra and are relating to the Western Gneiss Region, Lofoten-Vesterålen and the West-Troms Basement Complex. Combining subordinate juvenile Phanerozoic (90-350 Ma) and older Archean ages (2500-3300 Ma), with other studies, suggests the origin of the sediments are derived from provenance regions such as the High Arctic Large Igneous Province, Spitsbergen, and Novaya Zemlya in the Barents Sea, including the Varangerfjorden. The lack of a juvenile Phanerozoic and a late Proterozoic U-Pb zircon age spectra, with a significant Archean component, responds to provenance signatures originating from the northern Greenland region. U-Pb zircon dating results are supported by the hafnium isotope analysis pointing to a protosource from the same regions. Finally, this study emphasizes the importance of incorporating provenance methods, and stresses the use of U-Pb and hafnium isotope analysis, in order to comprehend the stratigraphic variability to unravel complex turbidite systems and predict the lateral extent.

Contents

List of figures

List of tables

1 Introduction

The confinement of the Lysing and Lange formations in the Mid-Norwegian margin is between 62˚ and 69˚ N (Figure 1; Bøe et al., 2010). The Cenomanian to Turonian-Coniacian formations are dispersed in the Halten and Dønna Terrace to the west of Trøndelag Platform and the Vøring and Møre basins in the Norwegian Sea (Koch and Heum, 1995). The evolution of the Lange-Lysing formations has been regionally studied for their depositional style, provenance source area by both seismic and core data. A regional study by (Morton and Grant, 1998) combined provenance on Cretaceous sandstones in the Norwegian Sea to expose evidence for differences in sediment provenance and assess if their geographic distribution was related to possible source terrains. This study revealed that there was a stratigraphic and lateral variability. The Cretaceous reservoir discoveries on the Dønna Terrace makes their evolution and extent important, and a motivation for the provenance study on the Cenomanian to Turonian-Coniacian Lange-Lysing. This study was designed to address four main questions.

1.1 How to correlate provenance study with stratigraphy

The theory is to combine traditional methods such as sedimentology, whole-rock geochemistry, optical petrography, and single-grain U-Pb radiometric dating and Lu/Hf isotopic analysis, with stratigraphy to observe if I can provide recorded signatures of sandstones within the stratigraphy of the megasequences. Testing if information about the weathering and recycling patterns, source rock composition and tectonic setting, combined with logarithmic ratios of trace elements versus depth (m) will reveal a difference in the recorded signature within individual sandstone in the stratigraphy of the megasequences of the Lange-Lysing.

1.2 Stratigraphical separation: chronostratigraphy (megasequence) vs lithostratigraphy

The Cenomanian to Coniacian-Turonian Lange-Lysing have been divided into chronostratigraphic megasequences by biostratigraphic analysis. Is it possible to separate them individually by performing a provenance study? By comparing provenance signatures and lithostratigraphy with chronostratigraphy, I will evaluate the possibility of distinguishing stratigraphic variability, and the lateral correlation within individual megasequence, and within both megasequences.

1.3 The Lysing-Lange depositional model

These formations were studied concerning their origin, geometry, and depositional style. Three concepts regarding their depositional style exist:

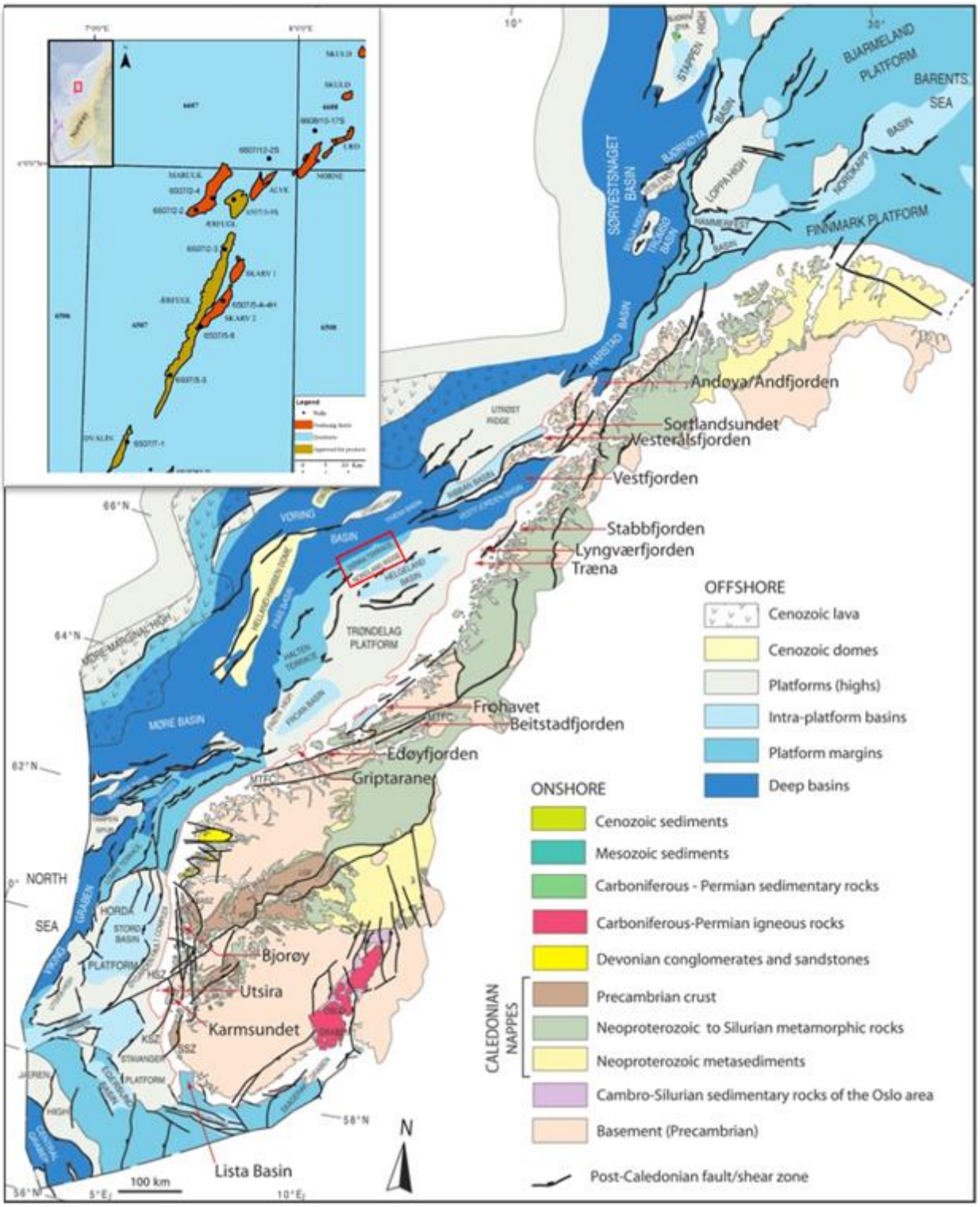

Figure 1: Summary of onshore geology and structures with offshore geological structures. The red box marks the Dønna Terrace (Bøe et al., 2010).

(1) mass-transport complexes or slump deposits, (2) complex transverse to longitudinal fed turbidites and (3) tidally influenced prograding delta (Shanmugam et al., 1994; Vergara et al., 2001; Martinsen et al., 2005; Lien et al., 2006). However, is it possible to relate gross

depositional environments with individual stratigraphic signatures? Is it possible to observe a lateral development by comparing gross depositional environment with individual provenance signatures? Gross depositional environment and stratigraphic and lateral contrasts will be tested by linking specific signatures such as provenance development to its designed gross depositional environment, to observe an eventual development and reveal a pattern. By using these patterns, I will test if it is possible to laterally contrast them across different gross depositional environments and discuss the rationale of lateral connectivity.

1.4 Discussion around Lysing-Lange

1.4.1 Assumed source locations: local vs. regional

The oldest and still recognized theory of their origin is that the Cenomanian to Turonian-Coniacian Lange-Lysing sandstones are derived from the local high of the Nordland Ridge (Hastings, 1987). In recent years, there have been some speculations about this theory, discussing that the Nordland Ridge is limited by its size to contain the amount of sediment that is needed to supply the spatial and temporal distribution of the Cretaceous fill in the Norwegian Sea (Koch and Heum, 1995). By performing a regional provenance study on the Lysing and Lange megasequences, authors such as Morton et al. (2005) and Fonneland et al. (2004) argued that the provenance signatures point to different source terrains such as: (1) Greenland, (2) the Norwegian Landmass, (3) the Western Gneiss Region, (4) the West Troms Basement Complex and (5) Lofoten/Vesterålen. A later addition comes from Tegle (2017), who added Sør-Varanger as a sixth possible source origin by U-Pb zircon dating, integrated whole-rock geochemical, and petrographic analysis. Source rock origin will be studied by utilizing U-Pb zircon dating and hafnium isotope analysis, combined with traditional provenance methods performed on stratigraphically separated sandstones within the megasequences. Source rock origin may enable the identification of possible source regions and transportation directions of the individual sand bodies.

1.5 Outline of this thesis

The provenance study was designed to address these questions by: (1) testing the validity of correlation between stratigraphy and provenance study, (2) unravel the stratigraphic variability between the Cenomanian to Turonian-Coniacian Lange-Lysing megasequences, and investigate the validity of lateral correlation on individual units by utilizing provenance data in field reservoir studies, (3) investigate a possible pattern between gross depositional environments and provenance by studying relevant discovery and dry wells of interest and (4) locate individual provenance sources to define potential sediment transport direction.

2 Analytical background

Provenance studies is a well-developed method for reconstructing the lithospheric history of the Earth (Basu, 2003). The aim by sedimentary provenance studies is to unravel the lineage of the sediment by reconstructing the history from the early erosion of parent rock to the final burial of their detritus (Weltje and Eynatten, 2004). Composition and texture are sedimentary signatures that may have specific reference to the parent rock and the climate from which the sediment is derived (Pettijohn et al., 1987; Weltje and Eynatten, 2004). Technological advancement within sediment provenance has enabled single-grain U-Pb radiometric dating of certain heavy minerals, e.g., zircon, of detrital grain populations (Morton et al., 2005). However, single-grain analysis alone will in most cases not give a complete and accurate provenance and is best used in combination with traditional methods such as whole-rock geochemistry and petrography (Morton et al., 2005; Andersen, 2013). According to Willner et al. (2003), loss of radiogenic lead from zircon by diagenetic processes can give inaccurate results in clastic sediment. However, Lu-Hf isotope data from zircon are unlikely to be affected by this process and are therefore encouraged to use in combination with U-Pb isotope data (Amelin et al., 2000; Andersen, 2013). Another aspect to consider for a more representative interpretation of zircon data for sedimentary provenance is the depositional environment and the transport path of the clastic sediments, as stated by Zimmermann et al. (2015).

3 Regional geology

3.1 Onshore regions: Norway and Greenland

3.1.1 Norway

The Archean rocks on the Norwegian continent are exposed predominantly in northern Norway, Lofoten-Vesterålen and the West Troms Basement Complex and are related to the tonalite-trondhjemite-granodiorite gneisses. The oldest protolithic age (2.9 Ga) within Norway is an orthogneiss located in Sør-Varanger (Levchenkov et al., 1995; Nordgulen et al., 1995; Koistinen et al., 2001). The Palaeoproterozoic rocks of the Svecokarelian/Svecofennian orogeny are predominantly situated in Sweden; however, it crops out in smaller areas in northern Norway consisting of large plutons of granite (Ramberg et al., 2008). The Trans-Scandinavian Igneous Belt was the next phase of crustal accretion in Scandinavia and is more widespread in Norway. The granitic plutonic rock (1650-1850 Ma) are emerging through windows of younger Caledonian nappes in the Western Gneiss Region and is a 1500 km long belt from Skåne in Sweden to Lofoten-Vesterålen in northern Norway (Ramberg et al., 2008). Crustal development in southern Scandinavia continued from 1750 to 900 Ma. Different plate

tectonic settings resulted in two orogenies: Gothian (1.7 to 1.5 Ga) and Sveconorwegian (1130 to 900 Ma), which produced a variety of metamorphosed and deformed rocks. The felsic to ultramafic plutonic rocks from the Gothian (1500-1750 Ma) orogeny comprises of 80 % of the southern area of the Western Gneiss Region (WGR; Kullerud et al., 1986; Austrheim and Mørk, 1988; Skår, 2000). Dolerite dikes, which intruded the Gothian plutonic rocks in the Hustad Igneous Complex within the Western Gneiss Region, are dated to 1251 Ma (Austrheim et al., 2003). The remaining 20 % of the southern rocks from the Sveconorwegian orogeny (900-1250 Ma) are the intrusions of mainly intermediate to felsic rocks (Kullerud et al., 1986; Skår, 1998; Skår, 2000). Large granite bodies (975-925 Ma) marks the end of the Precambrian evolution of the basement in southern Norway (Ramberg et al., 2008). The Caledonian nappes formed during the closure of the Iapetus Ocean and collision of the Laurentia and Baltica in the late Silurian (Gee, 1975). The thrust sheets produced during this collision is allocated from north to south in the mid-Norwegian region consisting of sedimentary and crystalline rocks, where abundant basement windows are exposed (Roberts and Gee, 1985). Mesozoic rocks in Norway are associated with the dated dikes, eclogite, and amphibolite located on the Flakstadøy on Lofoten (Hames and Andersen, 1996; Steltenpohl et al., 2003a; Steltenpohl et al., 2004; Corfu, 2004a; Corfu, 2004b; Steltenpohl et al., 2011a). Mesozoic rocks from the Barents Sea are related to the High Arctic Large Igneous Province sills, dikes and lavas dated to around 120-125 Ma. Frantz Josef Land in the Barents Sea has dikes and sills that are dated to around 94-192 Ma and 34-175 Ma, respectively (Koryakin and Shipilov, 2009; Corfu and Heim, 2013).

3.1.2 Greenland

An almost complete chronostratigraphy of the Archean age is located on Greenland within the North Atlantic Craton border in the southwestern and southeastern parts (Figure 2). Granite-greenstone and granite-gneiss complexes, with a hiatus from 3.20-3.55 Ga, represent the Archean rocks (Kolb et al., 2015 and reference herein). However, they are less exposed to the northern and western Greenland (Ramberg et al., 2008). The ice-free areas of Greenland are occupied of crystalline rocks of the Precambrian shield, wherein East Greenland, the basement rocks are of Early Proterozoic and Phanerozoic ages; also Early Proterozoic basement rocks are exposed north of 72°N (Watt and Thrane, 2001; Thrane, 2002). To the east of the Precambrian basement are predominantly younger sedimentary rocks, and metasedimentary rocks of the Caledonian thrust belt exposed (Thrane, 2002). Sediments which are derived from Archean and Proterozoic age rocks are located in Northern Greenland, close to Peary Land (Kirkland et al.,

2009). Dikes, which are cross-cutting the Early Cretaceous strata in northern Greenland, have been dated to around 82-103 Ma (Buchan and Ernst, 2006).

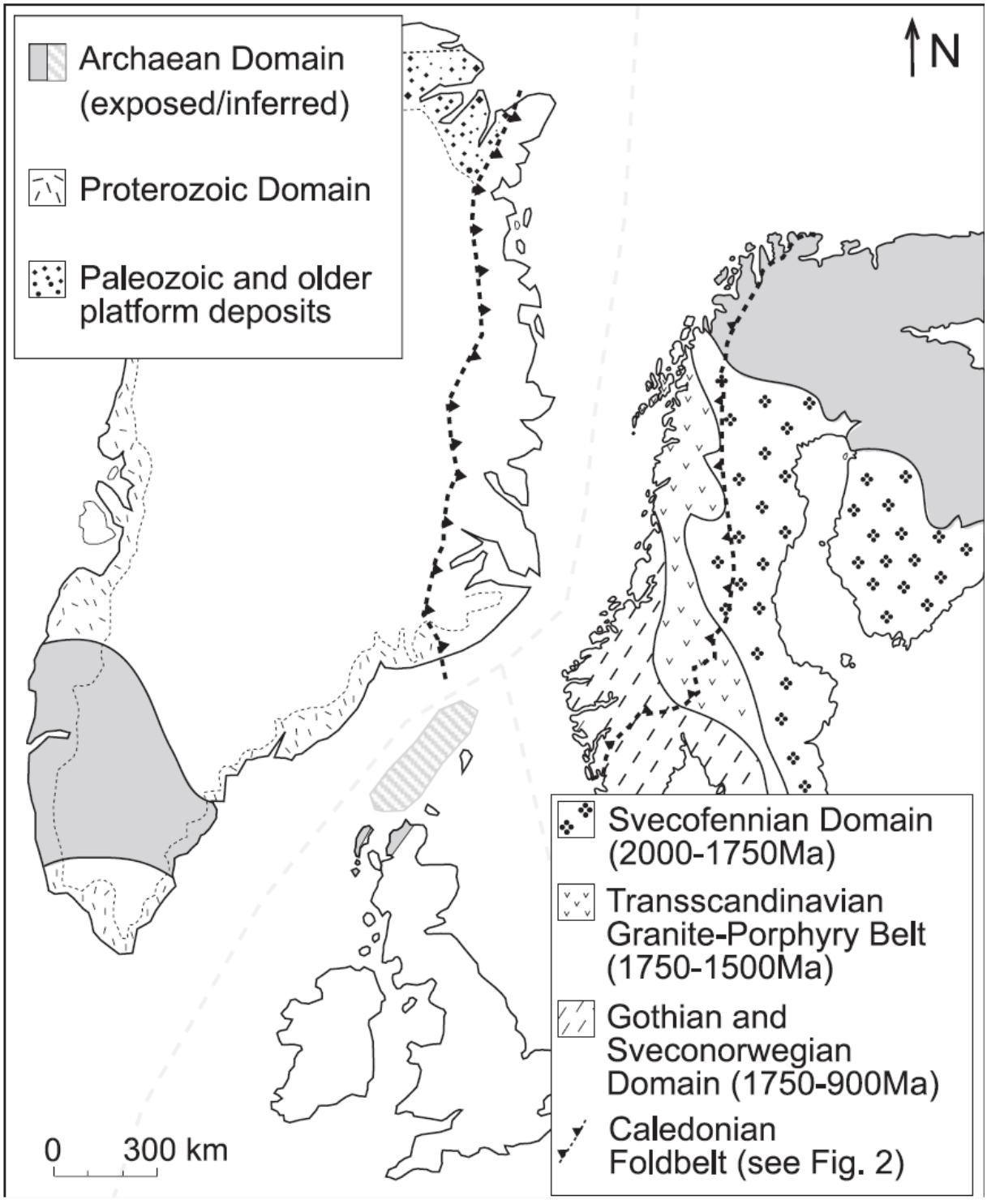

Figure 2: Greenland and Scandinavia age distribution presented in a pre-drift configuration (Fonneland et al., 2004).

3.2 Norway-Greenland offshore

3.2.1 Late Paleozoic-Mesozoic rifting (rift episodes)

3.2.1.1 Late Permian-Early Triassic

Episodic regional extensions induced the formation of the Middle Norwegian shelf of the North Atlantic's east side during the continental rifting. The first episodic rifting, which started in the Late Permian to early Triassic, created two major lineaments trending northeast-southwest. The offshore representation of the onshore Møre-Trøndelag Fault Zone is present in the southeastern margin by elongated fault blocks (Figure 3; Blystad et al., 1995; Berndt et al., 2001; Gernigon et al., 2003; Abdelmalak et al., 2017). A second lineament with this northeast-southwest trend extends from the Lofoten area to the northern Vøring Basin. The North-South bounding faults step towards the Trøndelag Platform where they are partly present and on the Halten Terrace and southern Fles Fault Zone (Doré et al., 1997; Brekke et al., 2001; Halland et al., 2013).

3.2.1.2 Late Jurassic

The Jan Mayen Lineament and Bivrost Lineament are northwest-southeast transfer zones that segment the Mesozoic and Cenozoic basins of the Norwegian Sea (Blystad et al., 1995; Doré et al., 1997). During the Jurassic rift phase, the North-South trending Halten Terrace and the Dønna Terrace basins developed and subsequently, subsided. Doré et al. (1997) proposed that during the Lower Cretaceous, the rift networks in the Jurassic were overprinted. A shift from extensional systems on the northern margin of the Tethys Ocean, by the propagating Atlantic spreading, with considerable crustal extension, produced the major northeast-southwest trending Møre Basin and Vøring Basin on the Norwegian Continental Shelf (Faleide et al., 2008).

3.2.1.3 Late Cretaceous-Early Paleogene

Eldholm et al. (2002) have suggested three different tectono-magmatic events that comprise the formation of the mid-Norwegian margin. The first occurred during the latest Cretaceous-Paleocene when a lithospheric extension during a rift episode lead to plate breakup and separation (Eldholm et al., 2002).

3.2.1.4 Early Paleogene fracturing and vulcanites

The second tectono-magmatic event was during the Early Eocene when immense emanation of basaltic lavas peaked during igneous activity (Eldholm et al., 2002).

3.2.2 Paleogene-Neogene passive margin

3.2.2.1 Early immature transition to mature in Neogene

The third tectono-magmatic event, during the Middle Eocene-Present, changed the increased igneous activity to a normal accretionary magma volume. Subsequently, continental margin subsidence and maturation occurred (Figure 3; Eldholm et al., 2002).

3.2.2.2 Neogene inversion

Evidence of a compressional phase during the Cenozoic is evident by numerous anticlines with a North-South trend (Figure 3; Blystad et al., 1995; Doré and Lundin, 1996). These structures (e.g., Ormen Lange Dome, Modgunn Arch) that extend on the Jan Mayen Fracture Zone are believed to originate from a minor sinistral wrenching. Similar structures are also seen on the Bivrost Lineament (Doré and Lundin, 1996).

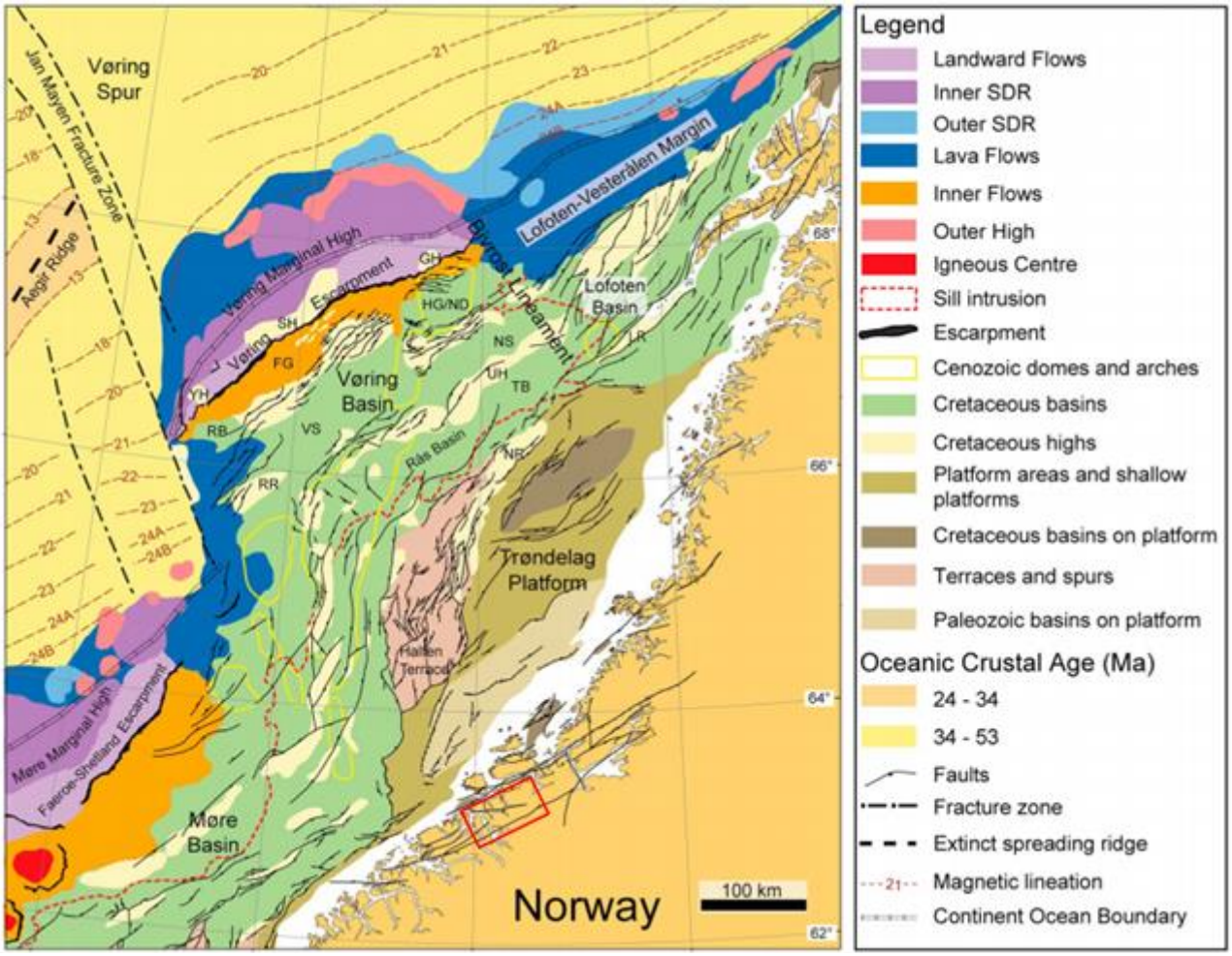

Figure 3: Main tectonic structures, fault zones and volcanic seismic facies units of the Norwegian Sea (Abdelmalak et al., 2017 modified from Blystad et al., 1995; Berndt et al., 2001; Gernigon et al., 2003). FG: Fenris Graben; GH: Grimm High; HG/ND: Hel Graben/Nagfar Dome; NR: Nordland Ridge; NS: Någrind Syncline; RB: Rån Basin; RR: Rån Ridge; SDRs: Seaward dipping reflectors; SH: Skoll High; TB: Træna Basin; UH: Utgard High; VS: Vigrid Syncline; YH: Ygg High.

3.2.2.3 Late Neogene glaciation

For the 6 Ma, the Norwegian Sea was a net exporter of deep-water with $\delta\,^{18}O$ indicating denser and colder waters. Starting from the late Miocene (5.45 Ma) through the Pliocene, a series of glacial episodes in the surroundings of the Norwegian-Greenland Sea took place. Major glacial episodes during 5.1-5 Ma and 3.7-3.1 Ma lowered the sea-level about 80 m below the present (Jansen et al., 1990).

3.3 Surrounding areas

3.3.1 The Barents Sea and North Greenland important sedimentary source regions

Metamorphic and granitic rocks with ages corresponding to the Archean, Proterozoic, and Phanerozoic are located on the northwest Spitsbergen (Ohta et al., 2002 and references therein). Sediments located in the Independence Fjord close to the Peary Land are recorded with a substantial Archean and Proterozoic component with no sign of a Phanerozoic input. The oldest zircon found was 3970 Ma, whereas the youngest was dated to around 970 Ma (Kirkland et al., 2009).

3.3.2 Barents-North Greenland volcanic activity

The High Arctic Large Igneous Province (HALIP) within the Barents Sea contains 120-125 Ma sills, dikes, and lavas stretching towards the Franz Josef Land, where they have a more extensive spread of ages from 35-190 Ma (Koryakin and Shipilov, 2009; Corfu and Heim, 2013). The High Arctic Large Igneous Province encompasses northern Greenland, where the Early Cretaceous strata have been crosscut by dikes dated to around 80-100 Ma (Buchan and Ernst, 2006).

3.4 Structural domains

3.4.1 Platform area

The Nordland Ridge and the Trøndelag Platform have been regarded as a constituent of the same geological framework, prior to the uplift during the Middle Jurassic to Early Cretaceous. The uplift separated them into two individual elements (Blystad et al., 1995). The Base Cretaceous Unconformity on the Nordland Ridge represents events of erosion and non-deposition (Blystad et al., 1995). The rocks truncated by the Base Cretaceous Unconformity (BCU) characterize strata from the Early Permian to Jurassic, whereas the overlying rocks are from Early Cretaceous to Pliocene, representing hiatus (Blystad et al., 1995). Erosional events on the Nordland Ridge suggest that the ridge existed as an emergent high throughout the Cretaceous (Hastings, 1987). The southern part of the Revfallet Fault Complex is made up of west dipping, NNW-SSE en-echelon normal faults (Blystad et al., 1995). The Trøndelag Platform was a stable area where it eroded down to a peneplain in the Early Cretaceous.

Westward tilting of the Platform followed by a transgression continued into to Late Cretaceous (Brekke and Riis, 1987).

3.4.2 Terraces

According to Blystad et al. (1995), the Dønna Terrace in the Norwegian Sea is perceived as a prolongation of the southward Halten Terrace. The boundaries of the Dønna Terrace are the Nordland Ridge, separated by the Revfallet Fault Complex to the southeast, and Rås Basin separated by the Ytreholmen Fault zone to the northwest (Figure 4a; NPD, 2019 and Figure 4b; Mjelde et al., 2010). The Dønna Terrace is separated from the Halten Terrace by the Heidrun-Smørbukk fault zone, represented by transfer fault induced by the first tectonic phase during the Late Permian to early Triassic (Doré et al., 1997; Brekke et al., 2001; Fugelli and Olsen, 2007). Structural features of the Dønna Terrace are local horsts, rotated fault blocks and grabens, created by deep-seated northeast and southwest transfer faults. North-South trending Jurassic structures produced differential bathymetry and a reservoir fairway for the Cretaceous sediment (Blystad et al., 1995; Færseth and Lien, 2002; Gjelberg et al., 2005; Martinsen et al., 2005).

3.4.3 Deep basins

The Vøring Basin is the eastern margin of the Dønna terrace and formed during the Late Jurassic-Early Cretaceous rifting phase. Further rifting in the Cretaceous and minor faulting in the Paleogene and Neogene affected the Vøring Basin (Brekke et al., 1999). The Møre Basin also formed during the Late Jurassic-Early Cretaceous and borders to the Norwegian Landmass; however, it was not affected by the Cretaceous and minor Paleogene and Neogene faulting (Brekke et al., 1999).

3.5 Halten-Dønna

3.5.1 Formation

The main tectonic episode during the Carboniferous to Late Permian is only evident in the Trøndelag Platform. First, during the Middle Jurassic to Early Cretaceous, intense fault activity on the Dønna Terrace is visible. In the course of the faulting, the Nordland Ridge was uplifted on the platform edge, in conjunction with the individual separation of the Dønna and Halten terraces during the Late Jurassic (Brekke, 2000). The elevation of the terraces relative to the Trøndelag Platform remained the same until later in the Cretaceous, culminating with the final separation and downfaulting of the Dønna Terrace relative to the Nordland Ridge (Blystad et al., 1995; Brekke, 2000). The Bremstein and Revfallet Fault Complexes controlled the separation along the eastern border during two phases of subsidence: (1) Early Cretaceous and

(2) one major in the post-Cenomanian time (Brekke, 2000). According to Bukovics et al. (1984), the rationale behind the subsidence is the gradual cooling of a thermal anomaly during the Late Jurassic rifting phase.

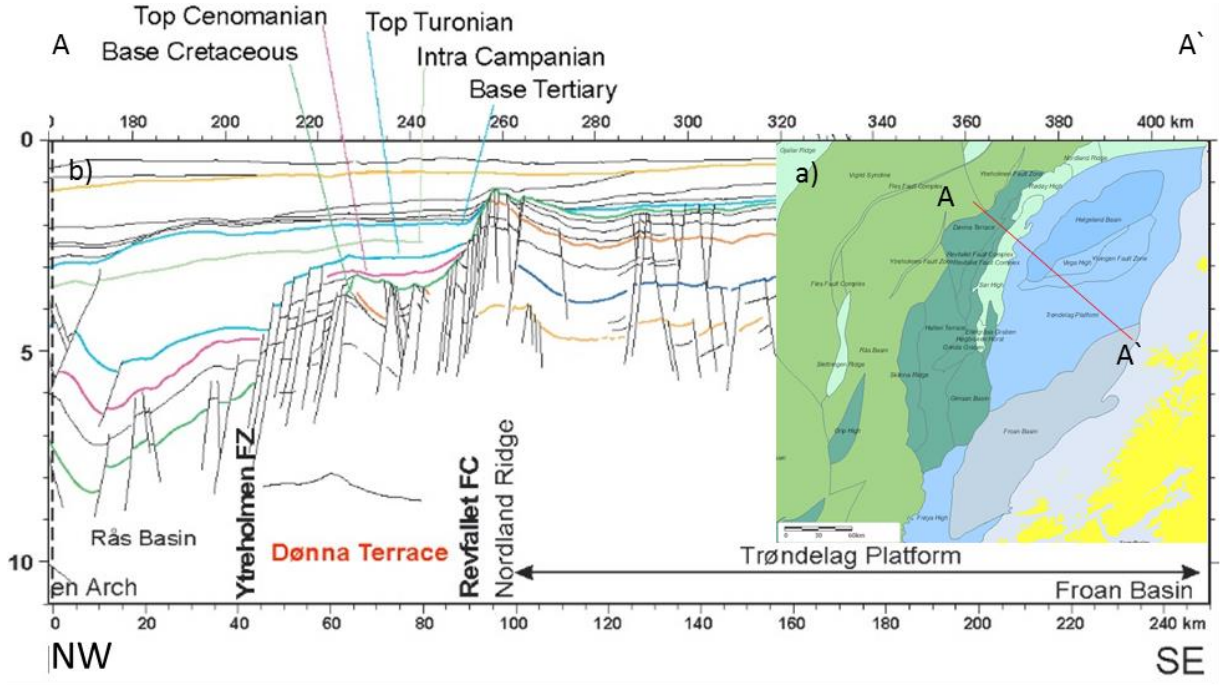

Figure 4: a) Inset map over the Dønna Terrace, Nordland Ridge and Trøndelag Platform (modified from NPD, 2019). b) is a cross section showing faults and formations on the Dønna Terrace and Trøndelag Platform (modified from Mjelde et al., 2010).

3.5.2 Cenomanian-Coniacian sedimentation

A low gradient deep-water slope consisting of the Halten and Dønna terraces was formed between the Trøndelag Platform to the east and the Vøring Basin to the west. Low relief accommodation on gentle regional slopes was formed by differential subsidence of underlying fine-grained rocks (Færseth and Lien, 2002). The low relief accommodation was controlled by the underlying Jurassic structure and subtle differential subsidence on major basin bounding faults. The underlying lithology of the Cretaceous fill consists of Lower-Middle Jurassic pre-rift sandstone that was dominated by fluvial to marine shelf deposition. In the Upper Jurassic-earliest Cretaceous (Figure 5; Fugelli and Olsen, 2005), the bathymetry changes and deep-water sedimentation dominates during syn-rift deposition (Koch and Heum, 1995; Kyrkjebø et al., 2001; Faleide et al., 2008). The post-rifting evolution culminated in thermal subsidence that caused the filling of the differential basin with thick Upper Cretaceous sediment (Færseth and Lien, 2002; Faleide et al., 2008). According to Færseth and Lien (2002) and Lien (2005), the highest sedimentation rate on the Dønna Terrace was 100 m/my towards the end of the post-rift stage during the Late Cretaceous. The long-term basin infill and the variations in clastic input were controlled by high-frequency climatic and eustatic fluctuations during the Cretaceous

(MacLeod et al., 2005; Miller et al., 2005a; Miller et al., 2005b; Price et al., 2011). Dalland et al. (1988) described the sediment of the early Late Cretaceous as predominantly mudstone and siltstone, interrupted by thin intervals of sandstone. The infill of the Late Turonian to Early Coniacian Lysing Formation consists of fine-grained clastic material. Also, glauconite that forms exclusively in a shallow-marine setting is present in the Lysing Formation (Smith and Hiscott, 1987; Dalland et al., 1988).

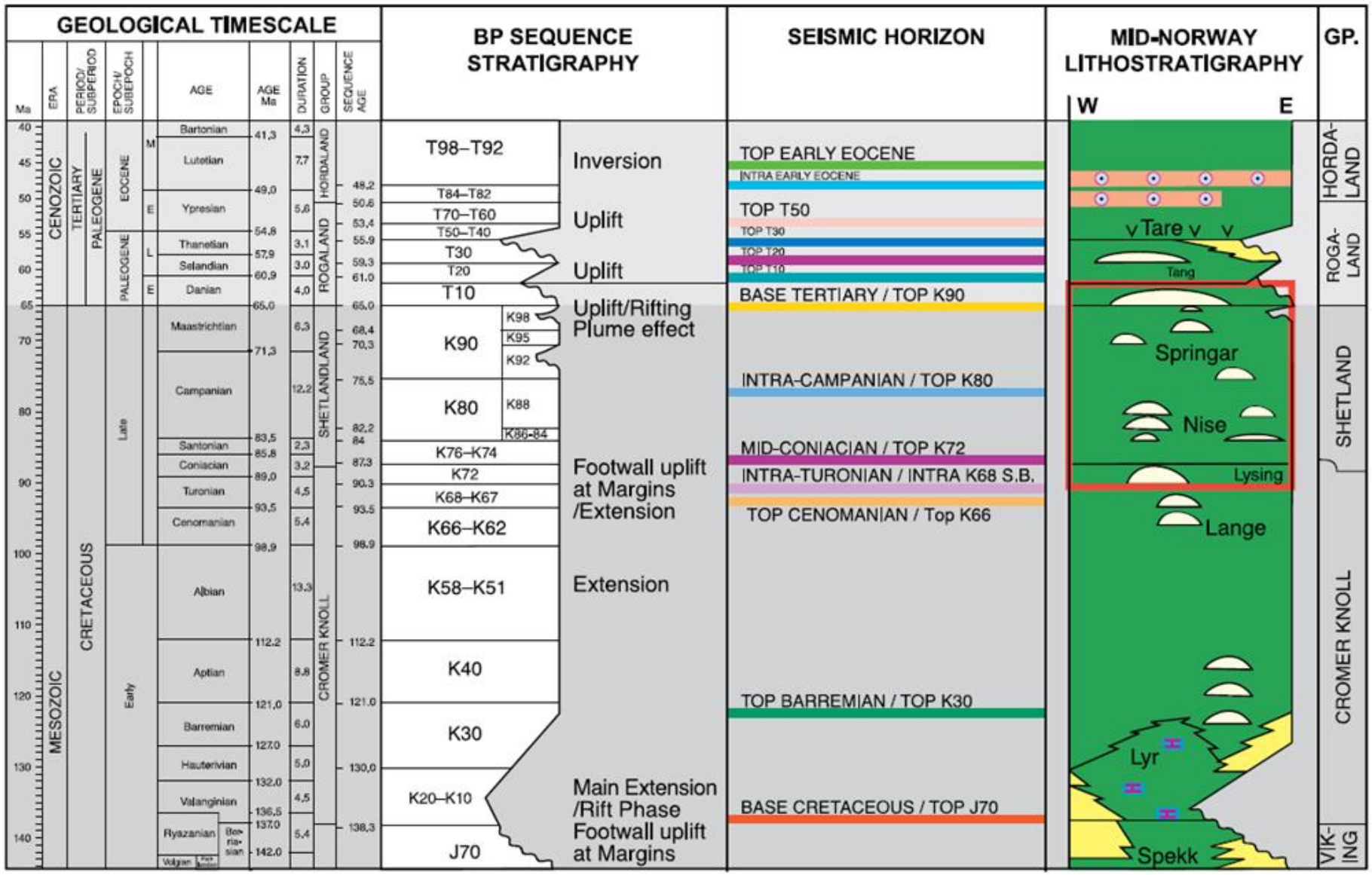

Figure 5: Sequence stratigraphic scheme for the Norwegian Sea. Yellow=sandstone, orange=silt, gray=mudstones (Fugelli and Olsen, 2005). K72 in this study equates to K72.2 and K72.1, and K74 to K72.3 (courtesy of Aker BP).

4 Dataset & analytical techniques

4.1 Dataset

225 m of core interval from six wells covering Cenomanian to Turonian-Coniacian Lange and Lysing formations on the Dønna Terrace, where described and sampled at the Weatherford Core storage in Sandnes, Norway. Aker BP ASA, Vår Energi AS, and ConocoPhilips AS provided the cores. Ninety samples were analyzed from sandstone intervals, including a few taken from shale intervals and sand injectites. 46 for geochemical analysis, 27 for petrography, and 11 for zircon analysis (Appendix 1-4). Labeling of the individual samples are according to their respective field, well number, and sample number, (e.g., ÆR5-8-4, which is Ærfugl field, well number 6507/5-8 and sample number 4).

4.2 Core description

Six cores (6507/2-2, 6507/2-4, 6507/5-8, 6507/3-9S, 6507/5-A-4H and 6507/7-1) were described, ranging from 9-65 m in thickness, and taken from fields located on the Dønna Terrace (Figure 1; inset map). Core 6607/12-2S only consists of cuttings, so no core description is available. The descriptions are based on rock type, grain size, sorting, bioturbation, and sedimentary structures. Classification of the facies are according to lithology: Breccia (Facies A), massive sandstone (Facies B), graded and laminated sandstone (Facies C), heterolithics (Facies D), hemipelagic and pelagic mudstone (Facies E) and massive sandstone with abundant bioturbation (Facies F). Facies formed by gravity flows are classified according to Bouma (1962) and Lowe (1982). Aker BP provided interpretation of the gross depositional environment and architectural element (GDE). GDE interpretations are based on Aker BPs internal regional interpretations and are founded in regional seismic, well, core and biostratigraphic data (Figure 6). Architectural elements are inferred from core interpretations and cross-checked with Aker BPs interpretation of GDE and depositional/architectural elements for internal consistency.

The samples have predominantly been taken from the massive sandstone facies, where a subordinate of the samples have been taken from heterolithics and hemipelagic and pelagic facies. By predominantly sampling from a homogeneous facies will reduce any affect of grain size differences (Savage and Potter, 1991). Composition is dependent on grain size which is why this method is preferred (Savage and Potter, 1991). The architectural elements are mainly slope channel complex and sandy fan with subordinate elements such as delta front, background and unstable slope. The gross depositional environments are predominantly lower slope and basinfloor, with subordinate environments such as marginal marine and upper slope (Table 1-

3). By defining facies, architectural element and gross depositional environment for each sample taken, it is possible to get realistic results when comparing provenance signature within the megasequences and to unravel any uncertainty related to different material from varying facies.

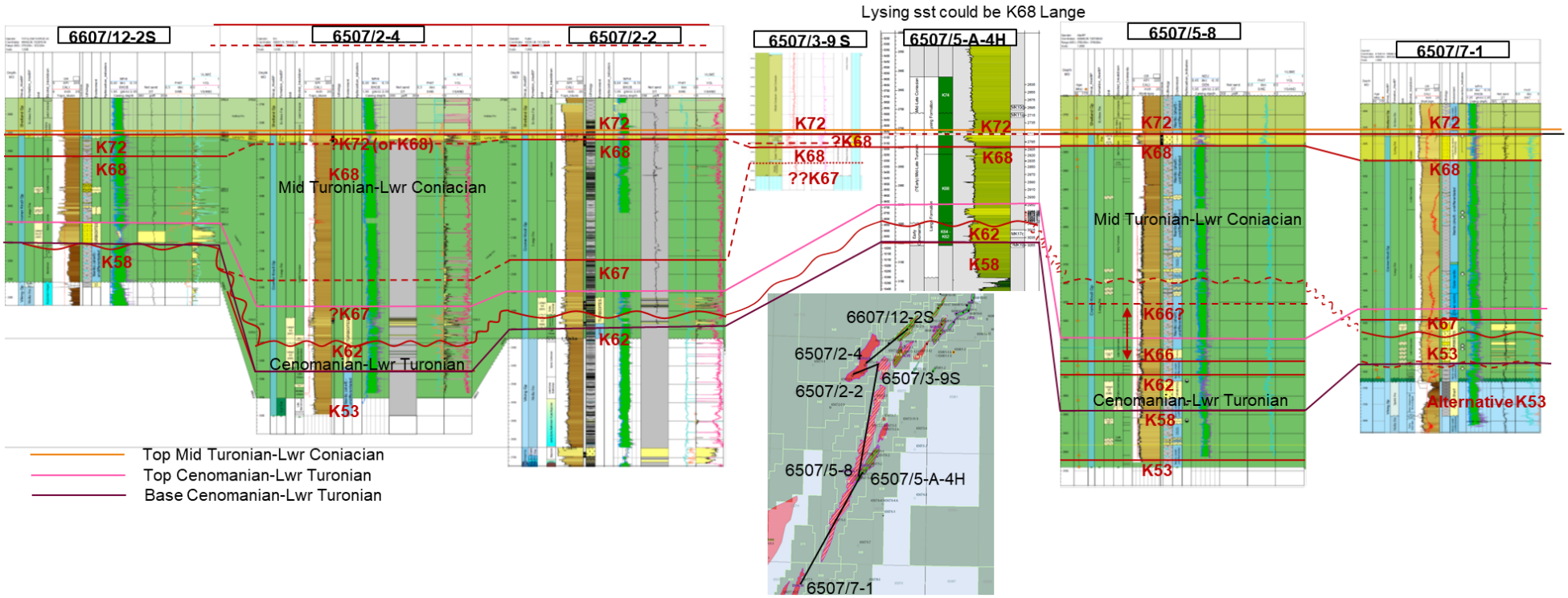

Figure 6: Well correlation of sequece stratigraphy units within the Cenomanian to Coniacian Lange-Lysing megasequence, covering all the wells within the scope of this study. Courtesy of Aker BP.

Table 1: Overview of all samples taken and at which interval. GDE=gross depositional environment. GC= geochemical, TS=thin section, Hf= hafnium.

Field	Well	Depth (m)	Sample	Formation	Megasequence	Part of unit	GDE	GrossArc	DepoElement	Lithology	GC	TS	U-Pb	Hf
Dvalin	6507/7-1	3504,22	DE1-1	Lange Fm	Cen-LowTur	Upper part	Lower Slope/Base-of-slope	Slope Channel Cplx	Channel-fill	Sandstone	x			
Dvalin	6507/7-1	3504,22	DE1-2	Lange Fm	Cen-LowTur	Upper part	Lower Slope/Base-of-slope	Slope Channel Cplx	Channel-fill	Sandstone			x	
Dvalin	6507/7-1	3504,32	DE1-3	Lange Fm	Cen-LowTur	Upper part	Lower Slope/Base-of-slope	Slope Channel Cplx	Channel-fill	Sandstone		x		
Dvalin	6507/7-1	3505,48	DE1-4	Lange Fm	Cen-LowTur	Upper part	Lower Slope/Base-of-slope	Slope Channel Cplx	Channel-fill	Sandstone				
Dvalin	6507/7-1	3505,54	DE1-5	Lange Fm	Cen-LowTur	Upper part	Lower Slope/Base-of-slope	Slope Channel Cplx	Channel-fill	Sandstone	x			
Dvalin	6507/7-1	3507,57	DE1-6	Lange Fm	Cen-LowTur	Upper part	Lower Slope/Base-of-slope	Slope Channel Cplx	Channel-fill	Sandstone		x		
Dvalin	6507/7-1	3507,66	DE1-7	Lange Fm	Cen-LowTur	Upper part	Lower Slope/Base-of-slope	Slope Channel Cplx	Channel-fill	Sandstone	x			
Dvalin	6507/7-1	3509,1	DE1-8	Lange Fm	Cen-LowTur	Upper part	Lower Slope/Base-of-slope	Slope Channel Cplx	Channel-fill	Sandstone	x			
Dvalin	6507/7-1	3509,1	DE1-9	Lange Fm	Cen-LowTur	Upper part	Lower Slope/Base-of-slope	Slope Channel Cplx	Channel-fill	Sandstone			x	
Dvalin	6507/7-1	3509,1	DE1-10	Lange Fm	Cen-LowTur	Upper part	Lower Slope/Base-of-slope	Slope Channel Cplx	Channel-fill	Sandstone		x		
Dvalin	6507/7-1	3511,3	DE1-11	Lange Fm	Cen-LowTur	Upper part	Lower Slope/Base-of-slope	Slope Channel Cplx	Channel-fill	Sandstone	x			
Dvalin	6507/7-1	3511,3	DE1-12	Lange Fm	Cen-LowTur	Upper part	Lower Slope/Base-of-slope	Slope Channel Cplx	Channel-fill	Sandstone				
Dvalin	6507/7-1	3512,7	DE1-13	Lange Fm	Cen-LowTur	Upper part	Lower Slope/Base-of-slope	Slope Channel Cplx	Channel-fill	Sandstone		x		
Dvalin	6507/7-1	3512,86	DE1-14	Lange Fm	Cen-LowTur	Upper part	Lower Slope/Base-of-slope	Slope Channel Cplx	Channel-fill	Sandstone	x			
Dvalin	6507/7-1	3512,86	DE1-15	Lange Fm	Cen-LowTur	Upper part	Lower Slope/Base-of-slope	Slope Channel Cplx	Channel-fill	Sandstone				
Ærfugl	6507/5-8	2802,80-87	ÆR5-8-1	Lysing Fm	MidTur-LowCon	Upper part	Basinfloor/Slope terrace	Sandy fan	Channelized-lobe complexes	Sandstone	x			
Ærfugl	6507/5-8	2802,80-87	ÆR5-8-2	Lysing Fm	MidTur-LowCon	Upper part	Basinfloor/Slope terrace	Sandy fan	Channelized-lobe complexes	Sandstone				
Ærfugl	6507/5-8	2802,80-87	ÆR5-8-3	Lysing Fm	MidTur-LowCon	Upper part	Basinfloor/Slope terrace	Sandy fan	Channelized-lobe complexes	Sandstone		x		
Ærfugl	6507/5-8	2811,64-70	ÆR5-8-4	Lysing Fm	MidTur-LowCon	Upper part	Basinfloor/Slope terrace	Sandy fan	Channelized-lobe complexes	Sandstone	x			
Ærfugl	6507/5-8	2811,64-70	ÆR5-8-5	Lysing Fm	MidTur-LowCon	Upper part	Basinfloor/Slope terrace	Sandy fan	Channelized-lobe complexes	Sandstone		x		
Ærfugl	6507/5-8	2815,40-46	ÆR5-8-6	Lysing Fm	MidTur-LowCon	Upper part	Basinfloor/Slope terrace	Sandy fan	Channelized-lobe complexes	Sandstone	x			
Ærfugl	6507/5-8	2815,40-46	ÆR5-8-7	Lysing Fm	MidTur-LowCon	Upper part	Basinfloor/Slope terrace	Sandy fan	Channelized-lobe complexes	Sandstone		x		
Ærfugl	6507/5-8	2821,82-88	ÆR5-8-8	Lysing Fm	MidTur-LowCon	Upper part	Basinfloor/Slope terrace	Sandy fan	Channelized-lobe complexes	Sandstone	x			
Ærfugl	6507/5-8	2821,82-88	ÆR5-8-9	Lysing Fm	MidTur-LowCon	Upper part	Basinfloor/Slope terrace	Sandy fan	Channelized-lobe complexes	Sandstone			x	x
Ærfugl	6507/5-8	2821,82-88	ÆR5-8-10	Lysing Fm	MidTur-LowCon	Upper part	Basinfloor/Slope terrace	Sandy fan	Channelized-lobe complexes	Sandstone		x		
Ærfugl	6507/5-8	2822,64-71	ÆR5-8-11	Lysing Fm	MidTur-LowCon	Upper part	Basinfloor/Slope terrace	Sandy fan	Channelized-lobe complexes	Sandstone	x			
Ærfugl	6507/5-8	2822,64-71	ÆR5-8-12	Lysing Fm	MidTur-LowCon	Upper part	Basinfloor/Slope terrace	Sandy fan	Channelized-lobe complexes	Sandstone			x	
Ærfugl	6507/5-8	2822,64-71	ÆR5-8-13	Lysing Fm	MidTur-LowCon	Upper part	Basinfloor/Slope terrace	Sandy fan	Channelized-lobe complexes	Sandstone		x		
Ærfugl	6507/5-8	2824,31-39	ÆR5-8-14	Lysing Fm	MidTur-LowCon	Upper part	Basinfloor/Slope terrace	Sandy fan	Channelized-lobe complexes	Sandstone	x			
Ærfugl	6507/5-8	2824,31-39	ÆR5-8-15	Lysing Fm	MidTur-LowCon	Upper part	Basinfloor/Slope terrace	Sandy fan	Channelized-lobe complexes	Sandstone				
Ærfugl	6507/5-8	2824,31-39	ÆR5-8-16	Lysing Fm	MidTur-LowCon	Upper part	Basinfloor/Slope terrace	Sandy fan	Channelized-lobe complexes	Sandstone		x		
Skarv	6507/5-A-4H	2966,40-49	SK5-A-1	Lange Fm	Cen-LowTur	Upper part	Marginal-marine (Shelf-edge	Delta-front2Prodelta	Tidal (mouth) bar	Sandstone	x			
Skarv	6507/5-A-4H	2966,40-49	SK5-A-2	Lange Fm	Cen-LowTur	Upper part	Marginal-marine (Shelf-edge	Delta-front2Prodelta	Tidal (mouth) bar	Sandstone			x	
Skarv	6507/5-A-4H	2966,40-49	SK5-A-3	Lange Fm	Cen-LowTur	Upper part	Marginal-marine (Shelf-edge	Delta-front2Prodelta	Tidal (mouth) bar	Sandstone		x		
Skarv	6507/5-A-4H	2970,46-53	SK5-A-4	Lange Fm	Cen-LowTur	Upper part	Marginal-marine (Shelf-edge	Delta-front2Prodelta	Tidal (mouth) bar	Sandstone	x			
Skarv	6507/5-A-4H	2970,46-53	SK5-A-5	Lange Fm	Cen-LowTur	Upper part	Marginal-marine (Shelf-edge	Delta-front2Prodelta	Tidal (mouth) bar	Sandstone				
Skarv	6507/5-A-4H	2970,46-53	SK5-A-6	Lange Fm	Cen-LowTur	Upper part	Marginal-marine (Shelf-edge	Delta-front2Prodelta	Tidal (mouth) bar	Sandstone		x		
Skarv	6507/5-A-4H	2973,52-60	SK5-A-7	Lange Fm	Cen-LowTur	Upper part	Marginal-marine (Shelf-edge	Delta-front2Prodelta	Tidal (mouth) bar	Sandstone	x			
Skarv	6507/5-A-4H	2973,52-60	SK5-A-8	Lange Fm	Cen-LowTur	Upper part	Marginal-marine (Shelf-edge	Delta-front2Prodelta	Tidal (mouth) bar	Sandstone			x	
Skarv	6507/5-A-4H	2973,52-60	SK5-A-9	Lange Fm	Cen-LowTur	Upper part	Marginal-marine (Shelf-edge	Delta-front2Prodelta	Tidal (mouth) bar	Sandstone		x		
Skarv	6507/5-A-4H	2983,71-76	SK5-A-10	Lange Fm	Cen-LowTur	Upper part	Upper Slope	Background		silt/shale	x			
Skarv	6507/5-A-4H	2991,60-65	SK5-A-11	Lange Fm	Cen-LowTur	Upper part	Upper Slope	Background		silt/shale	x			
Skarv	6507/5-A-4H	2994,73-78	SK5-A-12	Lange Fm	Cen-LowTur	Upper part	Upper Slope	Unstable slope	Remob sst/slump-inj ?	Sand injectites	x			
Skarv	6507/5-A-4H	2995,57-66	SK5-A-13	Lange Fm	Cen-LowTur	Upper part	Upper Slope	Unstable slope	Remob sst/slump-inj ?	Sand injectites	x			

Table 2: Overview of all samples taken and at which interval. GDE=gross depositional environment. GC= geochemical, TS=thin section, Hf= hafnium.

Field	Well	Depth (m)	Sample	Formation	Megasequence	Part of unit	GDE	GrossArc	DepoElement	Lithology	GC	TS	U-Pb	Hf
Marulk	6507/2-2	2823,80-90	MA2-2-1	Lysing Fm	MidTur-LowCon	Upper part	Basinfloor/Slope terrace	Sandy fan	Channelized-lobe complexes	Sandstone			x	
Marulk	6507/2-2	2824,3	MA2-2-2	Lysing Fm	MidTur-LowCon	Upper part	Basinfloor/Slope terrace	Sandy fan	Channelized-lobe complexes	Sandstone	x			
Marulk	6507/2-2	2824,3	MA2-2-3	Lysing Fm	MidTur-LowCon	Upper part	Basinfloor/Slope terrace	Sandy fan	Channelized-lobe complexes	Sandstone		x		
Marulk	6507/2-2	2831,40-50	MA2-2-4	Lysing Fm	MidTur-LowCon	Upper part	Basinfloor/Slope terrace	Sandy fan	Channelized-lobe complexes	Sandstone			x	x
Marulk	6507/2-2	2832,6	MA2-2-5	Lysing Fm	MidTur-LowCon	Upper part	Basinfloor/Slope terrace	Sandy fan	Channelized-lobe complexes	Sandstone	x			
Marulk	6507/2-2	2832,6	MA2-2-6	Lysing Fm	MidTur-LowCon	Upper part	Basinfloor/Slope terrace	Sandy fan	Channelized-lobe complexes	Sandstone		x		
Marulk	6507/2-2	2840,6	MA2-2-7	Lysing Fm	MidTur-LowCon	Upper part	Basinfloor/Slope terrace	Background		Silt/Shale	x			
Marulk	6507/2-2	3282,4	MA2-2-8	Lange Fm	Cen-LowTur	Upper part	Lower Slope/Base-of-slope	Slope Channel Cplx	Channel-fill	Sandstone			x	x
Marulk	6507/2-2	3282,55	MA2-2-9	Lange Fm	Cen-LowTur	Upper part	Lower Slope/Base-of-slope	Slope Channel Cplx	Channel-fill	Sandstone	x			
Marulk	6507/2-2	3282,55	MA2-2-10	Lange Fm	Cen-LowTur	Upper part	Lower Slope/Base-of-slope	Slope Channel Cplx	Channel-fill	Sandstone		x		
Marulk	6507/2-2	3288,1	MA2-2-11	Lange Fm	Cen-LowTur	Upper part	Lower Slope/Base-of-slope	Slope Channel Cplx	Channel-fill	Sandstone	x			
Marulk	6507/2-2	3288,1	MA2-2-12	Lange Fm	Cen-LowTur	Upper part	Lower Slope/Base-of-slope	Slope Channel Cplx	Channel-fill	Sandstone		x		
Marulk	6507/2-2	3334,7	MA2-2-13	Lange Fm	Cen-LowTur	Middle part	Lower Slope/Base-of-slope	Slope Channel Cplx	Channel-plugging/abondonm	Silt/Shale	x			
Marulk	6507/2-2	3337,6	MA2-2-14	Lange Fm	Cen-LowTur	Middle part	Lower Slope/Base-of-slope	Slope Channel Cplx	Channel-fill	Sandstone	x			
Marulk	6507/2-2	3337,6	MA2-2-15	Lange Fm	Cen-LowTur	Middle part	Lower Slope/Base-of-slope	Slope Channel Cplx	Channel-fill	Sandstone		x		
Marulk	6507/2-2	3338,1	MA2-2-16	Lange Fm	Cen-LowTur	Middle part	Lower Slope/Base-of-slope	Slope Channel Cplx	Channel-fill	Sandstone			x	x
Marulk	6507/2-4	2835,26	MA2-4-1	Lysing Fm	MidTur-LowCon	Upper part	Basinfloor/Slope terrace	Sandy fan	Channelized-lobe complexes	Sandstone	x			
Marulk	6507/2-4	2835,26	MA2-4-2	Lysing Fm	MidTur-LowCon	Upper part	Basinfloor/Slope terrace	Sandy fan	Channelized-lobe complexes	Sandstone				
Marulk	6507/2-4	2842,36	MA2-4-3	Lysing Fm	MidTur-LowCon	Upper part	Basinfloor/Slope terrace	Sandy fan	Channelized-lobe complexes	Sandstone	x			
Marulk	6507/2-4	2842,36	MA2-4-4	Lysing Fm	MidTur-LowCon	Upper part	Basinfloor/Slope terrace	Sandy fan	Channelized-lobe complexes	Sandstone			x	x
Marulk	6507/2-4	2842,46	MA2-4-5	Lysing Fm	MidTur-LowCon	Upper part	Basinfloor/Slope terrace	Sandy fan	Channelized-lobe complexes	Sandstone		x		
Marulk	6507/2-4	2843,77	MA2-4-6	Lysing Fm	MidTur-LowCon	Upper part	Basinfloor/Slope terrace	Sandy fan	Channelized-lobe complexes	Sandstone	x			
Marulk	6507/2-4	2843,9	MA2-4-7	Lysing Fm	MidTur-LowCon	Upper part	Basinfloor/Slope terrace	Sandy fan	Channelized-lobe complexes	Sandstone		x		
Marulk	6507/2-4	2846,8	MA2-4-8	Lysing Fm	MidTur-LowCon	Upper part	Basinfloor/Slope terrace	Sandy fan	Channelized-lobe complexes	Sandstone		x		
Marulk	6507/2-4	2846,94	MA2-4-9	Lysing Fm	MidTur-LowCon	Upper part	Basinfloor/Slope terrace	Sandy fan	Channelized-lobe complexes	Sandstone	x			
Marulk	6507/2-4	2846,94	MA2-4-10	Lysing Fm	MidTur-LowCon	Upper part	Basinfloor/Slope terrace	Sandy fan	Channelized-lobe complexes	Sandstone				
Marulk	6507/2-4	2848,4	MA2-4-11	Lysing Fm	MidTur-LowCon	Upper part	Basinfloor/Slope terrace	Sandy fan	Channelized-lobe complexes	Sandstone	x			
Marulk	6507/2-4	2848,4	MA2-4-12	Lysing Fm	MidTur-LowCon	Upper part	Basinfloor/Slope terrace	Sandy fan	Channelized-lobe complexes	Sandstone				
Marulk	6507/2-4	2848,53	MA2-4-13	Lysing Fm	MidTur-LowCon	Upper part	Basinfloor/Slope terrace	Sandy fan	Channelized-lobe complexes	Sandstone		x		
Marulk	6507/2-4	3336,17	MA2-4-14	Lange Fm	Cen-LowTur	Middle part	Lower Slope/Base-of-slope	Slope Channel Cplx	Channel-fill ?	Sandstone	x			
Marulk	6507/2-4	3336,17	MA2-4-15	Lange Fm	Cen-LowTur	Middle part	Lower Slope/Base-of-slope	Slope Channel Cplx	Channel-fill ?	Sandstone				
Marulk	6507/2-4	3336,5	MA2-4-16	Lange Fm	Cen-LowTur	Middle part	Lower Slope/Base-of-slope	Slope Channel Cplx	Channel-fill ?	Sandstone		x		
Marulk	6507/2-4	3340,5	MA2-4-17	Lange Fm	Cen-LowTur	Middle part	Lower Slope/Base-of-slope	Slope Channel Cplx	Channel-fill ?	Sandstone	x			
Marulk	6507/2-4	3340,6	MA2-4-18	Lange Fm	Cen-LowTur	Middle part	Lower Slope/Base-of-slope	Slope Channel Cplx	Channel-fill ?	Sandstone		x		
Marulk	6507/2-4	3343,03	MA2-4-19	Lange Fm	Cen-LowTur	Middle part	Lower Slope/Base-of-slope	Slope Channel Cplx	Channel-fill ?	Sandstone	x			
Marulk	6507/2-4	3343,03	MA2-4-20	Lange Fm	Cen-LowTur	Middle part	Lower Slope/Base-of-slope	Slope Channel Cplx	Channel-fill ?	Sandstone			x	
Marulk	6507/2-4	3343,2	MA2-4-21	Lange Fm	Cen-LowTur	Middle part	Lower Slope/Base-of-slope	Slope Channel Cplx	Channel-fill ?	Sandstone				

Table 3: Overview of all samples taken and at which interval. GDE=gross depositional environment. GC= geochemical, TS=thin section, Hf= hafnium.

Field	Well	Depth (m)	Sample	Formation	Megasequence	Part of unit	GDE	GrossArc	DepoElement	Lithology	GC	TS	U-Pb	Hf
Ærfugl	6507/3-9S	2851,52-59	ÆR3-9S-1	Lysing Fm	MidTur-LowCon	Upper part	Basinfloor/Slope terrace	Sandy fan	Channelized-lobe complexes	Sandstone	x			
Ærfugl	6507/3-9S	2851,52-59	ÆR3-9S-2	Lysing Fm	MidTur-LowCon	Upper part	Basinfloor/Slope terrace	Sandy fan	Channelized-lobe complexes	Sandstone			x	x
Ærfugl	6507/3-9S	2851,52-59	ÆR3-9S-3	Lysing Fm	MidTur-LowCon	Upper part	Basinfloor/Slope terrace	Sandy fan	Channelized-lobe complexes	Sandstone		x		
Ærfugl	6507/3-9S	2856,25-30	ÆR3-9S-4	Lysing Fm	MidTur-LowCon	Upper part	Basinfloor/Slope terrace	Sandy fan	Channelized-lobe complexes	Sandstone	x			
Ærfugl	6507/3-9S	2860,54-60	ÆR3-9S-5	Lysing Fm	MidTur-LowCon	Upper part	Basinfloor/Slope terrace	Sandy fan	Channelized-lobe complexes	Sandstone	x			
Ærfugl	6507/3-9S	2860,54-60	ÆR3-9S-6	Lysing Fm	MidTur-LowCon	Upper part	Basinfloor/Slope terrace	Sandy fan	Channelized-lobe complexes	Sandstone		x		
Ærfugl	6507/3-9S	2871,46-54	ÆR3-9S-7	Lysing Fm	MidTur-LowCon	Upper part	Basinfloor/Slope terrace	Sandy fan	Channelized-lobe complexes	Sandstone	x			
Ærfugl	6507/3-9S	2871,46-54	ÆR3-9S-8	Lysing Fm	MidTur-LowCon	Upper part	Basinfloor/Slope terrace	Sandy fan	Channelized-lobe complexes	Sandstone				
Ærfugl	6507/3-9S	2871,46-54	ÆR3-9S-9	Lysing Fm	MidTur-LowCon	Upper part	Basinfloor/Slope terrace	Sandy fan	Channelized-lobe complexes	Sandstone		x		
Ærfugl	6507/3-9S	2874,68-75	ÆR3-9S-10	Lysing Fm	MidTur-LowCon	Upper part	Basinfloor/Slope terrace	Sandy fan	Channelized-lobe complexes	Sandstone	x			
Ærfugl	6507/3-9S	2874,68-75	ÆR3-9S-11	Lysing Fm	MidTur-LowCon	Upper part	Basinfloor/Slope terrace	Sandy fan	Channelized-lobe complexes	Sandstone				
Ærfugl	6507/3-9S	2874,68-75	ÆR3-9S-12	Lysing Fm	MidTur-LowCon	Upper part	Basinfloor/Slope terrace	Sandy fan	Channelized-lobe complexes	Sandstone		x		
Ærfugl	6507/3-9S	2878,66-72	ÆR3-9S-13	Lysing Fm	MidTur-LowCon	Upper part	Basinfloor/Slope terrace	Sandy fan	Channelized-lobe complexes	Sandstone	x			
Ærfugl	6507/3-9S	2878,66-72	ÆR3-9S-14	Lysing Fm	MidTur-LowCon	Upper part	Basinfloor/Slope terrace	Sandy fan	Channelized-lobe complexes	Sandstone			x	x
Ærfugl	6507/3-9S	2878,66-72	ÆR3-9S-15	Lysing Fm	MidTur-LowCon	Upper part	Basinfloor/Slope terrace	Sandy fan	Channelized-lobe complexes	Sandstone		x		
Ærfugl	6507/3-9S	2879,83-90	ÆR3-9S-16	Lysing Fm	MidTur-LowCon	Upper part	Basinfloor/Slope terrace	Sandy fan	Channelized-lobe complexes	Sandstone	x			
Ærfugl	6507/3-9S	2879,83-90	ÆR3-9S-17	Lysing Fm	MidTur-LowCon	Upper part	Basinfloor/Slope terrace	Sandy fan	Channelized-lobe complexes	Sandstone			x	
Ærfugl	6507/3-9S	2879,83-90	ÆR3-9S-18	Lysing Fm	MidTur-LowCon	Upper part	Basinfloor/Slope terrace	Sandy fan	Channelized-lobe complexes	Sandstone		x		
Ærfugl	6507/3-9S	2883,83-90	ÆR3-9S-19	Lysing Fm	MidTur-LowCon	Upper part	Basinfloor/Slope terrace	Sandy fan	Channelized-lobe complexes	Sandstone	x			
Ærfugl	6507/3-9S	2883,83-90	ÆR3-9S-20	Lysing Fm	MidTur-LowCon	Upper part	Basinfloor/Slope terrace	Sandy fan	Channelized-lobe complexes	Sandstone				
Ærfugl	6507/3-9S	2883,83-90	ÆR3-9S-21	Lysing Fm	MidTur-LowCon	Upper part	Basinfloor/Slope terrace	Sandy fan	Channelized-lobe complexes	Sandstone		x		
Ærfugl	6507/3-9S	2885,34-41	ÆR3-9S-22	Lysing Fm	MidTur-LowCon	Upper part	Basinfloor/Slope terrace	Sandy fan	Channelized-lobe complexes	Silt/shale	x			
Ærfugl	6507/3-9S	2894,75-80	ÆR3-9S-23	Lysing Fm	MidTur-LowCon	Upper part	Basinfloor/Slope terrace	Sandy fan	Channelized-lobe complexes	Silt/shale	x			
Alve	6607/12-2S	2994	AL2S-1	Lange Fm	Cen-LowTur	Upper part	Lower Slope/Base-of-slope	Slope Channel Cplx	Channel-fill	Sandstone	x			
Alve	6607/12-2S	3094	AL2S-3	Lange Fm	Cen-LowTur	Upper part	Lower Slope/Base-of-slope	Slope Channel Cplx	Channel-fill	Sandstone	x			

4.3 Petrography

Twenty-seven thin sections with blue epoxy were made for the petrographic study of the sandstone samples (Appendix 1). For quantitative petrographic analysis, a minimum of 350 framework grains, in addition to intergranular components (porosity, matrix, and cement), were counted per thin section. The standard method of Ingersoll et al. (1984) was used to determine the mineralogical composition and framework mode, with a grid spacing of 1x1 mm. Minerals that are >63 µm within lithoclasts are counted as the type of lithoclast in which they occur (Von Eynatten and Gaup, 1999; Von Eynatten, 2003). Classification of sorting, roundness, sphericity, and grain-grain contacts are based on Pettijohn et al. (1973), Longiaru (1987) and Tucker (1988). The porosity loss due to compaction and cementation is based on Ehrenberg (1989):

$$COPL = OP - \frac{(100*IGV)-(OP*IGV)}{100-IGV} \qquad CEPL = (OP - COPL) * \frac{CEM}{IGV}$$

where COPL = porosity loss due to compaction, CEPL = porosity loss due to cementation, OP = original porosity, CEM = total volume of cement and IGV = intergranular volume.

The original porosity is assumed to 40 %, and the intergranular volume is the intergranular porosity, matrix and cement. The preconditions (e.g., original porosity value) should be used with caution as the composition and size of various sandstone types can affect the result (Ehrenberg, 1989).

Two independent studies of porosity detection within the Lysing Formation and Lange Formation samples on the Dønna Terrace were performed. Four individual samples ÆR5-8-3,5,7 and ÆR3-9S-18, within the Lysing Formation were used to compare results. In this thesis, the method has been the traditional point-counting method, separating cement, matrix, and porosity from the intergranular volume. The other method is from a bachelor study by Worum and Pedersen (2019), where they used a Matlab script in combination with a flatbed and slide scanner to single out the blue epoxy color within the pores of the thin sections. The method is supposed to make the estimation objective, cheaper and faster. From the results obtained by both parties, the intergranular volume from this study can be compared to the total porosity values obtained from the bachelor study.

4.4 Geochemical analysis

For the whole-rock geochemical analysis, 46 samples (including six of shales in ÆR3-9S-22,23, MA2-2-7,13 and SK5-A-10,11 and two from sand injectites in sample SK5-A-12,13; (See Table 4 and Appendix 2 for full coverage) were milled with the Retch Vibratory Disc Mill using an agate of 100 ml at the University of Stavanger. Subsequently, a whole-rock analysis was performed with Inductively Coupled Plasma Mass Spectrometry for refractory and rare earth elements, and Inductive Coupled Plasma Emission Spectrometer for the major and minor elements at the Acme laboratory (Vancouver, Canada; see ACME`s website http://acmelab.com for a detailed description of the analytical method and processing).

Table 4: Overview of dataset compiled during this study. (Dig.log=digitalized logs, Cen=Cenomanian, Tur=Turonian, Con=Coniacian, GDE=Gross depositional environment, GC=geochemical, TS=thin section, U-Pb=Uranium-lead, Hf=Hafnium and Fa=Facies association.

Field	Well	Dig. log (m)	Sample lab.	Megasequence	Formation	GDE	GC	TS	U-Pb	Hf	Fa
Dvalin	6507/7-1	9	DE1-X	Cen-LowTur	Lange Fm	Lower Slope/Base-of-slope	6	4	2		Yes
Ærfugl	6507/5-8	30	ÆR5-8-X	MidTur-LowCon	Lysing Fm	Basinfloor/Slope terrace	6	6	2	1	Yes
Skarv	6507/5-A-4H	45	SK5-A-X	Cen-LowTur	Lange Fm	Marginal-marine (Shelf-edge)	7	3	2		Yes
Marulk	6507/2-2	17	MA2-2-X	MidTur-LowCon	Lysing Fm	Basinfloor/Slope terrace	3	2	3	2	Yes
Marulk	6507/2-2	48	MA2-2-X	Cen-LowTur	Lange Fm	Lower Slope/Base-of-slope	4	3	1	1	Yes
Marulk	6507/2-4	13	MA2-4-X	MidTur-LowCon	Lysing Fm	Basinfloor/Slope terrace	5	4	1	1	Yes
Marulk	6507/2-4	12	MA2-4-X	Cen-LowTur	Lange Fm	Lower Slope/Base-of-slope	3	2	1		Yes
Ærfugl	6507/3-9S	50	ÆR3-9S-X	MidTur-LowCon	Lysing Fm	Basinfloor/Slope terrace	10	7	3	2	Yes
Alve	6607/12-2S	0	AL2S-X	Cen-LowTur	Lange Fm	Lower Slope/Base-of-slope	2				No

The Chemical Index of Alteration (CIA) is calculated by the major elements Al_2O_3, CaO, Na_2O_3, and K_2O. The calculation is based on the work by Fedo et al. (1995) and is shown in the equation below. The constituent of carbonate or apatite in the CaO was not accounted for in the CIA calculation, and this may result in an overestimating of the resulting CIA. Apart from a few samples, the values of CaO were relatively low, and the resulting error will only be minor.

$$CIA^{*} = Al_2O_3 / (Al_2O_3 + CaO + Na_2O_3 + K_2O) * 100$$

In order to understand the stratigraphic variability between the Cenomanian to Turonian-Coniacian Lange-Lysing samples, studies on eight trace element ratios with a logarithmic scale versus depth (m) were conducted. Samples that have the same concentration, or with a minute discrepancy within each trace element ratio, are considered to obtain the same provenance signature. Where they appear the same with a frequency of >5 times, they are of the same source.

4.5 Zircon sample preparation

Eleven zircon samples ranging from 57.5 to 185 g (Table 5 and Appendix 3 and 4 for full coverage) were selected. They were sampled concerning the grain size remaining medium sand for each sample. The consistent medium grain size was done to avoid heterogeneity and to preserve the validity of the produced results within each sample location. Zircon grains were separated using a standard technique at the University of Stavanger, starting with crushing the rock, in this case with a hammer and a mortar, to sufficiently separate all the grains. Then the grains were sieved to a fraction of 25-500 µm and subsequently, a heavy mineral separation was performed with sodium polytungstate liquid with a density of 2.95g/cm^3. The heavy mineral fraction was separated through a Frantz magnetic barrier laboratory separator (Model LB-1). A third separation by diiodinemethane liquid at 3.3 g/cm^3, was performed. At the Department of Geosciences, the University of Oslo, approximately 200 zircons per sample were picked and mounted on 1- inch epoxy mounts, finalizing it with a fine polish to reveal the center of the zircon grains. At the University of Stavanger, detailed imaging using a Zeiss Supra 35VP field emission gun scanning electron microscope, by cathodoluminescence and backscattered electrons, was performed on each zircon. The cathodoluminescence and backscatter images enabled a detailed study of the morphology and textures that each zircon produced.

Table 5: Samples and the number of analyzed zircons.

Sample	Analysed zircons
ÆR3-9S-2	108
ÆR3-9S-14	102
MA2-4-4	108
MA-2-4-20	109
MA2-2-4	97
MA2-2-8	110
MA2-2-16	109
SK5-A-2	21
SK5-A-8	23
ÆR5-8-9	109
DE1-2	106

4.6 U-Pb isotope analysis

At the Department of Geosciences in the University of Oslo, the U-Pb and Lu-Hf isotope analysis was performed using a Nu Plasma HR multi-collector ICP-MS equipped with a Cetac LSX-G2 and laser microprobe (with HelEx cell). A 40 µm beam diameter with a 10 Hz pulse was used during the U-Pb isotope analysis with a focused laser beam in aperture mode to produce circular ablation pits. For calibrating isotope fractionation, zircon standards GJ-01 (609±1 Ma; Belousova et al., 2006), 91500 (1065±1 Ma; Wiedenbeck et al., 1995) and A382 (concordia age=1876±2 Ma; Lauri et al., 2011) were run at the start and end of each analytical session, and GJ-01 and A382 at regular intervals (after each 15 ablations) during the session. The calculation and visualization of the concordia diagrams and relative probability density diagrams were performed using an in-house Microsoft Excel spreadsheet and with Isoplot, respectively. Zircon spots with elevated concentrations of lead that could not be corrected for common Pb or with discordance of more than 10 % from the $^{207}Pb/^{206}Pb$ and $^{206}Pb/^{238}U$ ratios

were not used for result presentation and interpretation. For a detailed description of the analytical method and processing, see Andersen et al. (2009) and Rosa et al. (2009) and references therein. The concordant data differs among the samples; however, an average of around 53 concordant zircons per sample have been used. The exception is in sample SK5-A-2 and SK5-A-8, which both have 11 concordant zircon each. The stratigraphic distance between them are seven meters, and in order to compile more compatible geochronology, they have been combined.

4.7 Lu-Hf isotope analysis

Ninety-seven zircons, divided on seven samples (ÆR3-9S-2,14, MA2-2-4,8,16, ÆR5-8-9, and MA2-4-4), which had concordant ages around the Caledonian (n=29) and the Gothian orogeny (n=68) were analyzed (Appendix 4). Hf isotope analysis was executed on the same spot as the U-Pb ablation had been performed. The same machine as for U-Pb dating (Nu Plasma HR multi-collector ICP-MS equipped with a Cetac LSX-G2 and laser microprobe (with HelEx cell)) was used for the Lu-Hf isotope analysis, but with a spot size of 50 µm and with a pulse frequency of 5 Hz. The program used for the isotope ratio calculations was the Nu Plasma time-resolved analysis software. An exponential law was used to correct for mass discrimination of the raw data. To control the quality of the data, the invariant ratio $^{178}Hf/^{177}Hf$ was monitored during the analytical sessions. Repeated analysis of the reference zircons Mud Tank (Woodhead and Hergt, 2005) and LV11 (Heinonen et al., 2010), gave $^{176}Hf/^{177}Hf$ = 0.282503±39 (2σ; n=117) and $^{176}Hf/^{177}Hf$ = 0.282835±63 (2 σ; n=128), respectively. $^{176}Hf/^{177}Hf$ is equivalent to ±2.2 ε_{Hf} - units and is accepted as a conservative estimate of the precision of the method. For a detailed description of the analytical method and processing, see Elburg et al. (2013) and references therein. All the constants used for calculation are listed in table 6 (Rudnick and Gao, 2003; Söderlund et al., 2004; Gerdes and Zeh, 2006; Bouvier et al., 2008; Chauvel et al., 2008).

Table 6: Constants, with their references, used for the calculation of model ages and epsilon values. From Gerdes & Zeh (2006) the ƐDM is equal to 0 at 4.07 Ga.

176Hf/177Hf (CHUR, today)	*0.282785*	(Bouvier et al. 2008)
176Lu/177Hf (CHUR, today)	*0.0336*	(Bouvier et al. 2008)
Decay constant	1.867E-11	(Söderlund et al. 2004)
176Lu/177Hf (crust, today)	0.0113	(Rudnick & Gao (2003)
176Hf/177Hf (DM, today)	0.283164	Chauvel et al. (2008)
176Lu/177Hf (DM, today)	0.0384	Gerdes & Zeh (2006)

5 Results

The results of the sedimentological core analysis is build up to describe the differences of the depositional processes and environment of the sandstones of the samples taken from the cores. It is critical for this study to investigate the differences within the facies of each sample to reveal variations of the recorded provenance signature. It is important to define any variabilities of the recorded signature between the facies before integrating the samples with other methods to reduce the uncertainty of the analythical data.

5.1 Sedimentological core analysis

5.1.1 Facies A: breccia

Description

Facies A is only represented in core 6507/3-9S, 6507/2-4 and 6507/2-2. The characteristics of facies A is that it consists of a thin 1 - 3 cm thick interval of matrix-supported breccia. It is composed of 3-6 mm large angular fragments of mudstone, glauconite, siderite and carbonate, surrounded by a coarse sand matrix. It occurs mainly as automictic, unsorted assemblages within ungraded beds. The base mainly is erosional with planar to uneven scouring structures (Figure 7).

Figure 7: Breccia (facies A) from core 6507/2-2 with 3 mm to 1 cm large angular grains (3290 m depth).

Interpretation

The angular clasts reflect textural immaturity, suggesting that the fragments are intraclasts or that they have an origin proximal to the depositional basin. The basal lag is interpreted as clast dropping out from the deposition of a turbidite flow (Fugelli and Olsen, 2007).

5.1.2 Facies B: massive sandstone

Description

Facies B is the most dominating facies in the Cenomanian to Turonian-Coniacian Lange-Lysing megasequences and is observed in all cores, except 6507/5-A-4H. It is represented by a thick bedded, coarse to medium sandstone. Facies B can be subdivided into subfacies B1, B2, and

B3. B1 is a massive sandstone that appears mostly structureless (Figure 8), however, faint dish structures with mm long pipes and weak planar lamination occur. Subfacies B1 ranges from 50 cm to 1.7 m in thickness. The facies may conform single beds, bedsets or amalgamated units, the latter with beds separated by indistinct to prominent amalgamation surfaces. Sedimentary structures such as water escape structure, dish structure, and planar lamination sandstone are represented in subfacies B2. Faint to clear dish structures, followed by vertical pipes up to 50 cm in size, are prominent fluid escape structures that are represented in subfacies B2. Along with planar lamination to planar bedding. Subfacies B3 is observed with rip-up mud clasts and plant fragment commonly without apparent organization; however, imbrication is identified.

Figure 8: Massive sandstone facies (facies B1) from core 6507/3-9S (2876-2875 m depth).

Interpretation

Facies B is regarded as the Ta unit in the Bouma division (Bouma, 1962). The non-sedimentary structured subfacies (B1) suggests high energy and rapid deposition by a hyperconcentrated to a concentrated density flow. It is supported by the lack of debris found, which suggests a non-cohesive flow and is more grain – to – grain supported (Mulder and Alexander, 2001). Dewatering structures in B2 represents cyclic currents that compress the underlying strata, often indicated by amalgamated sandstone (Kneller and McCaffrey, 2003). The dish and pillar structures could also be triggered by an earthquake event (Roy and Banerjee, 2016). The changes from amalgamated sandstones to a planer base of mud clast suggest a representation of accompanying amalgamated surface. The scouring could be produced by a concentrated flow representing different facies, whereas the planar surface could indicate a surge flow to quasi-steady turbidity current (Mulder and Alexander, 2001). The non-graded, rip-up mud clast supported subfacies B3 represents a layer of high-density subcritical turbulent flow defined by Lowe (1982) as stage S2 or division Tc by Bouma (1962). The evidence of a sharp shift from coarse to medium sandstone layer, to a layer of banded sandstone could indicate deposition from a high density current. Plant fragments could point the source of the sediments to originate from a vegetated environment, perhaps from a coastal plain (Henstra et al., 2016).

5.1.3 Facies C: graded and laminated sandstone

Description

Facies C has a range of grain sizes from fine to coarse sandstone. It is observed in all the cores, except core 6507/5-A-4H. It has an assortment of structures such as graded ripple cross-stratification to planar and quasi-planar lamination, and low to moderate angle cross-stratified sandstone (Figure 9). The facies is subdivided into facies C1 and C2. Medium to coarse-grained, 1 to 3 m ungraded, with rarely occurring planar to quasi-planar bedding and laminations is representative for subfacies C1. Interbedded mud laminations usually occur with a low abundance of bioturbation. The base of subfacies C1 is marked with coarse non-graded sandstone strata, and the occurrence of mud clasts in this layer is common. The coarse to very fine graded sandstone of (70 cm to 2 m thick) subfacies C2 is less common. The pronounced low angle and ripple cross-stratification are encountered upwards in the stratigraphy. 5 to 7 cm large clasts of lithic origin are observed, disturbing the surrounding structures. Sand injection and planar lamination are often observed in the upper section of subfacies C2, with a sharp contact at the top.

Figure 9: Graded and laminated sandstone facies (facies C). The picture is taken from core 6507/3-9S (2861-2862 m depth.

Interpretation

Bouma (1962) and Mutti (1992) have described the facies as Tb-c-d or F9a, respectively. The base of subfacies C1 is interpreted as a concentrated density flow. The undulating lamination in the upper interval is more indicative of interference from internal Helmholtz-waves (Baas et al., 2009). However, the lack of 2-3 cm large fragments or clasts in the upper layer does not support this theory, and quasi-steady turbidity current (Mulder and Alexander, 2001) is proposed for subfacies C1. The bioturbation with an index value of 1-2 is indicated as a break in the deposition in an oxygen-rich environment (Reineck, 1963; Taylor and Goldring, 1993; Bann and Fielding, 2004). The structures encountered in subfacies C2 is more indicative of a high density current switching between turbulent or Newtonian and laminar or non-Newtonian behavior (Baas et al., 2009). Another possibility is that the transport mechanism came from a transitional concentrated density flow (Mulder and Alexander, 2001), where a decrease in energy produced the planar laminations. The high

density current switches between turbulent or Newtonian and laminar or non-Newtonian behavior (Baas et al., 2009).

5.1.4 Facies D: heterolithics

Description

Facies D is represented by poorly sorted and disorganized mixture of sandy siltstones and silty sandstones. The siltstones comprise of poorly organized matrix rich intervals charachterized by a chaotic appearance defined by “floating” sand fragments of variably shape, geometries and dimensions. Sandstones appears as minute angular to rounded clasts, disrupted and distorted “clast-trains” and wisps of lamina/stratification to semirounded to rounded sand-balls and fragments of massive to laminated appearance. The interval ranges from around 6 cm to 2 meters and is observed in all cores, with the thinnest interval located in 6507/5-A-4H. A dark grey color distinguishes them from overlying pelagic/hemipelagic mud. Facies D appears in two varieties: D1) non-structured with clasts varying in size, and D2) water escape/bioturbation, slump, sand injectites, and ripples (Figure 10). Commonly both subfacies are incorporated into one unit, however, in most cases, subfacies D2 is the transition between facies C or D and facies E. Subfacies D1 occurs mainly as 20 cm to 50 cm graded units with a sharp upper contact within a massive sandstone. The clasts are 0.5 to 7 cm in size, ordinarily un-organized and have deformed the surrounding beds syn to post-depositionally. The clasts have a carbonaceous or sideritic composition with a rounded, elongated shape, and the largest clast often defines the base of this subfacies. Structures such as convoluted beds (Figure 11), vertical sand dikes, and horizontal sand injectites are representative of subfacies D2. These units tend to be thicker than those of subfacies D1. They range in thickness between 50 cm and 3 meters. Their contacts are typically graded from sandstone to mudstone, although, sharp to scoured boundaries are seen within thinner units. Subfacies D2 tends to start with

Figure 10: Core 6507/3-9S. Heterolithics (facies D2) with sand injectites, mud clasts and water escape structures (2881-2882 m depth).

Figure 11: Convoluted bedding in heterolithics (facies D2) taken from core 6507/3-9S (2876-2877 m depth).

a sequence of dewatering/bioturbation structures of 20-50 cm below more defined convoluted beds. These significant beds are of various thickness between 5 cm to 20 cm and are composed of mud/silt and fine sand. They have distinct asymmetrical folding patterns, where the folded layers are thin and observable or thicker and partially ambiguous, no disruption is evident. Upwards, low angle cross stratifications to ripple cross stratifications are seen, were lenticular laminations of fine sands are evident.

Interpretation

The elongated carbonate and siderite clasts have most likely been deposited during a co-genetic flow, were the hybrid flow has slightly rotated the elongated clast in a frozen upright position (Mulder and Alexander, 2001). The hybrid flow is the reason why there are partially no visible structures in these units. The origin of the clasts could originate from an adjacent slope or, their carbonaceous composition could point towards a more shallow water source (Haughton et al., 2009). Their rounded shape indicates some distance traveled, or it supports more grain-to-grain contact during a hybrid flow (Haughton et al., 2009). Subfacies D2, on the other hand, show distinct deformation or folding structures of preserved bedding, which is more indicative of a cohesive flow (Haughton et al., 2009). These debris flows are often deposited on an underlying substrate, fully laden with water, which will then be injected upwards into unconsolidated sands, creating sand injected dikes and sills (Hiscott, 1979).

5.1.5 Facies E: hemipelagic and pelagic mudstone

Description

Facies E is observed occasionally in the Lysing megasequence in core 6507/2-4 and 6507/3-9S. The thickness of the hemipelagic to pelagic mudstone facies differs from a few cm thick interbedded mud drapes to several meters' thick layer. Most common structures are flaser, lenticular bedding, and flame structures; additionally, sand injectites are observed at the base or the top of this facies (Figure 12). Siderite and light grey (carbonaceous material) nodules in mudstone beds frequently occur within a thicker layer.

Figure 12: Hemipelagic mudstone (facies E) with sand injectites and siderite clasts (core 6507/3-9S at 2894-2895 m depth).

Interpretation

Facies E originates as suspended fall-out from the water column or surface plumes (Nichols, 2009). Flaser and lenticular laminations represent deposition by settling of sediments in the aftermath of a diluted turbidity current, and larger nodules indicate remobilization.

5.1.6 Facies F: massive sandstone with abundant bioturbation

Description

Facies F is only observed in core 6507/5-A-4H within the Lange Megasequence. It is dominated by poorly sorted sandstone beds, rich in matrix with dispersed clay matrix. The thickness of the beds varies from 90 cm up to 6 m with an erosional contact at the top. The facies is dominated by an admixture of low-angle cross-laminated sandstones, ripple cross-laminated sandstones, cross-stratified sandstones and herringbone cross stratification (Figure 13, Figure 14 and Figure 15). Cross stratified varieties are dominated by large scale (0.5 to more than 2 cm in height) sigmoidal, tangential to angular cross-strata. Compound cross-stratification is present locally, with ripple cross-laminations formed on the inclined (downcurrent descending) cross-strata of larger scale bedforms. Cross-stratification and lamination is normally defined by claystone drapes or clast-trains of minute claystone fragments and chips. Double mud-drapes are common in all facies varieties. Sporadic bioturbation on foresets and topsets with vertical, lateral and u-shaped burrows (Figure 13-15) represents the more blocky and coarser sandstone. Draped low-high angle cross-stratification and ripple cross stratification (Figure 13) boundaries are partly indistinct. A paucity in the bioturbation is observed within high angle cross-stratification, and herringbone cross stratification where rounded to angular clasts or burrows are observed. The burrow infill consists of coarse sands, interbedded with mud drapes.

Figure 13: Facies F. Mottled, mud draped low angle cross stratification, with burrows of Cylindrichnus and Planolites with rhythmically infill patterns. Core 6507/5-A-4H (2973-2974 m depth).

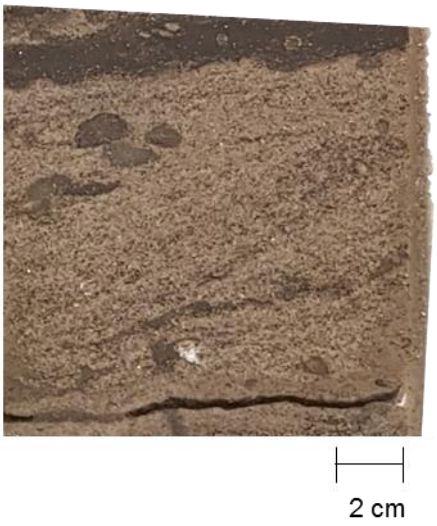

Figure 14: Facies F. Burrows of Planolites on bottomsets and topsets in core 6507/5-A-4H (2970-2971 m depth).

Interpretation

The low angle and ripple cross stratifications and herringbone cross stratification with abundant mud drapes, and especially double mud drapes represent deposition within a tidally influenced environment with currents periodically changing direction (Nichols, 2009). Storm events are evident by the paucity of bioturbation within high angle cross-stratification, which are more common in the middle to upper shoreface setting (Pemberton et al., 1992; Raychaudhuri and Pemberton, 1992). The diminutive and sporadic bioturbation and burrows within this facies, suggests migrating beds from sandstone to a more short accumulation of mud drapes, where animal colonization is limited (Howard, 1975; MacEachern and Pemberton, 1992). According to Gingras and MacEachern (2012), the vertical biogenic structure is indicative of burrowing by *Skolithos*, *Planolites*, and *Cylindrichnus* (Figure 13-15). The burrow infill pattern, mainly observed within the burrows of the *Planolites*, demonstrates rhythmically infill patterns like that of tidal processes (Figure 13), termed "tubular tidalites" by Gingras et al. (2007).

Figure 15: Facies F. Mottled structure in mud drapes. Burrows by Skolithos and Cylindrichnus in core 6507/5-A-4H (2963-2964 m depth).

5.1.7 Facies association

The lithofacies were assembled into seven major facies associations, with its representative subenvironment (Table 7; Figure 16). The associated central lobe (FA3) is interpreted within the Cenomanian to lower Turonian Lange sandstones (6507/7-1; upper part), middle Turonian-lower Coniacian upper unit of Lysing in 6507/5-8 and 6507/3-9S and 6507/2-4. The facies associated channel fill (FA1) are subordinate, however, located within middle Turonian-lower Coniacian upper unit of Lysing in 6507/5-8 and upper part of the Cenomanian to lower Coniacian Lange (6507/2-2). The peripheral to marginal lobe (FA4) is interpreted within the upper part of middle Turonian to lower Cenomanian Lysing (6507/2-2, 6507/5-8, and 6507/3-9S) and middle part of Cenomanian to lower Turonian Lange (6507/2-2 and 6507/2-4). Less

present in the channel to lobe transition (FA2), which is identified within the middle Turonian to lower Cenomanian Lysing (6507/5-8). Fan (lobe) fringe (FA5) is only established within the middle part and upper part of Cenomanian to lower Turonian Lange in 6507/2-4 and 6507/2-2 respectively, whereas the basinplain (FA6) is identified within all the megasequences. The tidal bars (FA7) are only recognized in the upper part of the Cenomanian to lower Turonian Lange (6507/5-A-4H; Figure 16).

Facies Association 1

Description

The association is composed of facies A, B3, C1, C2 and D2 arranged in fining upward motifs up to 5 meters thick. The association is present as simple and single fining upward motif commonly with a basal erosive boundary and with the lower motifs normally top truncated, i.e. with incomplete facies sequence. The facies association is commonly encased in mudstones of Facies Association FA6. The facies association is normally overlain by disorganized and slumped mudstones of Facies Association 6 which in such cases forms the transition between the two association.

Interpretation

Facies Association 1 is interpreted to represent slope to inner basin-floor fan channel-fills. The channels formed on lower part of the slope to basinfloor based on contact or interfingering relationship with associated facies association (GDE interpretation provided by Aker Bp). A channel-fill origin is inferred by the overall fining upward motif, the erosive base to the motifs, and the coarse fill of the basal part of the motifs in combination with the favored gravity flow origin of the channel-fill sandstones (Pickering et al., 1989). A gravity-flow origin is furthermore supported by and consistent with the overall slope to basinfloor setting (Pickering et al., 1989).

Single fining upward motifs are here inferred to represent a single channel-fill motif, i.e. it represents a single or solitary channel storey (Pickering et al., 1989). Interbedding and capping by the slumped slope mudstones of Facies Association 6 may have formed as a result of upslope and / or channel wall instability (see interpretation of Facies Association 6 below) and would favour an overall slope to base-to-slope setting.

Facies Association 2

Description

The association is composed of facies B2 and D2 arranged in fining upward motifs up to 13 meters thick. The association is present as a series of vertically stacked fining upward motif. Up to 5 fining upward motifs are present commonly with a non-erosive basal boundary and with the motifs normally top truncated, i.e. with incomplete facies sequence. The vertically stacked fining upward motifs occur with an incomplete motif with a basal erosive contact to individual fining upward sequences. The facies association stratigraphically overlie with an erosive contact to sandstones of Facies Association 3 which in such cases forms the transition between the two associations.

Interpretation

Facies Association 2 is interpreted to represent braided mid-fan to channel to lobe transition in proximal fan. The braided mid-fan formed on lower part of the slope to basinfloor based on contact or interfingering relationship with associated facies association (GDE interpretation provided by Aker Bp). A braided mid-fan origin is inferred by the overall vertically stacked fining upward motif, the non-erosive base to the motifs with the favored gravity flow origin of the braided mid-fan sandstones (Pickering et al., 1989). A gravity-flow origin is furthermore supported by and consistent with the overall slope to basinfloor setting (Pickering et al., 1989).

Vertically stacked fining upward motifs are here referred to represent a channel complex with the favoured overall sedimentary architecture. The incomplete fining upward motifs points to erosive basal contacts to individual channel fills and an gross architecture dominated by multistorey or multilateral-to-multistorey channel complexes (Pickering et al., 1989).

Facies Association 3

Description

The association is composed of facies B1, B2, B3, C1, C2, D1, D2 and E arranged in fining upward motifs up to 18 meters thick. The association is present as simple and single fining upward motifs or as a series of vertically stacked motifs. In the latter case, up to 6 motifs may be present commonly with a basal erosive boundary and with the lower motifs normally top truncated, i.e. with incomplete facies sequence. The facies association is commonly encased in mudstones of Facies Association FA6. The facies association is normally overlain by disorganized and slumped mudstones of Facies Association 6 which in such cases forms the

transition between the two associations. In other situations, the association appear to interfinger with or stratigraphically overlie with an erosive contact to sandstones of Facies Association 2.

Interpretation

Facies Association 3 is interpreted to represent mid-fan channels. The channels formed on the basinfloor to lower slope based on the contact or interfingering relationship with associated facies association (GDE interpretation provided by Aker BP). A mid-fan channel origin is inferred by the overall fining upward motifs, the erosive base to the motifs and the combination with the favoured gravity flow origin of the mid-fan channel sandstones. A gravity-flow origin is furthermore supported by and consistent with the overall lower slope to basinfloor setting (Pickering et al., 1989).

Single fining upward motifs are here inferred to represent a single channel-fill motif, i.e. it represents a single or solitary channel storey. In cases where there are vertically stacked motifs, a channel complex is the favoured overall sedimentary architecture. In such cases, incomplete fining upward motifs points to erosive basal contacts to individual channels and an gross architecture dominated by multistorey or multilateral-to-multistorey channel complexes (Pickering et al., 1989).

Interbedding and capping by slumped slope mudstones of Facies Association 6 may have formed as a result of upslope and / or channel wall instability (see interpretation of Facies Association 6 below) and would favour an overall lower slope to basinfloor setting (Pickering et al., 1989).

Facies Association 4

Description

The association is composed of facies B1, B2, B3, C1, C2, D1, D2 and E arranged in fining upward motifs up to 11 meters thick. The association is present as simple and single fining upward motif commonly with a basal erosive boundary and with the lower motifs normally top truncated, i.e. with incomplete facies sequence. The facies association is commonly encased in mudstones of Facies Association FA6. The facies association is normally overlain by disorganized and slumped mudstones of Facies Association 6 which in such cases forms the transition between the two association. In other situations, the association appear to interfinger with the sandstones of Facies Association 2.

Interpretation

Facies Association 4 is interpreted to represent scoured terminal lobes and splays. The lobes and splays formed on the basinfloor to lower slope based on the contact or interfingering relationship with associated facies association (GDE interpretation provided by Aker BP). A lobe and splay origin are inferred by the overall fining upward motifs, the erosive base to the motifs and the combination with the favoured gravity flow origin of the lobe and splay sandstones. A gravity-flow origin is furthermore supported by and consistent with the overall lower slope to basinfloor setting (Pickering et al., 1989).

Single fining upward motifs are here inferred to represent a single channel-fill motif, i.e. it represents a single or solitary channel storey (Pickering et al., 1989).

Interbedding and capping by slumped slope mudstones of Facies Association 6 may have formed as a result of upslope and / or channel wall instability (see interpretation of Facies Association 6 below) and would favour an overall lower slope to basinfloor setting (Pickering et al., 1989). Where Facies Association 4 occur in stratigraphic succession underlying mid-fan channel sandstones of Facies Association 3 a terminal lobe and splay origin is the preferred interpretation.

Facies Association 5

Description

The association is predominantly composed of facies C1, C2 and E arranged in fining upward motifs up to 10 meters thick. The association is present as thin single fining upward motif commonly with a basal erosive boundary. The facies association is commonly encased in mudstones of Facies Association FA6. The facies association is normally overlain by disorganized and slumped mudstones of Facies Association 6 which in such cases forms the transition between the two association.

Interpretation

Facies Association 5 is interpreted to represent gently scoured terminal sheets. The terminal sheets formed on the basinfloor to lower slope is based on the contact associated facies association (GDE interpretation provided by Aker BP). A terminal sheets origin is inferred by the overall fining upward motifs, the erosive base to the motifs and the combination with the favoured gravity flow origin of the terminal sheet sandstones. A gravity-flow origin is

furthermore supported by and consistent with the overall lower and upper slope to basinfloor setting (Pickering et al., 1989).

Single fining upward motifs are here inferred to represent a single channel-fill motif, i.e. it represents a single or solitary channel storey (Pickering et al., 1989).

Interbedding and capping by slumped slope mudstones of Facies Association 6 may have formed as a result of upslope and / or channel wall instability (see interpretation of Facies Association 6 below) and would favour an overall lower and upper slope to basinfloor setting (Pickering et al., 1989). Where Facies Association 5 occur in stratigraphic succession underlying gently scoured terminal lobes and splay sandstones of Facies Association 4 a gently scoured terminal sheet origin is the preferred interpretation.

Facies Association 6

Description

The association is composed of facies E with no visible grading essentially unbedded up to 18 meters thick sections. The association is present with a basal erosive boundary and with the upper motif normally top truncated, i.e. with incomplete facies sequence. It also contains slump structures. The facies association is normally underlying massive sandstones of all Facies Association which in such cases forms the sharp transition between them.

Interpretation

Facies Association 6 is interpreted to represent mudstone sheets. The mudstone sheets formed on the basinfloor to lower and upper slope is based on the contact associated facies association (GDE interpretation provided by Aker BP). A mudstone sheet origin is inferred by the overall non graded unbedded thick section, the erosive base to the motifs and the combination with the favoured gravity flow origin of the mudstone sheet. A gravity-flow origin is furthermore supported by and consistent with the overall lower and upper slope to basinfloor setting (Pickering et al., 1989). The slump structures could indicate remobilization of the basinfloor or channel wall instability (Nichols, 2009).

Facies Association 7

Description

The association is composed of facies F arranged in coarsening upward motifs up to 20 meters thick. The association is present as simple and single coarsening upward motif commonly with

a complete facies sequence in the basal boundary and normally top truncated, i.e. with incomplete facies sequence. The facies association is commonly encased in mudstones of Facies Association FA6. The facies association is normally overlain by mudstones sheets of Facies Association 6 which in such cases forms the transition between the two association.

Interpretation

Facies Association 7 is interpreted to represent tide dominated delta front. The tidal bars formed on the marginal marine is based on the contact associated facies association (GDE interpretation provided by Aker BP). A tide dominated delta front origin is inferred by the overall coarsening upward motifs, the complete facies sequence at the base to the motifs and the combination with the favoured suspended-sediment load origin of the tidal bar sandstones (Dalrymple and Choi, 2007). A suspended-sediment load origin is furthermore supported by and consistent with the overall marginal-marine setting (Dalrymple and Choi, 2007).

5.1.8 Gross depositional environment

The gross depositional environment data was given by Aker BP. The lower slope or base-of-slope are interpreted within the Cenomanian to lower Turonian Lange (6507/7-1) upper (6507/2-2) and middle part (6507/2-2 and 6507/2-4) and within the upper part of 6607/12-2S. Basinfloor or slope terrace are indicated within the upper part of middle Turonian to lower Coniacian Lysing Formation (6507/5-8, 6507/3-9S, 6507/2-2, and 6507/2-4). Marginal-marine (shelf-edge) and the upper slope are only established within the upper part of Cenomanian to lower Turonian Lange Formation in 6507/5-A-4H (Figure 16). Figure 17 gives a visualization of the megasequences divided into sequence stratigraphic units, combined with the interpreted facies, facies association and gross depositional environment (Figure 16).

Table 7: Facies association with its subenvironment.

Facies associations	Facies description	Subenvironment
FA1: Channel fills, margin and belts	The dominant facies are breccia (FA), rip-up mud clast massive sandstone (FB3), Planar, cross- and ripple stratification (FC1,2) and often occuring slide or slump facies FD2. These are often thick stacked beds commonly amalgamated with an erosive base.	Lower slope to inner basinfloor channelized fan
FA2: Channel to lobe transition-Proximal lobe	Facies (FA) is less observed and replaced by an erosive or amalgamated sandstone surface (B2). Heterolithics of slide or slump structures (FD2) are less occuring.	Braided mid-fan, channelized lobes in proximal fan
FA3: Central lobe	Dominant facies are massive sandstone (FB), planar laminated to cross stratification (FC 1,2), interbedded with hemipelagic mudstones (FE). Symmetrical thickening and thinning upward motifs. Subordinate slide or slump structured heterolithics (FD 1,2).	Mid-fan channels
FA4: Peripheral to marginal lobe	Primary facies are massive sandstone (FB1,2), ripple cross laminated and cross stratified sandstone (FC1,2), debrite, slump or slide of heterolithics (D1,2) and interbedding of mudstones (FE).	Channelized/scoured terminal lobes and splays
FA5: Distal lobe, fan fringe	This is dominated by cross stratification and planar laminations (FC). Frequency of interbedded mudstone has increased (FE).	Gently scoured terminal sheets
FA6: Basinplain/ Floodplain	Silt and fine sand laminations mm to cm thick, sand injectites occur. Predominantly mudstone (FE).	Mudstone sheets from slope to basinfloor
FA7: Tidal bars	Thickening upwards succession, with burrows by "tubular tidalites". Tough cross bedding, rhytmic bedding and mud draping on ripples.	Tide dominated delta front

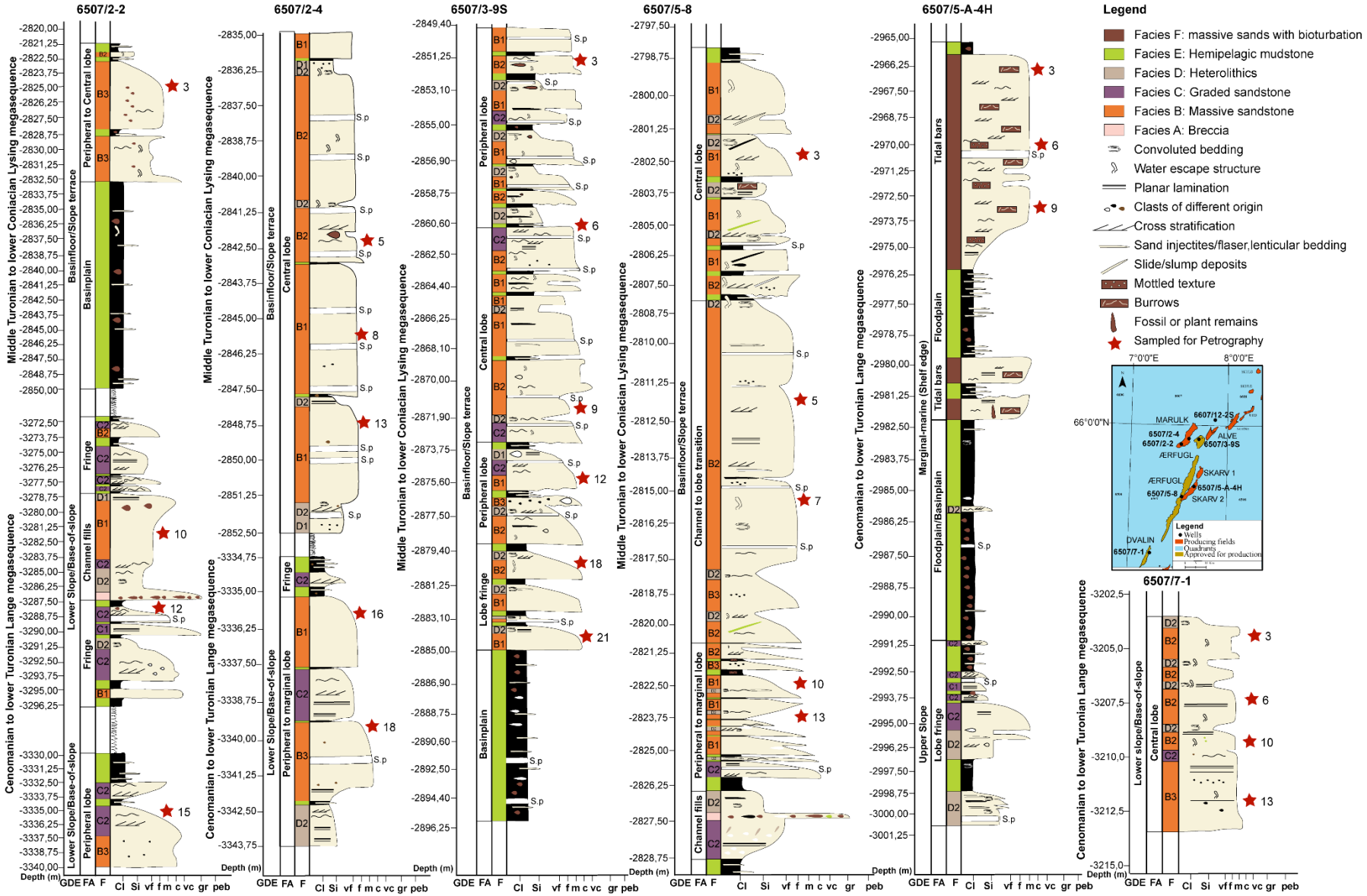

Figure 16: Interpreted core logs with facies association (FA) and gross depositional element (GDE). Red star indicates sampled for petrography. S.p=Seal peel.

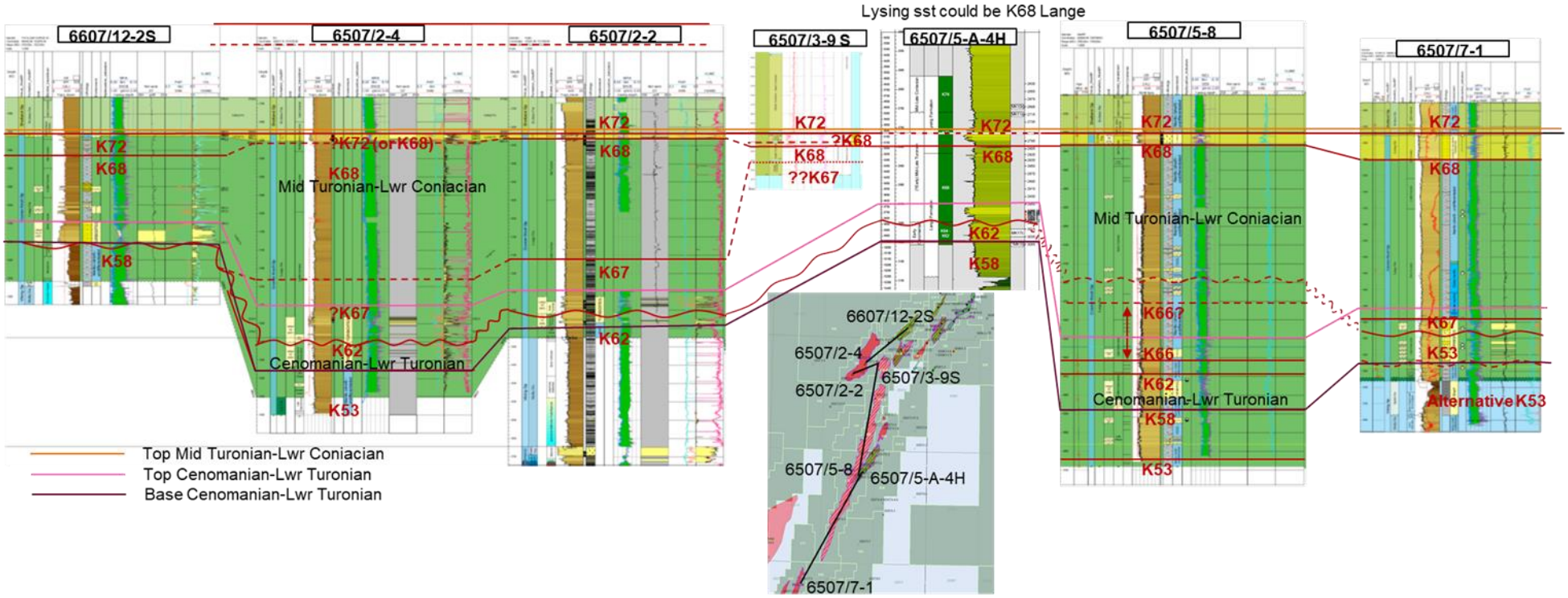

Figure 17: Well correlation of sequece stratigraphy units within the Cenomanian to Coniacian Lange-Lysing megasequence, covering all the wells within the scope of this study. Courtesy of Aker BP.

5.2 Petrographic composition

5.2.1 Granulometry

An overview of the granulometric data described in this sub-chapter, can be viewed in table 8 and figure 16 for sample location. The 27 analyzed thin sections are mostly composed of fine to medium sandstone; however, a finer input is observed in a basinfloor gross depositional environment in the Cenomanian (*Æ*R3-9S-21) to Coniacian (MA2-2-3) Lange-Lysing, with coarser sandstone in the lower slope (Cenomanian to lower Turonian Lange; DE1-3). The Cenomanian to lower Turonian Lange and middle Turonian to lower Coniacian lysing has an input of larger grains ranging from 480 µm to 8000 µm. The largest is a pelite clast consisting of micro quartz within the marginal-marine (SK5-A-6; Appendix 1). The sorting is mostly moderate to poor or moderate to good, however within the marginal-marine to the basinfloor (SK5-A-9, *Æ*R3-9S-6, and MA2-2-3) exhibit very good sorting. The Turonian to Coniacian Lysing megasequence from core 6507/3-9S, has overall good sorting, whereas rocks from the lower slope to the basinfloor (Lange megasequence; 6507/7-1 and Lysing megasequence; 6507/5-8), display moderately good to poor sorting. The grains are mainly subrounded to subangular but with exceptions in basinfloor of the Lysing megasequence (*Æ*R5-8-3 and *Æ*R3-9S-18; Figure 24.1-2) and the lower slope of the Lange megasequence (DE1-10), which is subangular. The dominant grain-to-grain contacts are sutured contact to concave-convex (Figure 24.1-2 and Figure 24.3-4). Point contact is represented within the Turonian to Coniacian Lysing megasequence (*Æ*R3-9S-3, MA2-4-8, MA2-4-13, *Æ*R5-8-5, and *Æ*R5-8-7). When observing the overall structure of each sample, little fabric is visible. However, visible alignment of muscovite and low to high sphericity grains are observed in sandstones within basinfloor (6507/2-4 upper unit) and lower slope (6507/2-4 middle unit and 6507/7-1; Figure 24.5-6), with weak to no alignments within the Turonian to Coniacian basinfloor (6507/5-8).

Table 8: Granulometric data over 27 thin section analyzed, covering the Lysing and Lange sandstones on the Dønna Terrace.

Sample	Depth (m)	Formation	Mean Grain size (µm)*	Max grain size (µm)*	Grain size Udden Wentworth	Sorting Longiaru 1987	Roundness Pettijohn et al., 1973	Sphericity Pettijohn et al., 1973	Grain-grain contact Tucker 1988	Fabric
ÆR3-9S-3	2851.55	Lysing	260 µm	2000 µm	Medium sand	Moderately good	Subrounded-Subangular	Low	Point contact to plane	no fabric
ÆR3-9S-6	2860.58	Lysing	280 µm	680 µm	Medium sand	Very good	Subrounded-Subangular	Low	Plane contact to sutured	no fabric
ÆR3-9S-9	2871.5	Lysing	250 µm	1000 µm	Medium sand	Very good to moderately good	Subrounded-Subangular	High	concave-convex	no fabric
ÆR3-9S-12	2874.72	Lysing	220 µm	800 µm	Fine to medium sand	Very good to moderately good	Subrounded-Subangular	High	concave-convex	no fabric
ÆR3-9S-18	2879.85	Lysing	280 µm	1200 µm	Medium sand	Moderately good	Subangular	Low	concave-convex	no fabric
ÆR3-9S-21	2885.35	Lysing	180 µm	600 µm	Fine sand	Very good to moderately good	Subrounded to subangular	High	concave-convex, sutured	no fabric
MA2-4-5	2842.46	Lysing	250 µm	1400 µm	Medium sand	Very good to moderately good	Subrounded-Subangular	High	Plane contact	aligned grains
MA2-4-8	2846.8	Lysing	400 µm	1600 µm	Medium sand	Moderate/poor	Subrounded-Subangular	High	Point contact	no fabric
MA2-4-13	2848.53	Lysing	280 µm	800 µm	Medium sand	Moderately good	Rounded to subrounded	High	Point to plane	aligned grains
MA2-4-16	3336.5	Lange	220 µm	600 µm	Fine to medium sand	Very good to moderately good	Rounded to subrounded	High	Plane contact	aligned grains
MA2-4-18	3340.5	Lange	280 µm	1000 µm	Medium sand	Moderately good	Subrounded-Subangular	High	concave-convex, sutured	no fabric
MA2-2-3	2824.3	Lysing	180 µm	480 µm	Fine sand	Very good	Subrounded	High	concave-convex	no fabric
MA2-2-10	3282.55	Lange	240 µm	720 µm	Fine to medium sand	Moderately good	Subrounded to subangular	Low	concave-convex, sutured	weak to no alignement
MA2-2-12	3288.1	Lange	300 µm	1000 µm	Medium sand	Moderately good	Subrounded-Subangular	Low	concave-convex	no fabric
MA2-2-15	3337.6	Lange	300 µm	1000 µm	Medium sand	Moderately good	Subangular-Angular	Low	concave-convex, sutured	aligned grains
SK5-A-3	2966.45	Lange	320 µm	1600 µm	Medium sand	Moderate/poor	Subrounded to angular	Low	concave-convex, sutured	no fabric
SK5-A-6	2970.51	Lange	400 µm	8000 µm	Medium sand	Moderately good	Subrounded-Subangular	Low	concave-convex	no fabric
SK5-A-9	2973.55	Lange	400 µm	1000 µm	Medium sand	Very good	Subrounded to subangular	High	Concave-convex to point	no fabric
ÆR5-8-3	2802.85	Lysing	240 µm	1800 µm	Fine to medium sand	Moderate/poor	Subangular	Low	point to concave-convex	no fabric
ÆR5-8-5	2811.66	Lysing	240 µm	1200 µm	Fine to medium sand	Moderate/poor	Rounded to subangular	Low	Point to plane	weak to no alignement
ÆR5-8-7	2815.43	Lysing	220 µm	1000 µm	Fine to medium sand	Moderately good	Subrounded-Subangular	High	Point to plane	no fabric
ÆR5-8-10	2821.85	Lysing	200 µm	780 µm	Fine to medium sand	Moderately good	Subrounded-Subangular	Low	Point contact to plane	aligned grains
ÆR5-8-13	2822.65	Lysing	320 µm	1400 µm	Medium sand	Moderate/poor	Rounded to subrounded	High	concave-convex, sutured	weak to no alignement
DE1-3	3504.32	Lange	600 µm	1200 µm	Coarse sand	Moderately good	Subrounded to angular	Low	concave-convex, sutured	no fabric
DE1-6	3507.57	Lange	300 µm	1000 µm	Medium sand	Moderate/poor	Subrounded to angular	Low	concave-convex, sutured	aligned grains
DE1-10	3509.1	Lange	320 µm	1000 µm	Medium sand	Moderately good	Subangular	High	Sutured contact	aligned grains
DE1-13	3512.7	Lange	500 µm	800 µm	Medium to Coarse sand	Moderately good	Subrounded-Subangular	Low	concave-convex, sutured	weak to no alignement

5.2.2 Framework grains

The major framework grains of the Cenomanian to lower Turonian Lange and the middle Turonian to lower Coniacian Lysing megasequences are of quartz, feldspar, and lithic fragments (Appendix 1). The average sum of quartz grains, including chert, is 90 % in the Lysing megasequence and 82 % in the Lange megasequence (Figure 18; QtFL diagram; Dickinson et al., 1983; Figure 19; QmFL diagram; Dickinson et al., 1983; Figure 20; sandstone classification diagram; Folk, 1980). The dominant quartz grains are monocrystalline and non-undulatory in the Lysing megasequence with 72 %, whereas the Lange megasequence has a lower average of 61 %. These quartz grains are often observed with inclusions of the accessory mineral's zircons, rutile and tourmaline. The lowest value is seen in the marginal-marine Lange megasequence (SK5-A-3) and the basinfloor of the Lysing megasequence (*Æ*R3-9S-21) with 37 %. From the quartz monocrystalline, undulatory grains there is a low difference of 3 % between the Lysing and the Lange megasequences. The sandstones from both formations show low content of polycrystalline quartz grains (Figure 24.7-8). Polycrystalline quartz with 2-3 crystals has an average value of 2.5 % and 2.7 % in the Lysing megasequence and the Lange megasequence sandstones respectively, with the highest value observed within the lower slope (MA2-4-18). The highest value of the polycrystalline mineral with >3 crystals is observed in the basinfloor (*Æ*R5-8-13), which is in the deepest depth within core 6507/5-8. The percentage of the polycrystalline mineral with >3 crystals decreases upwards to 5.8 % at the top. The same trend is observed in the basinfloor of the Lysing megasequence (6507/3-9S; Figure 21 quartz provenance diagrams of Basu et al., 1975 and Figure 22 source rock diagram by Tortosa et al., 1991). The content of chert is an accessory in most sandstones; however, a high value of 2.6 % is observed within the basinfloor of the Lysing megasequence (MA2-2-3).

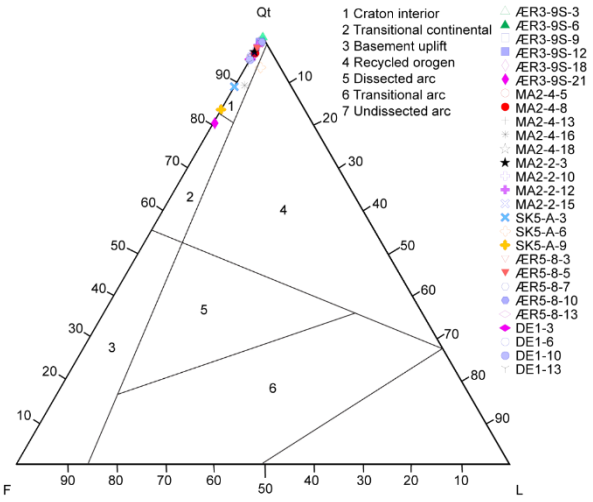

Figure 18: QtFL provenance diagram after Dickinson (1983). Qt=quartz monocrystalline, non-undulatory and undulatory, polycrystalline quartz and chert.

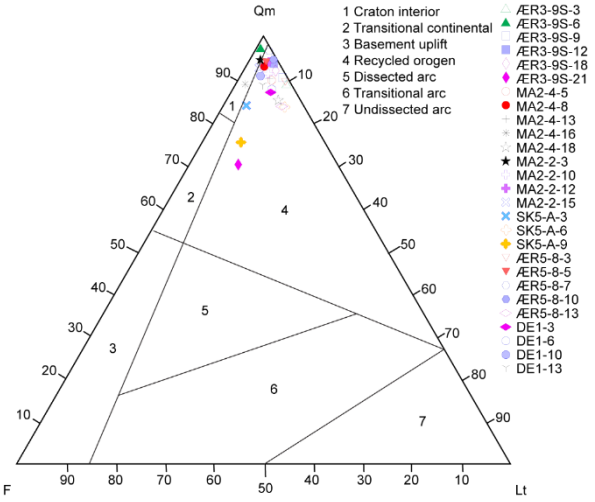

Figure 19: QmFL provenance diagram after Dickinson (1983). Qm=monocrystalline quartz and chert. Lt=lithic components and polycrystalline quartz.

The average sum of the feldspar grains in the Lange-Lysing megasequences are 3 % and 5.5 %, respectively. Alkali feldspar dominates with point-counting k-feldspar and microcline has the highest value within the basinfloor of the middle Turonian to lower Coniacian Lysing megasequence (ÆR3-9S-21). The average value of lithic fragments is below 0.5 % in both formations; the only lithic fragment observed was pelite. Bioclasts of former microfossils, are deformed and leached and have created secondary moldic porosity.

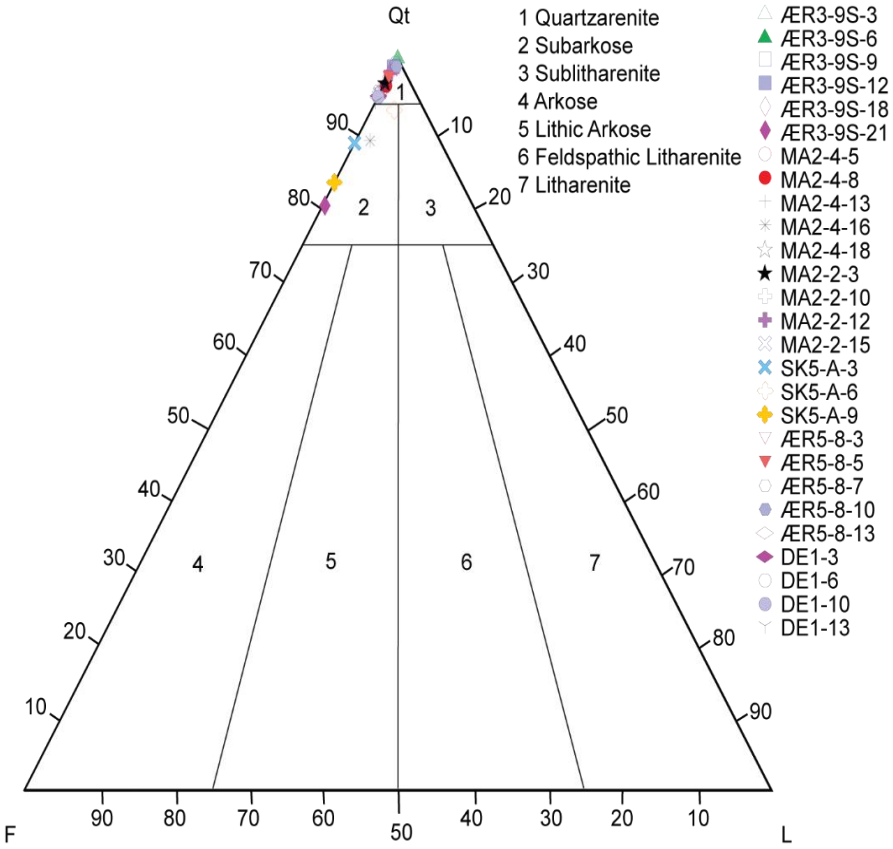

Figure 20: Sandstone classification scheme after Folk (1980).

The detrital minerals muscovite and biotite (mica group) dominant among other minerals. Muscovite, which is found within every sample, has an average concentration of 5 % within the Lysing megasequence and 8 % in the Lange megasequence. The highest concentration is found within the basinfloor of the middle Turonian to lower Coniacian Lysing megasequence (ÆR3-9S-21), with a value of 18 %. Additionally, the highest concentrations of muscovite are often observed within the deepest depth of each core and decreasing upwards. A common occurrence of the muscovite is in a bended shape between quartz grains (Figure 24.5-6). It is also aligned with the framework. The glauconite (Figure 24.3-4 and Figure 24.5-6) is sparse in most samples, however, within the marginal-marine (6507/5-A-4H) and basinfloor (6507/5-8) they exhibit relatively high values of 0.3 to 5 %, with the highest value in sample SK5-A-9.

Accessory minerals of the Lange-Lysing megasequences are spares. Angular zircons are observed within the basinfloor (ÆR3-9S-3 and ÆR5-8-10), lower slope (MA2-2-10), and marginal-marine (SK5-A-6) with a size ranging from 20 µm to 150 µm. Rounded garnets are present within the Lysing megasequence samples, with an average of 0.2 % with an average size of 30 µm.

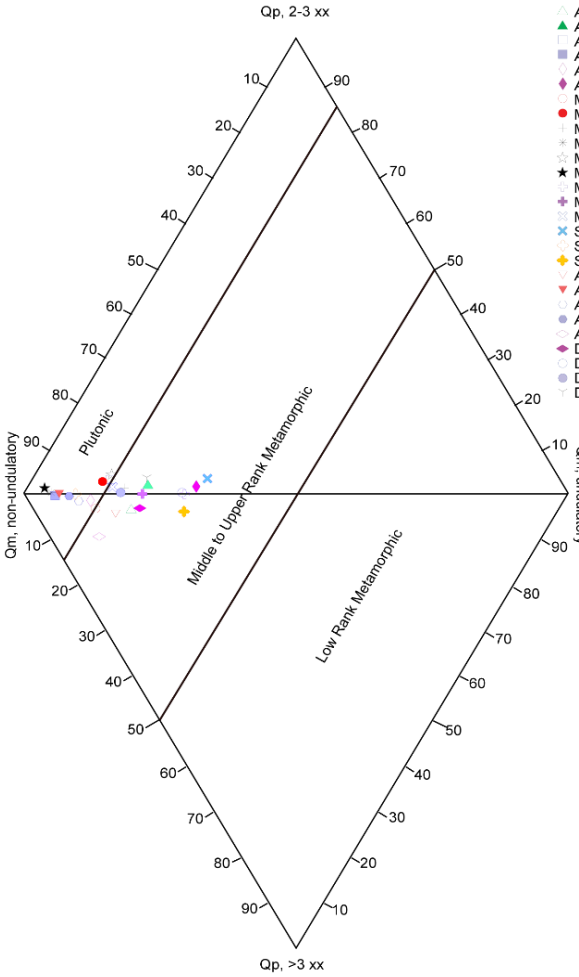

Figure 21: The quartz provenance scheme of Basu et al. (1975).

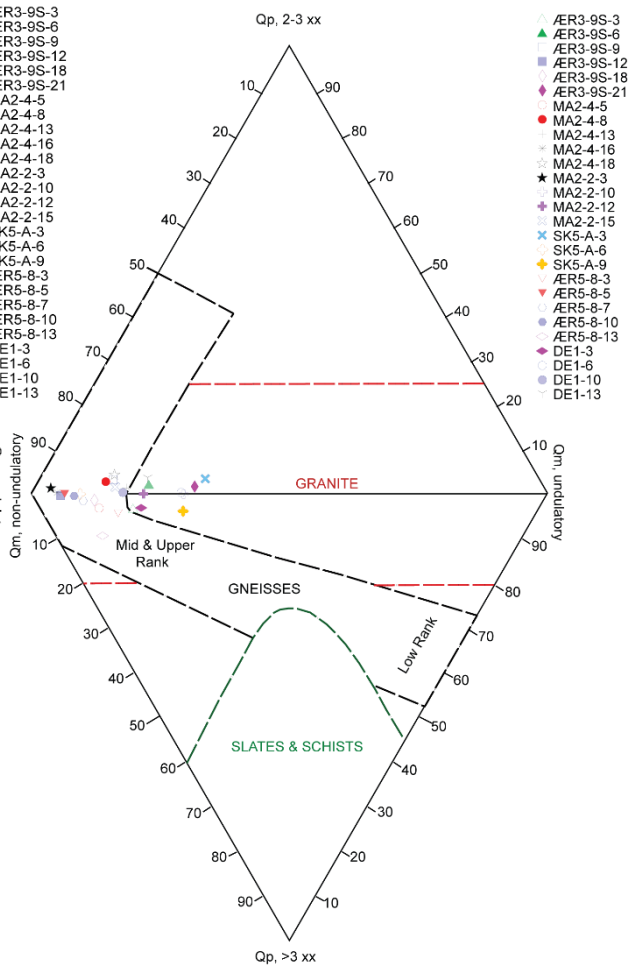

Figure 22: Types of source rocks are revealed by the diamond diagram of Tortosa et al. (1991).

5.2.3 Intergranular volume content and diagenesis

The major contributor to the intergranular volume content is porosity (total avg. 12 %) and cement (total avg. 11 %), with the content of matrix (total avg. 1 %) remaining a minor constituent (Appendix 1). The largest average sum of porosity (avg. 13 %) is seen within the Lysing megasequence sandstones; on the other hand, the highest individual value is observed within the marginal-marine (SK5-A-3). Primary intergranular porosity is the inordinate porosity (Figure 24.7-8), with moldic secondary intergranular porosity (Figure 24.3-4) being subordinate. Another intragranular porosity is most abundant within the basinfloor (ÆR3-9S-21; 8 %) and marginal-marine (SK5-A-3; 4 %) represented by honeycomb porosity of plagioclase (Figure 24.3-4), grain-rim porosity and the less abundant fracture porosity (Figure 24.3-4).

The most prominent cement minerals within the Lange-Lysing megasequence sandstones are calcite and kaolinite. The calcite cement is observed with a poikilotopic fabric within pores and is most abundant in the Cenomanian to lower Turonian Lange sandstones (3 %), with the

highest value of 12 % within the lower slope (MA2-4-16). The authigenic kaolinite is observed as booklets or with a botryoidal fabric within the blue epoxy filled pores (Figure 24.1-2). The constituent of kaolinite cement is most prominent in the deepest depth of each core; however, the basinfloor (*Æ*R5-8-3; 5 % and *Æ*R3-9S-3; 6 %) have its highest value in the shallowest depth within their respective cores. Chlorite cement occurs as fibrous fabric, surrounding quartz grains in the framework composition. Its abundance among the samples are minuscule; however, it is most common among the basinfloor of the middle Turonian to lower Coniacian Lysing megasequence (6507/3-9S and 6507/5-8). Overgrowth quartzite cement is sparse among the Lange samples, although it has one prominent sandstone in the marginal-marine (SK5-A-3), which has a significant amount of quartz cement (2 %). The average concentration among the Lysing sandstones is 0.3 %. Pyrite and iron-oxide cement are quite similar, albeit, a brown hue visible within the iron-oxides, separates it from the prominent dark color of the pyrite cement (Figure 24.7-8). High values of iron-oxide cement are only observed within two sandstone, marginal-marine (SK5-A-6 from the Lange megasequence) and basinfloor (*Æ*R5-8-3 from the Lysing megasequence), both with 2 %. The pyrite cement is a scarcity in the Lange megasequence sandstones, only within the lower slope (MA2-4-18) high value of 0.7 % is observed.

On the other hand, the Lysing megasequence sandstones exhibit higher values of pyrite cement with an average value of 1 % and the highest within the basinfloor (*Æ*R3-9S-3). A side note, angular detrital pyrite growth is observed within the pore systems of the Lysing megasequence sandstones; however, they were not included in the point counting as they were observed during a general overview of the thin sections. The glauconite cement is often observed with a greenish light hue rim, and towards the center increasing in a deeper green with microparticles of brown color, another variant is fibrous to needle-like shape. It is common as a pore-filling cement, and it is often hard to distinguish from the detrital form of glauconite. This cement type is occurring in both the Lange-Lysing megasequence sandstones, with a higher average value within the Lange sandstones of 1 % and the highest value of 6 % within the marginal-marine (SK5-A-9). The highest amount of illite and smectite cement is both observed within the same sandstones. The lower slope of the Lange sandstone (MA2-4-16) has a value of 6 % of illite cement and 11 % and smectite cement, whereas the basinfloor within the Lysing sandstone (MA2-2-3) show 2.70 % illite and 11.95 % smectite cement. The average values of both illite and smectite cement are highest in the Lange megasequence sandstone of 2 %.

The matrix content within the intergranular volume is not that frequent within the Lange sandstones, albeit in the Lysing sandstones it is observed as clustered micro quartz within pores. The average value within the Lysing sandstones is 2 %. Diagenetic dissolutions are point counted as dissolved feldspar, were a type of feldspar is beyond recognition. The average value of diagenetic dissolution reflects no discrepancies between the Lange-Lysing megasequence sandstones.

Combining all the components contributing to the intergranular volume content, present overall high values within all the samples. The highest average value is observed within the Lysing sandstones with a value of 25 % towards the slightly lower average value of 22 % within the Lange sandstones. The lowest and highest individual value is observed within the lower slopes of the Lange megasequence (DE1-6 and MA2-4-16, respectively).

5.2.4 Porosity

Although significant discrepancies are observed when comparing intergranular porosity with the total porosity, were the result of this study is almost half the value obtained by the bachelor study (Table 9). In the basinfloor (ÆR5-8-3) this value is reduced to one-fifth of the total porosity calculated by the Matlab script. These discrepancies can be induced by poor resolution obtained from the scanners and in combination with separating matrix and cement (which is often shaded with the blue epoxy color, seen within the kaolinite cement) from epoxy filled pores.

Table 9: Summary of the results of the two independent studies of porosity detection. Notice the similar results between the total porosity from the bachelor study and the intergranular volume (IGV) from this study.

Bachelor study						My study	
Sample	**dpi**	**First cluster porosity (%)**	**Second cluster porosity (%)**	**Total porosity (%)**		**Intergranular porosity**	**IGV**
ÆR5-8-5	2400	11.68	12.40	24.08		14.3	25.6
ÆR5-8-7	2400	11.68	12.40	24.08		14.4	25.6
ÆR3-9S-18	2400	11.68	12.40	24.08		18.0	33.1
ÆR5-8-3	2400	11.68	12.40	24.08		5.7	20.8

Samples of the Lange-Lysing megasequences have around 10 to 30 % of original porosity destroyed by cementation, and around 40 to 60 % destroyed by mechanical compaction. Outliners are observed outside this cluster, and the marginal-marine sandstones (6507/5-A-4H) have a value of around 10 % destroyed by cementation and from 60 % mechanical compaction, which is decreasing upwards in the stratigraphy. The mechanical compaction is reflected by the sutured to concave-convex grain-to-grain contacts. On the opposite side, sandstone within the lower slope (MA2-4-16) show over 80 % porosity destroyed by cementation, which is due to the total cement value of 34 %, with a low mechanical compaction value of 15 % seen by the

plane contacts in the sample (Figure 23 original porosity loss due to compaction and cementation diagram from Ehrenberg (1989).

From the equation of Ehrenberg (1989), porosity loss due to compaction (COPL) and porosity loss due to cementation (CEPL), the average total porosity loss of the Lange-Lysing sandstones and the highest value are 31 % and the highest value of around 42 %. The only discrepancies are observed for the lowest values, were within the basinfloor (ÆR3-9S-12) from the Turonian-Coniacian Lysing megasequence has a relatively low value of 20 % and the lower slope (MA2-4-16) within the Lange megasequence show a value of 9 %.

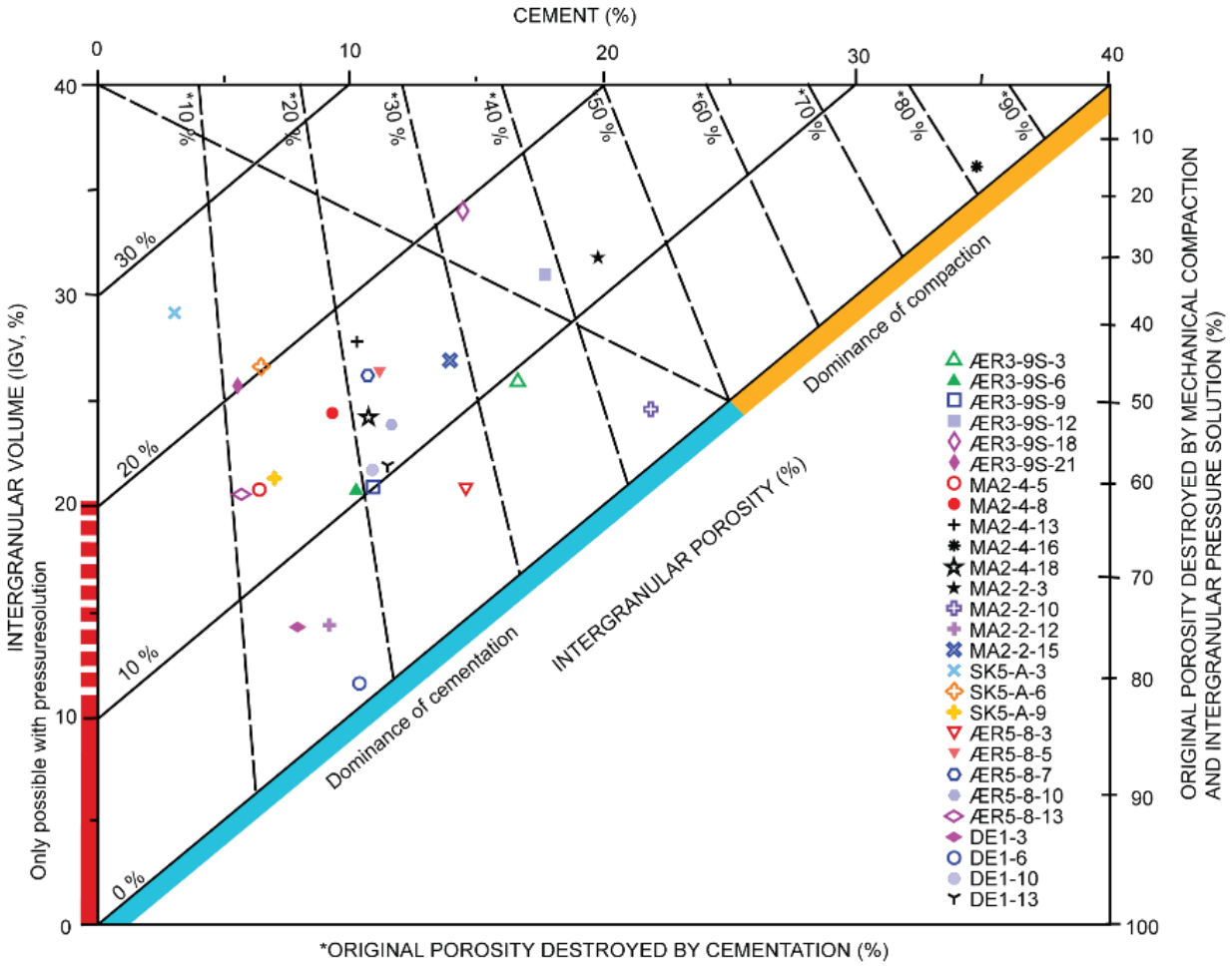

Figure 23: Ehrenberg (1989) diagram showing original porosity loss due to cementation and mechanical compaction.

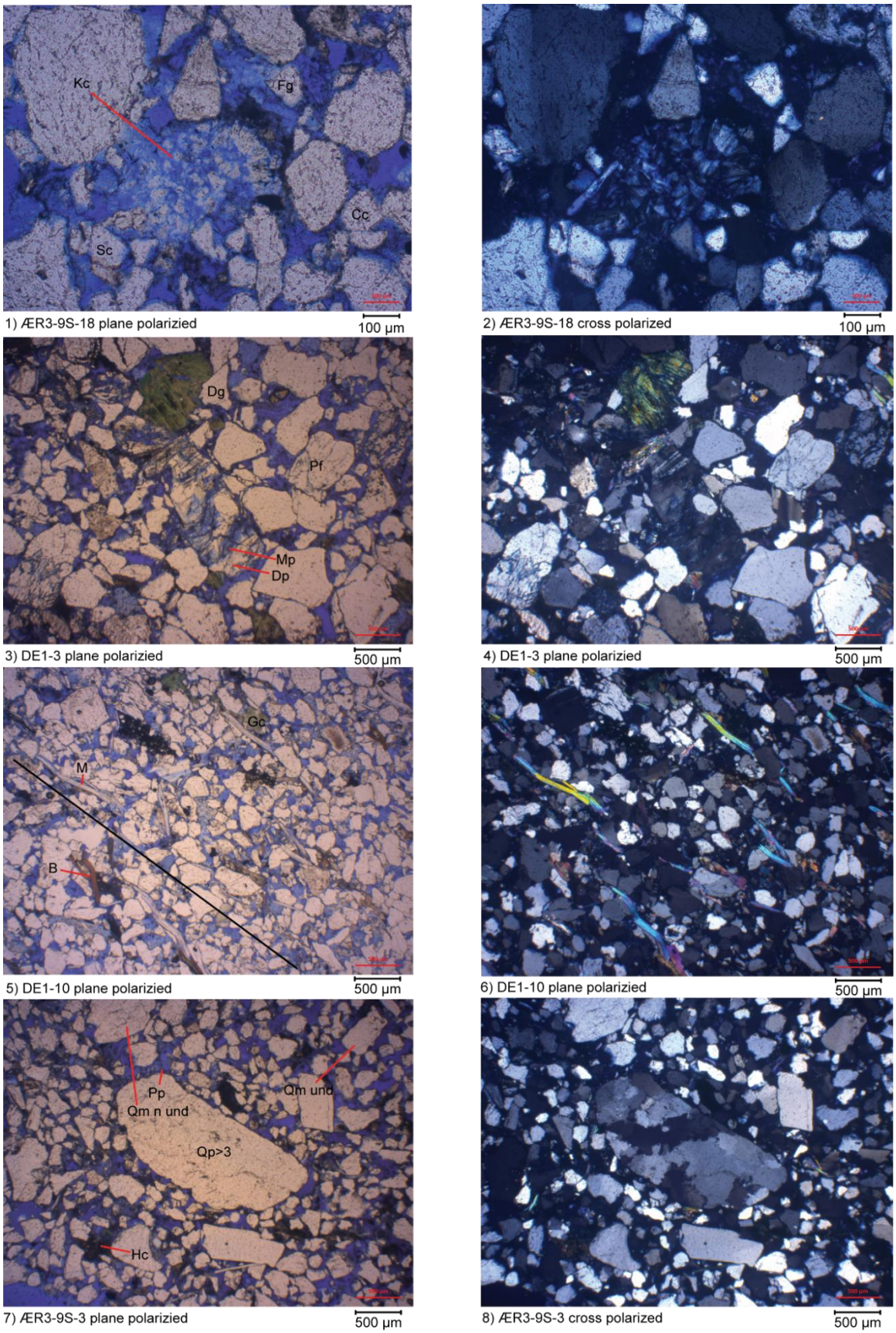

Figure 24: Plane and cross polarizied view of thin sections. Kc=kaolinite cement, Cc=concave-convex grain contact, Sc=sutured contact, Dg=dissolution of glauconite grain, Pf=fractured porosity, Mp=moldic porosity, Dp=dissolution of plagioclase, Gc=glauconite cement, M=muscovite, B=biotite, Pp=intergranular porosity, Qm und=monocrystalline quartz undulatory, Qm n und=monocrystalline quartz non-undulatory, polycrystalline quartz >3 crystalline lattice, Hc=hematite cement and black line indicates alignment in fabric.

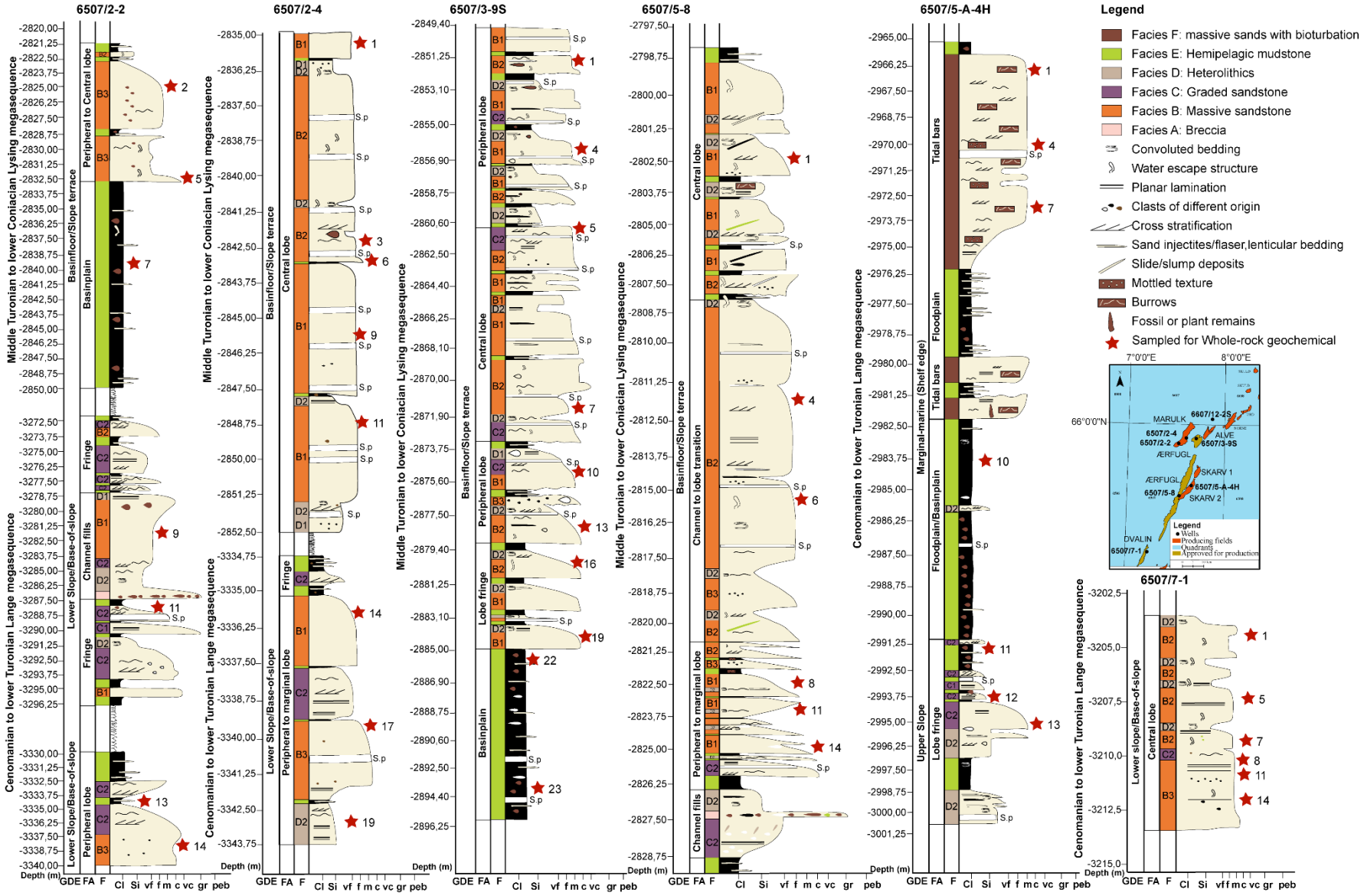

Figure 25: Interpreted core logs with facies association (FA) and gross depositional element (GDE). Red star indicates sampled for whole-rock geochemistry. S.p=Seal peel.

5.3 Geochemical composition

5.3.1 Major elements middle Turonian to lower Coniacian Lysing megasequence

An overview of the whole-rock geochemical sample location described in this subchapter can be viewed in figure 25. The major dominating element in the middle Turonian to lower Coniacian Lysing megasequence is SiO2, with an average value of 86 wt%. The lowest value of 67 wt% is seen in the shallowest sandstone within the basinfloor in core 6507/2-2 (MA2-2-5) and the highest of 90 wt% at the shallowest sandstone within the basinfloor in core 6507/5-8 (ÆR5-8-1; Figure 25). These trends are observed with the high abundance of quartz to the low from the petrography results. Additional important major elements include Al_2O_3, CaO, Na_2O_3, and K_2O, which have average values of 6, 1, 0.3, and 1 wt% respectively. The highest concentrations of Al_2O_3 (8 wt%) and K_2O (1 wt%) are all seen in the same sandstone within the basinfloor from core 6507/2-2, namely MA2-2-2. Comparable to the low abundance of feldspar from the petrography results. The sample representing the highest value of Na_2O_3 (0.6 wt%) is within the basinfloor of the Lysing megasequence (ÆR5-8-8).

The CIA values are calculated without CaO due to the significant discrepancies observed within the results (Table 10). The CIA in the Lysing megasequence has an average value of 79 % with the highest value of 85 % within the sandstone of the basinfloor (ÆR3-9S-1) and the lowest of 74 % (ÆR5-9-11; Table 10). It is following the ideal weathering trend (Figure 26).

The lowest values of TiO_2 (0.2 wt%) and Al_2O_3 (3 wt%), as well as the highest in CaO (9 wt%), is observed within the Lysing megasequence within the basinfloor (MA2-2-5), which represents the shallowest sandstone interval in core 6507/2-2. The average value of TiO_2 is 0.3 wt%, with the highest shown within the

Table 10: Overview of results from CIA calculations with and without CaO.

Sample	Formation	CIA total	CIA without CaO	Difference
AL2S-1	Lange	74.459	80.597	7.616
AL2S-3	Lange	73.229	82.428	11.161
ÆR3-9S-1	Lysing	77.970	84.636	7.876
ÆR3-9S-4	Lysing	76.597	84.191	9.019
ÆR3-9S-5	Lysing	77.666	83.276	6.737
ÆR3-9S-7	Lysing	74.661	78.799	5.251
ÆR3-9S-10	Lysing	61.568	79.558	22.613
ÆR3-9S-13	Lysing	70.316	79.649	11.718
ÆR3-9S-16	Lysing	70.659	78.291	9.748
ÆR3-9S-19	Lysing	43.315	77.718	44.267
ÆR3-9S-22	Lysing	80.152	81.710	1.908
ÆR3-9S-23	Lysing	77.946	79.606	2.085
MA2-4-1	Lysing	74.520	80.072	6.934
MA2-4-3	Lysing	75.261	80.507	6.516
MA2-4-6	Lysing	69.224	81.376	14.933
MA2-4-9	Lysing	68.378	80.540	15.100
MA2-4-11	Lysing	66.487	79.876	16.762
MA2-4-14	Lange	46.781	87.134	46.312
MA2-4-17	Lange	88.931	90.793	2.050
MA2-4-19	Lange	42.852	82.449	48.026
MA2-2-2	Lysing	50.432	80.094	37.033
MA2-2-5	Lysing	15.463	81.297	80.979
MA2-2-7	Lysing	79.147	82.607	4.189
MA2-2-9	Lange	61.516	83.694	26.499
MA2-2-11	Lange	76.648	84.806	9.620
MA2-2-13	Lange	75.501	77.977	3.176
MA2-2-14	Lange	58.823	74.524	21.069
SK5-A-1	Lange	66.313	68.173	2.729
SK5-A-4	Lange	65.637	68.647	4.385
SK5-A-7	Lange	60.461	67.431	10.337
SK5-A-10	Lange	76.274	81.229	6.100
SK5-A-11	Lange	80.033	82.400	2.872
SK5-A-12	Lange	47.574	70.489	32.508
SK5-A-13	Lange	64.228	72.116	10.938
ÆR5-8-1	Lysing	71.824	76.073	5.585
ÆR5-8-4	Lysing	69.808	75.476	7.510
ÆR5-8-6	Lysing	71.913	75.429	4.661
ÆR5-8-8	Lysing	72.987	75.455	3.270
ÆR5-8-11	Lysing	69.528	74.363	6.503
ÆR5-8-14	Lysing	70.231	74.531	5.769
DE1-1	Lange	65.124	68.590	5.053
DE1-5	Lange	65.729	68.917	4.625
DE1-7	Lange	66.551	72.126	7.730
DE1-8	Lange	62.560	71.550	12.564
DE1-11	Lange	65.186	71.972	9.429
DE1-14	Lange	68.121	71.870	5.217

basinfloor of the Lysing megasequence (MA2-4-1) in core 6507/2-4. From the chemical composition of the Upper Continental Crust (UCC; Taylor and McLennan, 1985), the average concentrations of the major elements from the Lysing megasequence samples have considerably lower concentrations, except for in SiO_2 were it is significantly higher (Appendix 2).

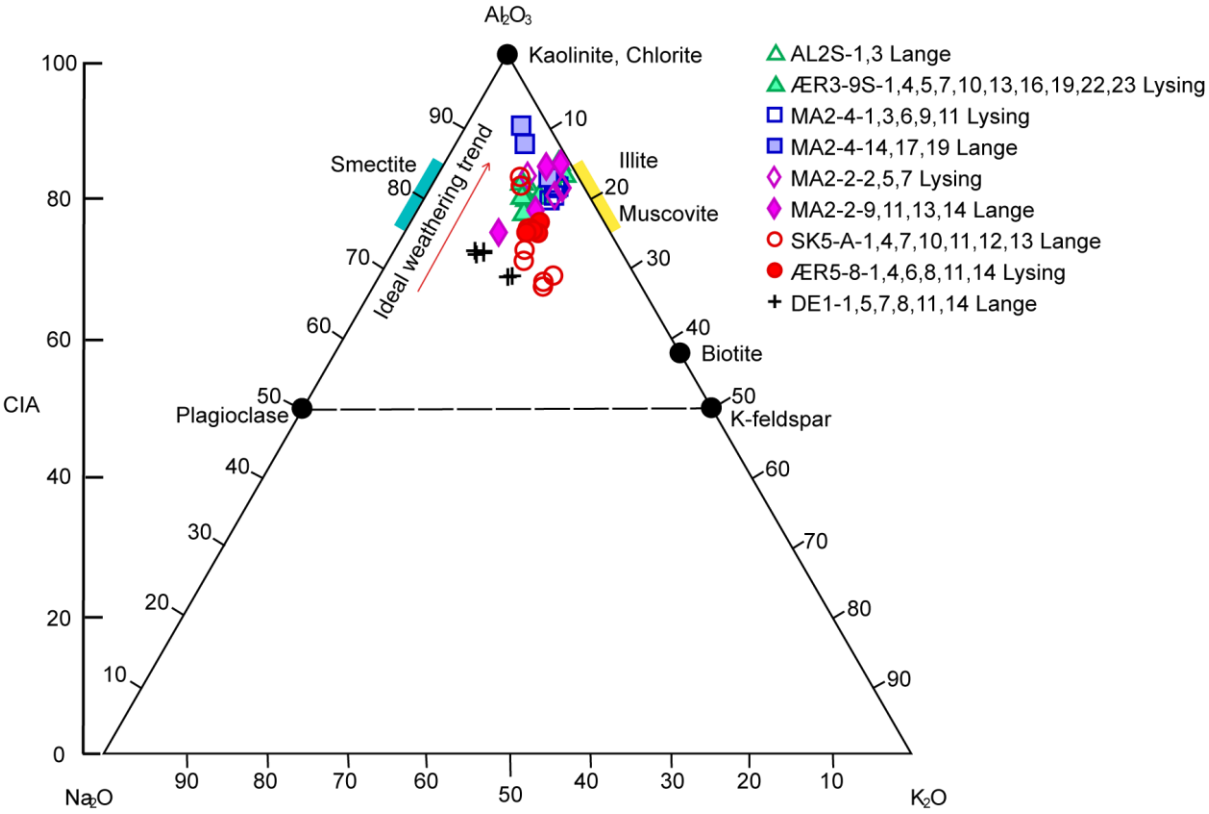

Figure 26: From the Chemical Index of Alteration (CIA) diagram by Nesbitt and Young (1984).

The mobile and incompatible elements (Large-ion lithophile elements (LILE)) Rubidium (Rb), Barium (Ba), Strontium (Sr) and Caesium (Cs) show average values lower than that of the Upper Continental Crust (UCC; Taylor and McLennan, 1985). The highest concentration of the immobile elements (High-field strength elements (HFSE) Thorium (Th), Hafnium (Hf), Titanium (Ti) and Zirconium (Zr) show unique values in sample MA2-4-1, which represents the shallowest basinfloor sandstone in core 6507/2-4. Whereas the lowest values of Hafnium (Hf), Nobium (Nb) and Zirconium (Zr) are denoted within the basinfloor (MA2-2-5) in core 6507/2-2.

5.3.2 The rare earth elements (REE)

The ΣREE concentrations are between 43 and 132 ppm, with an average of 68 ppm. The normalized chondrite diagram (Figure 27) reveals that the REE patterns from the sandstone intervals are comparable to the UCC and PAAS. Anomalies of a decrease in Eu within the upper

basinfloor sandstone (MA2-4-1) and a decrease in Tm lower in the stratigraphy (MA2-4-6) are observed. No other indications of anomalies, with enrichment of the LREE`s La, Sm, and Nd (McLennan et al., 1993) and no enrichment of Eu are observed. La_n/Yb_n values are well above 5 ppm (11 to 20 ppm; Appendix 2).

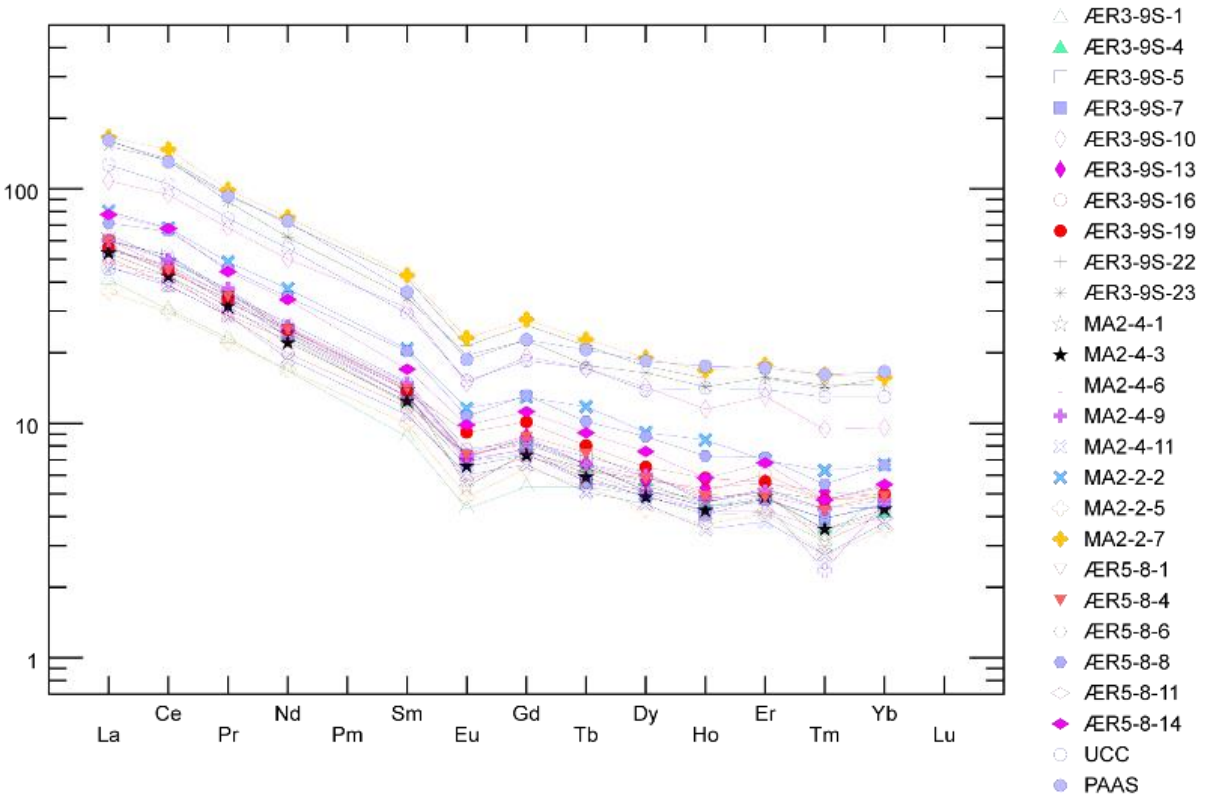

Figure 27: Chondrite-normalized REE diagram of Lysing samples, with UCC and PAAS values from Taylor and McLennan (1985).

5.3.3 Trace elements middle Turonian to lower Coniacian Lysing megasequence

The sandstones show La/Th and Hf results between 3 and 5 ppm and 3 to 6 ppm, respectively (Figure 28; Floyd and Leveridge, 1987). Upper sandstone within the basinfloor (MA2-4-1) is an exception, which has an increased concentration of Hf of 8 ppm. The samples taken from the shale intervals (ÆR3-9S-22,23 and MA2-2-7) have the same La/Th and Hf value of 4.1 ppm and 3.5 ppm, respectively.

The Ti/Zr ratios from the Lysing megasequence sandstones are between 9 and 15 ppm and with more dispersed values of 2 and 5 ppm with the La/Sc ratios (Figure 29; Bhatia and Crook, 1986), whereas three sandstones within the basinfloor (ÆR3-9S-7,10 and ÆR5-8-11) have an elevated La/Sc ratio up to 8 ppm. A clustering around Ti/Zr value of 30 ppm and La/Sc value of 2.1 ppm are observed of the three shales.

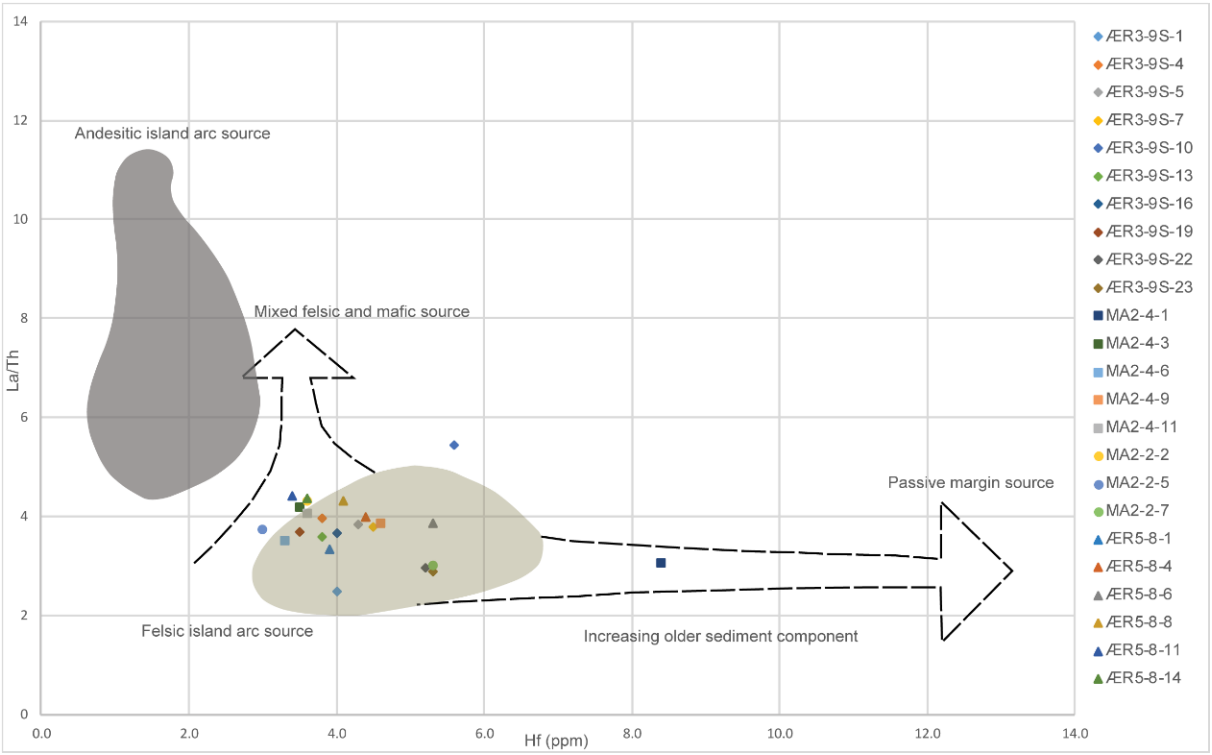

Figure 28: Source composition diagram by Floyd and Leveridge (1987).

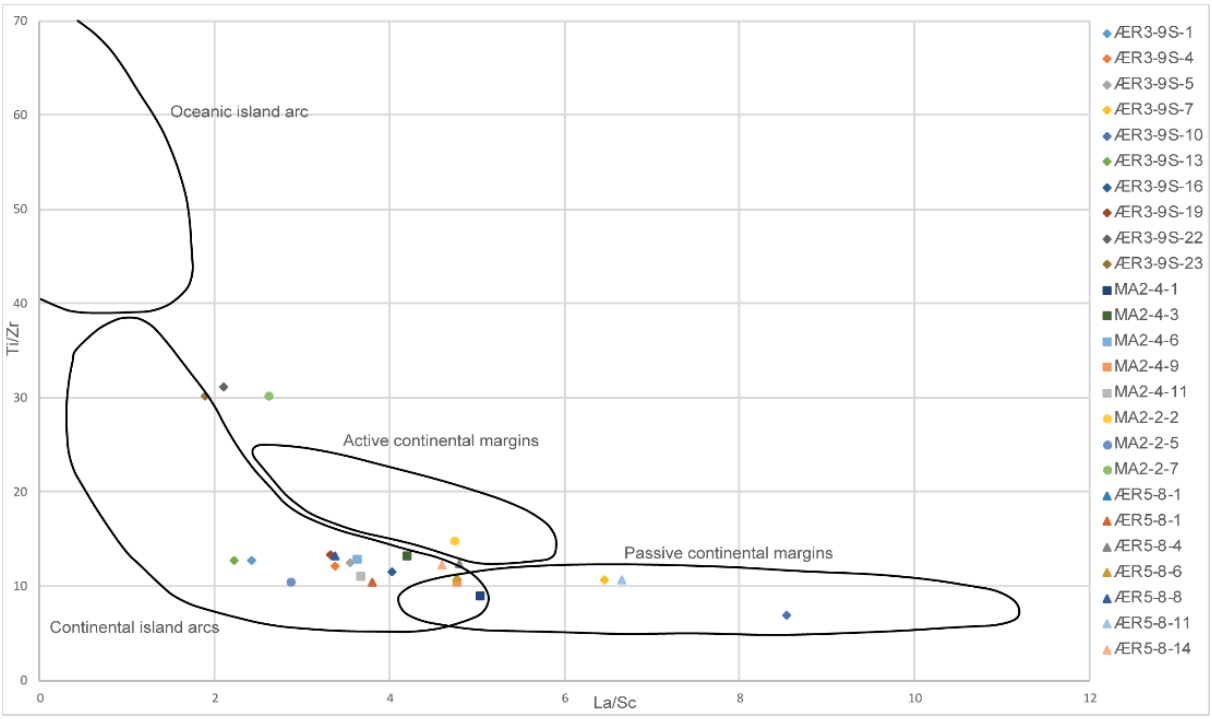

Figure 29: Tectonic setting diagram of Bhatia & Crook (1986).

The recycling discrimination plot of McLennan et al. (1993) display the samples following sediment recycling, with a different recycling degree (Figure 30). The ratios of Th/Sc are varying between 0.8 to 2 and 10 to 100 from Zr/Sc. Upper sandstone within the basinfloor (MA2-4-1) show ratios of 2 and 200 of Th/Sc and Zr/Sc, respectively whereas the other samples within the core 6507/2-4 have lower ratios Th/Sc of 1 and Zr/Sc of 50. The shale samples exhibit a clustering with ratios of 0.8 and 30 for Th/Sc and Zr/Sc, respectively. The Lysing sandstones exhibit ratios of Co/Th between 0.8 and 1 and ppm values of La/Sc between 2 and 5 (Figure 31; Condie, 1993; Gu et al., 2002). Basinfloor sandstone (ÆR3-9S-10) is observed with a high La/Sc value of 8.5 ppm, whereas the basinfloor (MA2-2-7; shale) has a higher logarithmic value of Co/Th of 5.

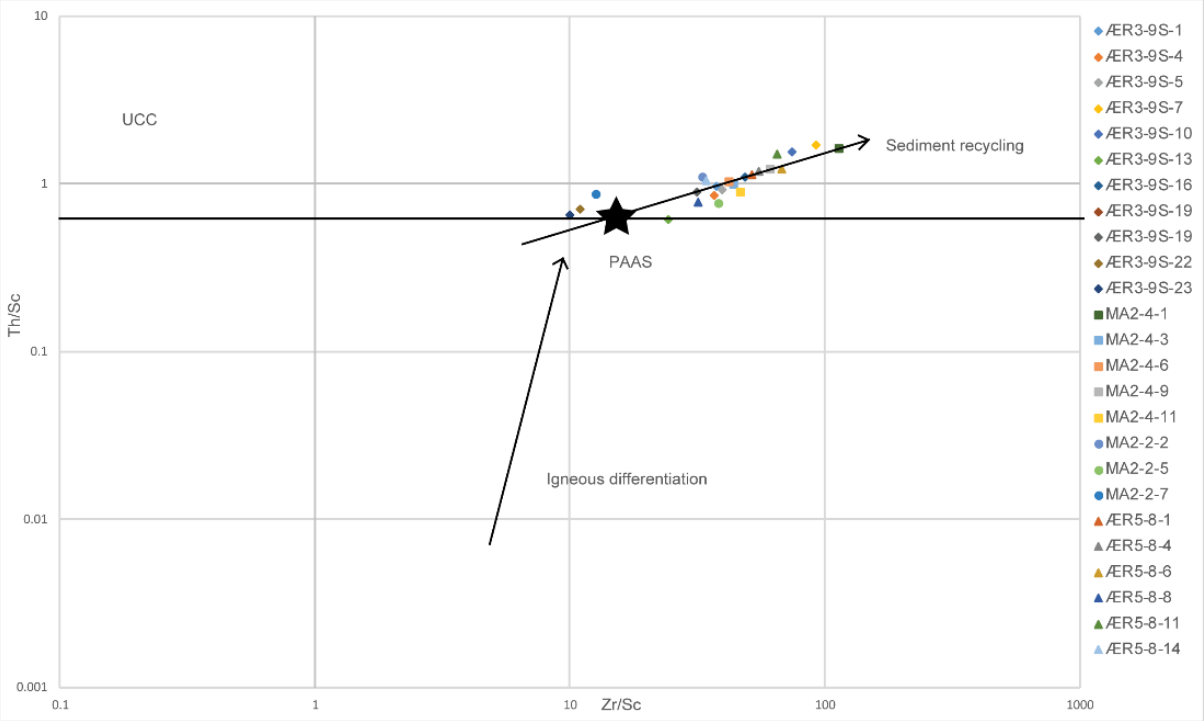

Figure 30: From the recycling discrimination diagram of McLennan et al. (1993).

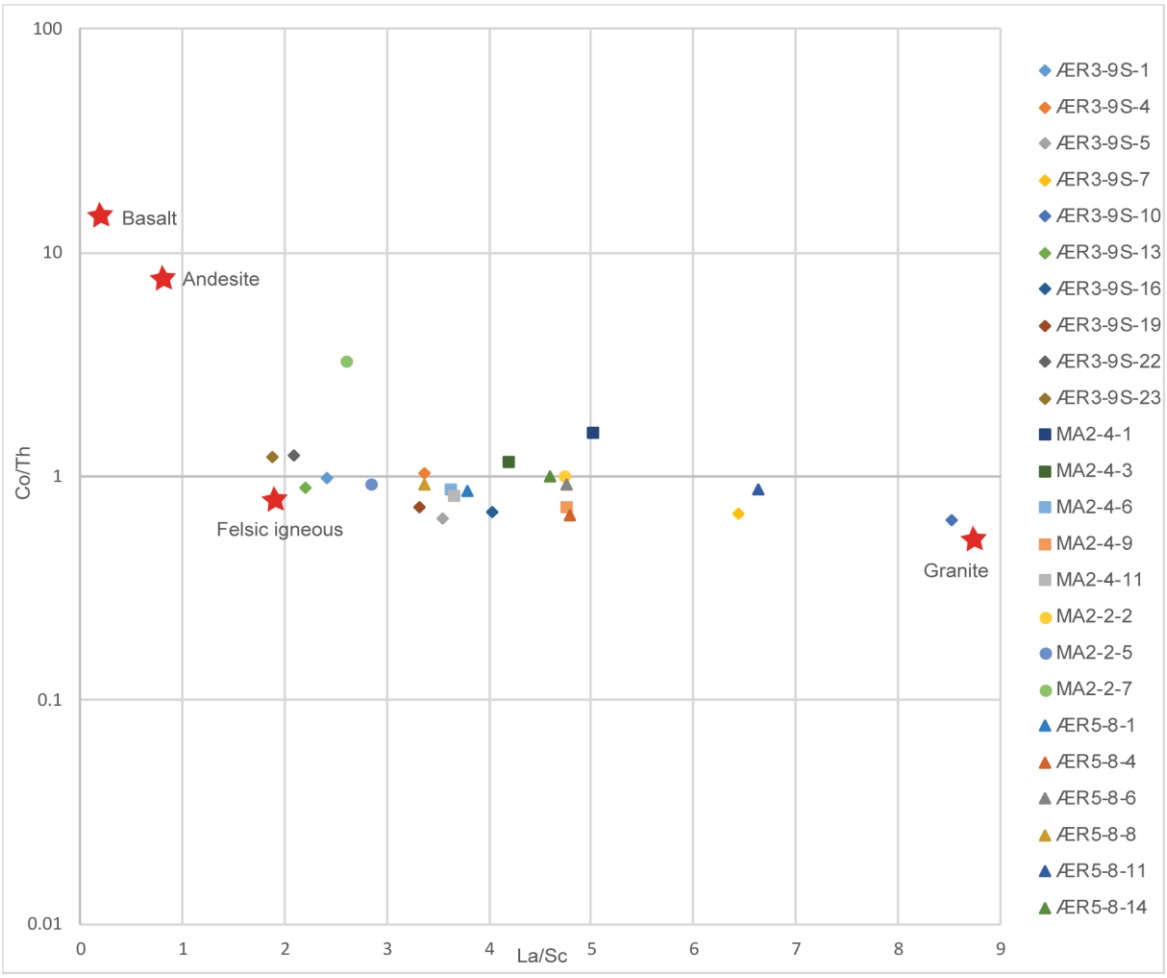

Figure 31: Average composition of volcanic rocks (Condie, 1993) and diagram by Gu et al. (2002).

5.3.4 Major elements Cenomanian to lower Turonian Lange megasequence

Concentrations of SiO_2 in the sandstone from the Lange megasequence are of substantial variation, relative to what is observed in the sandstone from the Lysing megasequence, with a lower average value of 78 wt%. The second lowest value of SiO_2 is seen in the deepest sandstone within the lower slope (MA2-4-19) in the core 6507/2-4, whereas one of the highest is observed on the superimposed sandstone (MA2-4-17) in the same core. The high and low SiO_2 concentration is comparable with the petrography results with lower abundance of quartz. Results from supplement major minerals of importance reveal that the lowest values are concentrated in the superimposed lower slope sandstone (MA2-4-17), while Al_2O_3, K_2O and TiO_2 display the highest concentrations within the lower slope sandstone (AL2S-1). The average concentrations of Al_2O_3, CaO, Na_2O_3, K_2O, and TiO_2 are 8, 1, 1, 1, and 0.5 wt%. Petrography observations are showing an abundance in alkali feldspar. In relation to the composition averages of the UCC (Taylor and McLennan, 1985), the average value of SiO_2 is high (80 %) with values representing the additional major elements are lower (Appendix 2).

The LILE elements Ba and Sr of the Lange megasequence show significantly higher values than those in Lysing megasequence. The highest concentration of Ba and Sr are 8122 and 393 ppm within the lower slope sandstone (AL2S-1) respectively, compared to those of the Lysing megasequence with values of 1378 and 167 ppm. The average values of the LILE represented in the Lange megasequence sandstones are lower than that of the Upper Continental Crust (UCC; Taylor and McLennan, 1985), apart from Ba of significantly higher value 3410 ppm. The lowest concentrations of HFSE elements of Hf and Zr of 9 ppm and 349 ppm, respectively are in the shallowest marginal-marina sandstone (SK5-A-1). On the other hand, the highest concentrations of Nb (15 ppm) and Th (12 ppm) are presented in the shallowest lower slope sandstone (AL2S-1) within well 6607/12-2S.

5.3.5 The rare earth elements (REE)

ΣREE concentrations are between 41 and 180 ppm, with an average of 73 ppm. Minute variations of the REE values of the Lange megasequence relative to those in the Lysing megasequence are observed. After normalizing the values, significant inconsistencies compared to the Lysing sandstones are observed (Figure 32; Taylor and McLennan, 1985). Most sandstones follow the same trend as the UCC and PAAS concentrations, albeit, enrichment in Eu is seen within the lower slopes (DE1-1,5 and MA2-4-14,17,19). Subsequently an enrichment in Tb of all the lower slope sandstones in core 6507/2-4. A decrease in concentration is observed

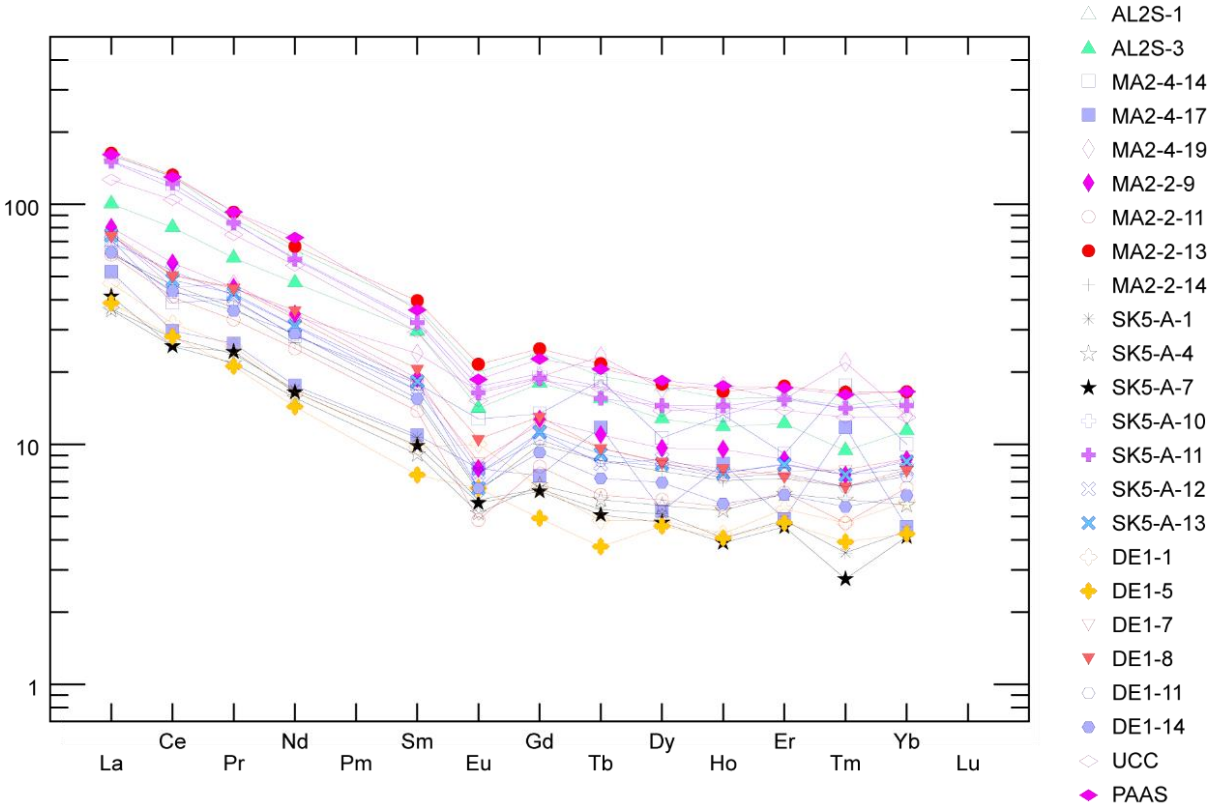

Figure 32: Chondrite-normalized REE diagram of Lange samples, with UCC and PAAS values from Taylor and McLennan (1985).

in the marginal-marine sandstones (SK5-A-1,7) in the REE element Tm. The La_n/Yb_n values from the Lange megasequence are relatively lower than that of the Lysing megasequence (Appendix 2).

5.3.6 Trace elements Cenomanian to lower Turonian Lange megasequence

Two main clusters are revealed from the results. One has the La/Th and Hf values between 2 and 4 ppm and 3.5 to 6 ppm, respectively. The second has ratios between 2 to 4 and 7 to 9 ppm from La/Th and Hf, respectively (Figure 33; Floyd and Leveridge, 1987). The three shales (MA2-2-7 and SK5-A-10,11) have the same La/Th (4) and Hf (3.5 ppm) values as the shales in the Lysing megasequence. The two upper slope sandstones taken from the sand injectites from core 6507/5-A-4H have the same values of La/Th (3.5 ppm) and Hf (8 ppm) as the basinfloor sandstone (MA2-4-1) of the Lysing megasequence.

The Ti/Zr ratios from the Lange sandstones are between 9 and 18 and 1 and 3 with the La/Sc ratios (Figure 34; Bhatia and Crook, 1986), whereas four shales (MA2-2-13, AL2S-1 and SK5-A-10,11) have an elevated La/Sc ratio of 35. The sand injectite have the same ratios as the basinfloor sandstones of the Lysing megasequence (ÆR3-9S-1 and ÆR3-9S-13) of 12 from the Ti/Zr ratio and 2 from the La/Sc ratio.

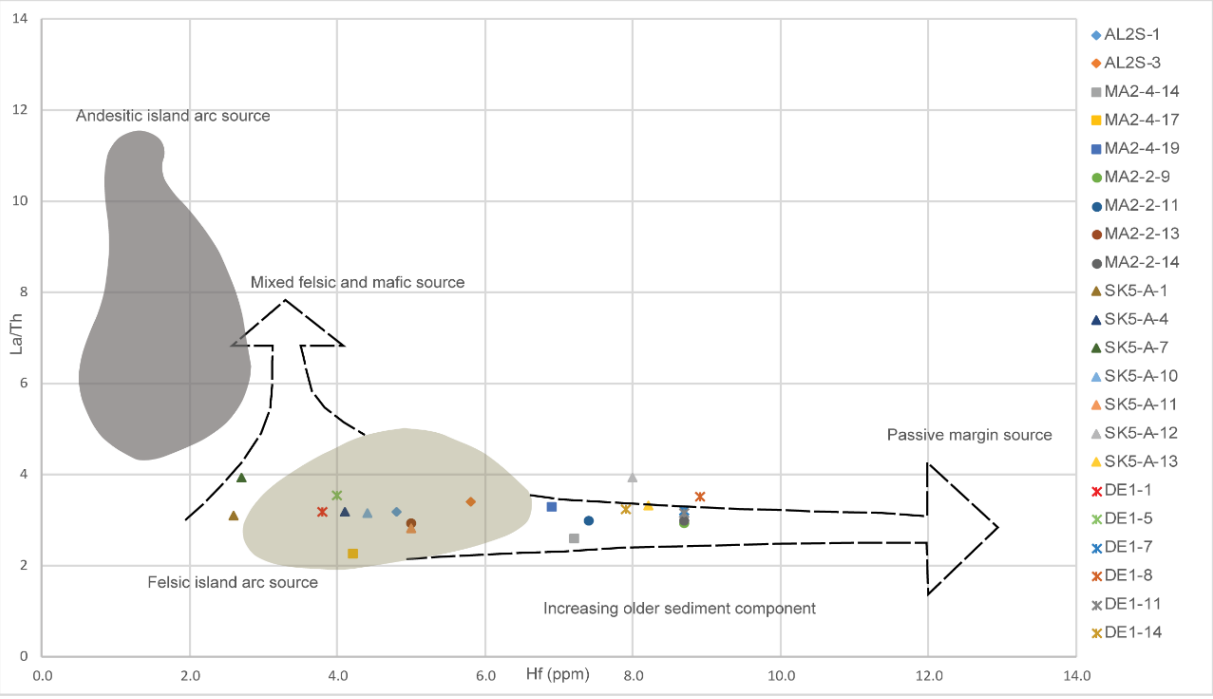

Figure 33: Source composition diagram by Floyd and Leveridge (1987).

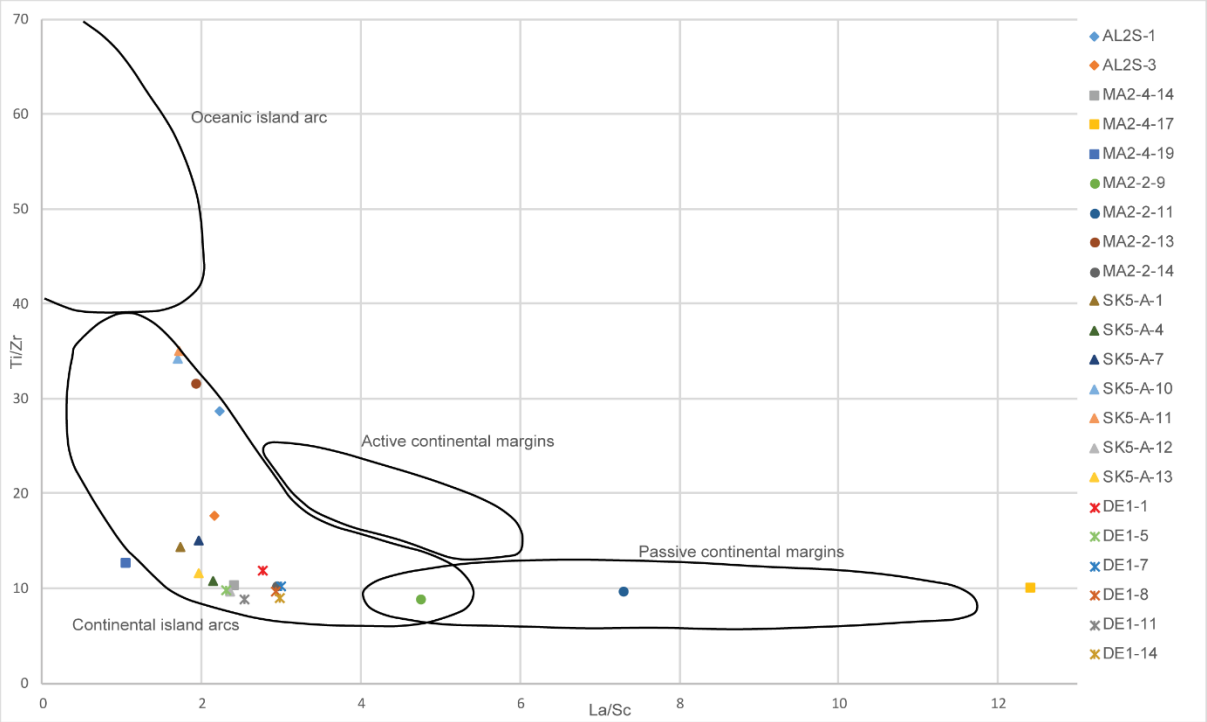

Figure 34: Tectonic setting diagram of Bhatia and Crook (1986).

Sediment recycling patterns of the Lange sandstones are following the same trend as with the Lysing sandstones with the logarithmic values of 0.8 and 5 of Th/Sc and Zr/Sc, respectively (Figure 35; McLennan et al., 1993). A cluster around the PAAS is observed, with the logarithmic value of Th/Sc and Zr/Sc of 0.5 to 0.8 and 8 to 12, respectively. The lower slope sandstone (MA2-4-17) show a high logarithmic value of 8 and 300 of Th/Sc and Zr/Sc compared to the deeper lower slope sandstone (MA2-4-19) which has a value of 0.5 and 12, respectively. The shales, including AL2S-1, have the same logarithmic values of 0.9 (Th/Sc) and 10 (Zr/Sc) as the shales of the Lysing megasequence. The sand injectites have the same logarithmic values of 0.8 with Th/Sc and 50 with Zr/Sc as with the basinfloor sandstone (MA2-2-5) of the Lysing megasequence.

A clustering of sandstones is observed with the logarithmic values of 0.8 with Co/Th and 1 to 3 ppm with La/Sc (Figure 36; Condie, 1993; Gu et al., 2002). The two sandstones from core 6507/2-4 show contradicting concentrations of La, where the superimposed sandstone (MA2-4-17) have a high value of 12 with the La/Sc ratio and the underlying sandstone (MA2-4-19) has the value 1 from the La/Sc ratio. The shales from Lange-Lysing megasequences, including both sandstones from core 6607/12-2S show comparable results of Co/Th ratio of 2 and 2 of La/Sc ratio.

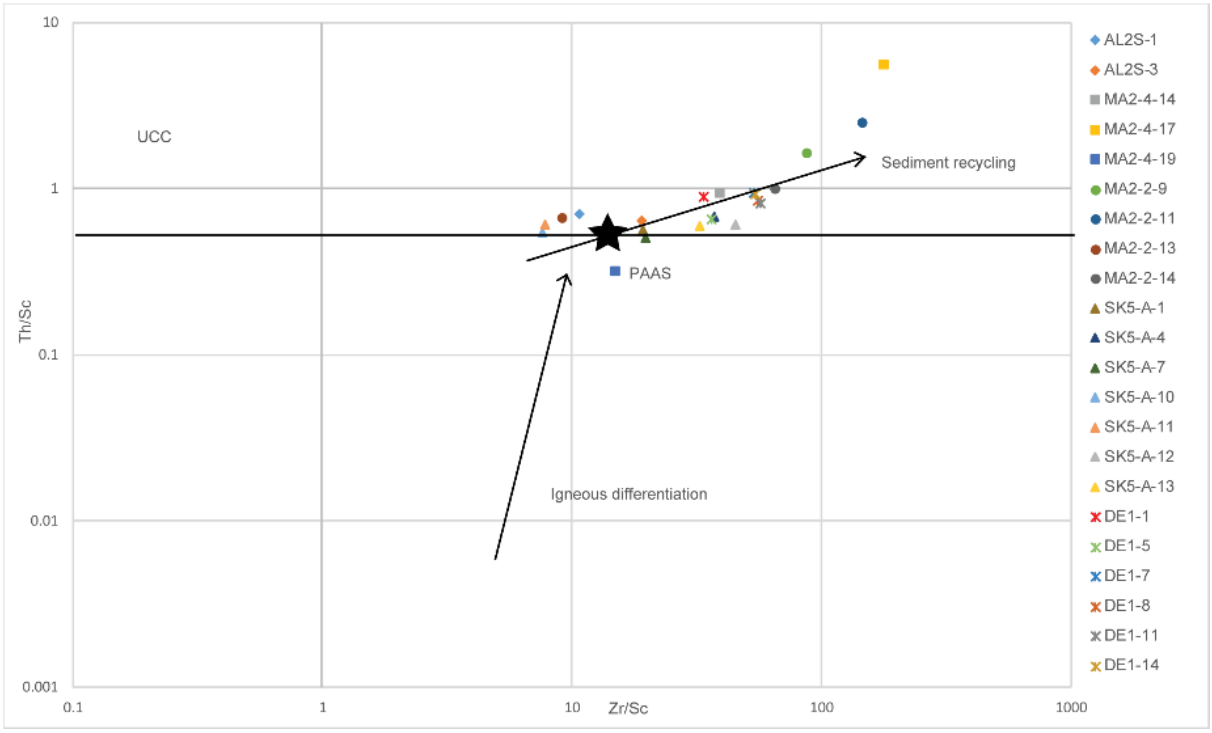

Figure 35: From the recycling discrimination diagram of McLennan et al. (1993).

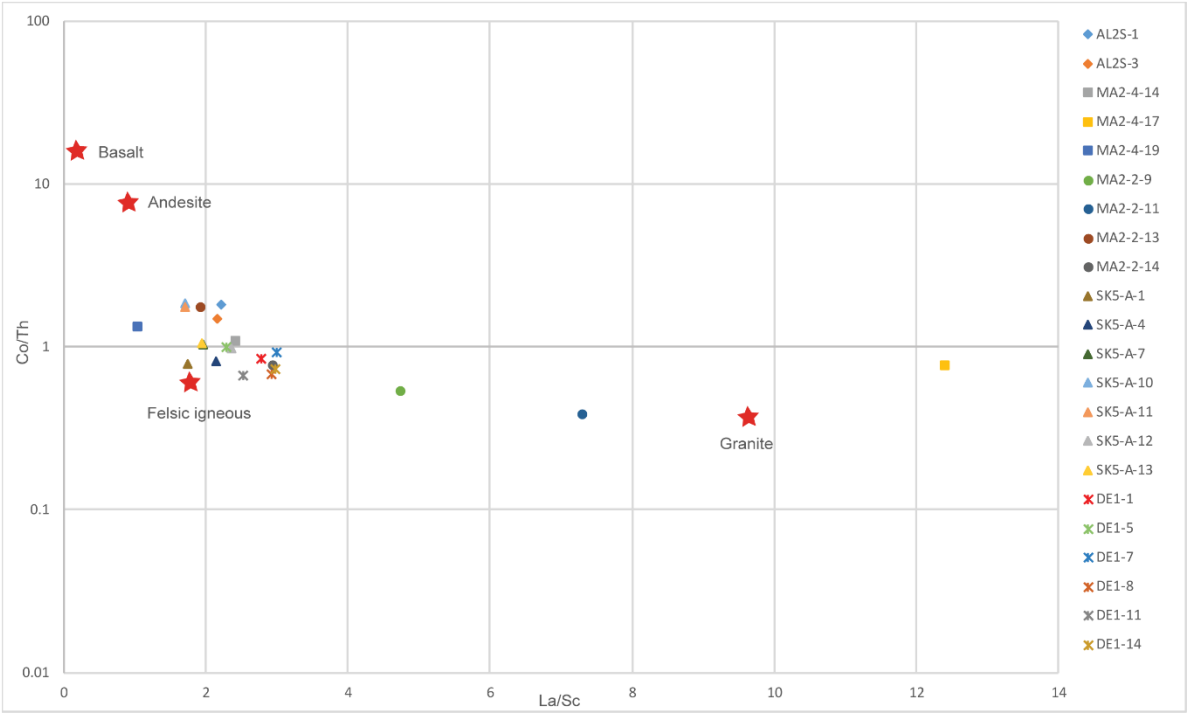

Figure 36: Average composition of volcanic rocks (Condie, 1993) and diagram by Gu et al. (2002).

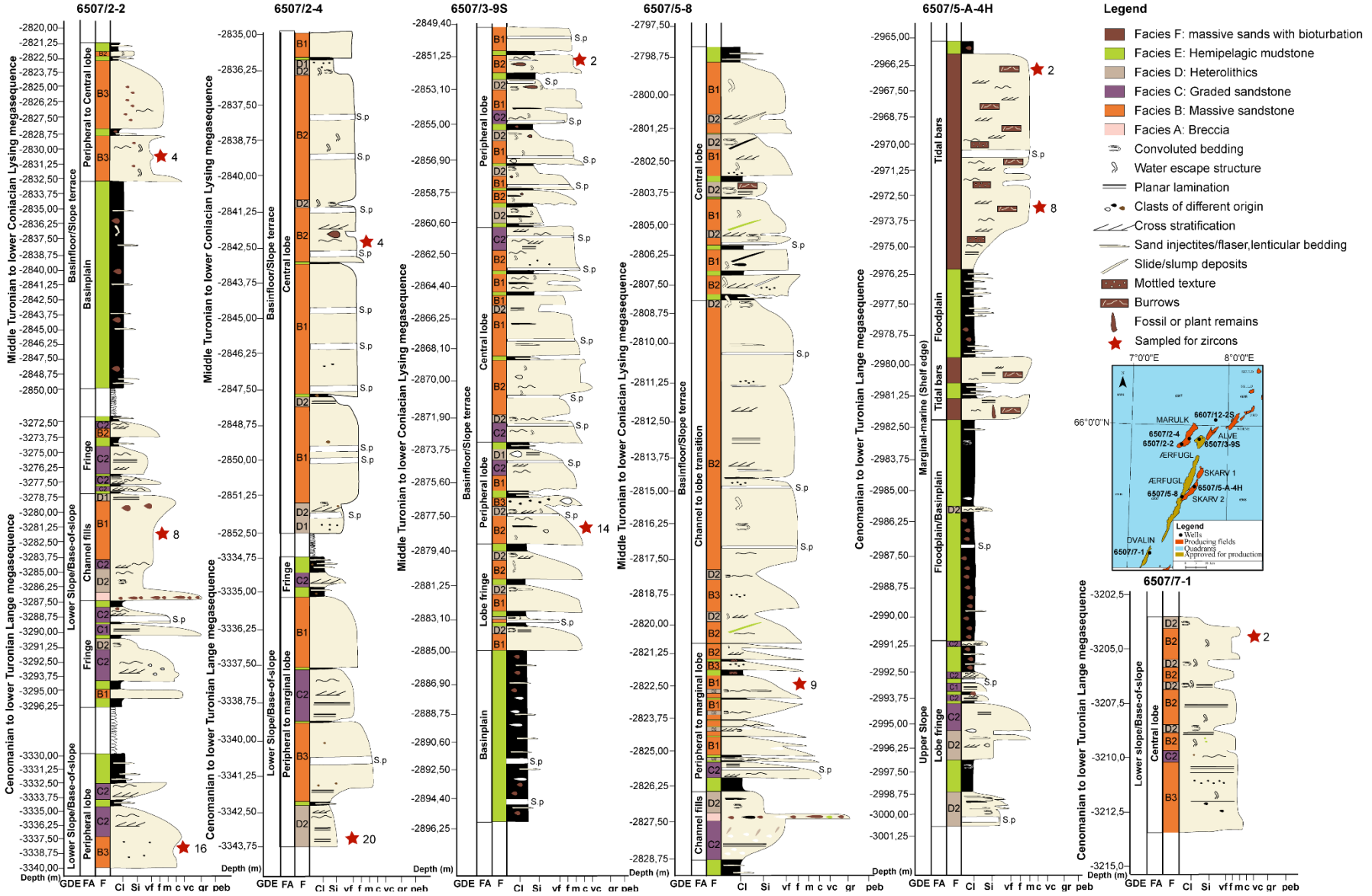

Figure 37: Interpreted core logs with facies association (FA) and gross depositional element (GDE). Red star indicates sampled for zircon analysis. S.p=Seal peel.

5.4 Zircon

An overview of the analyzed zircon sample location described in this subchapter can be viewed in figure 37.

5.4.1 Morphology and texture

Zircon grains mostly are elongated (Figure 38.b, g, r, s, u, w) and less common equant (Figure 38.a, o, t, v, x), often with rounded or broken edges (Figure 38.i, k). The smallest average size of 80 µm are observed within the Cenomanian to lower Turonian Lange megasequence within the marginal-marine sandstone (SK5-A-8), whereas the largest of 200 µm is represented in the lower slope sandstones (DE1-2; Figure 38.c, MA2-2-8; Figure 38.y and MA2-4-20). The morphology displays simple to complex growth history with single or multiple zonations, often with a non-visible or damaged early generation. Dominant single zonation is observed in the middle Turonian to lower Coniacian Lysing megasequence within the basinfloor sandstones (ÆR5-8-9), with an equal amount within the upper sandstone in core 6507/3-9S (ÆR3-9S-2; Figure 38.j). Moreover, in the sandstone of the northwestern core 6507/2-4 (MA2-4-4; Figure 38.p, q), whereas the middle sandstone (ÆR3-9S-14; Figure 38.d, f), the lower slope sandstone in the Lange megasequence (MA2-2-8; Figure 38.y). The lowest sandstone in the lower slope of core 6507/2-4 (MA2-4-20) represents abundance in multiple zonation zircons. Xenocryst inclusions with an unknown origin is a common occurrence among some of the samples (Figure 38.h, z, m). It often appears within or on the border of the first zonation, where black dots truncate the internal zoning surrounding the core. A rare occurrence of convoluted zoning (Figure 38.e, æ) is observed within all the sandstones; however, the sandstone in the lower slope of core 6507/2-2 (MA2-2-8) has the highest amount of both xenocrysts and convoluted zoning. The convoluted zoning is seen as wrapped or distorted inner core with a heterogeneous mix of trace elements. The rare occurrence of twin growth (Figure 38.l, n) is seen in sandstones from basinfloor and lower slope of both the Lange-Lysing megasequence (ÆR3-9S-2, MA2-4-4, and MA2-4-20).

5.4.2 U-Pb geochronology

Recurring age populations of 1750 Ma (Early Proterozoic), 1250 Ma (Middle Proterozoic) and 950 Ma (Late Proterozoic) are observed in all the sandstones within both the Lange-Lysing megasequences, with slightly different frequency. The population of Gothian age (1750 Ma) is the most prominent one within sandstones of both low to high concordant concentrations (Figure 39 and Figure 40).

A dominant, however, not repetitive within all the sandstones are the age population of 490 Ma. This age population is lacking within the upper basinfloor sandstone in core 6507/2-2 (MA2-2-4), furthermore no ages below 950 Ma is detected within this sandstone, despite the relatively high number of concordant zircons (n=56). The lower slope sandstone of the Lange megasequence within core 6507/2-2 (MA2-2-8) display relatively low occurrence of the 490 Ma age population, although the concentration of the concordant zircons is high (n=66). Stratigraphically this is observed as a decrease upwards in the input of Phanerozoic zircons in core 6507/2-2 (Figure 39 and Figure 40).

An opposite trend is observed for Archean ages in the same core, with an increase in Archean ages upwards. The same Archean and Phanerozoic ages are visible within cores 6507/2-4 and 6507/3-9S. Although a reverse of the Phanerozoic ages in core 6507/2-4 is represented by a stratigraphically upwards increase to stable input of younger zircons (Figure 39). No input of Archean zircons is observed in the Cenomanian to lower Turonian Lange sandstone of the upper slope and marginal-marine (MA2-4-20, MA2-2-16, and SK5-A-2+8), the latter is probably in combination with low amounts of concordant zircons (n=22). A trending Archean age population is 2850 Ma, which is observed within sandstones of the basinfloor, and lower slope (*Æ*R5-8-9, *Æ*R3-9S-2, *Æ*R3-9S-14, MA2-2-4, MA2-2-8 and MA2-4-4). Another significant age population in the Archean is that of 2680 Ma, revealed in sandstones of the lower slope and basinfloor (DE1-2, *Æ*R5-8-9, *Æ*R3-9S-2, and MA2-4-4). Oldest zircon ages are observed in the middle Turonian to lower Coniacian Lysing sandstones within the basinfloor (*Æ*R3-9S-2 and MA2-2-4) were both have an age population of 3150 Ma. Additionally, the upper basinfloor sandstone within core 6507/3-9S (*Æ*R3-9S-2) present two more age populations of Archean origin, the first is 3000 Ma and the second is 3350 Ma (Figure 39 and Figure 40).

90 Ma young zircons are observed within the basinfloor sandstones in core 6507/5-8 (*Æ*R5-8-9) and core 6507/3-9S (*Æ*R3-9S-14), which is around the depositional ages of the Cenomanian to Turonian formations (Appendix 3).

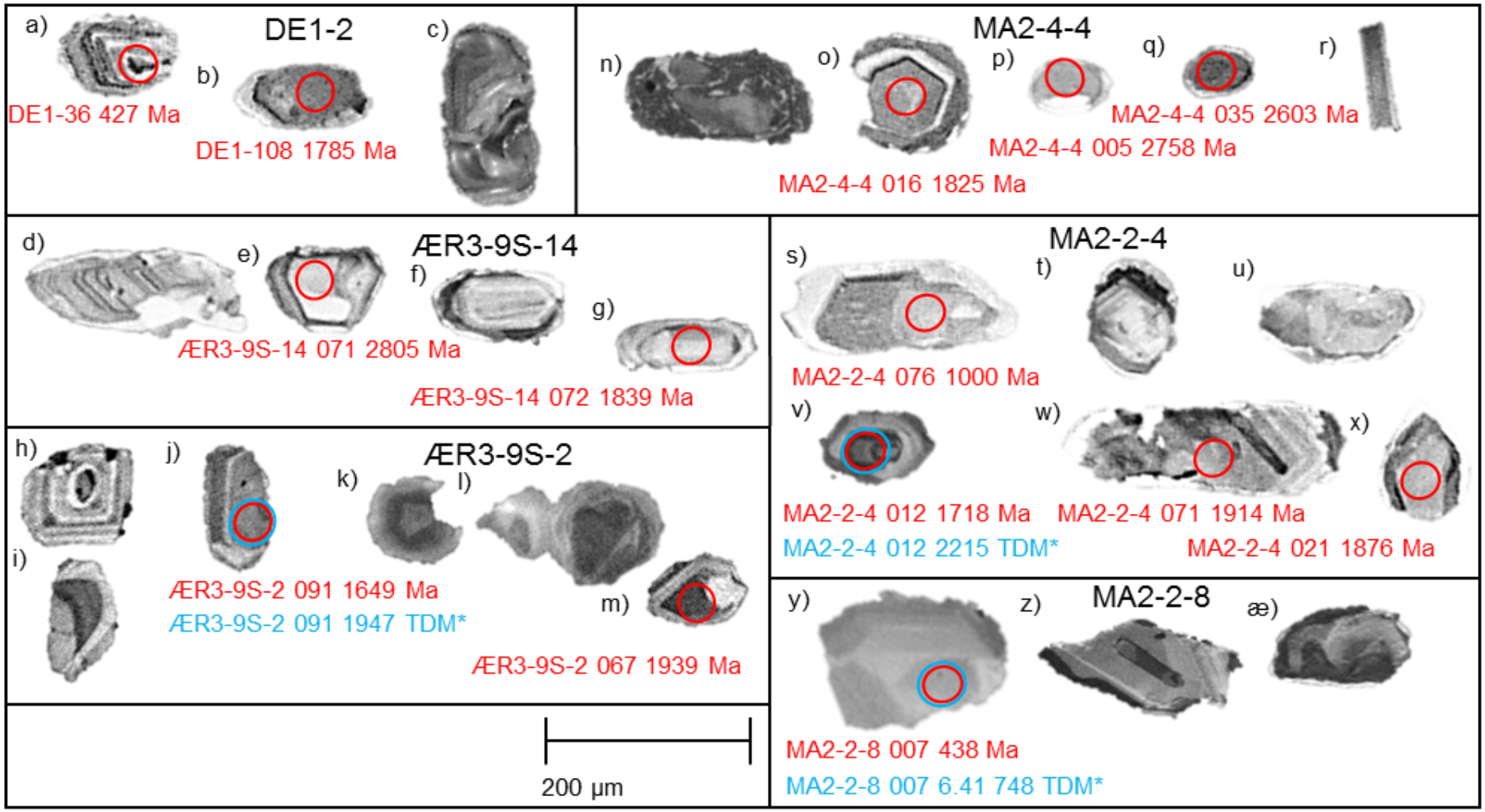

Figure 38: Morphology and texture among the analysed grains. Red circles (40 µm) U-Pb laser ablation. Light blue circles (50 µm) Hf ablation. a) multiple zonation and equant, b) single zonation and broken edges, C) convoluted zonation and elongated, d) multiple zonation with squared growth, e) convoluted zonation, f) single zonation and rounded, g) single zonation with bright rim, h) equant shape with xenocryst inclusion, i) broken zircon, j) single zonation, k) bright rim with squared core with round growth rim, l) twin growth, m) diamond shaped with annealed domain, n) recrystallization with twin cores, o) hexagon shaped core, p) single growth with light inclusion, q) single zonation, r) broken elongated zircon, s) complex growth and elongated, t) multiple zonation, u) sector zoning, v) multiple rounded zonation, w) complex growth in elongated zircon, x) recrystallization, y) multiple zonation, z) large elongated xencryst inclusion and æ) locally overprinted by zones of recrystallization or new growth. TDM=Model ages.

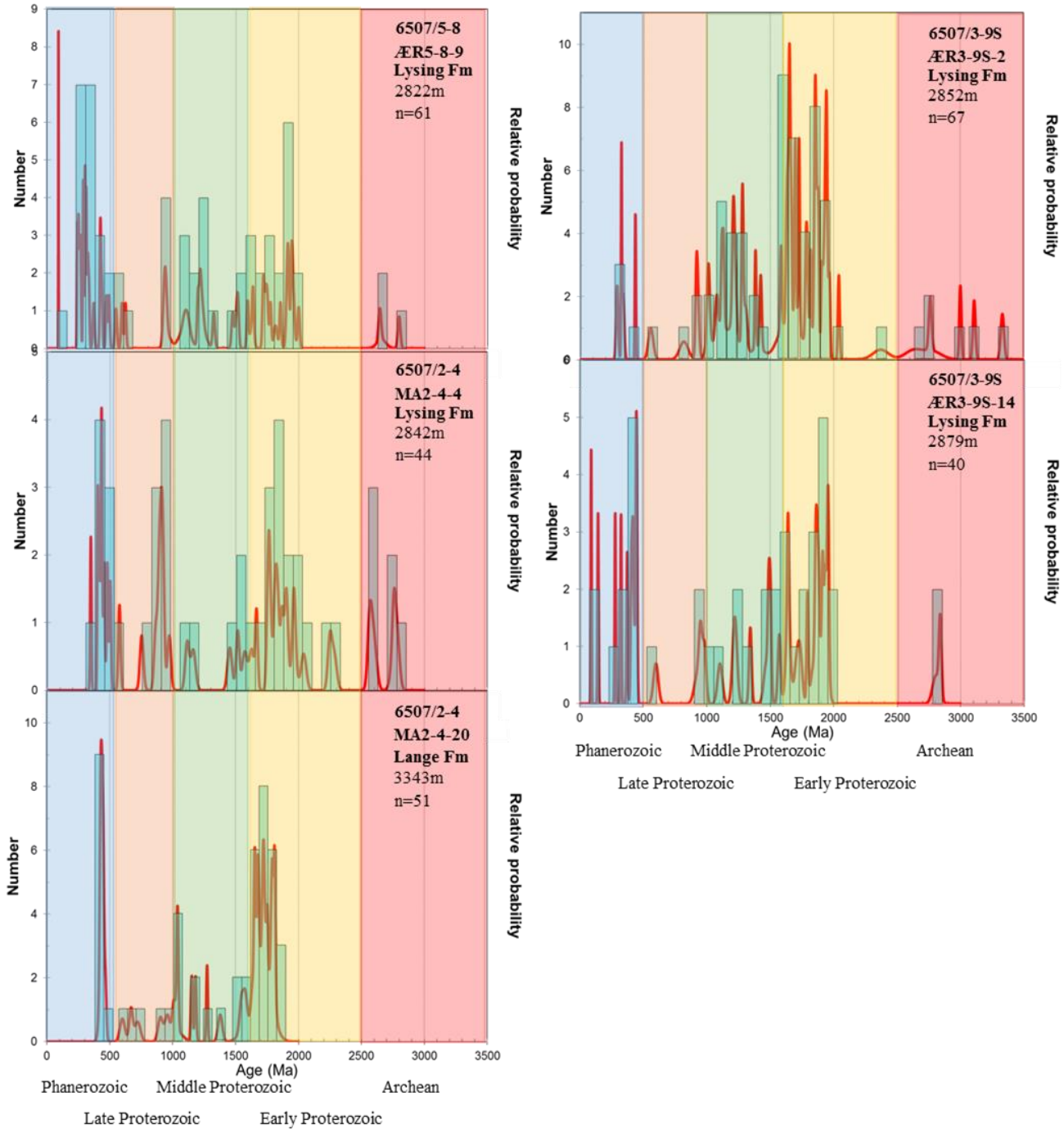

Figure 39: Zircon age spectra of 6507/8-9, 6507/2-4 and 6507/3-9S.

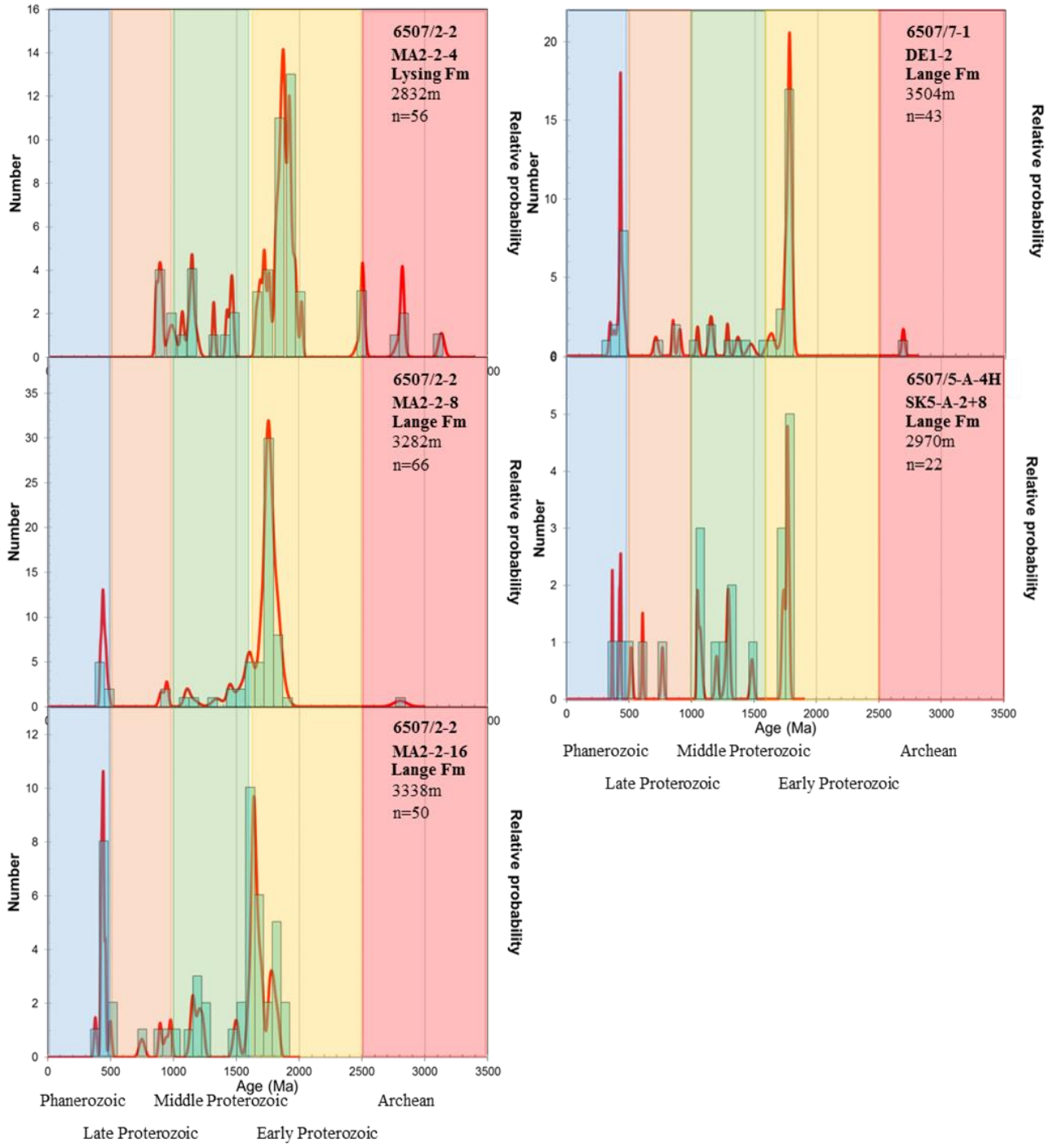

Figure 40: Zircon age spectra of 6507/2-2, 6507/7-1 and 6507/5-A-4H.

5.4.3 Hafnium isotopes

The results of the measured isotopes are compiled in appendix 4. The relative present-day $^{176}Hf/^{177}Hf_0$ values of the sampled sandstones are within the values of 0.281434 to 0.282832, corresponding to initial Hf_0 epsilon values of -10.72 and +10.44, respectively. Four outliners have been excluded and are observed with the $^{176}Hf/^{177}Hf_0$ values between 0.275677 and 0.277828 and the corresponding initial Hf_0 epsilon values between -214.12 and -137.85, respectively. The epsilon values at time T ($\varepsilon_{Hf}(t)$) have an average value among the Gothian

orogeny zircon ages of -0.42, and a minimum and maximum value of -10.72 and +7.66, represented by the basinfloor and lower slope sandstones (MA2-2-4 and MA2-2-16, respectively; Figure 41). The Caledonian orogeny zircon ages have an average value of -2.3 with a more extensive spread between -20.7 and +10.5. The minimum and maximum values are represented in the middle Turonian to lower Coniacian Lysing basinfloor sandstones (*Æ*R3-9S-14 and *Æ*R5-8-9, respectively). The average calculated depleted mantle ages (TDM*) within the Gothian orogeny zircon age is 2118 Ma with a minimum and maximum value of 1658 Ma and 2737 Ma within the lowest sandstone within the lower slope of core 6507/2-2 (MA2-2-16) and the upper sandstone within the basinfloor of the same core (MA2-2-4). The minimum and maximum depleted mantle ages are represented by the basinfloor sandstones of core 6507/5-8 (*Æ*R5-8-9) and core 6507/3-9S (*Æ*R3-9S-14) with the values of 513 Ma and 2204 Ma, respectively (Figure 41). The average depleted mantle age is 1221 Ma.

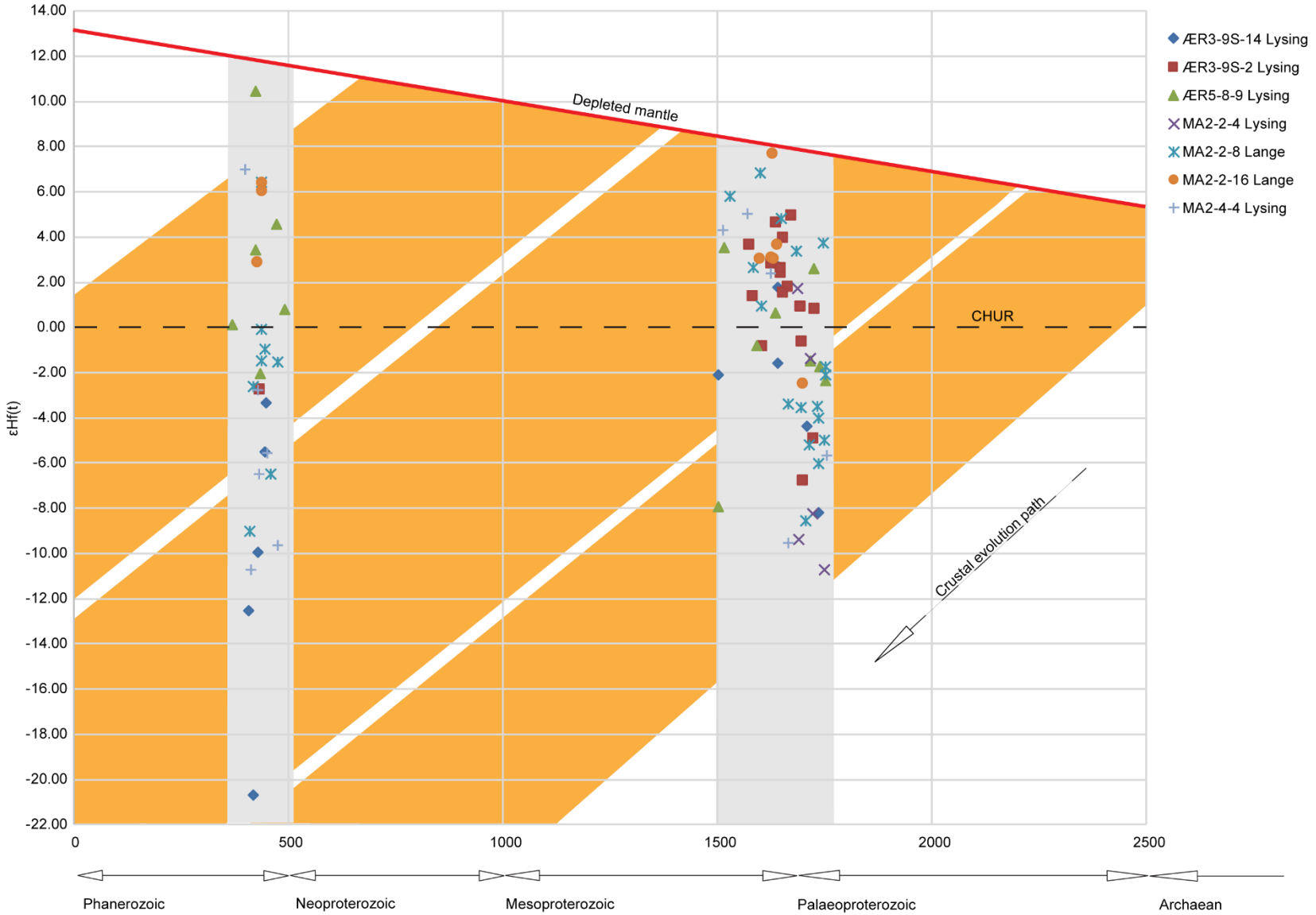

Figure 41: U-Pb ages vs initial Hf epsilon value. Red line is the depleted mantle and the black stipled line is the chondritic uniform reservoir. Three different crustal evolution trends are colored with a orange color. The two grey areas mark the Caledonian and Gothian orogeny ages.

5.5 A brief summary of the results

5.5.1 Cenomanian to lower Turonian Lange megasequence

Two main petrofacies are observed, consisting of a quartzarenite and the subordinate subarkose sandstone. The subarkose sandstone is originating from a cratonic environment from a continental island arc with a granitic source rock composition. However, the quartzarenite are predominantly from a recycled orogen with a mix of both granite and mid to upper gneisses. The weathering pattern for the subarkose petrofacies is predominantly low with less porosity obstructed by cement, whereas the quartzarenite varies between low to high weathering patterns with the corresponding degree of alteration of fragile minerals, inhibiting intergranular porosity. The sedimentary recycling patterns of the quartzarenite are a mix between low and high; however, the subarkose show no recycling pattern. From the REE patterns, the subarkose are following a normal trend resembling the upper continental crust (minute decrease in Tm), this is different from the quartzarenite, which show enrichment in the heavy REE elements Tm, Ho, and Tb. The quartzarenite have a wide age spectrum from 360-1900 Ma, besides a minute Archean input, relative to the subarkose sandstone (360-1800 Ma). The hafnium isotope analysis reveals scattered ε_{Hf} (t) values between -9 and +7 for the "Caledonian" and "Gothian" age dated zircons. The subarkose petrofacies is observed with a marginal-marine (shelf-edge) gross depositional environment, whereas the quartzarenite sandstones varies between a lower slope or base-of-slope and upper slope.

5.5.2 Middle Turonian to lower Coniacian Lysing megasequence

The Lysing megasequence consist predominantly of a quartzarenite petrofacies, originating from a recycled orogen. They reveal a mixed granitic to mid-upper gneisses source rock composition and a felsic igneous to granitic, volcanic rock composition. They are predominately originating from a felsic island arc source, whereas the tectonic setting of origin is varying between continental island arc, active continental margin and passive continental margin. The quartzarenite sediment recycling patterns are dispersed from no recycling (mature) to a high recycling trend, whereas the weathering patterns are clustered within a moderate to high ideal weathering trend. A dominance of cementation within the intergranular porosity is observed, shown by the high content of clay cement (illite, smectite, and kaolinite). The REE patterns from the middle Turonian to lower Coniacian Lysing sandstone are following the trend of the upper continental crust. The quartzarenite sandstones have a wide age spectrum ranging from 90-3300 Ma and the hafnium

isotope analysis displaying a broad dispersion of ε_{Hf} (t) values from -20 to +11 for the "Caledonian" age zircons and -11 to +5 for the "Gothian" age zircons. The gross depositional environment within the quartzarenite sandstones is predominantly basinfloor or slope terrace.

6 Interpretation

6.1 Subarkose

The low CIA values of the subarkose sandstone of the Cenomanian to lower Turonian Lange megasequence indicates low weathering, which suggests less exposure to surface erosion. The detrital feldspar content with less clay cement within the pore system implies early diagenesis with a shallow burial (eogenesis) before the final lithification (Boggs, 2012). The moderate amount of porosity and grain-to-grain point contact implies less affected by physical processes such as compaction. The introduction of calcite and carbonate cement infer diagenesis, and proximity to the paleoshelf (Martinsen et al., 2005). Low Zr/Sc ratio supports this notion, with low to none recycling of the sediments and detrital glauconite input, suggesting mature sediments with a direct contribution from its source origin. The proximity of the source origin is supported by the narrow age spectrum from the U-Pb zircon dating (400-1800 Ma) pointing to a source on the Norwegian Landmass containing rocks with this age spectra (Ramberg et al., 2008). High K_2O/Na_2O ratio support this notion, implying that the sediments are originating from a continental island arc of felsic origin, which is supported by the low La/Sc and Co/Th ratios (Engel et al., 1974; Taylor and McLennan, 1985), which is different from the intra-cratonic rift setting of deposition. The low feldspar content (detrital and altered) with coarse subangular, low sphericity grains supports a short transport distance from the source. The dominance of light REE elements over heavy supports an old felsic upper continental crust deposited in a passive margin setting. A negative Eu suggests a differentiated source similar to a granitoid source terrane (McLennan et al., 1993).

6.2 Quartzarenite

The quartzarenite sandstone of the Cenomanian to lower Turonian Lange and middle Turonian to lower Coniacian Lysing megasequences have an increased La/Sc ratio, suggesting a granitic source composition from a mixed passive continental margin and continental island arc. Sutured and concave-convex grain-to-grain contacts infer compaction and deep burial. The lack of detrital feldspar grains, with abundant clay cement (illite, smectite, and kaolinite) points to alteration during diagenesis and transport (Fedo et al., 1995). The high sphericity and subrounded to

subangular grains imply longer and more active transportation from the source or by reworking of sediments. However, the sinuous change of Zr/Sc ratios from moderate, low to high, reveals how sediment is either directly fed into the basin (first order), or progressively fed by second to third order cycle depositions. The concentration of quartz relative to feldspar supports this notion as the feldspar is more susceptible to mechanical abrasion and are less likely to survive second to third order recycling (Boggs, 2012). The increased broad age spectrum of 90 to 3300 Ma, which infers deposition of the progressively unroofed hinterland, most likely through recycling or reworking of dissimilar sediments of different geographical source origin (Brown, 1991; Gallagher et al., 1998; Carter and Moss, 1999). The indication of sediments of different origin is supported by the widespread La/Sc ratios, which points to a variation in composition and tectonic setting from felsic igneous (continental island arc) to granite (passive continental margin). A mixed setting and composition imply that sediments have their origin from a complex hinterland composition; alternatively, sediments originate from different geographical regions. The abundant monocrystalline quartz with a low content of mica suggests that the quartzarenite sandstone is derived from a felsic source (Dabbagh and Rogers, 1983). The low variability of weathering patterns can be influenced by the high frequency climatic and eustatic fluctuations during the Cretaceous (MacLeod et al., 2005; Miller et al., 2005a; Miller et al., 2005b; Price et al., 2011). A second possibility is that the degree of weathering is concealed by the high concentration of SiO_2 recorded in the quartzarenite sandstones and results in lower CIA values (Nesbitt and Young, 1982). The amount of heavy REE element concentrations observed in a few quartzarenites supports a variation in source terrane and tectonic setting (McLennan et al., 1993).

7 Discussion

7.1 Cenomanian to lower Turonian Lange megasequence

7.1.1 Stratigraphic comparison

The southeastern Cenomanian to lower Turonian Lange megasequence (6507/5-A-4H) consist of an upper slope gross depositional environment (sand injectites; SK5-A-12,13) with provenance signatures from trace element ratios inferring a variability upwards in the stratigraphy (Figure 42, Figure 43, Figure 44 and Figure 45) towards a marginal-marine (shelf edge). The sand injectites in the upper slope suggest that sediments were recycled before deposition. Upwards in the stratigraphy mature sediments from a tidal bar sub-environment (same coarsening upward motif) are likely directly fed from one source (first order recycling), which is suggested by the low Zr/Sc

ratio. The variability of trace element ratios establishes a link between petrofacies and sediment recycling patterns with the gross depositional environment, where the recycled sediments within the upper slope (similar facies C2) might be erosional products from the escarpment or shelf edge.

The southern quartzarenite lower slope or base-of-slope gross depositional environment (6507/7-1) has an established stratigraphic continuity. Supported by no variation in trace element ratios (Figure 42, Figure 43, Figure 44 and Figure 45), similar felsic igneous origin and all sandstones with an origin from a continental island arc setting. A change from felsic island arc source towards a passive margin source suggests a variability within the stratigraphy. Since this change is minute compared to the strong arguments for a continuity, further U-Pb dating could establish the importance of this minute variation. The minute variation could be related to facies change of the samples from B2 to C2. Significant more recycling within every sampled sand body is observed, which infers second order recycling, supported by the high sphericity and subrounded to subangular grain texture, implying longer and more energetic transportation from the source. This notion is supported by the minute input of Archean aged zircons.

The northwestern quartzarenite lower slope or base-of-slope gross depositional element (6507/2-4; 6507/2-2) infer large stratigraphic variability. Dispersed values among the various trace element ratios within the stratigraphy of the well 6507/2-4, and upper and middle unit in well 6507/2-2 (Figure 42, Figure 43, Figure 44 and Figure 45) supports this. These variations are interpreted within different facies, which could have an influence on the results. The provenance signatures support the notion of variability in detrital zircon age spectra (Figure 41; Parker, 1967; Harland, 1997; Dibner, 1998; Grogan et al., 1998; Dallmann, 1999; Midtkandal et al., 2008; Ramberg et al., 2008; Koryakin and Shipilov, 2009; Fossen, 2010; Corfu and Heim, 2013; Myhre et al., 2013; Bergh et al., 2015; 400-1900 Ma in MA2-2-8 and 350-1700 Ma in MA2-2-16) and the dispersed $\varepsilon_{Hf}(t)$ values (Figure 38; MA2-2-8 with -9 to 0 and MA2-2-16 with +3 to +6). The different U-Pb age population points to an origin from a complex hinterland composition; alternatively, sediments originate from different geographical regions such as the Western Gneiss Region and the West Troms Basement Complex (Ramberg et al., 2008). Stratigraphic variability is established by hafnium isotope analysis, where the crustal recycling of the protosource for the middle unit (MA2-2-16) pointing to crustal evolution path towards the Western Gneiss Region rocks (Ramberg et al., 2008). The upper unit (MA2-2-8) implies that zircons are derived from protosource compared to

the northern Norway and the Western Gneiss Region (Nordgulen et al., 1995; Koistinen et al., 2001; Ramberg et al., 2008). Moderate CIA values reveal a change in the weathering trend, which suggests progressively surface erosion. Sutured to point grain-to-grain contacts implies varying degree of compaction. The sinuous change of Zr/Sc ratio from moderate, low to high, within the same gross depositional environment of the lower slope and architectural element slope channel complex supports a variation. Two samples stratigraphically 4 meters apart (MA2-4-17 and MA2-4-19), suggests that the sediments are progressively recycled from one large mixed source, further originating from individual source regions (Pettijohn et al., 1987). Subsequently indicating an internally stratigraphic variability within a base-of-slope gross depositional environment of different facies (D2 and B3). The recycling from one large mixed source suggests a link between the gross depositional environment and stratigraphic variability unraveled by provenance signatures. The link infers that first to third order recycled sediments are likely to deposit in the base-of-slope environment either directly from the continental shelf and or by stacking of directionally alternating lobe systems. However, the large variability within a 4 meters depth with a thin mudstone interval separating the two fining upward motifs, may be influenced by facies change (Figure 45). The facies change to heterolithics implies a grain size and composition (MA2-4-19) change with an abundant input of dark material (e.g., Sc element), which could influence the results of the data. The same issue is implied to the northeast by the lower slope gross depositional environment (6607/12-2S), where ditch cuttings were retrieved. The provenance signature is established to have the same recordings as with the sampled shales (*Æ*R3-9S-22,23, MA2-2-7,13, and SK5-A-10,11), which implies a more considerable contribution of dark material, giving erroneous readings compared to the homogeneous medium grain sized sandstones. The contribution of dark material implies less provenance control, suggesting using heterolithics together with “clean” sandstones is not applicable within the scope of this provenance study.

7.1.2 Lateral comparison

The trace element ratios imply a lateral comparison from the marginal-marine and upper slope (6507/5-A-4H) to the deepest Cenomanian Lange quartzarenite in the northwest (6507/2-4 and MA2-4-14) and to the southwest (6507/7-1). The lateral comparison implies a link from the upper slope and marginal-marine to the lower slope or base-of-slope gross depositional environment (Figure 45). A link between the gross depositional environment is supported by the minute variations of U-Pb detrital zircon age spectra (Figure 44). The frequent 1.7-1.8 Ga and 1.2-1.25

Ga zircon ages (Figure 44; SK5-A-2+8, MA2-4-20, and MA2-2-16) are in accordance with a sediment source originating from rocks of the Norwegian Landmass. A lack of essential data from U-Pb zircon analysis makes a connection with the upper slope sand injectites outwards in the basin more uncertain. An expected change in petrofacies supports a link of the gross depositional environment away from the continent and onto the terrace from subarkose to quartzarenite petrofacies. Supported by a gradual decrease in coastal detrital glauconite and an increase in sediment recycling patterns. Additionally, this may infer the transport direction of the sediments deriving from the continent outwards onto the reservoir fairway on the terrace.

7.1.3 Conclusion

Stratigraphic variability is inferred with trace element ratios dependent on the gross depositional environment such as upper slope (6507/5-A-4H) to marginal-marine (6507/5-A-4H) and within the base-of-slope from the middle unit (6507/2-2; MA2-2-16) into the upper unit (6507/2-2; MA2-2-8). Provenance signatures elucidate a connection between the gross depositional environments and stratigraphic variability by a mixed setting and composition implying sediments origin from either a complex hinterland composition or from different geographical regions. Stratigraphic consistency, with minute variability, is suggested within the lower slope (6507/7-1); however, a lateral comparison is implied by U-Pb zircon dating within different gross depositional environments. Additionally, petrofacies and sediment recycling patterns are linked with the gross depositional environment. Stratigraphic variability is indicated where sediment recycling patterns increases independent on petrofacies. A caution in interpretation of various signatures from facies change of heterolithics to “clean” sandstones is suggested.

7.2 Middle Turonian to lower Coniacian Lysing megasequence

7.2.1 Stratigraphic comparison

The trace element ratios (Figure 42, Figure 43, Figure 44 and Figure 46) infer a stratigraphic variability of the basinfloor or slope terrace quartzarenite Lysing megasequence within facies B1 and B2 (6507/5-8). The constant moderate sediment recycling pattern supports this notion. The origin of tectonic setting from passive continental margin to continental island arc and a mixed source rock composition between felsic igneous to granitic have their origin from a complex hinterland composition; alternatively, sediments originate from different geographical regions. Supported by the broad U-Pb age spectrum (Figure 44; 90-2800 Ma from ÆR5-8-9) suggesting that the sediments are derived within a large source from the individual source regions in the

Barents Sea. The Norwegian Landmass to the east is in this case less likely as sediment recycling is too high. Excluding the Norwegian Landmass as a source region is supported by the hafnium isotope analysis, which suggests a juvenile to a Palaeoproterozoic protosource of the "Caledonian" and "Gothian" aged zircons (Levchenkov et al., 1995; Nordgulen et al., 1995; Koistinen et al., 2001; Ramberg et al., 2008). The assumption that recycling of sediments and variability is linked to the gross depositional environment mentioned previously, is also valid for the basinfloor. The assumption that recycling of sediments and variability is linked to the gross depositional environment infers that the basinfloor is subjected to sediment dispersal coming from one large supply system from the north, which has eroded into a larger hinterland. The notion of a large supply system from the north is supported by the abundant concentration of quartz minerals and clay cement.

The basinfloor or slope terrace of the middle Turonian to lower Coniacian Lysing in the middle of the Dønna Terrace (6507/3-9S) reveal a sinuous change of Zr/Sc ratios from moderate, low to high upwards in the stratigraphy, revealing a stratigraphic variability (Figure 42, Figure 43, Figure 44 and Figure 46). Scattered Zr/Sc ratios imply how sediment is either directly fed into the basin (first order), or progressively fed by second to third order cycle deposition. One sampled interval is interpreted with a subarkose petrofacies with low recycling (*Æ*R3-9S-21), which would imply a first order recycling with proximity to its source (Norwegian Landmass?). The wide U-Pb age spectrum supports the variability of Lysing sand bodies from 250-3300 Ma (Figure 44; *Æ*R3-9S-2) towards a spectrum of 90-2850 Ma (Figure 41; *Æ*R3-9S-14) downwards in the stratigraphy. The juvenile protosource supports this notion from the "Gothian" aged zircons (Figure 41; *Æ*R3-9S-2) and the older protosource from both the "Caledonian" and "Gothian" aged zircons (Figure 41; *Æ*R3-9S-14). The difference in age spectra corresponds to the variability of the degree of sediment and crustal recycling, which implies local (direct) to regional (recycled) origin of sediments. The same variability is observed from the trace element ratios (Figure 42 and Figure 43), where different sand bodies (different fining upward motifs) are interpreted with discordant values compared to the "norm" of the others. The stratigraphic variability is dependent on the basinfloor gross depositional environment, as mentioned before. In the sense that a large variability within a stratigraphy is more likely to occur on the basinfloor, as this would be a common depositional environment of sediments with a local origin and origin from a complex hinterland composition of different geographical regions.

The constant first to second order recycling combined with the trace element ratios (Figure 42, Figure 43, Figure 44 and Figure 46) suggest stratigraphic continuity for the northwestern basinfloor middle Turonian to lower Coniacian Lysing quartzarenites (6507/2-2). The clustered La/Sc ratio points to less variability of the source rock composition and tectonic setting within the same facies B3, which is supported by the missing Middle Proterozoic and Phanerozoic components from the U-Pb zircon ages (Figure 44; 850-3100 Ma). The hafnium isotope analysis indicates an Archean protosource for the "Gothian" age zircons (Figure 41) implies a different sediment source region. Supported by a significant constituent of Archean rocks, which was unaffected by the Caledonian orogeny. Alternatively, during transportation into the basin the eroded recycling sandstones or reworked sandstones of the Caledonian age were excluded.

Well 6507/2-4 located east of well 6507/2-2 in the northwestern sector has a basinfloor gross depositional environment within the middle Turonian to lower Coniacian Lysing megasequence. Stratigraphic variability is inferred by low to high degree sediment recycling patterns, with different source rock composition and tectonic setting (Figure 42, Figure 43, Figure 44 and Figure 46). However, the variability is limited to the shallowest part in the stratigraphy (MA2-4-1; facies B1). This notion is supported by the trace element ratios, where significant discrepancies separate the upper stratigraphy from the lower. The variability is not dependent on the facies, moreover a change of lobe systems. The broad age spectrum from the U-Pb zircon dating (Figure 44; MA2-4-4; 350-2800 Ma) implies that sediments are derived from the Norwegian Landmass, most likely in the north (Levchenkov et al., 1995; Nordgulen et al., 1995; Koistinen et al., 2001; Ramberg et al., 2008). ε_{Hf} (t) values imply crustal recycling from a juvenile to Archean protosources, which supports a northern source for the sediments (Figure 41).

7.2.2 Lateral comparison

A north (*Æ*R3-9S-14) to the south (*Æ*R5-8-9) lateral connectivity is inferred between the basinfloor elements with similar Phanerozoic provenance signature from the U-Pb dated zircons. The stratigraphic variability (*Æ*R3-9S-21) suggests that the sediments are provided by different sediment transportation direction on to the basinfloor (Figure 46). A vertical change in the stratigraphy (*Æ*R3-9S-2) by an older Archean input, suggesting an added source by a higher order recycling, or a change of sediment transport direction onto the basinfloor. The variability in sediment recycling supports this notion. Similar provenance signatures support lateral connectivity of the middle Coniacian to lower Turonian in the north (*Æ*R3-9S-2 and MA2-4-4). The age

spectrum (850-3100 Ma) implies lateral discontinuity from the northwestern-most Lysing megasequence (MA2-2-4). The 850-3100 Ma age spectrum is unidentified by other studies in the Norwegian Sea (Morton and Grant, 1998; Fonneland et al., 2004; Morton et al., 2005). The unidentified age spectrum draws an assumption that this system is limited to the northwestern part of the Dønna Terrace (6507/2-2). However, further downwards in the stratigraphy another provenance signature suggests internal sediment variation within the same depositional element of the channelized-lobe complex. However, by a slight hiatus in sediment input, and a different fining upward trend noted by the short interval of basinplain facies between two individual fining upward sand bodies could support the relocation of source transportation direction. This notion needs to be further supported by additional U-Pb zircon dating.

7.2.3 Conclusion

Stratigraphic variability and consistency by provenance signatures are implied for the middle Coniacian to lower Turonian Lysing megasequence. The basinfloor gross depositional environment creates variations in provenance signatures with sediment deposition from different directions. Lateral connectivity and discontinuity are inferred by provenance signatures, and especially single grain U-Pb and hafnium analysis.

7.3 Cenomanian Lange vs. Coniacian to Turonian Lysing

7.3.1 Stratigraphic comparison

Two cores (6507/2-2 and 6507/2-4) contain both lower slope Cenomanian to lower Turonian Lange megasequence and basinfloor middle Turonian to lower Coniacian Lysing megasequence. The stratigraphic variability is evident by the difference in the gross depositional environment, which creates different provenance signatures. Upwards in the stratigraphy (6507/2-4) variability is implied within the lower slope gross depositional environment in the middle unit (Cenomanian to lower Turonian Lange megasequence) to the basinfloor of the Lysing megasequence. Stratigraphic differences are evident upwards in the stratigraphy of well 6507/2-2 from a lower slope (Cenomanian to lower Turonian Lange megasequence) with provenance signatures pointing towards the Norwegian Landmass. A basinfloor gross depositional environment indicating a northern source (middle Turonian to lower Coniacian Lysing megasequence), and a last middle unit pointing to a unique source region from the northwest (middle Turonian to lower Coniacian Lysing megasequence). However, the variations in provenance regions might imply that a large sediment supply system which has eroded into a large hinterland in the North e.g. the Barents Sea.

The Barents Sea hinterland has then drainage systems connected to the different provenance regions. The variations in stratigraphic provenance signatures imply that gross depositional environment influences the stratigraphic variability independent of a change from one megasequence to another.

7.3.2 Lateral comparison

From the trace element ratios (Figure 42 and Figure 43), a lateral consistency is inferred by most sand bodies within both megasequences. Supported by the sand bodies that have similar tectonic setting and source rock composition. A similar pattern is observed within the recorded signature from the U-Pb zircon data (Figure 44). However, it is within the age spectrum that the differences are visible. The most persuasive evidence is the input of Phanerozoic and Archean input, which suggest different source regions. The different source regions are supported by hafnium analysis, which suggests juvenile protosources for the Cenomanian to lower Turonian Lange megasequences compared to the older Palaeoproterozoic and Archean protosource in the Lysing megasequence (Figure 41). However, the provenance signatures from the U-Pb and hafnium analysis contradicts with the recorded signatures within the whole-rock geochemical and petrographical analysis, in the sense that there is lateral variability between the megasequences. Specific age spectra are unrelated to each other, which denotes other provenance methods such as petrography and whole-rock geochemical analysis to be less practical in defining lateral connectivity. The repercussion is that previous assumptions from other studies are not reliable and it is difficult to base lateral connectivity purely on source rock composition and tectonic setting from which they originate, and that age of the zircons within a rock (crustal separation age and metamorphic age) is a key.

7.3.3 Conclusion

Stratigraphic contrasts are linked with the gross depositional environment, suggesting that both basinfloor and lower slope are related to stratigraphic variability. Lateral comparison is difficult, due to similar source rock composition and tectonic setting. However, single grain analysis such as U-Pb and hafnium are better tools for comparing lateral consistency by separating specific age spectra and protosources.

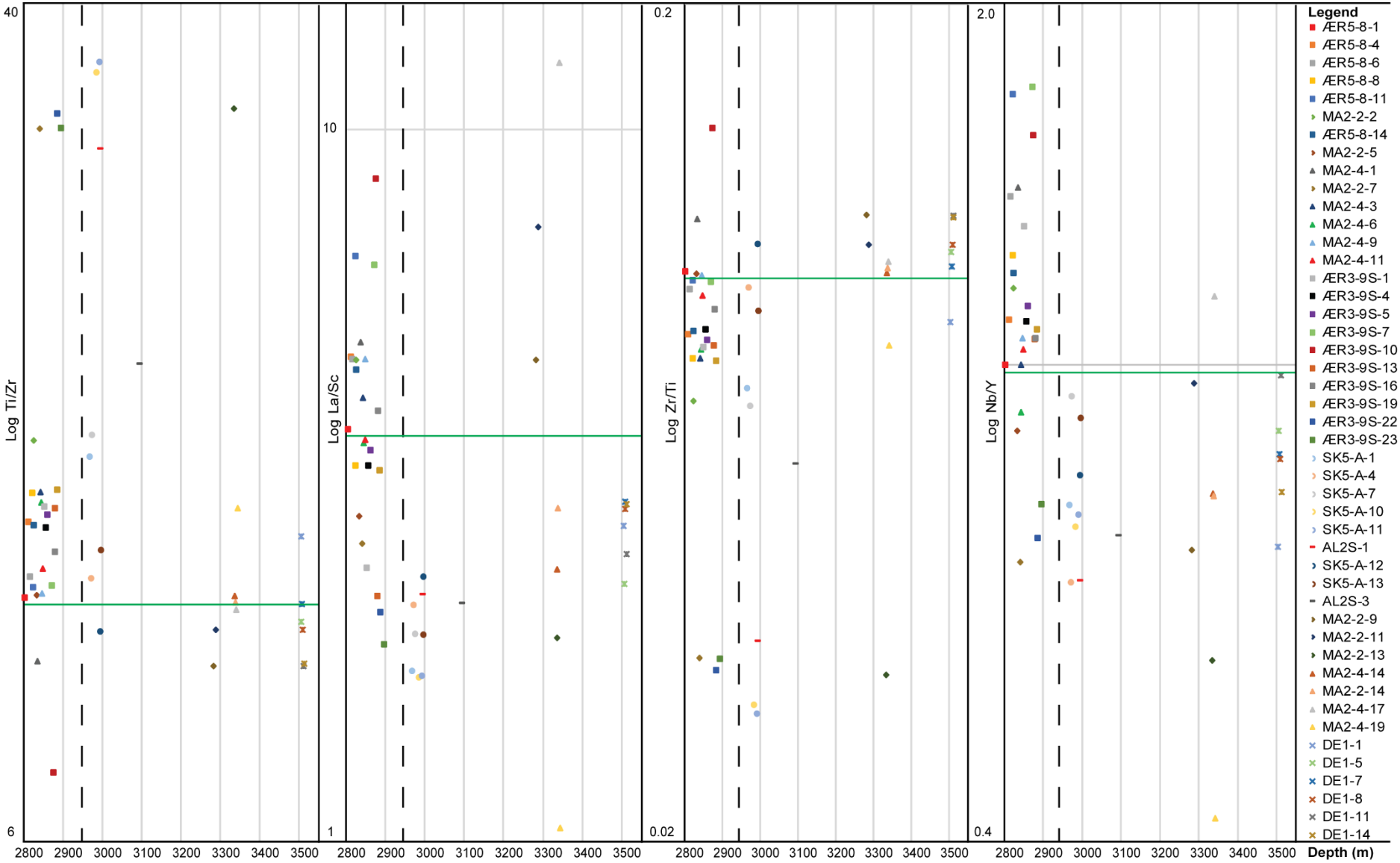

Figure 42: Provenance signatures and correlation of trace element ratios. Dotted black line is the boundary between the Lysing and Lange samples. Green line is the correlation line.

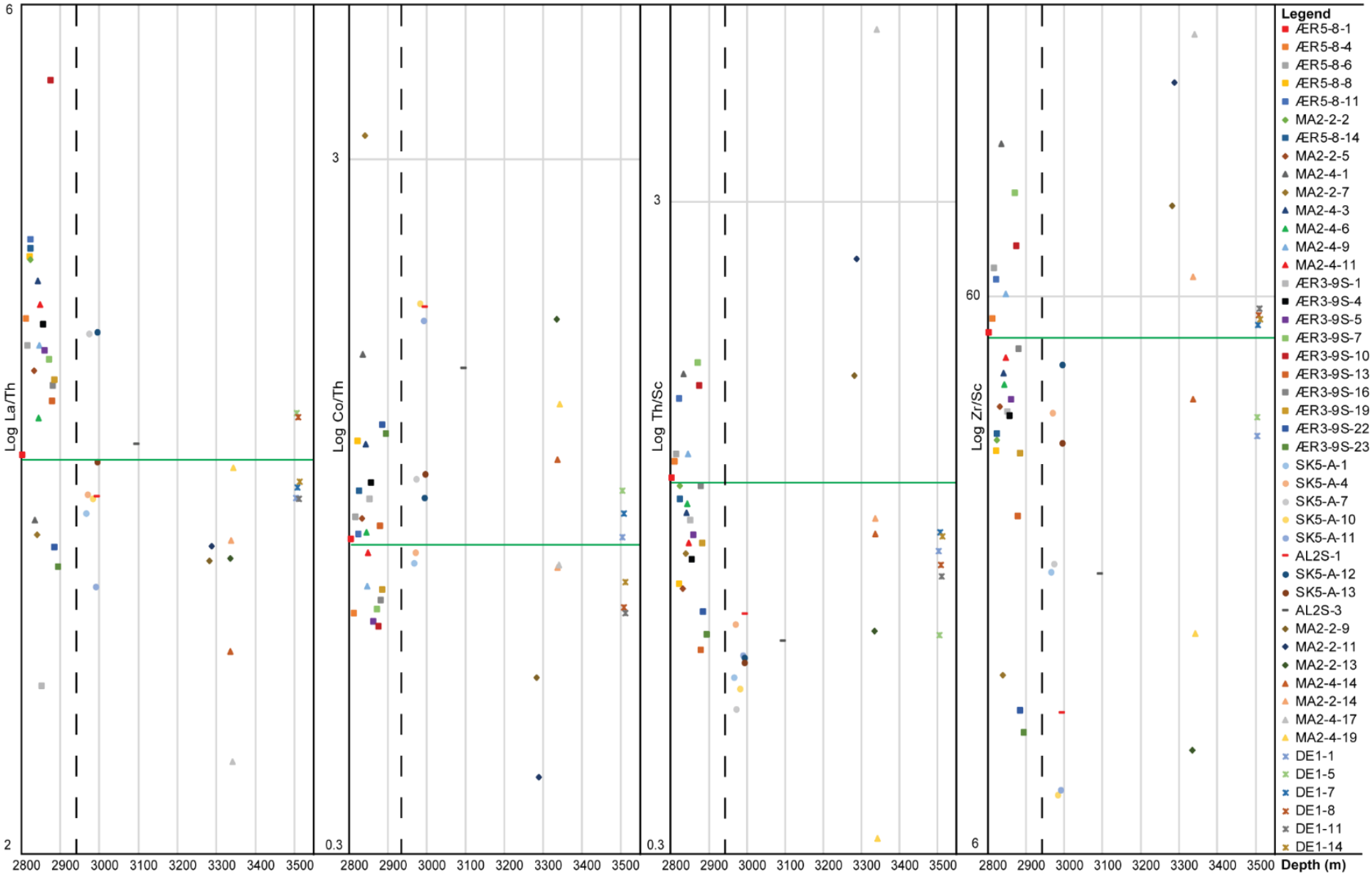

Figure 43: Provenance signatures and correlation of trace element ratios. Dotted black line is the boundary between the Lysing and Lange samples. Green line is the correlation line.

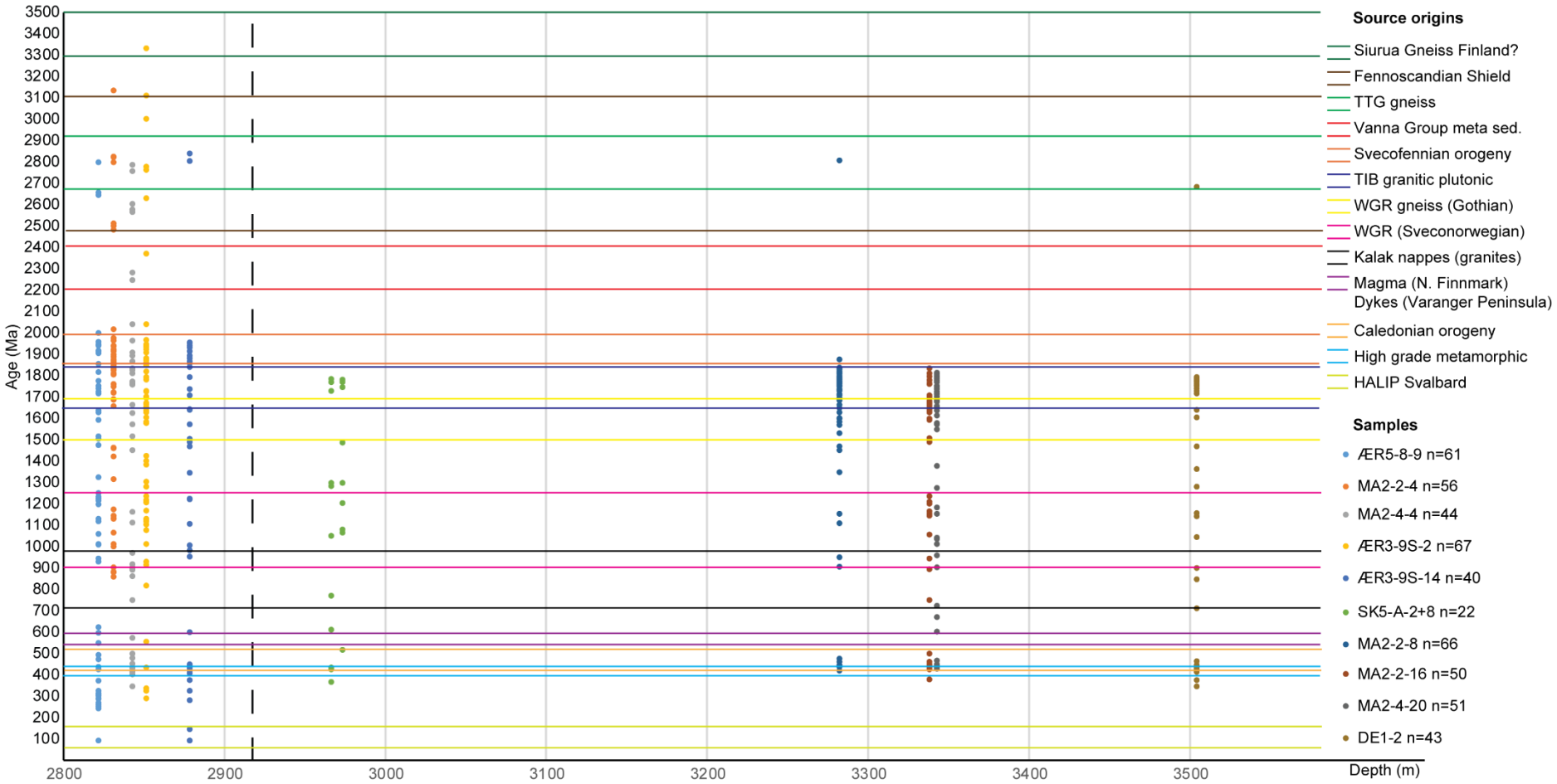

Figure 44: Stratigraphic variability of the U-Pb ages collected from the 11 samples. Dotted black line indicates the boundary of the Lysing Formation samples (2800-2920 m) and the Lange Formation (2920-3550 m). The colored lines indicate the possible source origin. Reference from the source origins are: Ramberg et al. (2008) Siurua Gneiss Finland?, Fennoscandian Shield, Vanna Group meta sed., TIB granitic plutonic,and Magma (N.Finnmark) Dikes (Varanger Peninsula), Fossen (2010) Western Gneiss Region (Sveconorwegian), Kalak nappes (granites), Caledonian orogeny and High grade metamorphic, Bergh et al. (2015) Svecofennian orogeny, Myhre et al. (2013) TTG gneiss and Midtkandal et al. (2008), Dallmann (1999), Grogan et al. (1998), Corfu et al. (2013), Harland (1997), Parker (1967), Dibner (1998) and Koryakin and Shipilov (2009) for the HALIP Svalbard.

7.4 Implications

7.4.1 Provenance development

The texture, sorting and clay content are essential factors which have a significant link to the lithofacies. The essential factors and lithofacies are controlled by the gross depositional environment, which suggest that reservoir quality and reservoir properties are controlled by provenance. The degree of compaction revealed by a progressively packing of detrital grains is linked to a decrease in intergranular porosity. The concentration in detrital feldspar with less clay cement represents chemical destruction from either diagenesis or dissolution by weathering (Boggs, 2012). The feldspars are also more prone to mechanical fragmenting, mechanical abrasion, and are less likely to survive recycling or reworking than the detrital quartz grains (Boggs, 2012). Reservoir quality is dependent on the clay content, sorting, and amount of matrix, which can affect the primary porosity.

7.4.1.1 Cenomanian to lower Turonian Lange megasequence

7.4.1.1.1 Stratigraphic comparison

The subarkose marginal-marine (6507/5-A-4H) was weakly compressed with progressively packing of detrital grains, followed by an increase of intergranular porosity upwards in the stratigraphy, pointing to variable reservoir quality. The very good sorting and subrounded grains could either point to a mass transport or a single sediment transport system. The entrainment process by suspended load points to a continuous energetic flow or current with less traction (Boggs, 2012). The abundant detrital alkali feldspar supports a single sediment transport system close to the continent, whereas in the top sampled sand body, this changes to poor sorting with angular grains (Boggs, 2012). The medium to coarse, poorly sorted angular sediments reveals a change to higher energy and reworking from temporary storage, containing coarser angular sediments. Another possibility is a change in erosion and weathering patterns, perhaps a variation in climate (Boggs, 2012). The notion of a change in climate is supported by the high frequency climatic and eustatic fluctuations during the Cretaceous (MacLeod et al., 2005; Miller et al., 2005a; Miller et al., 2005b; Price et al., 2011). Indication of a change in reservoir quality is observed by a variation in intergranular porosity and an increase in clay cement. Supported by the decrease in detrital feldspar upwards in the stratigraphy, which indicates a varying degree of chemical compaction (Boggs, 2012). The texture and sorting are important factors in defining the depositional environment of the delivery system. The important factors infer that provenance

signatures are strongly linked to the depositional environment and the transportation delivery system.

The quartzarenite in the upper slope in the southwest (6507/7-1) infer compaction predominantly by concave-convex and sutured grain-to-grain contacts, suggesting a more consistency within the stratigraphy (facies B2). The quartzarenite petrofacies with moderately poor to good sorting suggests reworking of grains within a mass transport system; subsequently, the aligned grains point to last depositional forces to be within a laminar flow (Dott, 1966). The decrease in feldspar content from the marginal marine to the upper slope combined with an increase in clay cement, point to a reduction in reservoir quality. A reduction in reservoir quality is suggested by a progressive reduction in intergranular porosity upwards in the stratigraphy of the upper slope. The decrease in detrital feldspar content and increase in clay cement points to an increase in chemical compaction and mechanical abrasion. The increase in chemical compaction and mechanical abrasion points to reworking or recycling of the less stable feldspar from long-term storage. Another suggestion is that they are originating from a source with less mineral feldspar composition. The architectural element of the slope channel complex infers a link between the reservoir quality and the stratigraphic consistency of the deposited sediments.

The quartzarenites within the lower slope in the northwest of the Dønna Terrace (6507/2-2; 6507/2-4) infers a variability by progressively increase in the distance from the continent, with a transition from angular to rounded grains. A further decrease in the feldspar content with an increase in clay cement, suggest further mechanical abrasion, chemical compaction, and compaction by plane to sutured grain-to-grain contact. However, intergranular porosity is increasing upwards in the stratigraphy followed by subrounded and concave-convex grain-to-grain contact. The shallowest sandstone (MA2-4-16) imply low reservoir quality by a high concentration of clay cement (33 %) and low intergranular porosity (0.5 %). The reduction of reservoir quality could be related to facies change from B3 to B1 (Figure 45). The indication of the total feldspar content (detrital and cement) suggest a source rock with a high composition of feldspar, relative to the other sandstones. The difference of feldspar content implies an internal stratigraphic variability within the architectural element of the slope channel complex.

7.4.1.1.2 Lateral comparison

It is difficult to laterally relate individual sandstones to each other based on provenance development. However, it is possible to link the gross depositional environments by comparing provenance development and reservoir quality. The link between the gross depositional environment, architectural element and reservoir quality is implied by a progressively lower reservoir quality from the marginal marine (architectural element delta front or prodelta), and outwards to the upper slope and into the lower slope environments (architectural element slope channel complex). From this point of view, lateral comparison of individual sandbodies gives inconclusive results as there is a large stratigraphic variability of the reservoir quality between both megasequences.

7.4.1.2 Middle Turonian to lower Coniacian Lysing megasequence

7.4.1.2.1 Stratigraphic comparison

The quartzarenite basinfloor in the middle of the Dønna Terrace (6507/5-8) is inferred with a stratigraphic variability of the reservoir properties. The sinuous change of sorting, rounded to subangular and sutured to point and plane contact, indicates different mechanical compaction. The sinuous change could imply internal variations within the same facies (B1) and the same lobe system. However, separated lobe systems by baffle zones could infer a variation in source origin from a local to a regional. The sinuous change of a local to a regional source is supported by the low amount of feldspar and high clay cement content, which suggests more extensive chemical alteration during transportation or burial.

The same signature is inferred from the quartzarenite basinfloor further north from well 6507/5-8 in well 6507/3-9S. However, the varying roundness and sphericity from rounded to subangular and low to high, suggest a difference in the entrainment process from bedload with more traction to a suspended load (Boggs, 2012). The different entrainment processes are supported by the alignment of grains within different facies (B1 and B2) and lobe systems, which suggest a laminar flow to turbulent flow with no alignment and moderately poor sorting. The only variability observed is that of the energy and flow changes, whereas a change in source origin or sediment transportation proves inconclusive. However, a variation in reservoir quality is evident by a difference in mechanical compaction, and the sorting degree, supported by the varying intergranular porosity from 6 % to 15 %. Although the high abundance in detrital feldspar, a decrease in clay cement and a high intergranular porosity (15 %) in the lowest sampled sandstone,

points to a proximal source not far from the basin. An indication of a local or a regional source is complicated to assume based on the basinfloor gross depositional environment. However, a link between the different reservoir quality within the stratigraphy could imply that either the processes within the depositional environment or the distance from the source have affected the different reservoir quality. Where the composition of a complex hinterland is implemented.

Only one quartzarenite sandstone was sampled in the basinfloor within the northwestern well 6507/2-2. Very good sorting and subrounded grains with concave-convex, support a continuous suspension of the grains, most likely within a turbulent flow (Boggs, 2012). Severe mechanical compaction is evident by the concave-convex grain-to-grain contact, with a deeper burial supported by the increase in clay content, suggesting diagenesis. However, intergranular porosity of 13 % suggests a quantity of the primary porosity is preserved, supported by the total porosity loss of 29 %.

The quartzarenite basinfloor of the northwest middle Turonian to lower Coniacian Lysing megasequence (6507/2-4) infer a variability of the reservoir quality by an increase in clay cement and reduction in intergranular porosity. An increase in clay cement suggests variable chemical alteration by weathering or diagenesis and varying mechanical compaction by different grain-to-grain contacts. The point to plane contacts suggests low mechanical compaction; however, the high sphericity supports a longer more energetic transportation towards the depositional basin. The variation is within different fining upward motifs (different facies B1 and B2 an lobe systems) and could imply a difference of source origin and an internal variation within the architectural element. The decrease in reservoir quality basinward supports the notion that reservoir quality is dependent on the gross depositional environment and the original composition of the parent rock.

7.4.1.2.2 Lateral comparison

A lateral comparison by provenance development is proving difficult. Although there are variabilities of the reservoir quality within the stratigraphy, where these are incomparable with other intervals from other wells. However, they give additional information for interpretation of U-Pb geochronology. An assumption that correlation by reservoir quality in between similar gross depositional environments gives inconclusive results, in the sense that they originate from different sources or parent rocks with different composition and by a mixed sediment supply system.

7.4.1.3 Cenomanian Lange vs. Coniacian to Turonian Lysing

7.4.1.3.1 Stratigraphic comparison

Indication of a gradual variability within both megasequences (6507/2-2 and 6507/2-4) is implied by the progressive changes of reservoir quality and properties from a basinfloor to lower slope. The gradual variability of reservoir quality infers a detachment from individual lobe systems (facies change from C2 and B2) within both megasequences. The variability of the reservoir quality implies a connection with the gross depositional environment within both megasequences.

7.4.1.3.2 Lateral comparison

The provenance development from the marginal marine (Cenomanian to lower Turonian) to the basinfloor gross depositional environment (Lysing megasequence) suggest a connection by the decrease in reservoir quality. The connection by a decrease in reservoir quality is only an assumption; however, it is crucial additional information to the U-Pb zircon dating, which can reveal a connection between individual lobe systems of the megasequences.

Figure 47 has been included to visualize the stratigraphic variability and consistency of provenance signatures within the different cores (Figure 45 and Figure 46), within the correlated sequence stratigraphic units of the megasequences.

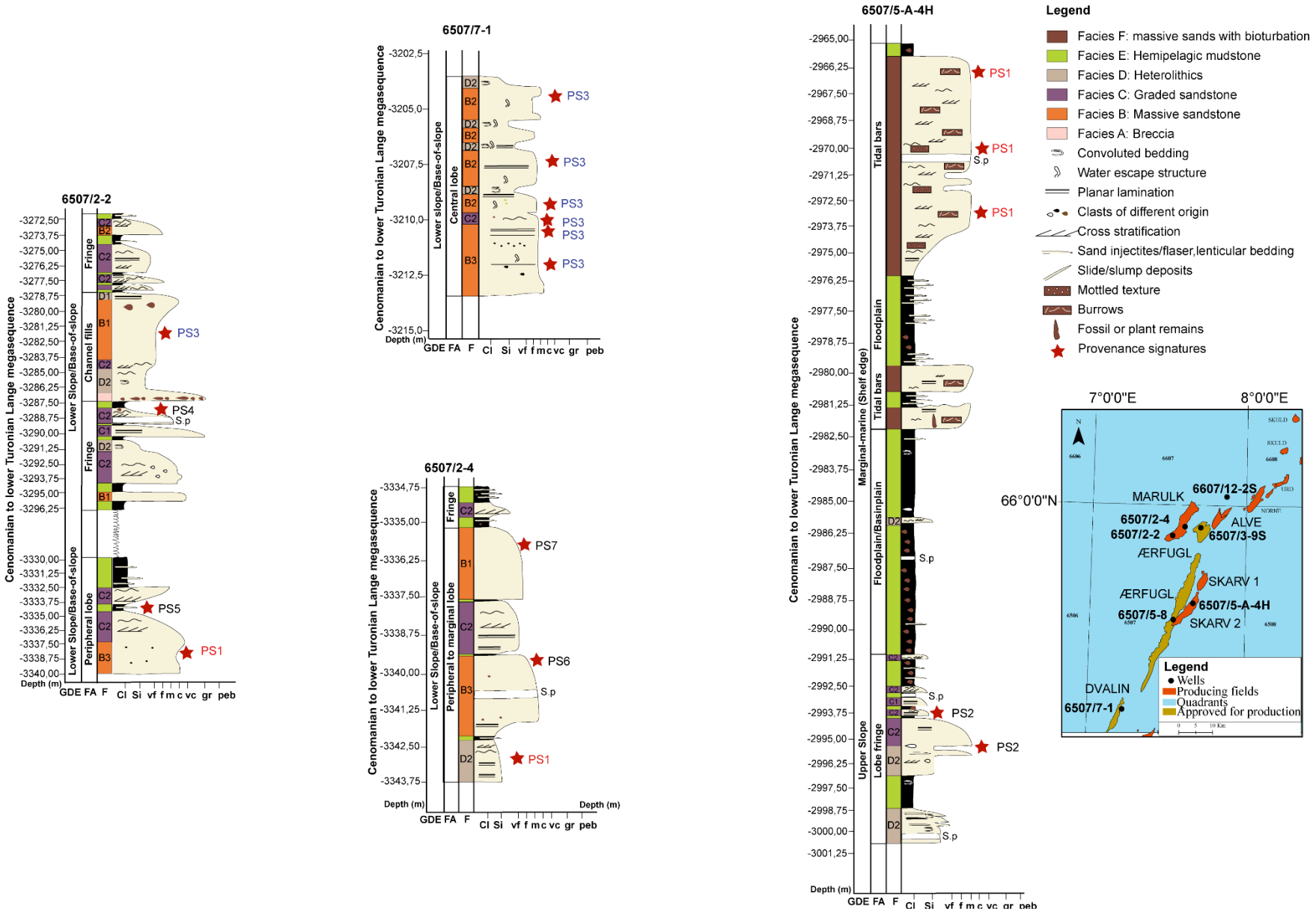

Figure 45: Provenance signatures from sand bodies within the Cenomanian to lower Turonian Lange megasequence. S.p=Seal peel. Red and blue letters infer lateral connectivity.

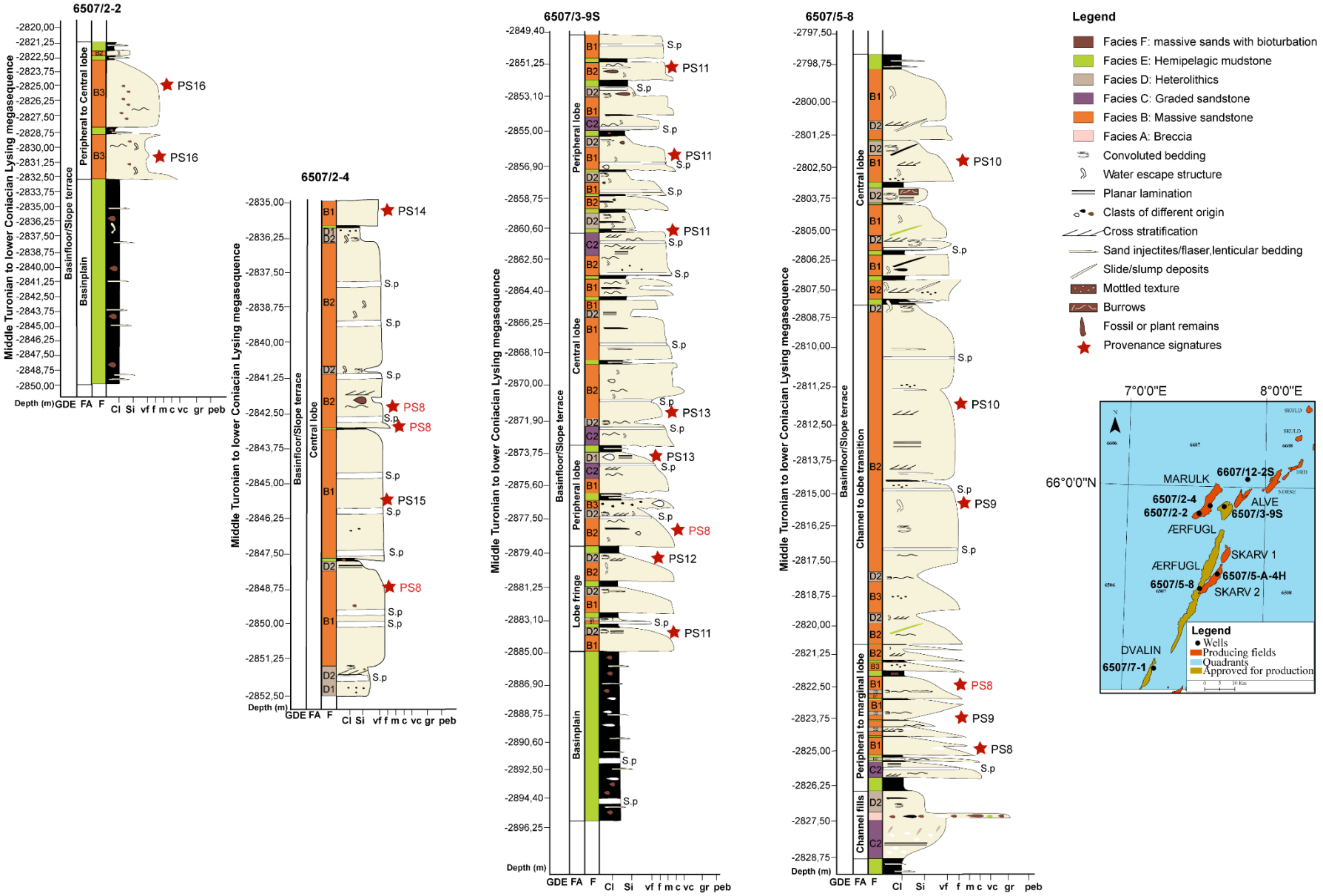

Figure 46: Provenance signatures from sand bodies within the middle Turonian to lower Coniacian Lysing megasequence. S.p=Seal peel. Red and blue letters infer lateral connectivity.

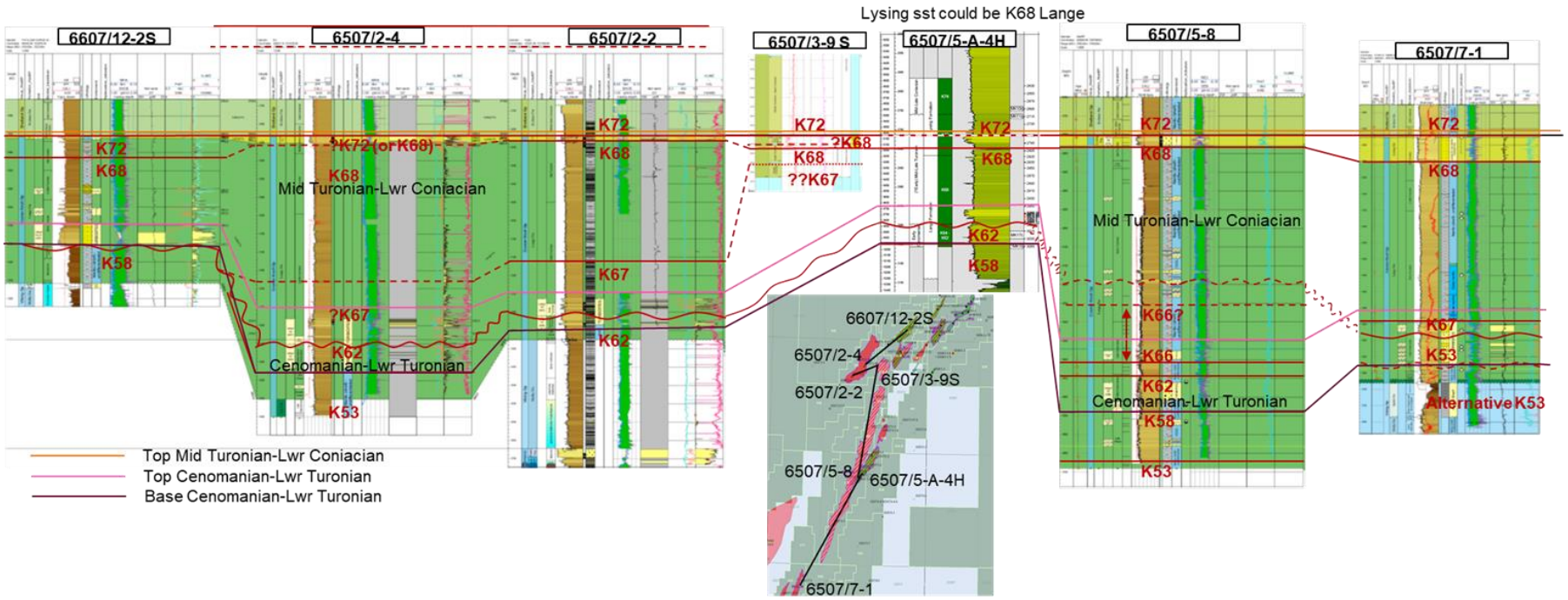

Figure 47: Well correlation of sequece stratigraphy units within the Cenomanian to Coniacian Lange-Lysing megasequence, covering all the wells within the scope of this study. Courtesy of Aker BP.

7.4.2 Sediment delivery system development

7.4.2.1 Southeastern direction

The frequent 1.7-1.8 Ga and 1.2-1.25 Ga zircon ages in the Cenomanian to lower Turonian Lange megasequence (SK5-A-2+8, MA2-4-20 and MA2-2-16) are in accordance with sediment transport from the southeast (Figure 48; modified from Fugelli and Olsen, 2007). The Trans-Scandinavian Intrusive Belt being of 1650-1850 Ma age in the northern part of the Western Gneiss Region (Ramberg et al., 2008) can explain this. There also felsic, and thus potentially zircon-bearing, 900-1250 Ma intrusive that is related to the Sveconorwegian orogeny occur (Kullerud et al., 1986; Skår, 1998; Skår, 2000). The detrital 400-500 Ma ages of the Caledonian orogeny could originate from the Western Gneiss Region. Although they are scarce in this region, they have been located within the ultrahigh pressure terrane (UHP; Terry and Robinson, 2003). The less frequent 1500-1750 Ma can be explained by the felsic to ultramafic plutonic rocks of the Gothian orogeny in the southern Western Gneiss Region (Kullerud et al., 1986; Austrheim and Mørk, 1988; Skår, 2000).

The notion of a southeastern source contradicts with that of Morton et al. (2005) provenance of Late Cretaceous to Paleocene submarine fan sandstones in the Norwegian Sea. Morton et al. (2005) study rule out a source from the Western Gneiss Region, due to the lack of a distinctive type C Garnet suite. Morton et al. (2005) argued that the juvenile Proterozoic ages represent erosional products of Caledonian granitoids. Although signature points to a Western Gneiss Region source provenance, the relatively low number of concordant zircons (n=22) could disguise a broader age spectrum than reflected from the U-Pb zircon age results. The low number of concordant zircons opens a debate for another source, coming from the Norwegian Landmass further north in western Trøndelag. Here a study by Gee et al. (2014) reveal the same age patterns, as within the Western Gneiss Region, from samples taken from schist in the Seve Nappe complex (Upper Allochthon). However, a prominent Caledonian and Archean age signature are recorded from the Seve northwestern-most complex, with a less prominent Early Proterozoic age spectrum. The lack of a prominent Archean age signature contradicts with the results obtained from samples MA2-4-20, MA2-2-16, and SK5-A-2+8. The narrow age population of 1250 Ma is distinctive of the dolerite dikes, which intruded the Gothian plutonic rocks in the Hustad Igneous Complex within the Western Gneiss Region, dated to 1251 Ma (Austrheim et al., 2003). Together with the recorded age spectrum from the Lange sandstone in the Agat Field (Fonneland et al., 2004), which are similar to those recorded in the Cenomanian to lower Turonian Lange sandstones on the Dønna

Terrace (MA2-4-20, MA2-2-16, and SK5-A-2+8), supports a southeastern source direction from the Western Gneiss Region. A southeastern source direction is supported by hafnium isotope analysis. The ε_{Hf} (t) values of +2 to +4 of the "Caledonian" age in the Cenomanian to lower Turonian Lange sandstones (MA2-2-16) is in accordance with a sediment transportation direction from the southeast (Figure 41). A sediment transport direction from the southeast is supported by the protosource of the "Caledonian" age dated zircons, which points to crustal recycling from a juvenile protosource with a crustal formation age in the Neoproterozoic. The Neoproterozoic age could point to an early (920-1300 Ma) felsic or mafic magmatism within the Sveconorwegian orogeny in the Western Gneiss Region (Andersen et al., 2011 and references therein). The "Gothian" zircon age suggest crustal recycling from a protosource originating from the Trans-Scandinavian Intrusive Belt, with a juvenile crustal formation age.

7.4.2.2 Northeastern direction

The Cenomanian to lower Turonian Lange megasequence in the south and north (6507/7-1 and 6507/2-2) with a frequent age spectrum of 1750-1800 Ma and 400-450 Ma, and its subordinate Archean age (2700 Ma) are in accordance with sediment transport from the northeast (Figure 48; modified from Fugelli and Olsen, 2007). The northeast sediment transport direction can be explained by the Trans Scandinavian Intrusive Belt of 1650-1850 Ma age, which corresponds to the second magmatic pulse. The second magmatic pulse intruded the Archean and the Proterozoic basement windows, where plutonic rocks solidified during a short period on the Lofoten-Vesterålen (Corfu, 2007; Ramberg et al., 2008). The short crystallization period of the Trans Scandinavian Intrusive Belt rocks on Lofoten corresponds to the elongated zircons observed in this sandstone (Corfu, 2003b). The Phanerozoic signature corresponds to the Caledonian nappes located on Lofoten, together with the Archean signature, which points to the Gullesfjorden Granite (Ramberg et al., 2008). The Archean granite on Lofoten is considered a part of the Baltic Shield with an age range of 2.6-2.7 Ga (Griffin et al., 1978).

The frequent age spectra recorded in the Cenomanian to lower Turonian Lange megasequence is also in accordance with the signatures deriving from the rocks on the West Troms Basement Complex. Especially the Ersfjord granite (1.79 Ga), which corresponds to the high peak in the Early Proterozoic. However, the Archean rocks around 2.6-2.7 Ga on the West Troms Basement Complex are of mafic origin, which contradicts with the felsic composition recorded within the samples (Ramberg et al., 2008). However, basement gneisses in the central West Troms Basement

Complex (Kvaløya and Senja), with its overlying felsic and mafic igneous rocks (1.7-1.8 Ga) are dated to around 2.6-2.7 Ga (Corfu et al., 2003a; Kullerud et al., 2006a). Setting aside the Archean age population in the samples from the interpretation still makes the Lofoten-Vesterålen or West Troms Basement Complex the most viable source location. The important Middle Proterozoic signature is missing, to sufficiently link them (DE1-2 and MA2-2-8) to the Western Gneiss Region. The provenance signatures on the Lofoten-Vesterålen or the West Troms Basement Complex support the northeast direction linked to the recorded age spectra of the samples in the southwest and north on the Dønna Terrace.

The hafnium analysis supports this notion by the low $\varepsilon_{Hf}(t)$ (-9 to 0) values of the "Caledonian" age zircons (MA2-2-8), where there is a change of sediment transportation direction from the east or northeast (Figure 41). A northeast sediment transport direction is in accordance with the suggested crustal formation age pointing to crustal recycling from a protosource originating from a Late Mesoproterozoic event. The Mesoproterozoic event could point to the Bratten-Landegode close to Bodø (Augland et al., 2014). However, a more likely protosource would be the Hallandian-Danopolonian or the Sveconorwegian orogeny in the West Troms Basement Complex (Bingen et al., 2008). The "Gothian" zircon ages with their $\varepsilon_{Hf}(t)$ values of +1 to +7 and -9 to -2, reflect two crustal formation ages (MA2-2-8). The youngest (+1 to +7) implies crustal recycling from a protosource from the Trans-Scandinavian Intrusive Belt on Lofoten-Vesterålen or West Troms Basement Complex (Ramberg et al., 2008). The oldest (-9 to -2) implies a protosource from the Early Palaeoproterozoic. Late Proterozoic rocks of this age are related to the tonalitic gneisses and dikes on the West Troms Basement Complex (Ramberg et al., 2008).

7.4.2.3 North and northeastern direction

The wide range of age spectra from the middle Turonian to lower Coniacian Lysing sandstones (ÆR5-8-9 (well 6507/5-8), MA2-4-4 (well 6507/2-4) and ÆR3-9S-14 (well 6507/3-9S)) demonstrates a complex evolution of the turbidite system on the Dønna Terrace. The frequent 2.6-2.9 Ga, 1.7-1.8 Ga, and 0.9-1.0 Ga, with a subordinate age spectrum of 90-450 Ma are in accordance with sediment transport from the north and northeast (Figure 48; modified from Fugelli and Olsen, 2007). The north and northeast sediment transport direction can be explained by the granite-granodiorite plutons (2.8-2.9 Ga) on the southern shores of the Varangerfjorden in Finnmark (Levchenkov et al., 1995; Nordgulen et al., 1995; Koistinen et al., 2001). The 2.6-2.8 Ga signature points to the West Troms Basement Complex and the 1.7-1.8 Ga combined with the

Caledonian age corresponds to the signatures found on Lofoten-Vesterålen. The 0.9-1.0 Ga points towards the megacrystic granite rocks on Bratten-Landegode (Augland et al., 2014 close to Bodø). The juvenile Cretaceous to Permo-Triassic ages corresponds to sources located in the Barents Sea region. Studies from the Northwest Spitsbergen reveals ages from metamorphic and granitic rocks corresponding to the age spectrum recorded in these samples (Ohta et al., 2002 and references therein). The wide age spectra within the Early and Middle Proterozoic, including the 2.6-2.8 Ga ages are similar to that recorded by Gee et al. (2014) in the Lower Seve Nappe in Sweden, suggesting an eastern source. The Permo-Triassic ages were described by Morton et al. (2005), which suggested an East Greenland source provenance. However, another source is suggested by the Permo-Triassic ages, comparable to dated dikes, eclogite, and amphibolite located on the Flakstadøy on Lofoten (Hames and Andersen, 1996; Steltenpohl et al., 2003a; Steltenpohl et al., 2004; Corfu, 2004a; Corfu, 2004b; Steltenpohl et al., 2011a). U-Pb detrital zircon dating on Novaya Zemlya (Permian sediments on the southern Novaya Zemlya) reveals a prominent peak at 310-320 Ma related to the Uralian orogeny, which is a more likely source origin (Lorenz et al., 2013). A proximal source for the Cretaceous aged zircons would be Flakstadøy on Lofoten, where dikes, eclogite facies, and pegmatite have been dated revealing younger ages from 184-206 Ma, with the youngest of 55.6 Ma (Hames and Andersen, 1996; Steltenpohl et al., 2003a; Steltenpohl et al., 2004; Corfu, 2004a; Corfu, 2004b; Steltenpohl et al., 2011a). However, these ages contradict with the age spectra observed within the samples. The ages of 90 and 130 Ma support a north directional sedimentary input from the High Arctic Large Igneous Province. Sills, dikes, and lavas within the Barents Sea are dated to around 120-125 Ma. However, studies on Northern Greenland have dated dikes, which are cross-cutting the Early Cretaceous strata, to around 82-103 Ma (Buchan and Ernst, 2006). Sills and dikes on Franz Josef Land are dated from 34-175 Ma and 94-192 Ma, respectively (Koryakin and Shipilov, 2009; Corfu and Heim, 2013). Morton et al. (2005) dated zircons from 90 to 100 Ma with significant error bars and accredited these to coeval air-fall volcanism. The 90 Ma zircons in this study are recorded with a miniscule error bar and are observed with heavy abrasion and rounding of the detrital zircons. Morton et al. (2005) observed the same heavy abrasion and rounding of the 90 Ma zircons and suggested that they are linked to distal sedimentary transport. Concordant zircon ages of c. 90 Ma was discovered by Tegle (2017) in the middle Turonian to lower Coniacian Lysing megasequence in well 6507/2-3, with no records within well 6507/5-3. This proposes two theories: (1) recycling or reworking from multiple source

regions including either eastern Norwegian Landmass, High Arctic Large Igneous Province/Spitsbergen, Lofoten-Vesterålen and West Troms Basement Complex or (2) multiple sediment recycling or reworking with a sediment direction from the Arctic region (HALIP and Spitsbergen), combined with the Varangerfjorden and Novaya Zemlya (Uralian orogeny). Both support a North-South sediment transport pattern recorded by the behavior of the middle Turonian to lower Coniacian Lysing megasequence sandstone located within well 6507/3-9S, 6507/2-3 (Tegle, 2017), 6507/5-3 (Tegle, 2017) and 6507/5-8. The variations of Zr/Sc ratios from moderate, low to high upwards in the stratigraphy, reveals how sediment is either directly fed into the basin (first order), or progressively fed by second to third order cycle depositions, which supports both theories. The ε_{Hf} (t) values of -2 to 10 of the "Caledonian" age in the sandstone (*Æ*R5-8-9) is following a sediment transportation direction from the Norwegian Landmass. A sediment transport direction from the Norwegian Landmass is suggested by crustal recycling of the protosource from the "Caledonian" age dated zircons, which points to a juvenile protosource with a crustal formation age in the Neoproterozoic. The Neoproterozoic age could point to an early (920-1300 Ma) felsic or mafic magmatism within the Sveconorwegian orogeny (Andersen et al., 2011 and references therein). The "Gothian" age zircon is suggested to have crustal recycling from a protosource originating from the Trans-Scandinavian Intrusive Belt, with a juvenile crustal formation age. Further implied by the low ε_{Hf} (t) (-11 to +7) values of the "Caledonian" age zircons (MA2-4-4; *Æ*R3-9S-2,14), suggesting a northeast sediment transportation direction. A northeast sediment transport direction is in accordance with the suggested crustal formation age pointing to crustal recycling from a protosource originating from a Late Mesoproterozoic event. A Late Mesoproterozoic event could point to the Bratten-Landegode close to Bodø (Augland et al., 2014). However, a more likely protosource would be the Hallandian-Danopolonian or the Sveconorwegian orogeny in the West Troms Basement Complex (Bingen et al., 2008). The "Gothian" zircon ages with their ε_{Hf} (t) values of -10 to -6 and +2 to +5, reflect two crustal formation ages (MA2-4-4). The youngest (+2 to +5) implies crustal recycling from a protosource from the Trans-Scandinavian Intrusive Belt on Lofoten-Vesterålen or West Troms Basement Complex (Ramberg et al., 2008). The oldest (-10 to -6) implies recycling from a protosource from the Early Palaeoproterozoic. Late Proterozoic rocks of this age are related to the tonalitic gneisses and dikes on the West Troms Basement Complex (Ramberg et al., 2008).

The U-Pb age dated zircon of 3.3 Ga within sample ÆR3-9S-2 (core 6507/3-9S) is the oldest zircon in this study. The oldest dated Archean rocks of this age are the Siurua trondhjemite gneiss in the Pudasjarvi Granulite Belt in northern Finland (Mutanen and Huhma, 2003). A source from the northern Finland implies either a transport direction over the continent towards the Norwegian Sea or longer transportation towards the Varangerfjorden and into the Barents Sea. These are just speculations, and more U-Pb zircon dating must be performed in order to reveal the significance of this detrital zircon age.

7.4.2.4 Northwestern direction

The ages from the middle Turonian to lower Coniacian Lysing megasequence (MA2-2-4) is recorded with a wide Early Proterozoic 1550-2100 Ma (major peak at 1900-1950 Ma), Middle Proterozoic and with a significant Archean input (peaks at 2500 and 2700 Ma). Interestingly, what separates this sample from others taken on the Dønna Terrace in this study is the lack of a Phanerozoic component with only a minor Late Proterozoic component. A lack of a Phanerozoic component implies that sediments transported to this location are not derived from Caledonian orogeny impacted regions, which excludes Norway, Sweden, Svalbard, and East Greenland. Sediment transportation from the eastern Barents Sea is a possibility, although this would infer an age spectrum of 600-630 Ma, derived from the Timanide orogeny from the northern parts of western Russia (Larionov et al., 2004). Subsequently, this would imply sediment recycling from the initial depositional basin towards the last depositional basin, where intermixing of "Caledonian" age sediments is very likely to occur. However, the Caledonian orogeny did not affect northern Greenland. A provenance study on sediments from the Independence Fjord, close to the Peary Land reveals the same age spectra as within this sample MA2-2-4 (Kirkland et al., 2009). The study in the Independence Fjord recorded no Phanerozoic input, with the youngest zircon ages dated to 970 Ma and a substantial age population around 1000-1400 Ma. The Archean component is prominent with the highest age dated to 3970 Ma with a prominent peak at 2700 Ma. The similar age populations suggest a northwestern sedimentary transportation pattern and infer a significant stratigraphically variability within well 6507/2-2 (Figure 48; modified from Fugelli and Olsen, 2007). A stratigraphic variability is supported by the shallowest sandstone unit (MA2-2-4) with "Gothian" ages has $\varepsilon_{Hf}(t)$ values of -10 to +2. The protosource of this sandstone unit is related to a crustal formation age of Neoarchean origin. A possible protosource could be the Precambrian Shield on Greenland (Nutman et al., 2008).

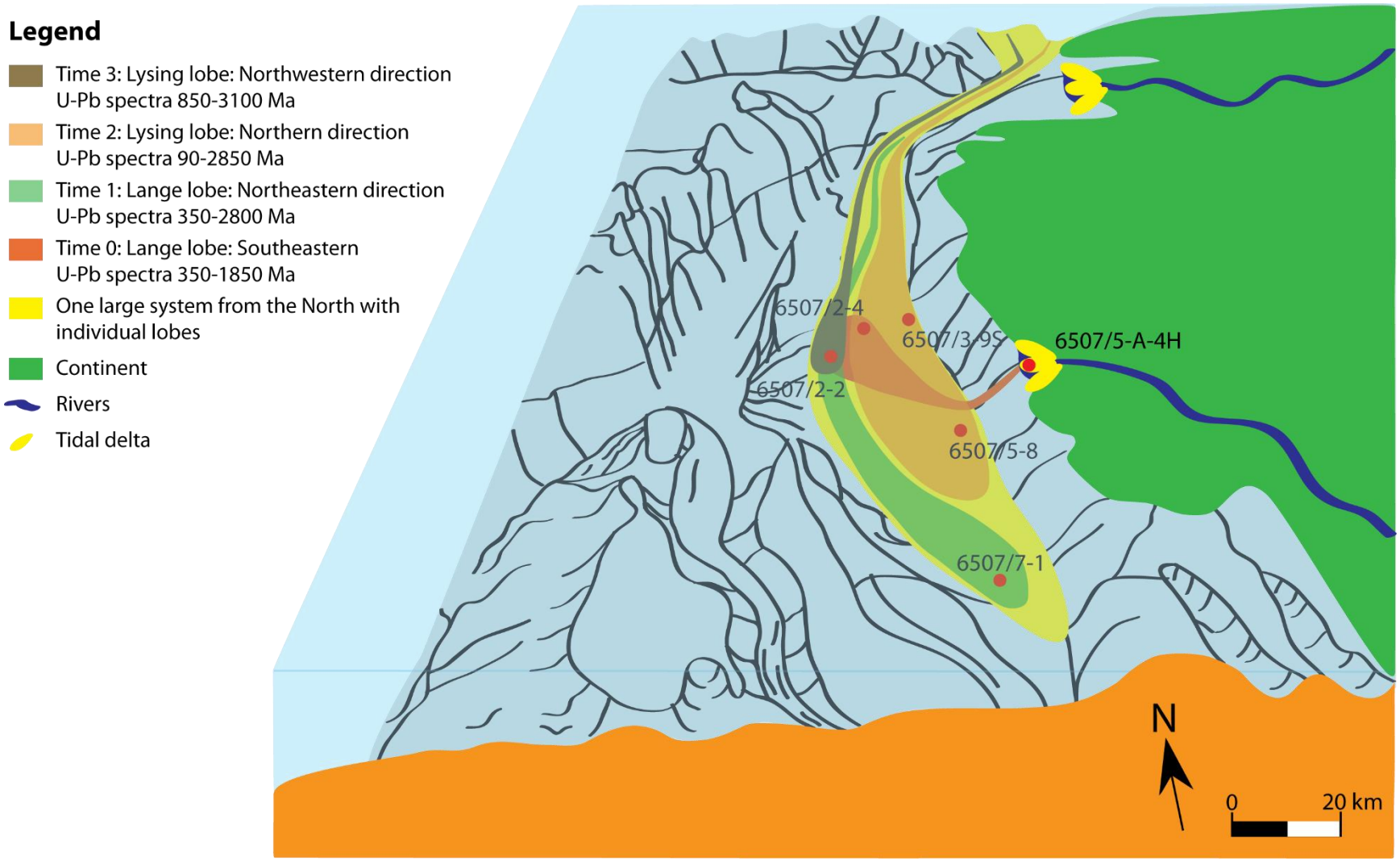

Figure 48: Conceptual model of sediment transportation directions on the Dønna Terrace (modified from Fugelli and Olsen, 2007).

7.5 Regional Context

The variability within the provenance signatures recorded by the U-Pb detrital zircon age dating combined with the stratigraphic and lateral variability with the provenance development, explains the complexity of the turbidite system of the Cenomanian to Coniacian Lange-Lysing megasequences. The development of the sedimentary delivery system observed from a regional context infer one large delivery system from the North which has eroded into a larger hinterland e.g. the Barents Sea. The hinterland has individual drainage systems originating from the North Greenland, northern Barents Sea, Novaya Zemlya and Finnmark (Figure 49; modified from GoogleEarth, 2019). The stratigraphic variability of the changing recycling order from low to high of sediments and the variability of the U-Pb zircon ages and crustal recycling ages within the basinfloor and lower slope of the Cenomanian to Coniacian Lange-Lysing megasequence in core 6507/2-2 supports this. The stratigraphic variability of the reservoir quality and consistent U-Pb zircon ages of 370-1800 Ma suggest an occasional sedimentary delivery from the Norwegian Landmass (Figure 49; modified from GoogleEarth, 2019).

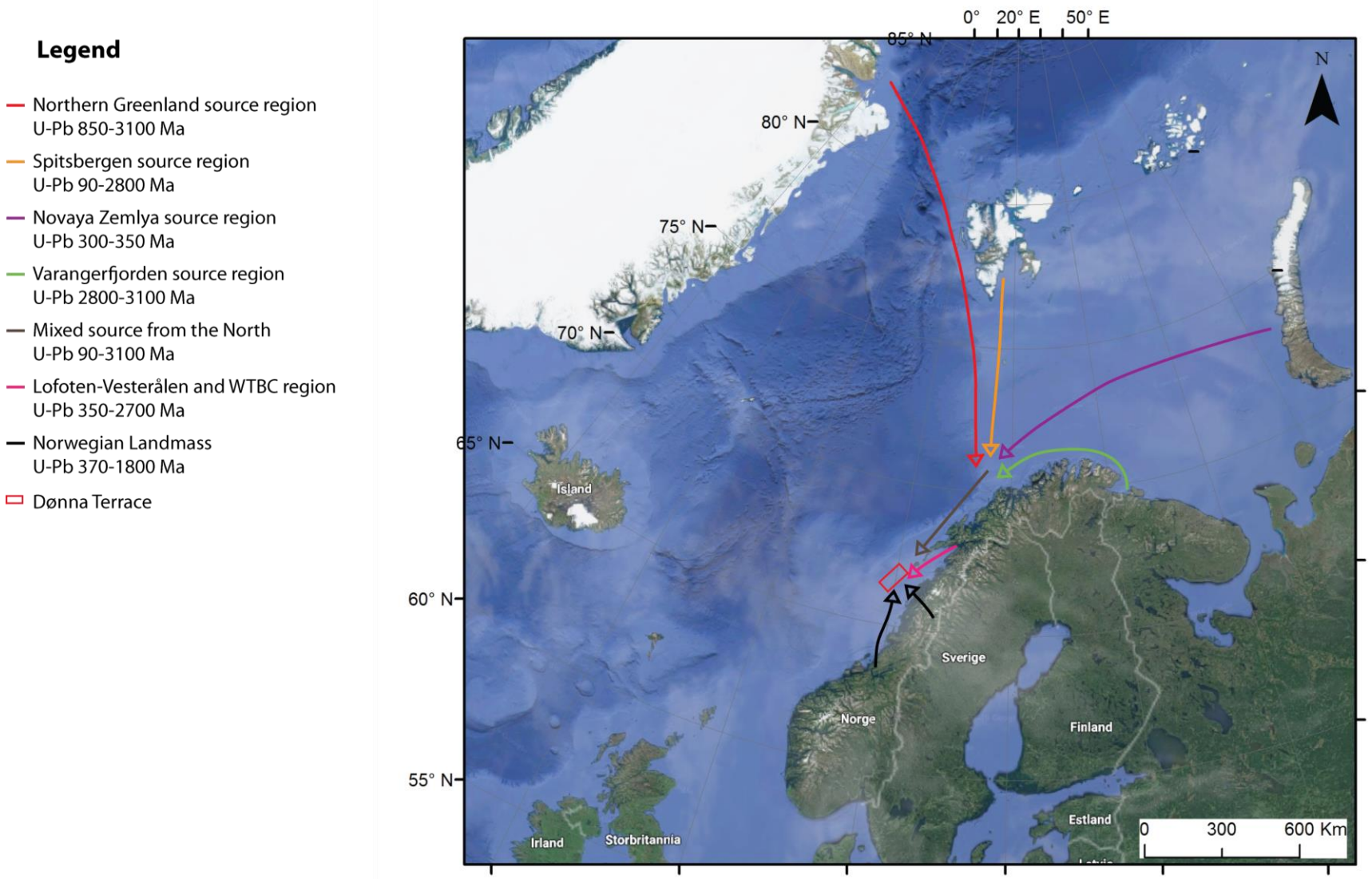

Figure 49: Regional context with the different source regions. The arrows of different colors show possible transport direction from the source regions and which zircon ages are related to them (GoogleEarth, 2019).

8 Conclusion

This study has demonstrated the importance and effectiveness to stratigraphically differentiate sandstone units by integrating traditional provenance methods such as whole-rock geochemistry and petrography, with U-Pb and Hafnium zircon isotope analysis. Petrography and whole-rock geochemistry provide the basis for characterizing each sandstone type in terms of lithology and mineralogy, enabling to delve into its stratigraphical provenance history. However, these methods are very dependent on a homogeneous representation of grain size within each sample, were a core description of each core was important. By defining individual facies to each sample, has revealed uncertainties regarding variation in sample material. This study has proven that provenance is a vital tool to elucidate stratigraphic variability within individual megasequence and laterally across both megasequences. Besides, it gives information on either a local or regional geographical source region. Identification of lateral connection is dependent on gross depositional environment combined with U-Pb geochronology and hafnium analysis, were other provenance signatures are less reliable. Provenance signatures have revealed a connection between the gross depositional environments, stratigraphic variability, and additionally, provenance development. Single grain analysis verifies the validity of the traditional provenance methods and supports the stratigraphic variability and lateral connectivity by providing a geochronological constraint on the source. The stratigraphic variability revealed the complexity of the turbidite system on the Dønna Terrace within each core and explained by the main four sediment transport directions:

1) Southwest from the Western Gneiss Region, suggested for the deepest part (in the Lange Formation) of core 6507/5-A-4H, 6507/2-4, and 6507/2-2.
2) Northeast from the Lofoten-Vesterålen and the West Troms Basement Complex implied by the upper Lange Formation interval of core 6507/7-1 and 6507/2-2, besides the upper Lysing Formation from core 6507/3-9S at a later time.
3) A northern combined with a northeastern direction is inferred by the younger input of the Phanerozoic aged zircons. The provenance source regime is mixed, originating from the High Arctic Large Igneous Province, Novaya Zemlya in the Barents Sea and the Varangerfjorden, combined with the Lofoten-Vesterålen and West Troms Basement Complex regions. A northern to northeastern direction is recorded within the middle and lower Lysing Formation within core 6507/5-8, 6507/3-9S and 6507/2-2.

4) A northwestern direction is suggested for the upper Lysing Formation within core 6507/2-2, with a provenance source originating from northern Greenland.

In a regional context, this suggests an extensive system from the North delivering sediments onto the Dønna Terrace, with a shifting delivery system from the east. Thus, a concentrated single-grain analysis of individual units within a succession reveals essential recordings from the sandstones, which is difficult to differentiate with isolated traditional provenance methods such as petrology and whole-rock geochemistry.

9 References

Abdelmalak, M.M., Faleide, J.I., Planke, S., Gernigon, L., Zastrozhnov, D., Shepard, G.E. and Myklebust, R., 2017. The T-Reflection and the deep crustal structure of the Vøring Margin, offshore mid-Norway. Tectonics, 36: 2497-2523.

Amelin, Y., Lee, D.C. and Halliday, A.N., 2000. Early-middle archaean crustal evolution deduced from Lu-Hf and U-Pb isotopic studies of single zircon grains. Geochemica et Cosmochimica Acta., 64(24): 4205-4225.

Andersen, T., 2013. Age, Hf isotope and trace element signatures of detrital zircons in the Mesoproterozoic Eriksfjord sandstone, southern Greenland: are detrital zircons reliable guides to sedimentary provenance and timing of deposition? Geological Magazine, 150(3): 426-440.

Andersen, T., Andersson, U.B., Graham, S., Aberg, G. and Simonsen, S.L., 2009. Granitic magmatism by melting of juvenile continental crust: new constraints on the source of Palaeoproterzoic granitoids in Fennoscandia from Hf isotopes in zircon. Geological Society, 166: 233-247.

Andersen, T., Saeed, A., Gabrielsen, R.H. and Olaussen, S., 2011. Provenance characteristics of the Brumunddal sandstone in the Oslo Rift derived from U-Pb, Lu-Hf and trace element analysis of detrital zircons by laser ablation ICPMS. Norwegian Journal of Geology, 91: 1-19.

Augland, L.E., Andresen, A., Gasser, D. and Steltenpohl, M.G., 2014. Early Ordovician to Silurian evolution of exotic terranes in the Scandinavian Caledonides of the Ofoten–Troms area – terrane characterization and correlation based on new U–Pb zircon ages and Lu–Hf isotopic data. Geological Society, London, Special Publications, 390(1): 655-678.

Austrheim, H., Corfu, F., Bryhni, I. and Andersen, T.B., 2003. The Proterozoic Hustad igneous complex: a low strain enclave with a key to the history of the Western Gneiss Region of Norway. Precambrian Research, 120: 149-175.

Austrheim, H. and Mørk, M.B.E., 1988. The lower continental crust of the Caledonian mountain chain: evidence from former deep crustal sections in western Norway. NGU (Norsk geologisk undersøkelse), 3: 102-113.

Baas, J.H., Best, J.L., Peakall, J. and Wang, M., 2009. A phase diagram for turbulent, transitional, and laminar clay suspension flows. Sedimentary Research, 79: 162-183.

Bann, K.L. and Fielding, C.R., 2004. An integrated ichnological and sedimentological comparison of non-deltaic shoreface and subaqueous delta deposits in Permian reservoir units of Australia. In: D. Mcllroy (Editor), The Application of Ichnology to Palaeoenvironmental and Stratigraphic Analysis. Geological Society, London, UK, pp. 273-307.

Basu, A., 2003. A perspective on quantitative provenance analysis. In: R. Valloni and A. Basu (Editors), Quantitative Provenance Studies in Italy, Memorie Descrittive della Carta. Geologica dell`Italia, Italy, pp. 11-22.

Basu, A., Young, S., Suttner, L.J., James, W.C. and Mack, C.H., 1975. Re-evaluation of the use of Undulatory extinction and polycrystallinity in detrital quartz for provenance interpretation. Sedimentary Petrology, 45: 873-882.

Belousova, E., Griffin, W. and O'Reilly, S., 2006. Zircon Crystal Morphology, Trace Element Signatures and Hf Isotope Composition as a Tool for Petrogenetic Modelling: Examples From Eastern Australian Granitoids, 47, 329-353 pp.

Bergh, S., Corfu, F., Priyatkina, N., Kullerud, K. and Myhre, P.I., 2015. Multiple post-Svecofennian 1750–1560 Ma pegmatite dykes in Archaean-Palaeoproterozoic rocks of the West Troms Basement Complex, North Norway: Geological significance and regional implications, 266.

Berndt, C., Planke, S., Alvestad, E., Tsikalas, F. and Rasmussen, T., 2001. Seismic volcanostratigraphy of the Norwegian margin: constraints on tectonomagmatic break-up process. Geological Society of London, 158: 413-426.

Bhatia, M.R. and Crook, K.A., 1986. Trace element characteristics of graywackes and tectonic setting discrimination of sedimentary basins. Contributions to mineralogy and petrology, 92(2): 181-193.

Bingen, B., Andersson, J., Söderlund, U. and Möller, C., 2008. The Mesoproterozoic in the Nordic countries. Episodes, 31: 29-34.

Blystad, P., Brekke, H., Færseth, R.B., Larsen, B.T., Skogseid, J. and Tørudbakken, B., 1995. Structural elements of the Norwegian Continental Shelf. Norwegian Petroleum Directorate publications: 8.

Boggs, S., 2012. Siliciclastic sedimentary rocks. In: S. Boggs (Editor), Principles of Sedimentology and Stratigraphy. Pearson Prentice Hall, pp. 585.

Bouma, A.H., 1962. Sedimentology of some Flysch deposits: A Graphic Approch to Facies Interpretation. Elsevier, Amsterdam: 168.

Bouvier, A., Vervoort, J.D. and Patchett, P.J., 2008. The Lu–Hf and Sm–Nd isotopic composition of CHUR: Constraints from unequilibrated chondrites and implications for the bulk composition of terrestrial planets. Earth and Planetary Science Letters, 273(1): 48-57.

Brekke, H., 2000. The tectonic evolution of the Norwegian Sea Continental Margin with emphasis on the Vøring and Møre Basins. Geological Society, London, Special Publications, 167(1): 327-378.

Brekke, H., Dahlgren, S., Nyberg, K. and Magnus, C., 1999. The prospectivity of the Vøring and Møre basins on the Norwegian Sea continental margin. In: A.J. Fleet and S.A.R. Boldy (Editors), Petroleum Geology of Northwest Europe. Geological Society, London, pp. 261-274.

Brekke, H. and Riis, F., 1987. Tectonics and basin evolution of the Norwegian shelf between 62°N and 72°N. Norsk Geologisk Tidsskrift, 67: 295-322.

Brekke, H., Sjulstad, H.I., Magnus, C. and Williams, R.W., 2001. Sedimentary environments offshore Norway - an overview. In: O.J. Martinsen and T. Dreyer (Editors), Sedimentary environments offshore Norway - Palaeozoic to Recent. Elsevier, Amsterdam.

Brown, R.W., 1991. Backstacking apatite fission-track `stratigraphy`: a method for resolving the erosional and isostatic components of tectonic uplift histories. Geology, 19: 74-77.

Buchan, K.L. and Ernst, R., 2006. Giant dyke swarms and the reconstruction of the Canadian Arctic islands, Greenland, Svalbard and Franz Josef Land. In: E. Hanski, S. Mertanen, T. Rämö and J. Vuollo (Editors), Dyke swarms — time markers of crustal evolution. Taylor and Francis/Balkema, London, UK, pp. 27-48.

Bukovics, C., Shaw, N.D., Cartier, E.G. and Ziegler, P.A., 1984. Structure and Development of the Mid-Norway Continental Margin. In: S.e.a. (1984a) (Editor), pp. 407-423.

Bøe, R., Fossen, H. and Smelror, M., 2010. Mesozoic sediments and structures onshore Norway and in the coastal zone. Norges geologiske undersøkelse, 450: 15-32.

Carter, A. and Moss, S.J., 1999. Combined detrital-zircon fission-track and U-Pb dating: A new approach to understanding hinterland evolution. Geology, 27: 235-238.
Chauvel, C., Lewin, E., Carpentier, M., Arndt, N.T. and Marini, J.-C., 2008. Role of recycled oceanic basalt and sediment in generating the Hf–Nd mantle array. Nature Geoscience, 1: 64.
Condie, K.C., 1993. Chemical composition and evolution of the upper continental crust: contrasting results from surface samples and shales. Chemical geology, 104(1-4): 1-37.
Corfu, F., 2003b. Atlas of Zircon Textures. In: J.M. Hanchar and P.W.O. Hoskin (Editors), Reviews in Mineralogy and Geochemistry, pp. 277-303.
Corfu, F., 2004a. U-Pb age, setting and tectonic significance of the anorthosite - magerite - charmockite - granite suite, Lofoten-Vesterålen, Norway. Journal of Petrology, 45: 1799-1819.
Corfu, F., 2004b. U-Pb geochronology of the Leknes Group: an exotic Early Caledonian metasedimentary assemblage stranded on Lofoten basement, northern Norway. Journal of the Geological Society, 161: 619-627.
Corfu, F., 2007. Comment to short-communication 'Comment: Hf-isotope heterogeneity in zircon 91500'. Chemical geology, 244: 350-353.
Corfu, F., Armitage, P.E.B., Kullerud, K. and Bergh, S.G., 2003a. Preliminary U-Pb geochronology in the West Troms Basement Complex, North Norway: Archaean and Palaeoproterozoic events and younger overprints. Norges geologiske undersøkelse, 441: 61-72.
Corfu, F. and Heim, M., 2013. Geology and U–Pb geochro-nology of the Espedalen Complex, southern Norway,and its position in the Caledonian nappe systems. In: F. Corfu, D. Gasser and D.M. Chew (Editors), New Perspectives on the Caledonides of Scandinavia and Related Areas. Geological Society, London.
Dabbagh, M.E. and Rogers, J.J., 1983. Depositional environments and tectonic significance of the Wajid sandstone of southern Saudia Arabia. African Earth Science, 1(1): 47-57.
Dalland, A., Worsley, D. and Ofstad, K., 1988. A lithostratigraphic scheme for the Mesozoic and Cenozoic succession offshore Mid and Northern Norway. Norwegian Petroleum Directorate, 4: 1-65.
Dallmann, W.K., 1999. Lithostratigraphic lexicon of Svalbard. Re-view and recommendations for nomenclature use. Late Palaeo-zoic to Quaternary Bedrock. Norwegian Polar Institute.
Dalrymple, R.W. and Choi, K., 2007. Morphologic and facies trends through the fluvial-marine transition in tide-dominated depositional systems: A schematic framework for environmental and sequence-stratigraphic interpretation. Earth-Science Reviews, 81: 135-174.
Dibner, V.D., 1998. Geology of Franz Josef Land. Norsk Polarinstitutt, 146: 190.
Dickinson, W.R., Bread, L.S., Brackenridge, G.R., Erjavec, J.L., Ferguson, R.C., Inman, K.F., Knepp, R.A., Lindberg, F.A. and Ryberg, P.T., 1983. Provenance of North American Phanerozoic sandstones in relation to tectonic setting. Geological Society of America Bulletin, 94(2): 222-235.
Doré, A.G. and Lundin, E.R., 1996. Cenozoic compressional structures on the NE Atlantic margin; nature, origin and potential significance for hydrocarbon exploration. Petroleum Geoscience, 2(4): 299-311.

Doré, A.G., Lundin, E.R., Birkeland, O., Eliassen, P.E. and Jensen, L.N., 1997. The NE Atlantic Margin: implications of late Mesozoic and Cenozoic events for hydrocarbon prospectivity. Petroleum Geoscience, 3: 117-131.

Dott, R.H., Jr., 1966. Late Jurassic unconformity exposed in southwestern Oregon. Ore Bin, 28: 85-97.

Ehrenberg, S.N., 1989. Assessing the relative importance of compaction processes and cementation to reduction of porosity in sandstones: discussio; compaction and porosity evolution of Pliocene sandstones, Ventura Basin, California: discussion. AAPG bulletin, 73(10): 1274-1276.

Elburg, M.A., Andersen, T., Bons, P.D., Simonsen, S.L. and Weisheit, A., 2013. New constraints on Phanerozoic magmatic and hydrothermal events in the Mt Painter Province, South Australia. Gondwana Research, 24(2): 700-712.

Eldholm, O., Tsikalas, F. and Faleide, J.L., 2002. The continental margin off Norway 62-75°N: Palaeogene tectono-magmatic segmentation and sedimentation. In: D.W. Jolley and B.R. Bell (Editors), The North Atlantic Igneous Province: stratigraphy, tectonics, volcanic and magmatic processes. Geological Society, London, pp. 39-68.

Engel, A.E.J., Itson, S.P., Engel, C.G., Stickney, D.M. and Cray, E.J.J., 1974. Crustal evolution and global tectonics: a petrogenic view. GSA Bulletin, 85(6): 843-858.

Faleide, J.L., Tsikalas, F., Breivik, A.J., Mjelde, R., Ritzmann, O., Engen, Ø., Wilson, J. and Eldholm, O., 2008. Structure and evolution of the continental margin off Norway and the Barents Sea. Episodes, 31(1): 82-90.

Fedo, C.M., Nesbitt, H.W. and Young, G.M., 1995. Unravelling the effects of potassium metasomatism in sedimentary rocks and paleosols, with implications for paleoweathering conditions and provenance. Geology, 23(10): 921-924.

Floyd, P.A. and Leveridge, B.E., 1987. Tectonic environment of the Devonian Gramscatho basin, south Cornwall: framework mode and geochemical evidence from turbiditic sandstones. Journal of the Geological Society, 144(4): 531-542.

Folk, R.L., 1980. Petrology of sedimentary rocks. Hemphill Publishing Company, Austin.

Fonneland, H.C., Lien, T., Martinsen, O.J., Pedersen, R.B. and Kosler, J., 2004. Detrital zircon ages: a key to understanding the deposition of deep marine sandstones in the Norwegian Sea. Sedimentary Geology, 164: 147-159.

Fossen, H., 2010. Extensional tectonics in the North Atlantic Caledonides: a regional view. Geological Society, 335: 767-793.

Fugelli, E.M.G. and Olsen, T.R., 2005. Screening for deep-marine reservoirs in frontier basins; Part 1; Examples from offshore Mid-Norway. AAPG bulletin, 89(7): 853-882.

Fugelli, E.M.G. and Olsen, T.R., 2007. Delineating confined slope turbidite systems offshore mid-Norway: The Cretaceous deep-marine Lysing Formation. AAPG bulletin, 91(11): 1577-1601.

Færseth, R.B. and Lien, B.T., 2002. Cretaceous evolution in the Norwegian Sea - a period characterized by tectonic quiescence. Marine and Petroleum Geology, 19: 1005-1027.

Gallagher, K., Brown, R. and Johnson, C., 1998. Fission track analysis and its applications to geological problems. Science, 26: 519-572.

Gee, D.G., 1975. A tectonic model for the central part of the Scandinavian Caledonides. American Journal of Science, 275: 468-515.

Gee, D.G., Ladenberger, A., Dahlqvist, P., Majka, J., Be'eri-Shlevin, Y., Frei, D. and Thomsen, T., 2014. The Baltoscandian margin detrital zircon signatures of the central Scandes. Geological Society, London, Special Publications, 390(1): 131-155.
Gerdes, A. and Zeh, A., 2006. Combined U–Pb and Hf isotope LA-(MC-)ICP-MS analyses of detrital zircons: Comparison with SHRIMP and new constraints for the provenance and age of an Armorican metasediment in Central Germany. Earth and Planetary Science Letters, 249(1): 47-61.
Gernigon, L., Ringenbach, J.C., Planke, S. and Jonquet-Kolsto, H., 2003. Extension, crustal structure and magmatism at the outer Vøring Basin, Norwegian margin. Journal of the Geological Society of London, 160: 197-208.
Gingras, M.K., Bann, K.L., MacEachern, J.A., Waldron, W. and Pemberton, S.G., 2007. A conceptual framework for the application of trace fossils. In: J.A. MacEachern, K.L. Bann, M.K. Gingras and S.G. Pemberton (Editors), Applied ichnology. SEPM Short Course Notes, pp. 1-25.
Gingras, M.K. and MacEachern, J.A., 2012. Tidal ichnology of shallow-water clastic settings. In: R.A.J. Davis and R.W. Dalrymple (Editors), Principles of Tidal Sedimentology. Springer, Dordrecht, pp. 57-77.
Gjelberg, J., J. Martinsen, O., Charnock, M., Møller, N. and Antonsen, P., 2005. The reservoir development of the Late Maastrichtian–Early Paleocene Ormen Lange gas field, Møre Basin, Mid-Norwegian Shelf, pp. 1165-1184.
GoogleEarth, 2019. Google Earth covering the North Atlantic Ocean.
Griffin, W., Taylor, P.N., Hakkinen, J.W., Heier, K.S., Iden, I.K., Ravna, E., Malm, O., Olsen, K.I., Ormaasen, D.E. and Tveten, E., 1978. Archaean and Proterozoic crustal evolution in Lofoten-Vesterålen, N. Norway, 135, 629-647 pp.
Grogan, P., Nyberg, K., Fotland, B., Myklebust, R., Dahlgren, S. and Riis, F., 1998. Cretaceous magmatism south and east of Svalbard: evidence from seismic reflection and magnetic data. Polarforschung, 68: 25-34.
Gu, X.X., Liu, J.M., Zheng, M.H., Tang, J.X. and Qi, L., 2002. Provenance and tectonic setting of the Proterozoic turbidites in Hunan, South China: geochemical evidence. Sedimentary Research, 72(3): 393-407.
Halland, E.K., Mujezinovic, J., Riis, F., Bjørnstad, A., Meling, I., Gjeldsvik, I., Tappel, I., Bjørheim, M., Rød, R. and Pham, V., 2013. CO2 Storage Atlas: Norwegian Continental Shelf. Norwegian Petroleum Directorate publications: 55.
Hames, W.E. and Andersen, A., 1996. Timing of Palaeozoic orogeny and extension in the continental shelf of north central Norway as indicated by laser 40Ar/40Ar muscovite dating. Geology, 24: 1005-1008.
Harland, W.B., 1997. Svalbard. Geological Society, London, Memoirs, 17(1): 3-15.
Hastings, D.S., 1987. Sand-prone facies in the Cretaceous of mid-Norway. In: J. Brooks and Glennie (Editors), Petroleum geology of North West Europe. Graham and Trotman, London, pp. 1065-1078.
Haughton, P., Davis, C., McCaffrey, W. and Barker, S., 2009. Hybrid sediment gravity flow deposits-classification, origin and significance. Marine and Petroleum Geology, 26: 1900-1918.
Heinonen, K., Strandvik, T., Mickelsson, J., Edvardsson, B., Sundström, E. and Andersson, P., 2010. A Customer-Dominant Logic of Service, 21, 531-548 pp.

Henstra, G.A., Grundvåg, S.-A., Johannessen, E.P., Kristensen, T.B., Midtkandal, I., Nystuen, J.P., Rotevatn, A., Surlyk, F., Sæther, T. and Windelstad, J., 2016. Depositional processes and stratigraphic architecture within a coarse-grained rift-margin turbidite system: The Wollaston Forland Group, east Greenland. Marine and Petroleum Geology, 76: 187-209.
Hiscott, N.R., 1979. Clastic Sills and Dikes Associated with Deep-Water Sandstones, Tourelle Formation, Ordovician, Quebec, 49, 1-10 pp.
Howard, J.D., 1975. The sedimentological significance of trace fossils. In: R.W. Frey (Editor), The study of Trace Fossils. Springer-Verlag, New York, NY, pp. 131-146.
Ingersoll, R.V., Bullard, T.F., Ford, R.L., Grimm, J.P., Pickle, J.D. and Sares, S.W., 1984. The effect of grain size on detrital modes: a test of the Gazzi-Dickinson point-counting method. Sedimentary Research, 54: 103-116.
Jansen, E., Sjøholm, J., Bleil, U. and Erichsen, J.A., 1990. Neogene and Pleistocene Glaciations in the Northern Hemisphere and Late Miocene — Pliocene Global Ice Volume Fluctuations: Evidence from the Norwegian Sea. In: U. Bleil and J. Thiede (Editors), Geological History of the Polar Oceans: Arctic versus Antarctic. Springer, Dordrecht.
Kirkland, C.L., Pease, V., Whitehouse, M.J. and Ineson, J.R., 2009. Provenance record from Mesoproterozoic-Cambrian sediments of Peary Land, North Greenland: Implications for the ice-covered Greenland Shield and Laurentian palaeogeography. Precambrian Research, 170(1): 43-60.
Kneller, B.C. and McCaffrey, W.D., 2003. The interpretation of vertical sequences in turbidite beds: the influence of longitudinal flow structure. Sedimentary Research, 73(5): 706-713.
Koch, J.O. and Heum, O.R., 1995. Exploration trends of the Halten Terrace. In: S. Hanslien (Editor), Petroleum Exploration and Exploitation in Norway. Elsevier, Amsterdam, pp. 235-251.
Koistinen, T., Stephens, M.B., Bogatchev, V., Nordgulen, Ø., Wennerstrøm, M. and Korhonen, J., 2001. Geological map of the Fennoscandian Shield, scale 1:2,000,000. Geological Survey of Finland, Trondheim: Geological Survey of Norway, Uppsala: Geological Survey of Sweden, Moscow: Ministry of Natural Resources of Russia.
Kolb, J., Bagas, L. and Fiorentini, M.L., 2015. Metallogeny of the North Atlantic Craton in Greenland. Mineralogical Magazine, 79(4): 815-855.
Koryakin, Y.V. and Shipilov, E.V., 2009. Geochemical specifics and 40Ar/39Ar age of the basaltoid magmatism of the Alexander Land, Northbrook, Hooker, and Hayes islands (Franz Josef Land Archipelago). Doklady Earth Sciences, 425(1): 260-263.
Kullerud, K., Corfu, F., Bergh, S.G., Davidsen, B. and Ravna, E.K., 2006a. U-Pb constraints on the Archaean and Early Proterozoic evolution of the West Troms Basement Complex, North Norway. Geological Survey of Finland.(1).
Kullerud, L., Tørudbakken, B.O. and Ilebekk, S., 1986. A compilation of radiometric age determinations from the Western Gneiss Region, south Norway. NGU (Norsk geologisk undersøkelse), 406: 17-42.
Kyrkjebø, R., Kjennerud, T., Gillmore, G., Faleide, J.I. and Gabrielsen, R., 2001. Cretaceous – Tertiary palaeo-bathymetry in the northern North Sea; integration of palaeo-water depth estimates obtained by structural restoration and micropalaentological analysis, 10.
Larionov, A.N., Andreichev, V.A. and Gee, D., 2004. The Vendian alkaline igneous suite of northern Timan: ion microprobe U-Pb zircon ages of gabbros and syenite. In: D. Gee and V. Pease (Editors), The Neoproterozoic Timanide Orogen of Eastern Baltica. Geological Society, London, pp. 69-74.

Lauri, L.S., Andersen, T., Hölttä, P., Huhma, H. and Graham, S., 2011. Evolution of the Archaean Karelian Province in the Fennoscandian Shield in the light of U–Pb zircon ages and Sm–Nd and Lu–Hf isotope systematics. Journal of the Geological Society, 168(1): 201-218.

Levchenkov, O.A., Levsky, L.K., Nordgulen, Ø., Dobrzhinetskaya., Vetrin, V.R., Cobbing, J., Nilsson, L.P. and Sturt, B.A., 1995. U-Pb zircon ages from sørvaranger, Norway, and the western part of the Kola Peninsula, Russia. NGU (Norsk geologisk undersøkelse), 7: 29-47.

Lien, T., 2005. From Rifting to drifting: effects on the development of deep-water hydrocarbon reservoirs in a passive margin setting, Norwegian Sea. . Norwegian Journal of Geology, 85: 319-332.

Lien, T., Midtbø, R.E. and Martinsen, O.J., 2006. Depositional facies and reservoir quality of deep-marine sandstones in the Norwegian Sea. Norsk Geologisk Tidsskrift, 2(86): 71.

Longiaru, S., 1987. Visual comparators for estimating the degree of sorting from plane and thin section. Sedimentary Petrology, 57(4): 791-794.

Lorenz, H., Gee, D., Korago, E., Kovaleva, G., C. McClelland, W., Gilotti, J. and Frei, D., 2013. Detrital zircon geochronology of Palaeozoic Novaya Zemlya—A key to understanding the basement of the Barents Shelf, 25.

Lowe, D.R., 1982. Sedimentary gravity flows II, Depositional models with special references of high-density turbidite currents. Sedimentary Petrology., 52: 279-297.

MacEachern, J.A. and Pemberton, S.G., 1992. Ichnological aspects of Cretaceous shoreface successions and shoreface variability in the Western Interior Seaway of North America. In: S.G. Pemberton (Editor), Applications of Ichnology to Petroleum Exploration. SEPM Core Workshop, Calgary, AB, pp. 57-84.

MacLeod, K.G., Huber, B.T. and Isaza-Londono, C., 2005. North Atlantic warming during global cooling at the end of the Cretaceous. Geology, 33: 437-440.

Martinsen, O.J., Lien, T. and Jackson, C., 2005. Cretaceous and Palaeogene turbidite systems in the North Sea and Norwegian Sea basins: source, staging area and basin physiography controls on reservoir development. In: A.G. Dore and B.A. Vining (Editors), Petroleum Geology: North-West Europe and Global Perspectives. Geological Society, London, pp. 1147-1164.

McLennan, S.M., Hemming, S., McDaniel, D.K. and Hanson, G.N., 1993. Geochemical approaches to sedimentation, provenance, and tectonics. Geological Society of America, 284: 21-40.

Midtkandal, I., Nystuen, J.P., Nagy, J. and Mørk, A., 2008. Lower Cretaceous lithostratigraphy across a regional subaerial unconformity in Spitsbergen: the

Rurikfjellet and Helvetiafjellet formations. Norwegian Journal of Geology, 88: 287-304.

Miller, K.G., Kominz, M.A., Browning, J.V., Wright, J.D., Mountain, G.S., Katz, M.E., Sugarman, P.J., Cramer, B.S., Christie-Blick, N. and Pekar, S.F., 2005a. The Phanerozoic record of global sea-level change. Science, 310: 1293-1298.

Miller, K.G., Wright, J.D. and Browning, J.V., 2005b. Visions of ice sheets in a greenhouse world. Mar.Geol., 217: 215-231.

Mjelde, R., Wessel, P. and Müller, R.D., 2010. Global pulsations of intraplate magmatism through the Cenozoic. Lithosphere, 2(5): 361-376.

Morton, A.C. and Grant, S., 1998. Cretaceous Depositional Systems in the Norwegian Sea: Heavy Mineral Constraints. AAPG bulletin, 82(2): 274-290.

Morton, A.C., Whitham, A.G. and Fanning, C.M., 2005. Provenance of Late Cretaceous to Paleocene submarine fan sandstones in the Norwegian Sea: integration of heavy mineral, mineral chemical and zircon age data. Sedimentary Geology, 182: 3-28.
Mulder, T. and Alexander, J., 2001. The physical character of subaqueous sedimentary density flows and their deposits. Sedimentology, 48: 269-299.
Mutanen, T. and Huhma, H., 2003. The 3.5 Ga Siurua trondhjemite gneiss in the Archean Pudasjärvi Granulite Belt, northern Finland. Geological Society of Finland, 75: 55-68.
Mutti, E., 1992. Turbidite sandstones. In: E. Mutti (Editor). AGIP, Italy, pp. 275.
Myhre, P.I., Corfu, F., Bergh, S.G. and Kullerud, K., 2013. U-Pb geochronology along an Archean geotransect in the West-Troms Basement complex, North Norway. Norwegian journal of Geology, 93: 1-24.
Nesbitt, H.W. and Young, G., 1982. Early Proterozoic climates and plate motions inferred from major element chemistry of lutites, 299.
Nichols, G., 2009. Sedimentology and stratigraphy. John Wiley & Sons.
Nordgulen, Ø., Solli, A. and Sundvoll, B., 1995. Caledonian granitoids in the Frøya-Froan area, central Norway, 427, 48-51 pp.
NPD, 2019. Norwegian Petroleum Directorate (NPD). Norwegian Petroleum Directorate (NPD), NPD Factpages.
Nutman, A.P., Dawes, P.R., Kalsbeek, F. and Hamilton, M.A., 2008. Palaeoproterozoic and Archaean gneiss complexes in northern Greenland: Palaeoproterozoic terrane assembly in the High Arctic. Precambrian Research, 161: 419-451.
Ohta, Y., Larionov, A.N., Tebenkov, A.M., Lepvrier, C., Maluski, H., Lange, M. and Hellebrant, B., 2002. Single-zircon Pb-evaporation and 40Ar/40Ar dating of the metamorphic and granitic rocks in the north-west Spitsbergen. Polar Research, 21: 73-89.
Parker, J.R., 1967. The Jurassic and Cretaceous sequence in Spitsbergen. Geological Magazine, 104(5): 487-505.
Pemberton, S.G., MacEachern, J.A. and Frey, R.W., 1992. Trace fossils facies models: environmental and allostratigraphic significance. In: R.G. Walker and N.P. James (Editors), Facies Models: Response to Sea Level Change. Geological Association of Canada, St. John`s, NF, pp. 47-72.
Pettijohn, F.J., Potter, P.E. and Siever, R., 1973. Sand and sandstones. Springer-Verlag, Berlin, pp. 617.
Pettijohn, F.J., Potter, P.E. and Siever, R., 1987. Sand and sandstones, 2nd ed. Springer-Verlag, New York, Berlin, Heidelberg, London, Paris, Tokyo, 533 pp.
Pickering, K.T., Hiscott, N.R. and Hein, F.J., 1989. Deep Marine Environments: Clastic Sedimentation and Tectonics. Chapman & Hall, London.
Price, G.D., Fozy, I., Janssen, N.M.M. and Palfy, J., 2011. Late Valanginan-Barremian (Early Cretaceous) palaeotemperatures inferred from belemnite stable isotope and Mg/Ca ratios from Bersek Quarry (Gerecse Mountains, Transdanubian Range, Hungary). Palaeogeogr. Palaeocl. Palaeoecol., 305: 1-9.
Ramberg, I.B., Bryhni, L., Nøttvedt, A. and Rangnes, K., 2008. The Making of a Land: Geology of Norway. Geological Society Publishing House.
Raychaudhuri, I. and Pemberton, S.G., 1992. Ichnologic and sedimentological characteristics of open-marine to storm dominated restricted marine settings within the Viking/Bow Island Formations, south-central Alberta. In: S.G. Pemberton (Editor), Applications of Ichnology to Petroleum Exploration. SEPM Core Workshop, Calgary, AB, pp. 119-139.

Reineck, H.E., 1963. Sedimentgefüge im Bereich der südlichen Nordsee. Abh Senkenberg Naturforsch Gesellschaft, 505: 1-138.
Roberts, D. and Gee, D.G., 1985. An introduction to the structure of the Scandinavian Caledonides. In: D.G. Gee and B.A. Stuart (Editors), The Caledonides Orogen-Scandinavia and related areas: Part 1. Wiley, New York, pp. 55-68.
Rosa, D., Finch, A.A., Andersen, T. and Inverno, C.M.C., 2009. U-Pb geochronology and Hf isotope ratios of magmatic zircons from the Iberian Pyrite Belt. Mineralogy and Petrology., 95(1-2): 47-69.
Roy, S.K. and Banerjee, S., 2016. Soft sediment deformation structures in the Andaman Flysch Group, Andaman Basin: evidence for Paleogene seismic activity in the Island Arc. Beri Sedimentology, 35: 55-64.
Rudnick, R. and Gao, S., 2003. Composition of the Continental Crust. Treatise Geochem 3:1-64, 3, 1-64 pp.
Savage, K.M. and Potter, P.E., 1991. Petrology of modern sands of the Rios Gauviare and Inirida, southern Colombia: Tropical climate and sand composition. Journal of Geology, 99: 289-298.
Shanmugam, G., Lehtonen, L.R., Straume, T., Syvertsen, S.E., Hodgkinson, R.J. and Skibeli, M., 1994. Slump and debris-flow dominated upper slope facies in the Cretaceous of the Norwegian and northern North Seas (61-67 N): Implications for sand distribution. AAPG bulletin, 78(6): 910-937.
Skår, Ø., 1998. Field relations and geochemical evolution of the pre-Sveconorwegian rocks in the Kvamsøy area, southern Western Gneiss Complex. Norway., University of Bergen, Norway.
Skår, Ø., 2000. Field relations and geochemical evolution of the Gothian rocks in the Kvamsoy area, southern Western Gneiss Complex, Norway. NGU (Norsk geologisk undersøkelse), 437: 5-24.
Smith, S.A. and Hiscott, R.N., 1987. Latest Precambrian to Early Cambrian basin evolution, Fortune Bay, Newfoundland fault-bounded basin to platform. Canadian Journal of Earth Sciences, 21: 3179-1392.
Steltenpohl, M.G., Andersen, A., Lindstrøm, M., Gromet, P. and Steltenpohl, L.W., 2003a. The roleof felsic and mafic igneous rocks in deciphering theevolution of thrust-stacked terranes: an example fromthe north Norwegian Caledonides. American Journal of Science, 303: 149-185.
Steltenpohl, M.G., Hames, W.E. and Andersen, A., 2004. The Silurian to Permian history of a metamorphic core complex in Lofoten, northern Scandinavian Caledonides. Tectonics, 23: 1-23.
Steltenpohl, M.G., Kassos, G., Andersen, A., Rehnstrøm, E.F. and Hames, W.E., 2011a. Eclogitization and exhumation of Caledonian continental basement in Lofoten, North Norway. Geosphere, 7: 202-218.
Söderlund, U., Patchett, P.J., Vervoort, J. and Isachsen, C., 2004. The 176Lu decay constant determined by Lu-Hf and U-Pb isotope systematics of Precambrian mafic intrusions, 219, 311-324 pp.
Taylor, A.M. and Goldring, R., 1993. Description and analysis of bioturbation and ichnofabric. Journal of the Geological Society, 150(1): 141-148.
Taylor, S.R. and McLennan, S.M., 1985. The Continental Crust: Its Composition and Evolution. Blackwell, Oxford.

Tegle, K., 2017. Provenance of the Late Cretaceous Lange-Lysing Megasequences, with implication for reservoir architecture and quality., University of Stavanger, Stavanger, UiS Brage.
Terry, M.P. and Robinson, P., 2003. Evolution of amphibolite-facies structural features and boundary conditions for deformation during exhumation of high-and ultrahigh-pressure rocks, Nordøyane, Western Gneiss Region, Norway. . Tectonics, 22(4).
Thrane, K., 2002. Relationships between Archean and Palaeoproterozoic crystalline basement complexes in the southern part of the East Greenland Caledonides: an ion microprobe study. Precambrian Research, 113: 19-42.
Tortosa, A., Palomares, M. and Arribas, J., 1991. Quartz grain types in Holocene deposits from the Spanish Central System: some problems in provenance analysis. Geological Society, 57: 47-54.
Tucker, M., 1988. Techniques in sedimentology. Blackwell Scientific, Oxford.
Vergara, L., Wreglesworth, I., Trayfoot, M. and Richardsen, G., 2001. The distribution of Cretaceous and Paleocene deep-water reservoirs in the Norwegian Sea basins. Petroleum Geoscience, 7(4): 395-408.
Von Eynatten, H., 2003. Petrography and chemistry of sandstones from the Swiss Molasse Basin: an archive of the Oligocene to Miocene evolution of the Central Alps. Sedimentology, 50(4): 703-724.
Von Eynatten, H. and Gaup, R., 1999. Provenance of Cretaceous synorogenic sandstones in the Eastern Alps: constrains from framework petrography, heavy minerals and mineral chemistry. Sedimentary Geology, 124: 81-111.
Watt, G.R. and Thrane, K., 2001. Early Neoproterozoic events in East Greenland. Precambrian Research, 110: 165-184.
Weltje, G.J. and Eynatten, H.V., 2004. Quantitative provenance analysis of sediments: review and outlook. Sedimentary Geology, 171(1-4): 1-11.
Wiedenbeck, M., Allé, P., Corfu, F., Griffin, W.L., Meier, M., Oberli, F., Quadt, A.v., Roddick, J.C. and Spiegel, W., 1995. Three natural zircon standards for u-th-pb, lu-hf, trace element and ree analyses. Geostandards Newsletter, 19(1): 1-23.
Willner, A.P., Sindern, S., Metzger, K., Ermolaeva, T., Kramm, U., Puchkov, V. and Kronz, A., 2003. Typology and single grain U/Pb ages of detrital zircons from Proterozoic sandstones in the SW Urals (Russia): early time marks at the eastern margin of Baltica. Precambrian Research, 124: 1-29.
Woodhead, J.D. and Hergt, J.M., 2005. A Preliminary Appraisal of Seven Natural Zircon Reference Materials for In Situ Hf Isotope Determination. Geostandards and Geoanalytical Research, 29(2): 183-195.
Worum, J. and Pedersen, H., 2019. Porosity Estimation using K-means clustering on Digital Images, University of Stavanger, UiS Brage.
Zimmermann, C., Stévant, I., Borel, C., Conne, B., Pitetti, J.L., Calvel, P., Kaessmann, H., Jégou, B., Chalmel, F. and Nef, S., 2015. Research resource: the dynamic transcriptional profile of sertoli cells during the progression of spermatogenesis. Mol Endocrinol, 29(4): 627-42.

10 Appendix

10.1 Appendix 1

Table 11: Overview of all petrographic results of sorting, roundness, sphericity, grain-grain contact and fabric.

Sample	Depth (m)	Formation	Mean Grain size (µm)*	Max grain size (µm)*	Grain size Udden Wentworth	Sorting Longiaru 1987	Roundness Pettijohn et al., 1973	Sphericity Pettijohn et al., 1973	Grain-grain contact Tucker 1988	Fabric
ÆR3-9S-3	2851.55	Lysing	260 µm	2000 µm	Medium sand	Moderately good	Subrounded-Subangular	Low	Point contact to plane	no fabric
ÆR3-9S-6	2860.58	Lysing	280 µm	680 µm	Medium sand	Very good	Subrounded-Subangular	Low	Plane contact to sutured	no fabric
ÆR3-9S-9	2871.5	Lysing	250 µm	1000 µm	Medium sand	Very good to moderately good	Subrounded-Subangular	High	concave-convex	no fabric
ÆR3-9S-12	2874.72	Lysing	220 µm	800 µm	Fine to medium sand	Very good to moderately good	Subrounded-Subangular	High	concave-convex	no fabric
ÆR3-9S-18	2879.85	Lysing	280 µm	1200 µm	Medium sand	Moderately good	Subangular	Low	concave-convex	no fabric
ÆR3-9S-21	2885.35	Lysing	180 µm	600 µm	Fine sand	Very good to moderately good	Subrounded to subangular	High	concave-convex, sutured	no fabric
MA2-4-5	2842.46	Lysing	250 µm	1400 µm	Medium sand	Very good to moderately good	Subrounded-Subangular	High	Plane contact	aligned grains
MA2-4-8	2846.8	Lysing	400 µm	1600 µm	Medium sand	Moderate/poor	Subrounded-Subangular	High	Point contact	no fabric
MA2-4-13	2848.53	Lysing	280 µm	800 µm	Medium sand	Moderately good	Rounded to subrounded	High	Point to plane	aligned grains
MA2-4-16	3336.5	Lange	220 µm	600 µm	Fine to medium sand	Very good to moderately good	Rounded to subrounded	High	Plane contact	aligned grains
MA2-4-18	3340.5	Lange	280 µm	1000 µm	Medium sand	Moderately good	Subrounded-Subangular	High	concave-convex, sutured	no fabric
MA2-2-3	2824.3	Lysing	180 µm	480 µm	Fine sand	Very good	Subrounded	High	concave-convex	no fabric
MA2-2-10	3282.55	Lange	240 µm	720 µm	Fine to medium sand	Moderately good	Subrounded to subangular	Low	concave-convex, sutured	weak to no alignement
MA2-2-12	3288.1	Lange	300 µm	1000 µm	Medium sand	Moderately good	Subrounded-Subangular	Low	concave-convex	no fabric
MA2-2-15	3337.6	Lange	300 µm	1000 µm	Medium sand	Moderately good	Subangular-Angular	Low	concave-convex, sutured	aligned grains
SK5-A-3	2966.45	Lange	320 µm	1600 µm	Medium sand	Moderate/poor	Subrounded to angular	Low	concave-convex, sutured	no fabric
SK5-A-6	2970.51	Lange	400 µm	8000 µm	Medium sand	Moderately good	Subrounded-Subangular	Low	concave-convex	no fabric
SK5-A-9	2973.55	Lange	400 µm	1000 µm	Medium sand	Very good	Subrounded to subangular	High	Concave-convex to point	no fabric
ÆR5-8-3	2802.85	Lysing	240 µm	1800 µm	Fine to medium sand	Moderate/poor	Subangular	Low	point to concave-convex	no fabric
ÆR5-8-5	2811.66	Lysing	240 µm	1200 µm	Fine to medium sand	Moderate/poor	Rounded to subangular	Low	Point to plane	weak to no alignement
ÆR5-8-7	2815.43	Lysing	220 µm	1000 µm	Fine to medium sand	Moderately good	Subrounded-Subangular	High	Point to plane	no fabric
ÆR5-8-10	2821.85	Lysing	200 µm	780 µm	Fine to medium sand	Moderately good	Subrounded-Subangular	Low	Point contact to plane	aligned grains
ÆR5-8-13	2822.65	Lysing	320 µm	1400 µm	Medium sand	Moderate/poor	Rounded to subrounded	High	concave-convex, sutured	weak to no alignement
DE1-3	3504.32	Lange	600 µm	1200 µm	Coarse sand	Moderately good	Subrounded to angular	Low	concave-convex, sutured	no fabric
DE1-6	3507.57	Lange	300 µm	1000 µm	Medium sand	Moderate/poor	Subrounded to angular	Low	concave-convex, sutured	aligned grains
DE1-10	3509.1	Lange	320 µm	1000 µm	Medium sand	Moderately good	Subangular	High	Sutured contact	aligned grains
DE1-13	3512.7	Lange	500 µm	800 µm	Medium to Coarse sand	Moderately good	Subrounded-Subangular	Low	concave-convex, sutured	weak to no alignement

Table 12: Composition values of all petrographic samples. Qt=total quartz, F= Feldspar, L= lithic fragments, Qm= monocrystalline quartz, Lt= total lithic including polycrystalline quartz, Qp= polycrystalline quartz, IGV= intergranular volume, COPL= porosity loss by compaction and CEPL= porosity loss by cementation.

Sample	Depth (m)	Formation	J-code	Qt	F	L	Qm	F	Lt	Qm, non-undulator	Qm, undulatory	Qp, 2-3 xx	Qp, >3 xx	Qp,2-3 ny	Qp,>3 ny	Intergranular porosity	Sum Cement	IGV	COPL	CEPL	Total porosity loss
ÆR3-9S-3	2851.55	Lysing	1	98.90	1.10	0.00	88.46	1.10	10.44	64.56	16.96	3.29	6.33	-3.04	3.04	8.0	14.6	24.3	20.75	11.58	32.33
ÆR3-9S-6	2860.58	Lysing	2	100.00	0.00	0.00	97.78	0.00	2.22	69.97	20.14	1.71	0.34	1.37	-1.37	11.1	7.6	18.7	26.20	5.60	31.80
ÆR3-9S-9	2871.5	Lysing	3	99.00	1.00	0.00	90.30	1.00	8.70	69.07	12.01	5.11	2.70	2.40	-2.40	8.8	9.1	20.7	24.34	6.86	31.20
ÆR3-9S-12	2874.72	Lysing	4	98.83	1.17	0.00	93.55	1.17	5.28	83.80	5.31	2.23	2.79	-0.56	0.56	8.8	15.9	31.8	11.98	14.01	25.99
ÆR3-9S-18	2879.85	Lysing	5	98.45	1.55	0.00	91.93	1.55	6.52	75.88	11.18	2.35	3.82	-1.47	1.47	18.0	13.0	33.1	10.34	11.66	22.00
ÆR3-9S-21	2885.35	Lysing	6	79.88	19.82	0.30	68.90	19.82	9.76	43.66	20.00	4.79	3.94	0.85	-0.85	19.3	5.4	24.6	20.39	4.28	24.67
MA2-4-5	2842.46	Lysing	7	96.21	3.54	0.25	89.65	3.54	6.82	73.08	12.26	1.68	4.57	-2.88	2.88	13.3	7.0	20.5	24.57	5.29	29.86
MA2-4-8	2846.8	Lysing	8	96.29	3.43	0.29	92.86	3.43	3.71	76.99	12.05	2.74	0.55	2.19	-2.19	15.0	8.7	23.7	21.36	6.87	28.23
MA2-4-13	2848.53	Lysing	9	96.15	3.85	0.00	89.94	3.85	6.21	70.94	15.67	3.42	2.56	0.85	-0.85	17.7	9.1	26.7	18.09	7.42	25.51
MA2-4-16	3336.5	Lange	10	88.73	9.31	1.96	88.73	9.31	1.96	74.14	3.88	0.00	0.00	0.00	0.00	0.6	33.9	34.4	8.47	31.02	39.49
MA2-4-18	3340.5	Lange	11	95.50	4.50	0.00	85.00	4.50	10.50	69.38	11.96	6.70	3.35	3.35	-3.35	13.1	10.2	23.3	21.80	7.96	29.76
MA2-2-3	2824.3	Lysing	12	96.58	3.42	0.00	94.41	3.42	2.17	84.00	2.86	1.43	0.57	0.86	-0.86	12.5	18.9	31.6	12.28	16.56	28.85
MA2-2-10	3282.55	Lange	13	96.55	3.45	0.00	91.22	3.45	5.33	57.10	23.96	2.23	2.51	-0.28	0.28	2.1	21.3	23.5	21.62	16.71	38.33
MA2-2-12	3288.1	Lange	14	98.06	1.94	0.00	93.91	1.94	4.16	71.05	19.84	1.88	2.14	-0.27	0.27	5.5	8.1	13.6	30.53	5.61	36.15
MA2-2-15	3337.6	Lange	15	95.40	4.60	0.00	92.53	4.60	2.87	72.65	13.67	1.88	0.80	1.07	-1.07	13.5	12.5	25.9	18.98	10.11	29.09
SK5-A-3	2966.45	Lange	16	88.41	11.59	0.00	83.77	11.59	4.64	36.50	18.14	2.38	0.65	1.73	-1.73	25.7	2.6	28.3	16.33	2.15	18.49
SK5-A-6	2970.51	Lange	17	92.92	4.00	3.08	83.38	4.00	12.62	69.01	7.32	4.23	4.51	-0.28	0.28	18.1	6.9	27.2	17.56	5.73	23.29
SK5-A-9	2973.55	Lange	18	83.03	16.97	0.00	75.15	16.97	7.88	46.38	20.11	2.14	4.83	-2.68	2.68	15.0	7.0	22.0	23.06	5.38	28.44
ÆR5-8-3	2802.85	Lysing	19	98.66	0.80	0.53	89.57	0.80	9.63	66.02	14.70	2.41	5.78	-3.37	3.37	5.7	12.6	20.8	24.24	9.54	33.78
ÆR5-8-5	2811.66	Lysing	20	97.69	2.31	0.00	94.22	2.31	3.47	80.90	5.57	1.59	1.59	0.00	0.00	14.3	10.9	25.6	19.37	8.82	28.19
ÆR5-8-7	2815.43	Lysing	21	99.41	0.59	0.00	96.44	0.59	2.97	82.86	10.00	0.57	2.29	-1.71	1.71	14.4	10.1	25.6	19.39	8.14	27.53
ÆR5-8-10	2821.85	Lysing	22	98.89	0.74	0.37	94.46	0.74	4.80	74.76	7.03	1.60	2.24	-0.64	0.64	9.9	8.5	24.8	20.25	6.77	27.02
ÆR5-8-13	2822.65	Lysing	23	95.45	4.55	0.00	83.52	4.55	11.93	67.22	13.77	2.20	9.37	-7.16	7.16	14.9	5.4	20.3	24.67	4.08	28.75
DE1-3	3504.32	Lange	24	94.86	5.14	0.00	86.82	5.14	8.04	60.34	17.24	2.30	4.89	-2.59	2.59	6.5	7.2	13.7	30.50	5.00	35.50
DE1-6	3507.57	Lange	25	95.48	4.52	0.00	87.57	4.52	7.91	50.46	20.64	3.21	3.21	0.00	0.00	1.2	8.8	10.4	33.01	5.89	38.90
DE1-10	3509.1	Lange	26	94.74	5.26	0.00	90.64	5.26	4.09	62.35	13.45	1.71	1.71	0.00	0.00	10.3	10.7	21.7	23.35	8.18	31.53
DE1-13	3512.7	Lange	27	94.14	5.86	0.00	88.58	5.86	5.56	63.38	17.46	3.94	1.13	2.82	-2.82	10.9	9.8	21.2	23.88	7.48	31.36

Table 13: Composition values of all petrographic samples. Ls= lithic sandstone.

Sample	Depth (m)	Formation	Qm, non-undulatory	Qm, undulatory	Qp, 2-3 xx	Qp, >3 xx	Chert	Sum Q	Alkali feldspar	Plagioclase	Sum F	Ls, Pelite	Sum L	Muscovite	Biotite	Chlorite	Fe oxide	Glauconite	Pyrite	Zircon	Garnet
ÆR3-9S-3	2851.55	Lysing	64.56	16.96	3.29	6.33	0.76	91.14	0.76	0.25	1.01	0.00	0.00	6.33	0.00	0.00	0.00	0.00	1.27	0.25	0.00
ÆR3-9S-6	2860.58	Lysing	69.97	20.14	1.71	0.34	0.00	92.15	0.00	0.00	0.00	0.00	0.00	6.48	0.00	0.00	0.34	0.00	0.00	0.00	1.02
ÆR3-9S-9	2871.5	Lysing	69.07	12.01	5.11	2.70	0.00	88.89	0.90	0.00	0.90	0.00	0.00	8.11	0.00	0.00	0.00	0.30	0.90	0.00	0.90
ÆR3-9S-12	2874.72	Lysing	83.80	5.31	2.23	2.79	0.84	94.13	0.56	0.56	1.12	0.00	0.00	1.40	0.00	0.56	0.00	1.12	1.68	0.00	0.00
ÆR3-9S-18	2879.85	Lysing	75.88	11.18	2.35	3.82	1.47	93.24	1.18	0.29	1.47	0.00	0.00	3.82	0.29	0.59	0.00	0.00	0.59	0.00	0.00
ÆR3-9S-21	2885.35	Lysing	43.66	20.00	4.79	3.94	1.41	73.80	17.75	0.56	18.31	0.28	0.28	3.66	0.28	0.85	1.41	1.13	0.00	0.00	0.28
MA2-4-5	2842.46	Lysing	73.08	12.26	1.68	4.57	0.72	91.59	3.13	0.24	3.37	0.24	0.24	3.37	0.24	0.00	0.00	0.96	0.24	0.00	0.00
MA2-4-8	2846.8	Lysing	76.99	12.05	2.74	0.55	0.82	92.33	3.01	0.27	3.29	0.27	0.27	3.56	0.00	0.00	0.00	0.55	0.00	0.00	0.00
MA2-4-13	2848.53	Lysing	70.94	15.67	3.42	2.56	0.00	92.59	3.42	0.28	3.70	0.00	0.00	3.42	0.00	0.00	0.00	0.00	0.28	0.00	0.00
MA2-4-16	3336.5	Lange	74.14	3.88	0.00	0.00	0.00	78.02	8.19	0.00	8.19	1.72	1.72	12.07	0.00	0.00	0.00	0.00	0.00	0.00	0.00
MA2-4-18	3340.5	Lange	69.38	11.96	6.70	3.35	0.00	91.39	4.31	0.00	4.31	0.00	0.00	4.31	0.00	0.00	0.00	0.00	0.00	0.00	0.00
MA2-2-3	2824.3	Lysing	84.00	2.86	1.43	0.57	2.57	88.86	2.57	0.57	3.14	0.00	0.00	8.00	0.00	0.00	0.00	0.00	0.00	0.00	0.00
MA2-2-10	3282.55	Lange	57.10	23.96	2.23	2.51	0.00	85.79	3.06	0.00	3.06	0.00	0.00	10.86	0.00	0.00	0.00	0.00	0.00	0.28	0.00
MA2-2-12	3288.1	Lange	71.05	19.84	1.88	2.14	0.00	94.91	1.88	0.00	1.88	0.00	0.00	2.95	0.00	0.00	0.00	0.27	0.00	0.00	0.00
MA2-2-15	3337.6	Lange	72.65	13.67	1.88	0.80	0.00	89.01	3.49	0.80	4.29	0.00	0.00	4.02	0.80	0.27	0.00	1.34	0.27	0.00	0.00
SK5-A-3	2966.45	Lange	36.50	18.14	2.38	0.65	0.00	57.67	4.75	3.02	7.56	0.00	0.00	4.10	1.30	0.22	0.65	0.22	3.46	0.00	0.43
SK5-A-6	2970.51	Lange	69.01	7.32	4.23	4.51	0.00	85.07	2.25	1.41	3.66	2.82	2.82	6.48	0.56	0.28	0.56	0.28	0.00	0.28	0.00
SK5-A-9	2973.55	Lange	46.38	20.11	2.14	4.83	0.00	73.46	10.99	4.02	15.01	0.00	0.00	4.02	1.88	0.80	0.00	4.83	0.00	0.00	0.00
ÆR5-8-3	2802.85	Lysing	66.02	14.70	2.41	5.78	1.20	88.92	0.00	0.72	0.72	0.48	0.48	8.19	0.00	0.24	0.00	0.72	0.72	0.00	0.00
ÆR5-8-5	2811.66	Lysing	80.90	5.57	1.59	1.59	0.53	89.66	1.86	0.27	2.12	0.00	0.00	6.63	0.00	0.27	0.27	1.06	0.00	0.00	0.00
ÆR5-8-7	2815.43	Lysing	82.86	10.00	0.57	2.29	0.00	95.71	0.57	0.00	0.57	0.00	0.00	2.57	0.00	0.00	0.00	0.29	0.86	0.00	0.00
ÆR5-8-10	2821.85	Lysing	74.76	7.03	1.60	2.24	0.32	85.62	0.00	0.64	0.64	0.32	0.32	10.54	0.00	0.32	0.00	0.32	1.60	0.32	0.32
ÆR5-8-13	2822.65	Lysing	67.22	13.77	2.20	9.37	0.00	92.56	4.13	0.28	4.41	0.00	0.00	1.38	0.00	0.00	0.00	0.55	0.00	0.00	1.10
DE1-3	3504.32	Lange	60.34	17.24	2.30	4.89	0.29	84.77	3.45	1.15	4.60	0.00	0.00	10.34	0.00	0.00	0.00	0.00	0.29	0.00	0.00
DE1-6	3507.57	Lange	50.46	20.64	3.21	3.21	0.00	77.52	1.83	1.83	3.67	0.00	0.00	18.35	0.46	0.00	0.00	0.00	0.00	0.00	0.00
DE1-10	3509.1	Lange	62.35	13.45	1.71	1.71	0.00	79.22	3.42	0.98	4.40	0.00	0.00	12.71	2.69	0.00	0.00	0.98	0.00	0.00	0.00
DE1-13	3512.7	Lange	63.38	17.46	3.94	1.13	0.00	85.92	3.38	1.97	5.35	0.00	0.00	6.20	0.28	0.00	0.00	2.25	0.00	0.00	0.00

Table 14: Composition values of all petrographic samples.

Sample	Depth (m)	Formation	Diagenetic dissolution	Q matrix	Sum matrix	Q cement	Cc cement	Pyrite cement	Fe oxide cement	Glauconite cement	Chlorite cement	Illite cement	Smectite cement	Kaolinite cement	Sum Cement	Intergranular porosity	Intragranular porosity	Sum Porosity	IGV
ÆR3-9S-3	2851.55	Lysing	0.76	1.71	1.71	0.19	3.04	4.17	0.38	0.38	0.00	0.57	0.19	5.69	14.61	7.97	0.00	7.97	24.29
ÆR3-9S-6	2860.58	Lysing	1.90	0.00	0.00	0.54	2.71	0.00	0.00	0.81	0.00	0.00	0.00	3.52	7.59	11.11	0.00	11.11	18.70
ÆR3-9S-9	2871.5	Lysing	1.86	2.79	2.79	0.93	5.58	0.00	0.00	0.23	0.00	0.00	0.00	2.33	9.07	8.84	0.00	8.84	20.70
ÆR3-9S-12	2874.72	Lysing	0.75	7.12	7.12	0.56	4.68	1.69	0.37	1.69	0.37	0.00	1.69	4.87	15.92	8.80	0.37	9.18	31.84
ÆR3-9S-18	2879.85	Lysing	1.72	2.10	2.10	0.00	4.21	2.87	0.19	0.19	0.00	1.34	0.19	4.02	13.00	17.97	0.19	18.16	33.08
ÆR3-9S-21	2885.35	Lysing	2.04	0.00	0.00	0.37	0.00	0.00	0.00	0.00	0.00	0.00	0.00	0.37	5.37	19.26	7.59	26.85	24.63
MA2-4-5	2842.46	Lysing	0.76	0.19	0.19	0.00	2.08	0.00	0.00	1.14	0.00	0.95	0.76	2.08	7.01	13.26	0.00	13.26	20.45
MA2-4-8	2846.8	Lysing	0.42	0.00	0.00	0.00	1.66	0.00	0.00	1.66	0.21	1.04	2.29	1.87	8.73	14.97	0.00	14.97	23.70
MA2-4-13	2848.53	Lysing	1.03	0.00	0.00	0.00	2.06	0.41	0.41	0.62	0.00	1.23	1.03	3.29	9.05	17.70	0.00	17.70	26.75
MA2-4-16	3336.5	Lange	1.11	0.00	0.00	0.00	12.22	0.28	0.28	0.56	0.00	6.39	10.56	3.61	33.89	0.56	0.00	0.56	34.44
MA2-4-18	3340.5	Lange	0.73	0.00	0.00	0.00	5.45	0.73	0.36	0.36	0.00	0.73	0.00	2.55	10.18	13.09	0.00	13.09	23.27
MA2-2-3	2824.3	Lysing	0.77	0.19	0.19	0.00	2.70	0.00	0.00	0.39	0.00	2.70	11.95	1.16	18.88	12.52	0.19	12.72	31.60
MA2-2-10	3282.55	Lange	0.00	0.00	0.00	0.00	10.66	0.00	0.21	0.21	0.00	1.28	6.61	2.35	21.32	2.13	0.00	2.13	23.45
MA2-2-12	3288.1	Lange	0.23	0.00	0.00	0.00	0.00	0.00	0.00	0.00	0.00	1.39	0.92	5.77	8.08	5.54	0.00	5.54	13.63
MA2-2-15	3337.6	Lange	0.20	0.00	0.00	0.00	0.20	0.20	0.00	1.58	0.00	2.77	2.18	5.54	12.48	13.47	0.00	13.47	25.94
SK5-A-3	2966.45	Lange	0.00	0.00	0.00	2.00	0.00	0.00	0.00	0.00	0.00	0.57	0.00	0.00	2.57	25.71	4.00	29.71	28.29
SK5-A-6	2970.51	Lange	3.86	2.12	2.12	0.58	1.16	0.00	2.32	0.58	0.19	0.00	0.00	2.12	6.95	18.15	0.39	18.53	27.22
SK5-A-9	2973.55	Lange	0.21	0.00	0.00	0.41	0.00	0.00	0.00	5.97	0.00	0.41	0.00	0.62	7.00	15.02	0.62	15.64	22.02
ÆR5-8-3	2802.85	Lysing	2.92	2.55	2.55	0.18	0.91	3.10	2.37	0.18	0.00	0.73	0.18	4.93	12.59	5.66	0.55	6.20	20.80
ÆR5-8-5	2811.66	Lysing	0.78	0.39	0.39	0.20	1.76	1.95	0.00	0.98	0.00	1.37	0.78	3.91	10.94	14.26	0.00	14.26	25.59
ÆR5-8-7	2815.43	Lysing	2.27	1.03	1.03	0.21	1.24	1.86	0.21	0.82	0.00	0.41	0.21	5.15	10.10	14.43	0.00	14.43	25.57
ÆR5-8-10	2821.85	Lysing	1.42	6.37	6.37	0.24	5.19	0.00	0.00	0.00	0.47	0.24	0.00	2.36	8.49	9.91	0.00	9.91	24.76
ÆR5-8-13	2822.65	Lysing	0.65	0.00	0.00	0.87	2.16	0.00	0.00	0.43	0.00	0.00	0.00	1.95	5.41	14.94	2.60	17.53	20.35
DE1-3	3504.32	Lange	2.88	0.00	0.00	0.00	2.88	0.00	0.00	0.96	0.00	1.44	0.00	1.92	7.19	6.47	0.00	6.47	13.67
DE1-6	3507.57	Lange	2.88	0.41	0.41	0.00	3.07	0.41	0.20	1.02	0.20	1.43	0.41	2.04	8.79	1.23	0.00	1.23	10.43
DE1-10	3509.1	Lange	2.88	0.75	0.75	0.00	4.31	0.19	0.00	0.94	0.19	3.18	0.75	1.12	10.67	10.30	0.00	10.30	21.72
DE1-13	3512.7	Lange	2.88	0.44	0.44	0.00	1.53	0.00	0.00	2.62	0.00	1.31	0.87	3.49	9.83	10.92	0.00	10.92	21.18

10.3 Appendix 2

Table 15: Overview concentrations of major elements from the whole-rock geochemical analysis.

	Analyte	Wgt	SiO2	Al2O3	Fe2O3	MgO	CaO	Na2O	K2O	TiO2	P2O5	MnO	Cr2O3	Ba	Ni	Sc	LOI	Sum
	Unit	KG	%	%	%	%	%	%	%	%	%	%	%	PPM	PPM	PPM	%	%
	MDL	0	0.01	0.01	0.04	0.01	0.01	0.01	0.01	0.01	0.01	0.01	0.002	1	20	1	-5.1	0.01
Sample	Type																	
AL2S-1	Rock	0.014	52.68	19.02	6.19	1.52	1.07	1.02	2.68	0.88	0.14	0.19	0.015	8122	61	17	13.5	99.80
AL2S-3	Rock	0.014	64.39	11.81	7.41	1.15	0.99	0.30	1.87	0.62	0.17	0.10	0.009	4419	32	11	10.6	99.86
ÆR3-9S-1	Rock Pulp	0.012	86.58	6.12	1.56	0.29	0.34	0.07	0.92	0.32	0.04	0.02	0.005	229	<20	4	3.6	99.92
ÆR3-9S-4	Rock Pulp	0.012	88.03	5.25	1.28	0.28	0.34	0.04	0.85	0.30	0.04	0.02	0.006	150	<20	4	3.5	99.92
ÆR3-9S-5	Rock Pulp	0.012	87.98	5.45	1.28	0.28	0.26	0.06	0.92	0.33	0.05	0.01	0.005	282	<20	4	3.2	99.91
ÆR3-9S-7	Rock Pulp	0.012	89.11	5.17	0.88	0.16	0.20	0.26	0.89	0.33	0.04	<0.01	0.006	358	<20	2	2.8	99.92
ÆR3-9S-10	Rock Pulp	0.012	84.60	5.99	1.82	0.37	1.21	0.35	0.89	0.26	0.06	0.03	0.004	275	<20	3	4.3	99.88
ÆR3-9S-13	Rock Pulp	0.012	82.84	6.11	3.36	0.66	0.56	0.37	0.88	0.31	0.04	0.06	0.004	229	<20	6	4.7	99.91
ÆR3-9S-16	Rock Pulp	0.012	88.33	5.14	1.24	0.22	0.39	0.34	0.80	0.28	0.04	0.02	0.005	180	<20	3	3.1	99.92
ÆR3-9S-19	Rock Pulp	0.012	79.33	5.96	2.01	1.12	3.35	0.44	0.91	0.28	0.05	0.06	0.004	260	<20	4	6.3	99.91
ÆR3-9S-22	Rock Pulp	0.012	58.00	21.39	3.89	1.33	0.28	1.18	2.63	1.02	0.14	0.04	0.018	436	53	18	9.9	99.84
ÆR3-9S-23	Rock Pulp	0.012	58.80	20.39	4.49	1.53	0.30	1.32	2.82	0.95	0.11	0.02	0.016	418	47	19	9.0	99.84
MA2-4-1	Rock	0.012	88.56	4.69	1.14	0.24	0.24	0.17	0.82	0.51	0.05	0.01	0.007	1378	<20	3	3.3	99.88
MA2-4-3	Rock	0.012	87.59	5.67	1.08	0.23	0.27	0.17	1.01	0.29	0.05	0.01	0.005	709	<20	3	3.5	99.91
MA2-4-6	Rock	0.012	88.14	5.31	1.13	0.33	0.63	0.14	0.91	0.27	0.05	0.01	0.005	226	<20	3	3.0	99.91
MA2-4-9	Rock	0.012	87.97	4.94	1.31	0.32	0.60	0.14	0.89	0.32	0.06	0.03	0.005	353	<20	3	3.3	99.91
MA2-4-11	Rock	0.012	88.38	4.76	0.92	0.32	0.66	0.15	0.88	0.26	0.05	0.01	0.002	172	<20	3	3.5	99.92
MA2-4-14	Rock	0.012	67.73	8.43	3.72	2.35	4.59	0.25	0.77	0.48	0.05	0.07	0.005	153	<20	7	11.4	99.85
MA2-4-17	Rock	0.012	88.21	5.52	0.31	0.10	0.07	0.11	0.35	0.30	0.05	<0.01	<0.002	246	<20	1	4.9	99.90
MA2-4-19	Rock	0.012	63.14	9.15	4.28	2.89	5.64	0.23	1.45	0.54	0.12	0.08	0.008	450	28	17	12.3	99.86
MA2-2-2	Rock	0.014	75.84	7.75	1.95	1.41	3.13	0.23	1.43	0.33	0.05	0.02	0.005	1236	<20	4	7.6	99.92
MA2-2-5	Rock	0.014	66.84	3.09	3.36	3.54	8.90	0.09	0.52	0.20	0.01	0.06	<0.002	129	<20	3	13.3	99.90
MA2-2-7	Rock	0.014	58.27	20.61	4.11	1.03	0.60	0.96	2.55	0.95	0.09	0.04	0.015	948	96	15	10.5	99.83
MA2-2-9	Rock	0.014	80.75	7.26	1.33	0.79	1.72	0.09	1.17	0.52	0.04	0.02	0.004	5701	<20	4	5.6	99.88
MA2-2-11	Rock	0.014	88.74	5.36	0.58	0.23	0.37	0.11	0.72	0.47	0.03	<0.01	0.004	3118	<20	2	3.0	99.93
MA2-2-13	Rock	0.014	55.77	20.75	4.79	1.56	0.48	1.22	3.56	0.97	0.11	0.03	0.017	861	69	20	10.5	99.82
MA2-2-14	Rock	0.014	82.72	6.65	1.62	0.59	1.31	0.77	0.93	0.56	0.03	0.03	0.006	2806	<20	5	4.4	99.92
SK5-A-1	Rock Pulp	0.012	85.02	7.07	1.57	0.44	0.16	0.73	1.94	0.23	0.04	<0.01	0.005	267	<20	5	2.7	99.91
SK5-A-4	Rock Pulp	0.012	85.71	6.26	1.46	0.39	0.23	0.58	1.76	0.27	0.05	0.02	0.003	1332	<20	4	3.0	99.91
SK5-A-7	Rock Pulp	0.012	79.96	7.87	2.98	0.69	0.74	0.85	2.22	0.25	0.04	0.02	0.004	662	<20	5	4.2	99.92
SK5-A-10	Rock Pulp	0.012	53.34	20.46	7.40	1.92	0.90	1.17	2.59	0.92	0.10	0.21	0.016	454	64	21	10.7	99.84
SK5-A-11	Rock Pulp	0.012	54.29	22.29	5.62	1.82	0.44	1.19	2.59	0.96	0.10	0.18	0.017	482	76	21	10.3	99.85
SK5-A-12	Rock Pulp	0.012	75.42	9.10	2.48	0.76	3.42	1.00	2.00	0.51	0.05	0.06	0.006	334	<20	7	5.0	99.88
SK5-A-13	Rock Pulp	0.012	75.16	10.57	3.57	1.02	0.99	1.05	2.18	0.57	0.05	0.03	0.006	394	25	9	4.6	99.87
ÆR5-8-1	Rock Pulp	0.012	89.78	4.91	1.05	0.31	0.21	0.34	0.91	0.27	0.05	0.01	0.006	225	<20	3	2.1	99.91
ÆR-8-4	Rock Pulp	0.012	89.35	5.07	1.07	0.28	0.30	0.35	0.99	0.34	0.05	0.01	0.005	172	<20	3	2.1	99.91
ÆR5-8-6	Rock Pulp	0.012	88.57	5.61	1.16	0.26	0.20	0.42	1.05	0.37	0.05	0.01	0.006	193	<20	3	2.2	99.90
ÆR5-8-8	Rock Pulp	0.012	83.82	7.71	2.07	0.38	0.19	0.61	1.39	0.35	0.06	0.01	0.004	433	<20	5	3.3	99.90
ÆR5-8-11	Rock Pulp	0.012	89.33	4.86	1.27	0.22	0.25	0.40	0.94	0.23	0.04	0.01	0.003	177	<20	2	2.3	99.92
ÆR5-8-14	Rock Pulp	0.012	84.63	6.64	2.13	0.39	0.30	0.57	1.23	0.28	0.06	0.02	0.006	379	<20	4	3.6	99.90
DE1-1	Rock	0.012	84.51	7.03	1.24	0.36	0.30	0.97	1.50	0.27	0.05	0.02	0.005	7739	<20	4	2.8	99.89
DE1-5	Rock	0.012	85.15	6.46	1.69	0.31	0.25	0.85	1.40	0.24	0.05	0.04	0.005	6084	<20	4	2.8	99.89
DE1-7	Rock	0.012	79.18	8.61	3.34	0.62	0.55	1.22	1.22	0.55	0.05	0.02	0.007	3169	28	6	4.1	99.87
DE1-8	Rock	0.012	80.13	8.51	1.99	0.71	0.94	1.32	1.12	0.54	0.05	0.04	0.008	4562	<20	6	4.0	99.85
DE1-11	Rock	0.012	81.90	8.17	1.74	0.55	0.65	1.23	1.07	0.51	0.06	0.03	0.008	5808	<20	6	3.3	99.86
DE1-14	Rock	0.012	82.37	7.36	2.97	0.39	0.31	1.08	1.02	0.41	0.05	0.01	0.006	3339	<20	5	3.5	99.87

Table 16: Overview concentrations of trace elements from the whole-rock geochemical analysis.

	Be	Co	Cs	Ga	Hf	Nb	Rb	Sn	Sr	Ta	Th	U	V	W	Zr	Y	La	Ce
	PPM	PPM	PPM	PPM	PPM	PPM	PPM	PPM	PPM	PPM	PPM	PPM	PPM	PPM	PPM	PPM	PPM	PPM
	1	0.2	0.1	0.5	0.1	0.1	0.1	1	0.5	0.1	0.2	0.1	8	0.5	0.1	0.1	0.1	0.1
Sample																		
AL2S-1	2	21.9	7.9	20.8	4.8	15.4	103.0	2	392.7	1.1	11.9	2.7	190	3.1	183.1	23.3	37.8	80.2
AL2S-3	<1	10.5	3.5	14.2	5.8	13.7	62.2	2	254.2	1.0	7.0	2.0	108	1.1	210.0	19.0	23.8	49.1
ÆR3-9S-1	<1	3.8	0.7	6.1	4.0	7.7	26.1	<1	23.0	0.4	3.9	0.3	47	1.0	149.6	5.9	9.7	18.7
ÆR3-9S-4	3	3.5	0.7	5.6	3.8	7.5	25.7	<1	24.4	0.4	3.4	0.3	46	<0.5	147.1	6.9	13.5	27.3
ÆR3-9S-5	2	2.4	0.7	6.3	4.3	8.4	27.7	1	29.7	0.6	3.7	0.2	47	1.0	157.1	7.5	14.2	31.8
ÆR3-9S-7	1	2.3	0.7	6.0	4.5	9.9	25.8	<1	32.8	0.4	3.4	0.5	36	0.6	184.4	5.8	12.9	29.0
ÆR3-9S-10	<1	3.0	0.7	10.1	5.6	28.3	27.8	2	48.0	1.4	4.7	0.9	48	1.9	221.8	18.2	25.6	57.8
ÆR3-9S-13	3	3.3	0.9	6.1	3.8	8.2	27.8	<1	37.7	0.5	3.7	0.5	52	0.9	145.6	7.8	13.3	28.3
ÆR3-9S-16	1	2.3	0.6	4.7	4.0	8.1	23.1	<1	31.7	0.4	3.3	0.5	34	0.7	145.1	7.7	12.1	23.7
ÆR3-9S-19	<1	2.6	0.7	6.1	3.5	9.0	26.0	<1	75.3	0.4	3.6	0.4	38	0.7	125.9	8.4	13.3	27.1
ÆR3-9S-22	2	15.8	7.0	24.7	5.2	17.0	100.8	2	91.2	1.3	12.7	1.9	250	2.4	196.0	23.7	37.8	81.9
ÆR3-9S-23	2	15.0	6.4	22.3	5.3	16.3	109.5	2	105.1	1.2	12.4	1.8	234	1.6	188.6	21.3	36.0	81.2
MA2-4-1	<1	7.7	1.0	5.0	8.4	10.4	19.9	<1	71.7	0.6	4.9	0.7	40	0.8	338.5	7.4	15.1	30.2
MA2-4-3	2	3.5	1.0	6.3	3.5	7.0	26.1	<1	56.3	0.5	3.0	0.4	39	1.1	131.3	7.0	12.6	25.9
MA2-4-6	<1	2.7	0.9	5.5	3.3	6.3	20.9	<1	51.7	0.5	3.1	0.4	36	0.8	125.2	6.9	10.9	24.9
MA2-4-9	1	2.7	0.8	5.6	4.6	8.1	21.0	<1	57.7	0.4	3.7	0.6	40	0.6	182.2	7.7	14.3	30.4
MA2-4-11	1	2.2	0.4	4.7	3.6	6.8	20.0	<1	52.2	0.4	2.7	0.2	32	<0.5	139.8	6.6	11.0	23.6
MA2-4-14	<1	7.2	1.9	9.5	7.2	10.7	19.2	4	169.2	0.5	6.5	4.0	49	1.2	274.9	13.7	16.9	23.8
MA2-4-17	<1	4.3	0.7	6.5	4.2	7.3	10.1	3	35.7	0.4	5.5	3.4	24	0.9	177.3	6.4	12.4	18.2
MA2-4-19	3	7.2	1.6	10.9	6.9	9.8	37.3	2	276.7	0.8	5.4	2.9	75	0.8	253.5	23.4	17.8	27.7
MA2-2-2	<1	4.4	0.7	9.0	3.6	13.1	34.6	2	134.0	0.6	4.4	1.1	44	0.6	132.8	11.3	19.0	41.6
MA2-2-5	<1	2.1	0.4	2.5	3.0	5.2	14.3	<1	166.5	0.3	2.3	0.5	27	<0.5	114.2	5.9	8.6	18.2
MA2-2-7	<1	42.2	7.2	23.9	5.3	16.7	106.5	2	154.4	0.9	13.0	2.4	221	1.7	188.7	24.4	39.3	90.1
MA2-2-9	<1	3.5	0.6	7.7	8.7	9.6	30.0	1	228.5	0.8	6.5	1.7	32	1.1	349.0	13.7	19.0	34.9
MA2-2-11	2	1.9	0.3	4.9	7.4	8.5	13.6	<1	107.6	0.7	4.9	1.8	22	1.4	290.6	8.8	14.6	25.1
MA2-2-13	5	23.3	8.5	24.0	5.0	13.5	143.8	3	180.5	1.0	13.2	2.6	215	2.1	184.1	23.8	38.7	81.0
MA2-2-14	2	3.8	0.4	6.5	8.7	8.7	22.8	1	128.3	0.6	4.9	1.7	29	0.8	325.2	11.2	14.7	28.2
SK5-A-1	<1	2.2	1.5	7.8	2.6	5.5	61.4	2	57.1	0.4	2.8	0.4	56	<0.5	96.0	7.2	8.7	17.0
SK5-A-4	<1	2.2	1.0	7.1	4.1	5.6	53.5	<1	87.1	0.4	2.7	0.5	46	0.6	148.6	8.5	8.6	15.7
SK5-A-7	1	2.6	1.2	9.2	2.7	6.4	67.1	1	69.9	0.4	2.5	0.4	45	0.7	99.4	6.8	9.8	15.7
SK5-A-10	2	21.0	6.5	23.4	4.4	13.7	102.6	2	132.5	1.0	11.3	1.6	198	1.6	161.0	18.7	35.8	71.5
SK5-A-11	5	22.3	6.8	25.7	5.0	15.0	105.6	2	123.8	1.0	12.7	2.1	201	2.0	163.9	20.0	35.9	75.1
SK5-A-12	<1	4.1	1.4	9.4	8.0	9.3	61.3	1	115.8	0.6	4.2	1.1	47	1.0	316.4	11.5	16.5	32.3
SK5-A-13	3	5.6	1.8	11.0	8.2	11.2	71.0	2	90.3	0.6	5.3	1.1	59	1.1	294.2	12.4	17.6	29.6
ÆR5-8-1	2	2.9	2.4	4.9	3.9	7.0	25.4	<1	31.9	0.4	3.4	0.6	37	1.5	155.2	7.0	11.4	26.0
ÆR-8-4	<1	2.4	1.5	5.6	4.4	8.4	28.8	1	28.2	0.5	3.6	0.6	45	1.2	164.6	7.7	14.4	27.9
ÆR5-8-6	<1	3.4	1.5	5.8	5.3	9.4	28.2	1	32.3	0.6	3.7	0.8	40	0.8	202.8	6.8	14.3	31.7
ÆR5-8-8	<1	4.6	3.0	8.9	4.1	13.7	43.8	1	52.2	0.8	3.9	1.0	65	1.0	158.6	11.1	16.9	40.3
ÆR5-8-11	3	2.6	1.6	4.8	3.4	10.1	25.9	<1	35.3	0.6	3.0	0.4	44	1.1	129.0	6.0	13.3	27.6
ÆR5-8-14	2	4.2	3.8	7.0	3.6	11.1	37.4	<1	51.0	0.6	4.2	0.7	70	3.2	136.6	9.3	18.4	41.4
DE1-1	1	3.0	1.0	8.3	3.8	5.5	43.6	1	294.0	0.5	3.5	0.5	34	1.7	135.0	7.8	11.1	19.5
DE1-5	<1	2.6	0.9	7.1	4.0	5.2	40.4	<1	240.8	0.4	2.6	0.5	25	0.7	145.7	5.9	9.2	17.2
DE1-7	4	5.2	0.9	10.5	8.7	10.7	38.9	2	147.6	0.7	5.6	1.9	49	1.5	320.6	12.7	18.0	31.1
DE1-8	3	3.4	0.7	10.1	8.9	10.1	34.8	2	202.1	0.7	5.0	1.6	53	1.6	333.8	12.1	17.6	30.9
DE1-11	<1	3.2	0.6	8.6	8.7	10.1	31.5	1	222.9	0.7	4.8	1.1	46	1.1	342.1	10.3	15.2	26.3
DE1-14	<1	3.4	0.6	8.5	7.9	7.6	30.7	4	144.3	0.6	4.6	1.4	45	2.5	273.4	9.7	14.9	26.7

Table 17: Overview concentrations of trace elements from the whole-rock geochemical analysis.

	Pr	Nd	Sm	Eu	Gd	Tb	Dy	Ho	Er	Tm	Yb	Lu	TOT/C	TOT/S
	PPM	PPM	PPM	PPM	PPM	PPM	PPM	PPM	PPM	PPM	PPM	PPM	%	%
	0.02	0.3	0.05	0.02	0.05	0.01	0.05	0.02	0.03	0.01	0.05	0.01	0.02	0.02
Sample														
AL2S-1	8.24	30.1	5.71	1.16	4.94	0.72	4.42	0.88	2.59	0.37	2.65	0.40	3.79	1.09
AL2S-3	5.68	22.0	4.52	0.82	3.69	0.58	3.24	0.67	2.02	0.24	1.94	0.29	2.90	0.57
ÆR3-9S-1	2.19	7.8	1.34	0.25	1.10	0.20	1.25	0.23	0.69	0.08	0.87	0.11	0.75	0.46
ÆR3-9S-4	3.19	10.9	1.87	0.42	1.71	0.24	1.43	0.25	0.81	0.09	0.70	0.11	1.03	0.28
ÆR3-9S-5	3.49	11.7	2.18	0.42	1.71	0.27	1.56	0.26	0.87	0.11	0.74	0.11	0.77	0.16
ÆR3-9S-7	3.29	10.9	1.98	0.40	1.60	0.21	1.25	0.23	0.79	0.10	0.77	0.10	0.63	0.34
ÆR3-9S-10	6.47	23.4	4.76	0.86	3.95	0.64	3.62	0.65	2.15	0.24	1.63	0.23	1.02	0.43
ÆR3-9S-13	3.07	11.8	2.14	0.41	1.80	0.25	1.44	0.30	0.92	0.13	0.83	0.12	1.17	0.51
ÆR3-9S-16	2.72	9.3	1.79	0.33	1.49	0.23	1.49	0.29	1.00	0.12	0.82	0.12	0.57	0.43
ÆR3-9S-19	3.23	11.7	2.10	0.53	2.08	0.30	1.65	0.33	0.93	0.12	0.85	0.12	1.61	0.35
ÆR3-9S-22	9.01	33.1	6.36	1.24	5.38	0.80	4.45	0.88	2.58	0.36	2.65	0.38	2.11	0.63
ÆR3-9S-23	8.36	29.0	5.26	1.13	4.64	0.66	4.17	0.81	2.60	0.37	2.50	0.39	2.02	0.24
MA2-4-1	3.46	11.3	2.12	0.31	1.55	0.24	1.37	0.26	0.85	0.12	0.91	0.14	1.06	0.22
MA2-4-3	2.99	10.3	1.90	0.38	1.50	0.22	1.23	0.24	0.80	0.09	0.73	0.11	1.00	0.25
MA2-4-6	2.85	11.2	1.99	0.40	1.52	0.21	1.32	0.25	0.76	0.06	0.78	0.09	0.61	0.20
MA2-4-9	3.55	12.0	2.25	0.42	1.76	0.25	1.52	0.27	0.85	0.11	0.80	0.11	0.70	0.26
MA2-4-11	2.73	8.8	1.66	0.35	1.37	0.19	1.15	0.20	0.63	0.07	0.64	0.09	1.16	0.18
MA2-4-14	3.81	13.2	2.74	0.74	2.76	0.69	2.70	0.75	1.51	0.45	1.70	0.50	3.28	0.11
MA2-4-17	2.50	8.2	1.67	0.46	1.52	0.44	1.34	0.47	0.81	0.30	0.77	0.36	2.55	0.06
MA2-4-19	4.42	16.0	3.66	0.97	3.92	0.87	4.33	0.99	2.55	0.56	2.24	0.55	3.33	0.12
MA2-2-2	4.63	17.5	3.17	0.67	2.65	0.44	2.32	0.48	1.15	0.16	1.13	0.17	1.47	0.23
MA2-2-5	2.12	7.9	1.52	0.28	1.32	0.20	1.09	0.21	0.68	0.07	0.60	0.09	3.81	0.08
MA2-2-7	9.41	35.3	6.55	1.34	5.69	0.85	4.82	0.95	2.93	0.41	2.66	0.43	1.62	0.48
MA2-2-9	4.28	16.3	2.88	0.46	2.62	0.41	2.45	0.54	1.43	0.19	1.47	0.22	0.94	0.19
MA2-2-11	3.14	11.7	2.10	0.28	1.66	0.23	1.49	0.31	1.04	0.12	1.12	0.19	0.32	0.13
MA2-2-13	8.81	31.2	6.07	1.25	5.14	0.81	4.53	0.94	2.89	0.42	2.81	0.40	2.19	0.59
MA2-2-14	3.52	12.3	2.28	0.37	2.05	0.32	1.96	0.40	1.19	0.17	1.29	0.21	0.90	0.31
SK5-A-1	2.26	7.9	1.63	0.34	1.34	0.20	1.30	0.23	0.80	0.09	0.74	0.09	0.86	<0.02
SK5-A-4	2.07	7.3	1.39	0.30	1.39	0.22	1.41	0.30	1.03	0.15	0.95	0.13	1.32	0.06
SK5-A-7	2.31	7.7	1.51	0.33	1.31	0.19	1.20	0.22	0.75	0.07	0.70	0.09	1.68	0.02
SK5-A-10	7.92	27.8	5.01	1.01	4.05	0.65	3.68	0.75	2.58	0.36	2.52	0.36	2.19	1.03
SK5-A-11	7.97	27.5	4.91	0.95	3.86	0.58	3.69	0.82	2.55	0.36	2.46	0.37	1.90	0.19
SK5-A-12	3.96	14.5	2.57	0.44	2.30	0.31	2.20	0.43	1.37	0.19	1.34	0.18	1.50	0.18
SK5-A-13	4.04	14.6	2.79	0.38	2.32	0.34	2.10	0.43	1.36	0.19	1.44	0.21	1.51	0.19
ÆR5-8-1	2.74	10.6	1.85	0.43	1.67	0.25	1.30	0.27	0.84	0.08	0.70	0.11	0.41	0.21
ÆR-8-4	3.35	11.9	2.18	0.43	1.82	0.28	1.49	0.28	0.81	0.11	0.84	0.10	0.37	0.20
ÆR5-8-6	3.36	12.5	2.29	0.45	1.72	0.25	1.31	0.25	0.78	0.10	0.76	0.11	0.32	0.27
ÆR5-8-8	4.32	16.1	3.10	0.62	2.70	0.38	2.23	0.41	1.18	0.14	1.13	0.14	0.49	0.74
ÆR5-8-11	3.11	11.5	1.99	0.41	1.58	0.23	1.28	0.24	0.70	0.09	0.67	0.09	0.40	0.41
ÆR5-8-14	4.20	15.7	2.60	0.57	2.30	0.34	1.92	0.33	1.12	0.12	0.93	0.13	0.77	0.74
DE1-1	2.43	7.7	1.49	0.58	1.37	0.18	1.22	0.24	0.89	0.12	0.98	0.12	0.44	0.28
DE1-5	2.01	6.7	1.14	0.38	1.01	0.14	1.16	0.23	0.78	0.10	0.72	0.11	0.47	0.70
DE1-7	4.29	15.6	2.75	0.49	2.50	0.36	2.13	0.42	1.28	0.20	1.48	0.21	0.61	1.50
DE1-8	4.25	16.9	3.16	0.61	2.68	0.36	2.15	0.45	1.22	0.17	1.33	0.21	0.79	0.31
DE1-11	3.75	13.3	2.57	0.44	2.15	0.32	2.06	0.41	1.25	0.17	1.25	0.22	0.64	0.42
DE1-14	3.42	13.5	2.37	0.38	1.90	0.27	1.76	0.32	1.02	0.14	1.04	0.17	0.49	1.62

Table 18: Overview concentrations of trace elements from the whole-rock geochemical analysis.

	Mo	Cu	Pb	Zn	Ni	As	Cd	Sb	Bi	Ag	Au	Hg	Tl	Se
	PPM	PPM	PPM	PPM	PPM	PPM	PPM	PPM	PPM	PPM	PPB	PPM	PPM	PPM
	0.1	0.1	0.1	1	0.1	0.5	0.1	0.1	0.1	0.1	0.5	0.01	0.1	0.5
Sample														
AL2S-1	0.4	37.4	20.5	109	50.5	22.4	<0.1	0.1	0.4	<0.1	2.0	0.05	0.1	0.6
AL2S-3	0.3	17.5	11.2	76	26.7	9.3	<0.1	<0.1	0.2	<0.1	<0.5	0.04	0.1	<0.5
ÆR3-9S-1	0.1	6.2	4.3	32	9.9	5.2	<0.1	0.1	<0.1	<0.1	<0.5	0.02	<0.1	<0.5
ÆR3-9S-4	0.1	5.8	4.6	21	7.7	4.0	<0.1	0.1	<0.1	<0.1	<0.5	0.02	<0.1	<0.5
ÆR3-9S-5	0.1	5.2	4.7	20	6.6	2.5	<0.1	<0.1	<0.1	<0.1	<0.5	0.03	<0.1	<0.5
ÆR3-9S-7	0.1	3.9	4.2	19	6.5	2.4	<0.1	0.1	<0.1	<0.1	<0.5	0.02	<0.1	<0.5
ÆR3-9S-10	0.5	4.1	5.9	44	6.3	3.1	<0.1	0.1	<0.1	<0.1	<0.5	0.53	<0.1	<0.5
ÆR3-9S-13	0.1	4.9	4.1	38	9.0	2.2	<0.1	<0.1	<0.1	<0.1	<0.5	0.02	<0.1	<0.5
ÆR3-9S-16	0.1	4.9	4.2	22	7.9	2.2	<0.1	0.1	<0.1	<0.1	<0.5	0.06	<0.1	<0.5
ÆR3-9S-19	0.1	3.7	4.1	23	6.9	3.3	<0.1	<0.1	<0.1	<0.1	<0.5	0.02	<0.1	<0.5
ÆR3-9S-22	0.4	33.2	18.6	99	35.8	16.2	<0.1	0.1	0.3	<0.1	<0.5	0.03	<0.1	<0.5
ÆR3-9S-23	0.2	30.6	16.7	108	36.8	7.0	<0.1	0.1	0.3	<0.1	<0.5	0.04	<0.1	<0.5
MA2-4-1	0.3	7.5	4.7	25	7.7	2.7	<0.1	<0.1	<0.1	<0.1	<0.5	0.02	<0.1	<0.5
MA2-4-3	0.1	5.9	5.1	20	6.4	2.9	<0.1	<0.1	<0.1	<0.1	<0.5	0.03	<0.1	<0.5
MA2-4-6	<0.1	4.0	4.5	22	5.8	2.4	<0.1	<0.1	<0.1	<0.1	<0.5	<0.01	<0.1	<0.5
MA2-4-9	0.2	3.5	3.7	22	5.9	2.2	<0.1	<0.1	<0.1	<0.1	<0.5	<0.01	<0.1	<0.5
MA2-4-11	<0.1	3.0	3.3	14	3.9	1.4	<0.1	<0.1	<0.1	<0.1	<0.5	<0.01	<0.1	<0.5
MA2-4-14	0.2	4.6	11.8	40	9.7	2.0	<0.1	0.1	<0.1	<0.1	2.8	0.02	<0.1	<0.5
MA2-4-17	<0.1	2.8	6.4	17	2.6	0.8	<0.1	<0.1	<0.1	<0.1	1.9	<0.01	<0.1	<0.5
MA2-4-19	0.3	6.9	6.0	48	14.8	1.7	<0.1	0.1	<0.1	<0.1	2.0	0.02	<0.1	<0.5
MA2-2-2	0.4	5.5	11.0	36	9.1	3.1	<0.1	<0.1	<0.1	<0.1	1.8	0.02	<0.1	<0.5
MA2-2-5	<0.1	2.1	2.3	20	3.7	1.2	<0.1	<0.1	<0.1	<0.1	0.6	<0.01	<0.1	<0.5
MA2-2-7	0.4	39.7	19.7	110	89.5	7.8	<0.1	<0.1	0.4	<0.1	<0.5	0.04	<0.1	<0.5
MA2-2-9	0.2	7.1	44.9	45	6.0	1.2	0.1	0.2	<0.1	0.2	<0.5	0.02	<0.1	<0.5
MA2-2-11	0.1	3.6	20.1	20	3.2	<0.5	<0.1	0.1	<0.1	<0.1	1.6	0.03	<0.1	<0.5
MA2-2-13	0.2	42.9	22.7	95	46.2	15.6	<0.1	<0.1	0.4	<0.1	2.3	0.07	0.1	0.8
MA2-2-14	0.2	5.9	20.6	38	10.2	3.4	0.1	0.3	<0.1	<0.1	1.0	0.06	<0.1	<0.5
SK5-A-1	<0.1	9.1	5.8	27	7.5	1.0	<0.1	<0.1	<0.1	<0.1	<0.5	0.03	<0.1	<0.5
SK5-A-4	<0.1	5.3	3.6	23	6.1	<0.5	<0.1	<0.1	<0.1	<0.1	<0.5	0.01	<0.1	<0.5
SK5-A-7	<0.1	4.3	4.7	28	7.4	0.5	<0.1	<0.1	<0.1	<0.1	<0.5	0.02	0.1	<0.5
SK5-A-10	0.3	40.7	16.4	102	43.6	28.8	<0.1	<0.1	0.3	<0.1	1.2	0.04	0.1	<0.5
SK5-A-11	0.3	47.6	20.5	97	48.7	22.3	<0.1	<0.1	0.3	<0.1	<0.5	0.03	0.1	<0.5
SK5-A-12	0.3	5.9	3.7	36	12.1	3.5	<0.1	<0.1	<0.1	<0.1	<0.5	0.02	0.1	<0.5
SK5-A-13	0.1	9.2	5.5	59	18.3	5.1	<0.1	<0.1	<0.1	<0.1	<0.5	0.02	0.1	<0.5
ÆR5-8-1	<0.1	5.0	4.0	21	10.2	3.1	<0.1	<0.1	<0.1	<0.1	1.5	<0.01	<0.1	<0.5
ÆR-8-4	<0.1	5.1	4.1	19	7.9	2.4	<0.1	<0.1	<0.1	<0.1	<0.5	<0.01	<0.1	<0.5
ÆR5-8-6	<0.1	5.6	4.3	20	7.7	2.9	<0.1	<0.1	<0.1	<0.1	<0.5	<0.01	<0.1	<0.5
ÆR5-8-8	1.1	6.4	4.9	49	14.4	5.4	<0.1	0.1	<0.1	<0.1	<0.5	0.02	0.1	<0.5
ÆR5-8-11	0.5	3.2	4.1	21	7.7	3.5	<0.1	<0.1	<0.1	<0.1	<0.5	<0.01	<0.1	<0.5
ÆR5-8-14	0.4	5.5	5.5	35	10.1	6.2	<0.1	<0.1	<0.1	<0.1	<0.5	<0.01	<0.1	<0.5
DE1-1	0.2	7.9	15.6	34	7.5	3.0	<0.1	0.6	<0.1	<0.1	<0.5	0.08	0.2	<0.5
DE1-5	0.3	5.5	12.7	30	7.4	3.6	<0.1	0.4	<0.1	<0.1	<0.5	0.06	<0.1	<0.5
DE1-7	0.3	9.7	13.4	45	14.9	4.2	<0.1	0.4	<0.1	<0.1	<0.5	0.11	<0.1	<0.5
DE1-8	0.4	9.9	17.5	48	11.1	2.6	<0.1	0.4	<0.1	<0.1	3.4	0.07	<0.1	<0.5
DE1-11	0.2	6.1	15.9	42	9.4	2.6	<0.1	0.4	<0.1	<0.1	<0.5	0.08	<0.1	<0.5
DE1-14	0.6	26.7	13.2	40	9.9	3.3	<0.1	0.5	<0.1	<0.1	<0.5	0.11	<0.1	<0.5

10.4 Appendix 3

Table 19: Raw data of concordant and disconcordant U-Pb analysis of all samples.

	ppm			Ratios								Discordance		Ages					
Name	U	^{206}Pb	$^{206}Pb_c$(%)	206/204	$^{207}Pb/^{206}Pb^*$	1SE	$^{207}Pb/^{235}U^*$	1SE	$^{206}Pb/^{238}U^*$	1SE	Rho	Central (%)	Minimum rim (%)	207/206	1σ	207/235	1σ	206/238	1σ
ER3-9S-2-001	84	16.4	1.90E+00	836	0.09415	0.00105	2.82297	0.10763	0.217474	0.007932	0.957	-17.7	-13.6	1511	20	1362	29	1269	42
ER3-9S-2-002	62	23.7	0.00E+00	7866	0.15217	0.00554	8.71557	0.50715	0.415387	0.018855	0.780	-6.5		2371	61	2309	53	2240	86
ER3-9S-2-003	173	44.1	0.00E+00	17716	0.09747	0.00277	3.83504	0.17938	0.285367	0.010606	0.795	3		1576	52	1600	38	1618	53
ER3-9S-2-004	308	119	7.90E-02	52890	0.18659	0.00787	10.91094	0.67881	0.424099	0.019394	0.735	-18.9	-10	2712	64	2516	58	2279	88
ER3-9S-2-005	345	70.2	7.60E-01	2252	0.10587	0.00319	3.3408	0.1532	0.228863	0.007907	0.753	-25.6	-17.8	1729	54	1491	36	1329	41
ER3-9S-2-006	1479	480.8	6.90E-03	118159	0.1361	0.0017	6.63272	0.26751	0.35345	0.013553	0.951	-12.1	-8.2	2178	21	2064	36	1951	65
ER3-9S-2-007	135	24.3	0.00E+00	3774	0.08059	0.00074	2.2709	0.07329	0.204364	0.006325	0.959	-1.2		1212	17	1203	23	1199	34
ER3-9S-2-008	290	56.6	0.00E+00	12406	0.0816	0.00219	2.46912	0.1123	0.219451	0.008057	0.807	3.8		1236	49	1263	33	1279	43
ER3-9S-2-009	64	28	4.30E-02	10835	0.20502	0.00316	13.44446	0.73584	0.4756	0.02498	0.960	-15.1	-11.1	2867	25	2711	52	2508	109
ER3-9S-2-010	77	18.4	7.80E-01	4608	0.09896	0.0032	3.66032	0.18494	0.268264	0.010406	0.768	-5.1		1605	58	1563	40	1532	53
ER3-9S-2-011	790	120.4	0.00E+00	25931	0.07287	0.00064	1.73062	0.05315	0.172253	0.00507	0.958	1.5		1010	18	1020	20	1025	28
ER3-9S-2-012	557	83.8	4.30E-01	3278	0.10365	0.00309	2.41995	0.11812	0.169338	0.00655	0.792	-43.5	-37.3	1690	52	1249	35	1008	36
ER3-9S-2-013	142	69.3	0.00E+00	24875	0.19396	0.00856	13.95441	0.98674	0.521791	0.028828	0.781	-3.1		2776	72	2747	67	2707	122
ER3-9S-2-014	273	121.1	0.00E+00	41422	0.17743	0.00733	11.75276	0.77711	0.480403	0.024804	0.781	-4.6		2629	66	2585	62	2529	108
ER3-9S-2-015	88	15.8	0.00E+00	142	0.18915	0.00963	5.34032	0.32869	0.204767	0.007075	0.561	-61.2	-57.1	2735	80	1875	53	1201	38
ER3-9S-2-016	256	64.3	2.80E-01	8057	0.1024	0.00114	3.71689	0.11973	0.263254	0.007959	0.939	-10.9	-6.8	1668	20	1575	26	1506	41
ER3-9S-2-017	656	58.3	2.10E-01	11436	0.06558	0.00055	0.91684	0.02738	0.101395	0.002906	0.960	-22.5	-17.8	793	17	661	15	623	17
ER3-9S-2-018	310	63.8	0.00E+00	27683	0.08874	0.00251	2.896	0.13186	0.236687	0.008447	0.784	-2.3		1399	51	1381	34	1369	44
ER3-9S-2-019	943	36	1.20E+00	1226	0.05352	0.00062	0.32537	0.01032	0.044091	0.001302	0.931	-21.2	-6.2	351	26	286	8	278	8
ER3-9S-2-020	348	88.1	0.00E+00	87312	0.10423	0.00316	4.11142	0.19906	0.2861	0.010806	0.78	-5.2		1701	53	1657	40	1622	54
ER3-9S-2-021	3	0.2	0.00E+00	66	0.13307	0.01051	1.39661	0.17359	0.07612	0.007306	0.772	-80.7	-75.6	2139	140	887	74	473	44
ER3-9S-2-022	41	6.3	0.00E+00	2326	0.07623	0.0022	1.84613	0.08543	0.175639	0.006361	0.783	-5.7		1101	57	1062	30	1043	35
ER3-9S-2-024	1093	295.9	2.90E-02	34424	0.1095	0.00351	4.39092	0.25486	0.290823	0.014081	0.834	-9.2		1791	56	1711	48	1646	70
ER3-9S-2-023	73	13	3.60E-01	3425	0.1052	0.00326	2.91027	0.13757	0.200635	0.007155	0.754	-34.3	-27.2	1718	53	1385	36	1179	38
ER3-9S-2-025	473	18.7	7.00E-01	2899	0.05165	0.00048	0.32697	0.01007	0.045918	0.001347	0.953	7.4		270	20	287	8	289	8
ER3-9S-2-026	78	9.7	4.70E-01	4890	0.06754	0.00187	1.25624	0.06422	0.134894	0.005794	0.84	-4.8		855	56	826	29	816	33
ER3-9S-2-027	323	82.1	1.50E-01	10786	0.11561	0.0013	4.49019	0.17714	0.281686	0.010651	0.958	-17.3	-13.8	1889	20	1729	33	1600	54
ER3-9S-2-028	374	65.2	0.00E+00	26415	0.08964	0.00259	2.45292	0.11734	0.198467	0.007568	0.797	-19.3	-9.5	1418	54	1258	35	1167	41
ER3-9S-2-029	205	53.1	0.00E+00	27672	0.10259	0.00314	4.12415	0.21586	0.291549	0.012383	0.811	-1.5		1672	56	1659	43	1649	62
ER3-9S-2-030	603	110.5	7.80E-02	22177	0.10893	0.00343	3.12646	0.15564	0.208171	0.008032	0.775	-34.6	-27.4	1782	55	1439	38	1219	43
ER3-9S-2-031	426	112	0.00E+00	26936	0.10156	0.0031	4.13602	0.21692	0.295377	0.012596	0.813	1.1		1653	55	1661	43	1668	63
ER3-9S-2-032	826	38.3	0.00E+00	12339	0.05306	0.00047	0.3918	0.01187	0.05356	0.001553	0.956	1.6		331	19	336	9	336	9
ER3-9S-2-033	547	127.2	1.90E-01	10148	0.1108	0.00352	3.96841	0.21515	0.259769	0.011404	0.81	-20	-10.8	1813	55	1628	44	1489	58
ER3-9S-2-034	1254	204.2	0.00E+00	56281	0.07714	0.00213	2.00399	0.08951	0.18841	0.00661	0.785	-1.2		1125	55	1117	30	1113	36
ER3-9S-2-035	186	31.6	0.00E+00	16480	0.07879	0.0022	2.13902	0.09722	0.19689	0.007057	0.789	-0.8		1167	53	1162	31	1159	38
ER3-9S-2-036	256	69.5	0.00E+00	24640	0.10127	0.00036	3.91631	0.04822	0.280468	0.00331	0.958	-3.7	-2.3	1648	7	1617	10	1594	17
ER3-9S-2-037	386	121.4	0.00E+00	52451	0.11112	0.0004	4.95606	0.07078	0.323483	0.004474	0.968	-0.7		1818	6	1812	12	1807	22
ER3-9S-2-038	302	100.8	1.10E-02	51394	0.11848	0.00054	5.37165	0.05432	0.328823	0.002973	0.894	-6	-4.5	1933	8	1880	9	1833	14
ER3-9S-2-039	211	58.9	0.00E+00	24308	0.1007	0.00037	3.94682	0.04438	0.28425	0.003025	0.947	-1.7	-0.2	1637	7	1623	9	1613	15
ER3-9S-2-040	248	16.5	0.00E+00	12603	0.05554	0.00024	0.53262	0.00522	0.069547	0.000612	0.897	-0.2		434	9	434	3	433	4
ER3-9S-2-041	79	15.5	0.00E+00	7181	0.08035	0.00036	2.21739	0.02293	0.20014	0.001865	0.901	-2.7	-0.5	1206	8	1187	7	1176	10
ER3-9S-2-042	1089	355.9	0.00E+00	123415	0.11501	0.00042	5.26777	0.06637	0.332187	0.004007	0.957	-1.9	-0.6	1880	6	1864	11	1849	19
ER3-9S-2-043	238	48.2	7.30E-01	2865	0.08085	0.0005	2.30058	0.03605	0.206387	0.002968	0.918	-0.7		1218	12	1212	11	1210	16
ER3-9S-2-044	489	158.7	1.40E-02	59355	0.11353	0.00046	5.1	0.05651	0.3246	0.003364	0.932	-2.7	-1.3	1857	7	1833	9	1812	16
ER3-9S-2-045	283	53.2	0.00E+00	19487	0.07733	0.00028	2.03695	0.02124	0.191051	0.001865	0.936	-0.2		1130	7	1128	7	1127	10
ER3-9S-2-046	77	15.1	0.00E+00	8005	0.09064	0.00043	2.51053	0.02763	0.200889	0.001996	0.903	-19.7	-18	1439	9	1275	8	1180	11
ER3-9S-2-047	340	56.8	3.50E-01	3845	0.16923	0.00084	3.96931	0.12145	0.170112	0.005136	0.987	-64.9	-64.4	2550	8	1628	25	1013	28
ER3-9S-2-048	434	70.9	8.10E-02	24602	0.07827	0.00032	1.75268	0.01918	0.162403	0.001646	0.926	-17.1	-15.4	1154	8	1028	7	970	9
ER3-9S-2-049	107	28.5	1.00E-01	17881	0.1002	0.00039	3.77745	0.05968	0.273428	0.004187	0.969	-4.8	-3.3	1628	7	1588	13	1558	21
ER3-9S-2-050	141	76.7	2.50E-02	126763	0.22262	0.00118	16.47891	0.37182	0.536871	0.011776	0.972	-9.4	-8	3000	8	2905	22	2770	49

Table 20: Raw data of concordant and disconcordant U-Pb analysis of all samples.

ER3-9S-2-051	698	117	0.00E+00	61071	0.07529	0.00052	1.81408	0.03149	0.17474	0.00278	0.916	-3.8	-0.1			1076	13	1051	11	1038	15
ER3-9S-2-052	313	146.1	0.00E+00	298	0.249	0.00317	15.8	0.31029	0.459239	0.006894	0.763	-27.9	-25.7			3178	19	2863	19	2436	30
ER3-9S-2-053	456	88.8	3.70E-02	34130	0.08666	0.00032	2.43074	0.02413	0.203441	0.001876	0.929	-12.9	-11.4			1353	7	1252	7	1194	10
ER3-9S-2-054	191	67.6	0.00E+00	22856	0.12581	0.00051	6.20389	0.07527	0.357641	0.004086	0.942	-3.9	-2.5			2040	7	2005	11	1971	19
ER3-9S-2-055	205	41.7	1.30E+00	2073	0.08449	0.00061	2.38048	0.03113	0.204353	0.002221	0.831	-8.8	-5.9			1304	13	1237	9	1199	12
ER3-9S-2-056	762	99.1	9.20E-01	1501	0.09617	0.00056	1.78147	0.02229	0.134349	0.001489	0.886	-50.6	-49.4			1551	11	1039	8	813	8
ER3-9S-2-057	1026	209.6	4.80E-01	3187	0.11302	0.00043	3.2106	0.07759	0.206033	0.004917	0.988	-38	-37.1			1849	7	1460	19	1208	26
ER3-9S-2-058	346	63.6	0.00E+00	30502	0.07678	0.00027	2.01505	0.0211	0.190341	0.001879	0.943	0.8				1116	7	1121	7	1123	10
ER3-9S-2-059	20	2.2	0.00E+00	916	0.09272	0.00338	1.36589	0.12843	0.106842	0.009261	0.922	-58.7	-51.6			1482	67	874	55	654	54
ER3-9S-2-060	142	13.2	1.50E+00	1347	0.05998	0.00059	0.74362	0.02722	0.089924	0.003169	0.963	-8.2				603	21	565	16	555	19
ER3-9S-2-061	294	53.6	6.20E-02	20856	0.08498	0.00031	2.21454	0.02307	0.188997	0.001846	0.938	-16.5	-15			1315	7	1186	7	1116	10
ER3-9S-2-062	322	52.5	0.00E+00	90031	0.07211	0.00021	1.68591	0.01811	0.169563	0.001754	0.963	2.3				989	6	1003	7	1010	10
ER3-9S-2-063	271	70.1	1.80E-01	9468	0.11416	0.00042	4.17736	0.05027	0.265394	0.00304	0.952	-21	-19.9			1867	6	1670	10	1517	15
ER3-9S-2-064	132	26.8	1.90E-01	7950	0.0834	0.00032	2.36498	0.03452	0.205655	0.0029	0.966	-6.3	-4.5			1279	7	1232	10	1206	16
ER3-9S-2-065	52	7.6	0.00E+00	3280	0.07169	0.00043	1.50699	0.0172	0.152464	0.001486	0.854	-6.8	-3.7			977	12	933	7	915	8
ER3-9S-2-066	129	1.7	0.00E+00	1159	0.0495	0.00064	0.09549	0.00151	0.013992	0.000127	0.575	-48.1	-13.5			172	30	93	1	90	1
ER3-9S-2-067	83	28.3	0.00E+00	4372	0.11885	0.00052	5.80143	0.13382	0.354026	0.008018	0.982	0.9				1939	8	1947	20	1954	38
ER3-9S-2-068	296	73.5	0.00E+00	22083	0.11119	0.00051	3.91978	0.04347	0.255671	0.002584	0.911	-21.6	-20.2			1819	8	1618	9	1468	13
ER3-9S-2-069	411	26.1	7.90E-01	2528	0.06423	0.00048	0.58386	0.00691	0.065932	0.000604	0.774	-46.5	-43.8			749	16	467	4	412	4
ER3-9S-2-070	424	147	0.00E+00	59698	0.11771	0.00051	5.68027	0.06308	0.349981	0.003573	0.919	0.8				1922	8	1928	10	1935	17
ER3-9S-2-072	103	68.6	5.90E-02	28875	0.27455	0.00227	23.09005	0.5372	0.609957	0.013268	0.935	-9.9	-7.8			3332	13	3231	23	3070	53
ER3-9S-2-073	141	28	0.00E+00	9996	0.08343	0.00035	2.36177	0.02793	0.205316	0.002274	0.937	-6.5	-4.6			1279	8	1231	8	1204	12
ER3-9S-2-074	239	78.3	0.00E+00	40682	0.11924	0.00049	5.43129	0.06661	0.33036	0.003822	0.943	-6.2	-4.8			1945	7	1890	11	1840	19
ER3-9S-2-075	161	51.2	0.00E+00	11996	0.11376	0.00045	5.04516	0.06103	0.321654	0.003679	0.946	-3.8	-2.4			1860	7	1827	10	1798	18
ER3-9S-2-076	81	8.2	8.60E-01	2093	0.07186	0.00051	1.0669	0.02929	0.10768	0.002856	0.966	-34.6	-31.7			982	14	737	14	659	17
ER3-9S-2-077	426	94.7	0.00E+00	33073	0.0899	0.00036	2.84826	0.03524	0.22978	0.002694	0.948	-7	-5.3			1423	8	1368	9	1333	14
ER3-9S-2-078	130	37.2	0.00E+00	20317	0.10405	0.00038	4.21463	0.05219	0.293776	0.003474	0.955	-2.5	-1			1698	6	1677	10	1660	17
ER3-9S-2-079	366	39	1.30E-01	14575	0.08397	0.00086	1.2607	0.03077	0.10889	0.00241	0.907	-50.9	-48.5			1292	19	828	14	666	14
ER3-9S-2-080	483	140.8	0.00E+00	31275	0.10383	0.00037	4.23891	0.05863	0.296093	0.003959	0.967	-1.5	-0.1			1694	6	1682	11	1672	20
ER3-9S-2-081	185	52.4	0.00E+00	23505	0.10223	0.00036	4.07158	0.04927	0.288869	0.003342	0.956	-2	-0.6			1665	6	1649	10	1636	17
ER3-9S-2-082	166	48.8	0.00E+00	16254	0.10892	0.00041	4.5229	0.05627	0.30118	0.003571	0.953	-5.4	-4			1781	7	1735	10	1697	18
ER3-9S-2-083	447	55.3	7.00E-02	21518	0.09223	0.0008	1.69769	0.03964	0.133504	0.002895	0.929	-48	-46			1472	15	1008	15	808	16
ER3-9S-2-084	796	148.5	1.90E-02	83596	0.09783	0.00035	2.57396	0.03315	0.190817	0.002363	0.962	-31.5	-30.4			1583	6	1293	9	1126	13
ER3-9S-2-085	70	40.7	0.00E+00	28625	0.23829	0.00148	18.81402	0.3462	0.572634	0.009915	0.941	-7.6	-5.9			3109	10	3032	18	2919	41
ER3-9S-2-086	413	113.3	6.30E-02	62791	0.11537	0.00043	4.44157	0.05785	0.279227	0.003485	0.958	-17.8	-16.7			1886	7	1720	11	1587	18
ER3-9S-2-087	493	147.8	0.00E+00	65257	0.11325	0.00041	4.75342	0.06557	0.304414	0.004054	0.965	-8.5	-7.3			1852	6	1777	12	1713	20
ER3-9S-2-088	154	43.9	0.00E+00	23442	0.10562	0.00039	4.25284	0.0557	0.292023	0.00367	0.959	-4.8	-3.4			1725	6	1684	11	1652	18
ER3-9S-2-089	256	86.3	0.00E+00	24670	0.1206	0.00046	5.67918	0.07529	0.341539	0.004338	0.958	-4.2	-2.8			1965	7	1928	11	1894	21
ER3-9S-2-091	156	43.7	0.00E+00	24703	0.10138	0.00036	4.02316	0.05174	0.287829	0.003558	0.961	-1.3				1649	6	1639	10	1631	18
ER3-9S-2-092	151	43	0.00E+00	17394	0.10164	0.00037	4.09789	0.05176	0.292416	0.003533	0.956					1654	6	1654	10	1654	18
ER3-9S-2-093	419	101.4	6.00E-02	85992	0.11793	0.00043	4.07339	0.05471	0.250506	0.003236	0.962	-28	-27			1925	6	1649	11	1441	17
ER3-9S-2-094	199	51.2	0.00E+00	21939	0.09786	0.00036	3.58457	0.04504	0.265655	0.003195	0.957	-4.6	-3.1			1584	7	1546	10	1519	16
ER3-9S-2-095	63	9.5	4.30E-01	4387	0.07032	0.00033	1.49938	0.01927	0.154654	0.001847	0.929	-1.2				938	9	930	8	927	10
ER3-9S-2-096	174	39.3	0.00E+00	30488	0.08798	0.00031	2.82806	0.03309	0.233125	0.002598	0.952	-2.5	-0.9			1382	6	1363	9	1351	14
ER3-9S-2-097	166	49.2	0.00E+00	23905	0.10575	0.00039	4.41368	0.05885	0.302719	0.00388	0.961	-1.5				1727	6	1715	11	1705	19
ER3-9S-2-098	436	223.5	0.00E+00	52513	0.19231	0.00132	12.79235	0.1549	0.482449	0.004818	0.825	-9.8	-8.1			2762	11	2664	11	2538	21
ER3-9S-2-099	340	71.8	1.00E-01	18751	0.08941	0.0004	2.70022	0.03642	0.219033	0.002787	0.943	-10.6	-8.8			1413	8	1329	10	1277	15
ER3-9S-2-100	323	98.7	0.00E+00	84353	0.11665	0.00046	5.04689	0.07329	0.313784	0.004389	0.963	-8.8	-7.4			1906	7	1827	12	1759	22
ER3-9S-2-101	209	61	1.10E-01	13317	0.11456	0.00049	4.59501	0.05797	0.290914	0.003454	0.941	-13.7	-12.3			1873	8	1748	11	1646	17
ER3-9S-2-102	70	20.7	2.90E-01	9511	0.11572	0.00051	4.80459	0.08052	0.301137	0.00487	0.965	-11.7	-10.2			1891	8	1786	14	1697	24
ER3-9S-2-103	140	44.6	0.00E+00	8446	0.11447	0.00042	5.13459	0.08028	0.325325	0.004946	0.972	-3.4	-2.1			1872	6	1842	13	1816	24
ER3-9S-2-104	711	86.2	1.10E-01	18804	0.07204	0.00025	1.25723	0.01536	0.126567	0.001481	0.958	-23.5	-21.9			987	7	827	7	768	8
ER3-9S-2-105	222	10.8	0.00E+00	3038	0.05303	0.00026	0.37591	0.00438	0.051412	0.000542	0.904	-2.1				330	10	324	3	323	3
ER3-9S-2-106	58	16.5	4.00E-01	6997	0.10958	0.00048	4.40084	0.05998	0.291287	0.003758	0.946	-9.1	-7.6			1792	8	1712	11	1648	19
ER3-9S-2-107	117	38.8	0.00E+00	5040	0.11916	0.0005	5.51849	0.07676	0.335878	0.004453	0.953	-4.6	-3.1			1944	7	1903	12	1867	21
ER3-9S-2-108	158	45.7	2.30E-01	7976	0.11464	0.00044	4.61812	0.07356	0.292158	0.004517	0.971	-13.4	-12.2			1874	6	1753	13	1652	23
ER3-9S-2-109	134	42.7	2.50E-01	8488	0.12611	0.00055	5.60677	0.07901	0.322439	0.004321	0.951	-13.6	-12.3			2044	8	1917	12	1802	21
ER3-9S-2-110	111	34.1	4.00E-01	4277	0.11291	0.00057	4.65662	0.05762	0.299108	0.003382	0.914	-9.8	-8.1			1847	9	1759	10	1687	17

Table 21: Raw data of concordant and disconcordant U-Pb analysis of all samples.

	ppm				Ratios								Discordance			Ages					
Name	U	^{206}Pb	$^{206}Pb_c$(%)	206/204	$^{207}Pb/^{206}Pb^*$	1SE	$^{207}Pb/^{235}U^*$	1SE	$^{206}Pb/^{238}U^*$	1SE	Rho	Central (%)	Minimum rim (%)		207/206	1σ	207/235	1σ	206/238	1σ
HR3-9S-14-001	144	2.2	0.00E+00	136	0.09358	0.00305	0.18765	0.00655	0.014543	0.000181	0.356	-94.4	-93.8		1500	60	175	6	93	1
HR3-9S-14-002	65	23.4	0.00E+00	4960	0.11998	0.00059	5.6093	0.0915	0.339082	0.00527	0.953	-4.3	-2.6		1956	8	1918	14	1882	25
HR3-9S-14-003	426	140.4	0.00E+00	9494	0.11704	0.0005	5.0176	0.08234	0.310922	0.004927	0.966	-9.9	-8.5		1912	7	1822	14	1745	24
HR3-9S-14-005	557	123.2	0.00E+00	93667	0.0862	0.00044	2.48481	0.04229	0.209073	0.003392	0.953	-9.7	-7.5		1343	10	1268	12	1224	18
HR3-9S-14-006	87	50.2	0.00E+00	7173	0.20147	0.00126	14.92046	0.32559	0.537111	0.011226	0.958	-2.9	-1.1		2838	10	2810	21	2771	47
HR3-9S-14-007	118	30.4	0.00E+00	4863	0.09303	0.00041	3.15439	0.05041	0.245927	0.003778	0.961	-5.3	-3.5		1488	8	1446	12	1417	20
HR3-9S-14-008	656	223.7	0.00E+00	27185	0.1141	0.00048	5.04993	0.08672	0.321002	0.005343	0.969	-4.4	-2.8		1866	8	1828	15	1795	26
HR3-9S-14-009	536	181.3	0.00E+00	21099	0.11498	0.0005	5.06282	0.08475	0.319363	0.005162	0.966	-5.7	-4.1		1880	8	1830	14	1787	25
HR3-9S-14-010	517	172.5	0.00E+00	766	0.13523	0.00156	5.89636	0.10913	0.316235	0.004568	0.781	-20.9	-18.1		2167	20	1961	16	1771	22
HR3-9S-14-011	598	208.2	0.00E+00	7464	0.11979	0.00057	5.43592	0.08821	0.329119	0.005107	0.956	-7	-5.4		1953	8	1891	14	1834	25
HR3-9S-14-012	663	49.7	3.50E-01	6426	0.05531	0.00033	0.54946	0.00798	0.07205	0.000952	0.91	5.8	.		425	13	445	5	448	6
HR3-9S-14-013	257	18.9	0.00E+00	1861	0.05565	0.00031	0.54877	0.00756	0.071519	0.000901	0.915	1.6	.		438	12	444	5	445	5
HR3-9S-14-014	577	29.5	0.00E+00	2046	0.0517	0.00025	0.35187	0.0062	0.049364	0.000837	0.962	14.5	5		272	10	306	5	311	5
HR3-9S-14-015	249	83.3	5.40E-01	2343	0.16956	0.00106	7.37175	0.13158	0.315308	0.005271	0.937	-35.1	-33.8		2553	10	2158	16	1767	26
HR3-9S-14-016	270	80.7	0.00E+00	18840	0.10086	0.00042	3.9441	0.07045	0.283623	0.004925	0.972	-2.1	-0.4		1640	7	1623	14	1610	25
HR3-9S-14-017	223	43.6	9.20E-01	1369	0.09921	0.00051	2.53784	0.03751	0.185534	0.002569	0.937	-34.6	-33.2		1609	9	1283	11	1097	14
HR3-9S-14-018	256	80.4	1.90E-01	7954	0.11574	0.00052	4.72283	0.07963	0.295942	0.004806	0.963	-13.2	-11.7		1891	8	1771	14	1671	24
HR3-9S-14-019	371	24.6	0.00E+00	3598	0.05727	0.0007	0.50058	0.00986	0.063397	0.00098	0.785	-21.7	-11.5		502	26	412	7	396	6
HR3-9S-14-020	391	24.1	0.00E+00	1623	0.05451	0.00031	0.44885	0.00616	0.059716	0.000744	0.907	-4.8	.		392	13	376	4	374	5
HR3-9S-14-021	550	29.6	0.00E+00	9061	0.05372	0.00027	0.38355	0.00556	0.051782	0.000704	0.938	-9.7	-3		359	11	330	4	325	4
HR3-9S-14-022	86	5.7	0.00E+00	1527	0.0555	0.00044	0.49694	0.00865	0.064936	0.001007	0.891	-6.4	.		433	17	410	6	406	6
HR3-9S-14-023	330	87.7	0.00E+00	11678	0.0937	0.0004	3.25444	0.05677	0.2519	0.004264	0.97	-4	-2.2		1502	8	1470	14	1448	22
HR3-9S-14-024	182	12.7	0.00E+00	3872	0.05569	0.00031	0.51407	0.00787	0.066944	0.000954	0.931	-5.3	.		440	12	421	5	418	6
HR3-9S-14-025	165	7.5	0.00E+00	1087	0.05195	0.00038	0.31704	0.00539	0.044265	0.000678	0.901	-1.4	.		283	17	280	4	279	4
HR3-9S-14-026	194	57.7	1.90E-01	10252	0.11026	0.00052	4.30217	0.08065	0.28298	0.005136	0.968	-12.4	-10.8		1804	8	1694	15	1606	26
HR3-9S-14-027	392	45.9	7.10E-01	1657	0.09379	0.00045	1.44595	0.02222	0.111809	0.001633	0.95	-57.4	-56.6		1504	9	908	9	683	9
HR3-9S-14-028	223	3.4	0.00E+00	412	0.05083	0.00045	0.10377	0.00175	0.014806	0.000213	0.853	-59.8	-51		233	19	100	2	95	1
HR3-9S-14-029	251	62.3	2.10E-01	7119	0.10893	0.00046	3.53129	0.05992	0.23511	0.003865	0.969	-26.1	-24.9		1782	8	1534	13	1361	20
HR3-9S-14-030	223	38.5	0.00E+00	4365	0.0717	0.00032	1.62736	0.02595	0.164622	0.002517	0.959	0.6	.		977	9	981	10	982	14
HR3-9S-14-031	600	104.2	8.90E-02	21294	0.10653	0.00085	2.48635	0.0584	0.169267	0.003739	0.94	-45.4	-43.7		1741	14	1268	17	1008	21
HR3-9S-14-032	140	6.9	0.00E+00	268	0.08891	0.00369	0.69074	0.05848	0.056348	0.004158	0.872	-76.8	-72.2		1402	75	533	35	353	25
HR3-9S-14-033	36	9.9	0.00E+00	1284	0.09721	0.00057	3.534	0.0783	0.263675	0.00563	0.964	-4.5	-2.1		1571	11	1535	18	1509	29
HR3-9S-14-034	346	89.3	3.30E-01	5917	0.12641	0.00063	4.26953	0.07168	0.244959	0.00393	0.955	-34.5	-33.4		2049	9	1688	14	1412	20
HR3-9S-14-035	342	112.6	0.00E+00	1752	0.12448	0.00088	5.35064	0.09802	0.311757	0.00527	0.923	-15.4	-13.2		2021	12	1877	16	1749	26
HR3-9S-14-036	42	7.3	0.00E+00	2395	0.07752	0.00051	1.79848	0.03674	0.168256	0.003254	0.947	-12.6	-9.5		1135	13	1045	13	1002	18
HR3-9S-14-038	1389	136.4	1.70E-01	9071	0.07638	0.00039	0.98715	0.01623	0.093735	0.001467	0.952	-49.9	-48.5		1105	10	697	8	578	9
HR3-9S-14-039	463	116.8	2.80E-01	5688	0.11045	0.0005	3.6628	0.0607	0.240518	0.003837	0.963	-25.7	-24.4		1807	8	1563	13	1389	20
HR3-9S-14-040	205	66.2	0.00E+00	11201	0.10963	0.00048	4.63984	0.08247	0.306961	0.005289	0.969	-4.3	-2.7		1793	7	1756	15	1726	26
HR3-9S-14-041	434	72	0.00E+00	12107	0.06964	0.00028	1.52569	0.02378	0.158884	0.002393	0.966	3.8	0.1		918	8	941	10	951	13
HR3-9S-14-042	508	169.8	0.00E+00	21204	0.11838	0.00054	5.15483	0.09431	0.315824	0.005595	0.968	-9.6	-8.1		1932	8	1845	16	1769	27
HR3-9S-14-043	304	94.3	8.00E-02	72890	0.1146	0.00049	4.63423	0.08261	0.293295	0.005074	0.971	-13	-11.6		1874	8	1755	15	1658	25
HR3-9S-14-044	64	0.9	0.00E+00	141	0.07741	0.00279	0.14979	0.00609	0.014035	0.000265	0.464	-92.7	-91.3		1132	69	142	5	90	2
HR3-9S-14-045	443	214.7	2.00E-02	49222	0.18696	0.0011	11.65137	0.25445	0.451993	0.009503	0.963	-13.7	-12.2		2716	9	2577	20	2404	42
HR3-9S-14-046	880	148.5	3.50E-01	3723	0.1504	0.00099	3.29508	0.06569	0.158901	0.002992	0.944	-63.9	-63.1		2350	11	1480	16	951	17
HR3-9S-14-047	607	85.1	3.70E-01	4149	0.09292	0.00075	1.727	0.04045	0.134796	0.002966	0.94	-48	-46.2		1486	15	1019	15	815	17
HR3-9S-14-048	659	119.1	1.80E-01	12305	0.10791	0.00056	2.58035	0.04041	0.173427	0.002563	0.944	-44.9	-43.8		1764	9	1295	11	1031	14
HR3-9S-14-049	140	43	1.40E-01	8410	0.11757	0.0006	4.73054	0.08102	0.291828	0.004772	0.955	-15.9	-14.3		1920	9	1773	14	1651	24
HR3-9S-14-050	182	58	0.00E+00	16153	0.11354	0.00051	4.71096	0.08758	0.300922	0.005428	0.97	-9.9	-8.3		1857	8	1769	16	1696	27

Table 22: Raw data of concordant and disconcordant U-Pb analysis of all samples.

HR3-9S-14-051	379	119.2	4.20E-02	56993	0.11334	0.00118	4.254	0.18387	0.272207	0.011419	0.971	-18.3	-15			1854	18	1685	36	1552	58
HR3-9S-14-052	682	284.8	3.00E-02	116845	0.14705	0.00179	7.2209	0.36078	0.356155	0.017257	0.970	-17.4	-14.1			2312	20	2139	45	1964	82
HR3-9S-14-053	467	137.6	7.30E-02	40548	0.11515	0.00122	4.09805	0.16908	0.258113	0.010292	0.966	-23.9	-20.8			1882	19	1654	34	1480	53
HR3-9S-14-054	261	93	2.00E-01	8428	0.11591	0.00123	4.96002	0.22502	0.310367	0.01369	0.972	-9.1	-5.5			1894	18	1813	38	1743	67
HR3-9S-14-055	154	23.9	5.00E-01	3641	0.07285	0.00071	1.40674	0.04838	0.140053	0.004621	0.959	-17.4	-12.6			1010	18	892	20	845	26
HR3-9S-14-056	244	3.7	0.00E+00	4980	0.0494	0.00059	0.09795	0.00303	0.014379	0.000411	0.923	-45.2	-16.8			167	27	95	3	92	3
HR3-9S-14-057	263	73.9	9.40E-02	61218	0.10585	0.0011	3.77463	0.16241	0.258628	0.010801	0.971	-15.9	-12.4			1729	18	1587	35	1483	55
HR3-9S-14-058	451	33.1	3.10E-01	5622	0.05527	0.00049	0.52426	0.01624	0.068795	0.002041	0.958	1.4				423	19	428	11	429	12
HR3-9S-14-059	141	44.7	3.20E-01	7976	0.10464	0.00112	4.1	0.17098	0.287415	0.011448	0.966	-5.3	-1.2			1708	19	1664	34	1629	57
HR3-9S-14-060	326	83.9	0.00E+00	35947	0.09205	0.00096	3.00101	0.11243	0.236452	0.008507	0.960	-7.6	-3.2			1468	19	1408	29	1368	44
HR3-9S-14-061	114	33.1	2.10E-01	9905	0.11295	0.00126	4.20001	0.16676	0.269694	0.010277	0.96	-18.7	-15.2			1847	21	1674	33	1539	52
HR3-9S-14-062	197	66.8	2.00E-01	9824	0.11929	0.0014	5.11423	0.22468	0.310944	0.013165	0.964	-11.7	-7.9			1946	20	1838	37	1745	65
HR3-9S-14-063	476	7.2	0.00E+00	2014	0.05473	0.00066	0.11088	0.00342	0.014692	0.000417	0.921	-77.1	-73.2			401	25	107	3	94	3
HR3-9S-14-064	287	57.9	3.20E-01	4615	0.08095	0.00079	2.14711	0.07396	0.192363	0.006353	0.959	-7.7	-3			1220	18	1164	24	1134	34
HR3-9S-14-065	165	14.6	0.00E+00	499	0.0718	0.0018	0.85977	0.0367	0.086846	0.003003	0.81	-47.1	-39.5			980	50	630	20	537	18
HR3-9S-14-066	294	85.6	0.00E+00	11929	0.11073	0.00118	4.24883	0.16995	0.278288	0.010727	0.964	-14.2	-10.7			1811	19	1684	33	1583	54
HR3-9S-14-067	585	97.8	2.40E-01	9843	0.08055	0.0008	1.8	0.06116	0.161905	0.005269	0.957	-21.6	-17.6			1210	19	1045	22	967	29
HR3-9S-14-068	454	41.1	2.80E-01	5521	0.05696	0.00053	0.69976	0.02205	0.089097	0.002684	0.956	12.8	1.5			490	19	539	13	550	16
HR3-9S-14-069	266	76.6	1.40E-01	45785	0.10084	0.00108	3.89005	0.14916	0.279788	0.010299	0.960	-3.4				1640	19	1612	31	1590	52
HR3-9S-14-070	116	39.1	3.30E-01	5442	0.11895	0.0014	5.3498	0.22274	0.326178	0.013025	0.959	-7.1	-3			1941	21	1877	36	1820	63
HR3-9S-14-071	110	55.8	0.00E+00	4012	0.19746	0.00327	13.53715	0.70614	0.497225	0.024595	0.948	-8.8	-4.2			2805	27	2718	49	2602	106
HR3-9S-14-072	145	43	5.30E-01	3803	0.11242	0.00131	4.60328	0.18913	0.296966	0.011699	0.959	-10	-6			1839	21	1750	34	1676	58
HR3-9S-14-073	161	2.3	0.00E+00	362	0.0509	0.00105	0.10751	0.00366	0.01532	0.000416	0.797	-58.9	-29.4			236	46	104	3	98	3
HR3-9S-14-074	704	188.9	4.60E-02	13798	0.12061	0.00116	4.57545	0.15416	0.275148	0.008882	0.958	-22.8	-20			1965	17	1745	28	1567	45
HR3-9S-14-075	223	65.2	2.00E-01	14544	0.11764	0.00134	4.87874	0.19373	0.300794	0.011439	0.958	-13.3	-9.6			1921	20	1799	33	1695	57
HR3-9S-14-076	398	58.3	3.10E-01	8329	0.07263	0.00071	1.54981	0.04833	0.15476	0.004581	0.949	-8.1	-2.7			1004	20	950	19	928	26
HR3-9S-14-077	88	6	0.00E+00	860	0.06211	0.00069	0.63316	0.0198	0.073935	0.002161	0.935	-33.3	-27			678	23	498	12	460	13
HR3-9S-14-078	1430	29.6	0.00E+00	5281	0.04891	0.00043	0.15193	0.00467	0.022528	0.000664	0.959	-0.1				144	20	144	4	144	4
HR3-9S-14-080	898	210.7	7.40E-02	25148	0.1117	0.00126	3.88632	0.13865	0.252331	0.00854	0.949	-23	-19.6			1827	20	1611	29	1450	44
HR3-9S-14-079	857	240.4	0.00E+00	20638	0.11417	0.00135	4.65762	0.16484	0.295873	0.009872	0.943	-11.9	-7.9			1867	20	1760	30	1671	49
HR3-9S-14-081	477	26.5	0.00E+00	1799	0.05803	0.00057	0.49648	0.01512	0.062056	0.00179	0.947	-27.7	-20.2			531	22	409	10	388	11
HR3-9S-14-082	448	15.8	0.00E+00	1049	0.05508	0.0006	0.30321	0.0096	0.039929	0.001187	0.939	-40	-31			415	24	269	7	252	7
HR3-9S-14-083	138	12.3	9.60E-01	1818	0.0614	0.00087	0.82424	0.02921	0.097357	0.003163	0.917	-8.7				653	29	610	16	599	19
HR3-9S-14-084	199	62.3	0.00E+00	7059	0.11709	0.0011	4.65332	0.16736	0.288237	0.010007	0.965	-16.5	-13.6			1912	16	1759	30	1633	50
HR3-9S-14-085	442	120.6	0.00E+00	40826	0.11405	0.0012	3.82576	0.13343	0.243285	0.008092	0.954	-27.5	-24.6			1865	19	1598	28	1404	42
HR3-9S-14-086	129	36.9	2.00E-01	13902	0.11922	0.00131	4.18461	0.15017	0.254566	0.008699	0.952	-27.7	-24.7			1945	18	1671	29	1462	45
HR3-9S-14-087	130	25.8	7.30E-01	3535	0.07633	0.00072	1.87181	0.05961	0.177862	0.005408	0.955	-4.8				1104	19	1071	21	1055	30
HR3-9S-14-088	158	2.4	0.00E+00	741	0.05065	0.00081	0.09704	0.00306	0.013897	0.000378	0.863	-60.8	-40.7			225	36	94	3	89	2
HR3-9S-14-089	132	45.3	0.00E+00	15040	0.11449	0.00094	4.74446	0.19579	0.300547	0.012155	0.980	-10.8	-8.1			1872	14	1775	35	1694	60
HR3-9S-14-090	390	6.2	0.00E+00	1621	0.04852	0.00053	0.09825	0.00291	0.014685	0.000406	0.931	-24.9				125	24	95	3	94	3
HR3-9S-14-091	176	54.6	0.00E+00	17180	0.10091	0.00101	3.87215	0.14897	0.27829	0.010335	0.965	-4				1641	18	1608	31	1583	52
HR3-9S-14-092	594	8.9	0.00E+00	733	0.04784	0.00047	0.09271	0.00277	0.014056	0.000396	0.943	-1.4				91	23	90	3	90	3
HR3-9S-14-093	482	159.9	0.00E+00	11409	0.10625	0.00108	4.35177	0.17265	0.29706	0.011391	0.967	-3.9				1736	17	1703	33	1677	57
HR3-9S-14-094	151	42	0.00E+00	6271	0.09971	0.00097	3.42791	0.13672	0.24935	0.009644	0.970	-12.6	-9.1			1619	18	1511	31	1435	50
HR3-9S-14-095	173	2.8	0.00E+00	624	0.06121	0.0011	0.12532	0.00404	0.01485	0.000397	0.830	-85.9	-83.7			646	37	120	4	95	3
HR3-9S-14-096	74	1.4	0.00E+00	335	0.04922	0.00119	0.12035	0.0045	0.017736	0.000504	0.761	-28.6				158	55	115	4	113	3
HR3-9S-14-097	97	26.1	6.30E-01	2384	0.09803	0.00102	3.28869	0.11954	0.243304	0.008474	0.958	-12.8	-9			1587	19	1478	28	1404	44
HR3-9S-14-098	553	46.2	9.30E-01	1475	0.06492	0.00059	0.68873	0.02143	0.076947	0.002289	0.956	-39.5	-35.3			772	18	532	13	478	14
HR3-9S-14-099	49	16.2	8.10E-01	1287	0.17733	0.00253	7.26607	0.31503	0.297183	0.012165	0.944	-41	-38.3			2628	23	2145	39	1677	60
HR3-9S-14-100	255	3.9	0.00E+00	543	0.04888	0.00064	0.09785	0.00309	0.014518	0.000417	0.909	-34.9				142	31	95	3	93	3
HR3-9S-14-102	206	45.7	0.00E+00	7046	0.08102	0.00074	2.29577	0.07732	0.205505	0.006663	0.963	-1.5				1222	17	1211	24	1205	36
HR3-9S-14-103	337	5.2	0.00E+00	793	0.04918	0.0006	0.09822	0.00322	0.014484	0.000441	0.929	-41.1	-6.1			157	28	95	3	93	3
HR3-9S-14-104	152	46.9	2.00E-01	6102	0.1153	0.00124	4.40408	0.18652	0.277026	0.011346	0.967	-18.4	-15.1			1885	18	1713	35	1576	57
HR3-9S-14-105	199	61.9	0.00E+00	7454	0.11721	0.00133	4.60817	0.18635	0.28515	0.011066	0.960	-17.5	-14			1914	20	1751	34	1617	56

Table 23: Raw data of concordant and disconcordant U-Pb analysis of all samples.

	ppm			Ratios								Discordance		Ages					
Name	U	^{206}Pb	$^{206}Pb_c$(%)	206/204	$^{207}Pb/^{206}Pb^*$	1SE	$^{207}Pb/^{235}U^*$	1SE	$^{206}Pb/^{238}U^*$	1SE	Rho	Central (%)	Minimum rim (%)	207/206	1σ	207/235	1σ	206/238	1σ
MA2-4-4-001	109	37.9	0.00E+00	6652	0.1204	0.00087	5.8416	0.14744	0.3519	0.008507	0.958	-1.1		1962	12	1953	22	1944	41
MA2-4-4-002	340	15	0.00E+00	355	0.07981	0.00127	0.50675	0.01242	0.046048	0.000861	0.763	-77.3	-75.7	1192	29	416	8	290	5
MA2-4-4-003	839	64.7	0.00E+00	584	0.10684	0.00086	1.17734	0.02711	0.079919	0.001725	0.937	-74.3	-73.5	1746	14	790	13	496	10
MA2-4-4-005	99	48.1	0.00E+00	7651	0.19188	0.00171	12.78904	0.40024	0.483402	0.014504	0.959	-9.5	-7	2758	14	2664	29	2542	63
MA2-4-4-006	762	111.2	0.00E+00	11068	0.06766	0.00037	1.40222	0.02894	0.150306	0.002993	0.965	5.6	0.4	858	11	890	12	903	17
MA2-4-4-007	898	31	0.00E+00	3969	0.05206	0.00029	0.25721	0.00575	0.03583	0.000776	0.969	-21.7	-13.4	288	12	232	5	227	5
MA2-4-4-008	100	31.3	0.00E+00	6565	0.1074	0.00072	4.67784	0.11769	0.31589	0.007661	0.964	0.9		1756	12	1763	21	1770	38
MA2-4-4-009	209	41.6	0.00E+00	4290	0.07521	0.00044	2.10688	0.04752	0.203165	0.004422	0.965	12	6.2	1074	11	1151	16	1192	24
MA2-4-4-010	716	227	0.00E+00	19134	0.1079	0.00071	4.7	0.14188	0.314009	0.009313	0.977	-0.3		1764	12	1762	25	1760	46
MA2-4-4-011	458	36.8	1.60E-01	7590	0.06449	0.00064	0.74258	0.0189	0.083507	0.001957	0.921	-33.1	-28.1	758	21	564	11	517	12
MA2-4-4-012	217	73.3	0.00E+00	222323	0.11411	0.00079	5.30163	0.16799	0.336962	0.01042	0.976	0.4		1866	11	1869	27	1872	50
MA2-4-4-013	241	41.6	2.00E-01	8640	0.10142	0.0007	2.53045	0.06048	0.180947	0.004139	0.957	-38	-36.2	1650	13	1281	17	1072	23
MA2-4-4-014	132	36.8	1.30E-01	10599	0.11247	0.00078	4.48582	0.10502	0.289258	0.006465	0.955	-12.4	-10.1	1840	12	1728	19	1638	32
MA2-4-4-015	231	37.2	3.40E-01	4281	0.08161	0.0005	1.91469	0.03925	0.170155	0.003326	0.953	-19.5	-17	1236	12	1086	14	1013	18
MA2-4-4-016	288	85.9	6.70E-02	19200	0.11155	0.00104	4.52963	0.15492	0.294517	0.00969	0.962	-10	-6.7	1825	16	1736	28	1664	48
MA2-4-4-017	241	77	1.60E-01	12376	0.11203	0.00086	4.87912	0.16714	0.315876	0.010546	0.975	-3.9	-1.1	1833	14	1799	29	1770	52
MA2-4-4-018	115	35.7	1.10E-01	9304	0.11062	0.00078	4.9	0.12011	0.323078	0.007541	0.958	-0.3		1810	12	1807	21	1805	37
MA2-4-4-019	274	3.7	0.00E+00	695	0.05229	0.00084	0.10679	0.00269	0.014813	0.000288	0.771	-68.7	-57.9	298	35	103	2	95	2
MA2-4-4-020	218	64.9	7.10E-02	35654	0.22955	0.00386	10.45455	0.57274	0.330321	0.017224	0.952	-45.4	-42.7	3049	27	2476	51	1840	83
MA2-4-4-021	695	87.5	8.90E-04	30925	0.08963	0.00109	1.72637	0.05712	0.139694	0.004297	0.93	-43.2	-40	1418	22	1018	21	843	24
MA2-4-4-022	926	150	3.40E-02	222120	0.10266	0.00072	2.41835	0.06971	0.170849	0.004776	0.97	-42.3	-40.7	1673	12	1248	21	1017	26
MA2-4-4-023	349	84.3	3.80E-02	22758	0.11028	0.00091	3.92	0.09359	0.25781	0.005772	0.938	-20.2	-17.6	1804	15	1618	19	1479	30
MA2-4-4-024	268	68.4	3.70E-01	4603	0.10217	0.00057	3.74338	0.07994	0.265722	0.005476	0.965	-9.8	-7.7	1664	10	1581	17	1519	28
MA2-4-4-025	319	59.6	4.30E-02	17955	0.16721	0.00176	4.79313	0.15208	0.207895	0.006225	0.944	-56.7	-55.3	2530	18	1784	27	1218	33
MA2-4-4-026	280	108.4	0.00E+00	46718	0.13269	0.001	7.28989	0.13647	0.398462	0.006823	0.915	1.6		2134	12	2148	17	2162	31
MA2-4-4-027	1265	79.3	1.90E-01	8461	0.08251	0.00055	0.73637	0.01324	0.064728	0.001082	0.93	-70	-69	1258	12	560	8	404	7
MA2-4-4-028	260	61	0.00E+00	5312	0.0876	0.00054	2.92679	0.04584	0.24233	0.003485	0.918	2		1374	11	1389	12	1399	18
MA2-4-4-029	160	54.8	7.50E-02	14246	0.2049	0.00324	10.26921	0.23012	0.363485	0.00578	0.710	-35.1	-32.6	2866	26	2459	21	1999	27
MA2-4-4-030	252	92.1	0.00E+00	73902	0.13492	0.00119	7.07421	0.15313	0.380289	0.007523	0.914	-4.6	-1.7	2163	15	2121	19	2078	35
MA2-4-4-031	363	112.6	3.30E-02	35499	0.17123	0.00177	7.69399	0.16621	0.325882	0.006185	0.879	-33.5	-31.4	2570	17	2196	19	1818	30
MA2-4-4-032	171	2.3	0.00E+00	836	0.05558	0.00092	0.10828	0.00232	0.01413	0.000193	0.637	-79.8	-75.2	436	35	104	2	90	1
MA2-4-4-033	211	93.7	0.00E+00	16308	0.17074	0.00172	10.87538	0.26691	0.461958	0.01034	0.912	-5.5	-2.5	2565	16	2513	23	2448	46
MA2-4-4-034	552	101.6	2.80E-01	5002	0.14589	0.0015	3.8776	0.06984	0.19277	0.002847	0.82	-55	-53.6	2298	17	1609	15	1136	15
MA2-4-4-035	254	111.9	0.00E+00	28087	0.1747	0.00247	11.17648	0.21992	0.463999	0.006347	0.695	-6.7	-3.5	2603	22	2538	18	2457	28
MA2-4-4-036	276	68.2	3.50E-02	21133	0.11593	0.00092	4.17684	0.08239	0.261317	0.004715	0.915	-23.5	-21.2	1894	14	1669	16	1497	24
MA2-4-4-037	591	36.6	1.70E-01	7029	0.05573	0.00051	0.492	0.00673	0.064031	0.000657	0.749	-9.7		442	20	406	5	400	4
MA2-4-4-038	644	160.5	0.00E+00	57874	0.10005	0.00104	3.60653	0.05292	0.26145	0.00272	0.709	-8.8	-5.6	1625	19	1551	12	1497	14
MA2-4-4-039	443	171	0.00E+00	28606	0.14439	0.00183	8.04994	0.13791	0.404343	0.004667	0.674	-4.7	-1.6	2281	21	2237	15	2189	21
MA2-4-4-040	392	5.3	6.60E-02	1862	0.04931	0.00048	0.09874	0.00163	0.014521	0.000194	0.809	-43.2	-20.5	163	23	96	2	93	1
MA2-4-4-041	468	55.7	9.60E-02	11918	0.06997	0.00047	1.21729	0.01585	0.126177	0.001404	0.855	-18.5	-15.2	927	13	809	7	766	8
MA2-4-4-042	2204	179.3	1.30E+00	2391	0.07476	0.00104	0.85913	0.01984	0.083352	0.001539	0.799	-53.5	-50.1	1062	26	630	11	516	9
MA2-4-4-043	695	45.8	6.90E-01	2096	0.06852	0.00049	0.65147	0.01707	0.06896	0.001739	0.962	-53.1	-50.9	884	14	509	10	430	10
MA2-4-4-044	477	96.2	4.50E-01	3666	0.10967	0.00109	3.3	0.09445	0.218233	0.005859	0.938	-32	-29.4	1794	17	1481	22	1273	31
MA2-4-4-045	854	330.1	0.00E+00	111409	0.14163	0.00131	7.92058	0.18096	0.405606	0.008471	0.914	-2.8		2247	16	2222	21	2195	39
MA2-4-4-046	25	12.2	0.00E+00	3213	0.19505	0.00228	13.79408	0.32087	0.512917	0.010316	0.865	-5.1	-1.9	2785	19	2736	22	2669	44
MA2-4-4-047	488	9.5	0.00E+00	3525	0.05008	0.00039	0.14283	0.00207	0.020683	0.000252	0.843	-34	-18.8	199	18	136	2	132	2
MA2-4-4-048	430	49.9	1.00E+00	3071	0.09674	0.00156	1.60513	0.0381	0.120332	0.00209	0.732	-56.1	-53.6	1562	30	972	15	732	12
MA2-4-4-049	142	6.7	0.00E+00	1455	0.05584	0.00047	0.39272	0.00636	0.05101	0.000703	0.851	-28.8	-21.6	446	18	336	5	321	4
MA2-4-4-050	149	46.6	0.00E+00	11148	0.11585	0.00093	5.24468	0.1021	0.328335	0.005818	0.910	-3.8	-0.9	1893	14	1860	17	1830	28

Table 24: Raw data of concordant and disconcordant U-Pb analysis of all samples.

MA2-4-4-051	266	62.8	0.00E+00	19966	0.09431	0.00069	3.21824	0.05599	0.24749	0.003902	0.906	-6.5	-3.6			1514	13	1462	13	1426	20
MA2-4-4-052			0.00E+00	13	0.8569	0.03987	925.7285	892.9498	7.83523	7.549	0.999	564.9				5019	63	6937	978	14045	5508
MA2-4-4-053	141	5.8	0.00E+00	1288	0.05392	0.00055	0.32557	0.00559	0.043793	0.000606	0.805	-25.4	-14.1			368	23	286	4	276	4
MA2-4-4-054	105	18.2	0.00E+00	5402	0.07664	0.00063	1.93597	0.03367	0.183196	0.002807	0.881	-2.7				1112	16	1094	12	1084	15
MA2-4-4-055	104	1.5	0.00E+00	521	0.07276	0.00173	0.15063	0.00423	0.015015	0.000223	0.530	-91.1	-90			1007	46	142	4	96	1
MA2-4-4-056	175	13.4	0.00E+00	5613	0.05857	0.00046	0.64944	0.01044	0.080422	0.00113	0.874	-9.9	-3.2			551	16	508	6	499	7
MA2-4-4-057	281	95.5	8.40E-02	20052	0.14074	0.00127	6.69448	0.1337	0.344991	0.006141	0.891	-16.8	-14.3			2236	14	2072	18	1911	29
MA2-4-4-058	574	45.1	6.30E-01	3335	0.07259	0.00084	0.83547	0.01453	0.083471	0.001084	0.747	-50.4	-47.4			1003	22	617	8	517	6
MA2-4-4-059	397	28.3	0.00E+00	7661	0.05708	0.00043	0.57068	0.00926	0.072512	0.001044	0.887	-9.1	-1.8			495	16	458	6	451	6
MA2-4-4-060	484	113.1	8.90E-01	5683	0.09608	0.00061	2.93616	0.04178	0.221636	0.002819	0.894	-18.4	-16.3			1549	11	1391	11	1291	15
MA2-4-4-061	191	53.1	0.00E+00	60320	0.10839	0.0009	4.42265	0.08846	0.295935	0.005388	0.91	-6.5	-3.5			1773	14	1717	17	1671	27
MA2-4-4-062	272	86.3	0.00E+00	73390	0.11671	0.00088	5.36093	0.10286	0.333146	0.005883	0.920	-3.2	-0.5			1906	13	1879	16	1854	28
MA2-4-4-063	523	72.2	1.70E+00	1223	0.0888	0.0018	1.77178	0.04664	0.144714	0.00243	0.638	-40.3	-35.9			1400	38	1035	17	871	14
MA2-4-4-064	449	43.1	3.50E-02	26025	0.09095	0.00069	1.28717	0.02818	0.102645	0.002109	0.939	-59.2	-57.8			1446	14	840	13	630	12
MA2-4-4-065	13	2.2	0.00E+00	768	0.08361	0.00128	2.10892	0.0652	0.182934	0.004911	0.868	-17	-10.9			1284	28	1152	21	1083	27
MA2-4-4-066	69	17.2	7.80E-01	4200	0.16756	0.00247	5.72174	0.14913	0.247662	0.005322	0.824	-48.6	-46.3			2533	24	1935	23	1426	27
MA2-4-4-067	257	86.9	0.00E+00	28334	0.12038	0.00141	5.5268	0.12094	0.332974	0.006154	0.845	-6.4	-2.6			1962	20	1905	19	1853	30
MA2-4-4-068	266	40.4	0.00E+00	23382	0.07141	0.00066	1.50711	0.02483	0.153079	0.002083	0.826	-5.6	-0.7			969	19	933	10	918	12
MA2-4-4-069	350	88.2	0.00E+00	41640	0.09119	0.00091	3.14921	0.05769	0.25047	0.003848	0.839	-0.7				1451	18	1445	14	1441	20
MA2-4-4-070	316	19.3	0.00E+00	3727	0.05661	0.00049	0.53993	0.00877	0.069171	0.000953	0.848	-9.8	-1.3			476	18	438	6	431	6
MA2-4-4-071	282	45.7	0.00E+00	12678	0.07206	0.00068	1.6114	0.02893	0.162176	0.002477	0.851	-2.1				988	19	975	11	969	14
MA2-4-4-072	162	60.4	0.00E+00	276837	0.12573	0.00152	6.30379	0.14876	0.363646	0.007376	0.859	-2.3				2039	21	2019	21	1999	35
MA2-4-4-073	282	54.2	0.00E+00	17837	0.07851	0.00076	2.08255	0.03732	0.192384	0.002893	0.839	-2.4				1160	19	1143	12	1134	16
MA2-4-4-074	447	21.7	0.00E+00	9021	0.05411	0.00048	0.4	0.0057	0.050036	0.000623	0.816	-16.7	-6.2			376	19	322	4	315	4
MA2-4-4-075	450	29.9	2.10E-01	14420	0.05602	0.00051	0.51082	0.00878	0.066133	0.000961	0.845	-9.2				453	20	419	6	413	6
MA2-4-4-076	242	18.1	0.00E+00	11276	0.05724	0.00051	0.60529	0.00981	0.076695	0.001034	0.832	-5.1				501	19	481	6	476	6
MA2-4-4-078	153	2.1	0.00E+00	1666	0.05242	0.00082	0.10368	0.00207	0.014345	0.00018	0.626	-70.3	-59.8			304	34	100	2	92	1
MA2-4-4-077	278	15.4	8.20E-01	2233	0.05413	0.00057	0.41077	0.00763	0.05504	0.00084	0.822	-8.5				376	23	349	5	345	5
MA2-4-4-079	205	64.5	0.00E+00	13601	0.12111	0.00141	5.18932	0.10771	0.310772	0.005343	0.828	-13.2	-9.8			1973	19	1851	18	1745	26
MA2-4-4-080	549	40.1	4.30E-01	7124	0.05923	0.00055	0.56628	0.0155	0.069341	0.001785	0.941	-25.8	-19			576	20	456	10	432	11
MA2-4-4-081	248	66.6	5.20E-02	34101	0.12023	0.00137	4.47496	0.08613	0.269948	0.00419	0.807	-24	-21.1			1960	19	1726	16	1541	21
MA2-4-4-082	243	88.3	4.80E-02	31209	0.18455	0.00272	9.3	0.21971	0.364885	0.006755	0.782	-29.7	-26.9			2694	23	2367	22	2005	32
MA2-4-4-083	291	13.7	3.80E-01	2872	0.05465	0.00063	0.3666	0.00609	0.048647	0.000584	0.722	-23.6	-11.6			398	25	317	5	306	4
MA2-4-4-084	93	4.7	0.00E+00	1843	0.05471	0.00067	0.39397	0.00674	0.052223	0.000628	0.703	-18.5	-4.9			401	26	337	5	328	4
MA2-4-4-085	164	7.3	0.00E+00	1636	0.05918	0.0008	0.36624	0.00704	0.04488	0.000613	0.711	-51.8	-45.8			574	28	317	5	283	4
MA2-4-4-086	176	14.3	0.00E+00	1648	0.06025	0.00057	0.67965	0.01107	0.081818	0.001085	0.814	-17.9	-11.3			612	20	527	7	507	6
MA2-4-4-087	83	21.6	0.00E+00	2384	0.09715	0.00108	3.33309	0.07273	0.248842	0.00467	0.86	-9.8	-5.7			1570	20	1489	17	1433	24
MA2-4-4-088	500	89.4	7.00E-02	32757	0.1029	0.00119	2.6834	0.06783	0.18913	0.004248	0.889	-36.3	-33.4			1677	21	1324	19	1117	23
MA2-4-4-089	46	5.5	6.60E-01	1727	0.06569	0.00073	1.11715	0.02479	0.123336	0.002365	0.864	-6.2				797	23	762	12	750	14
MA2-4-4-090	129	1.8	0.00E+00	593	0.08052	0.00445	0.16057	0.00914	0.014464	0.000198	0.240	-93	-90.8			1210	104	151	8	93	1
MA2-4-4-091	384	38	0.00E+00	11487	0.06082	0.00056	0.77926	0.01497	0.092929	0.001565	0.876	-9.9	-2.8			633	19	585	9	573	9
MA2-4-4-092	191	12.8	0.00E+00	11345	0.05618	0.00054	0.53494	0.00847	0.069054	0.000869	0.794	-6.6				460	20	435	6	430	5
MA2-4-4-093	237	120.8	0.00E+00	32016	0.1919	0.00297	12.80718	0.36914	0.484041	0.011769	0.844	-9.4	-5.3			2758	25	2666	27	2545	51
MA2-4-4-094	89	13.3	0.00E+00	2898	0.07195	0.00069	1.51419	0.02556	0.152634	0.002113	0.820	-7.5	-2.6			985	19	936	10	916	12
MA2-4-4-095	307	93.2	1.60E-01	10357	0.11844	0.00139	4.92676	0.10888	0.301686	0.005656	0.848	-13.7	-10.2			1933	20	1807	19	1700	28
MA2-4-4-096	70	33	0.00E+00	3404	0.17204	0.00248	10.82761	0.36897	0.456447	0.014092	0.906	-7.2	-3			2578	22	2508	32	2424	62
MA2-4-4-097	689	101.8	0.00E+00	27446	0.06889	0.00064	1.41747	0.02501	0.149239	0.002233	0.848	0.2				895	18	896	11	897	13
MA2-4-4-098	778	82.5	1.40E-01	13102	0.08085	0.00081	1.19105	0.02229	0.106841	0.001686	0.843	-48.6	-46.2			1218	18	796	10	654	10
MA2-4-4-099	115	1.5	0.00E+00	513	0.05047	0.00112	0.09771	0.0025	0.014041	0.000177	0.493	-58.9	-6.2			217	51	95	2	90	1
MA2-4-4-100	291	42.9	0.00E+00	14628	0.07047	0.00069	1.4386	0.02592	0.148054	0.002242	0.840	-5.9	-0.6			942	20	905	11	890	13
MA2-4-4-101	60	3.3	0.00E+00	602	0.05501	0.00062	0.41796	0.00757	0.055106	0.000781	0.783	-16.6	-4.2			413	25	355	5	346	5
MA2-4-4-102	106	20.2	3.00E-01	6344	0.09388	0.001	2.5001	0.04997	0.193148	0.003266	0.846	-26.6	-23.4			1506	20	1272	14	1138	18
MA2-4-4-103	79	1.1	0.00E+00	283	0.0517	0.00142	0.10282	0.00314	0.014423	0.000194	0.441	-66.6	-24.8			272	65	99	3	92	1
MA2-4-4-104	342	48.1	3.20E-01	4941	0.06944	0.00067	1.36725	0.02555	0.142812	0.00229	0.858	-6	-0.5			912	19	875	11	861	13
MA2-4-4-105	119	37.2	3.10E-01	9133	0.11947	0.00145	4.99087	0.12469	0.302984	0.006612	0.873	-14.1	-10.4			1948	21	1818	21	1706	33
MA2-4-4-106	314	33.1	2.80E-01	8567	0.10456	0.00127	1.56709	0.03184	0.108696	0.001767	0.800	-64.1	-62.6			1707	21	957	13	665	10
MA2-4-4-107	237	48.7	1.30E-01	8470	0.17046	0.00263	4.94717	0.13638	0.210495	0.004807	0.828	-56.9	-54.9			2562	26	1810	23	1231	26
MA2-4-4-108	232	39.2	3.10E-01	4934	0.10209	0.00123	2.40023	0.0548	0.170509	0.003306	0.849	-42	-39.4			1663	22	1243	16	1015	18
MA2-4-4-109	264	70.9	2.10E-01	6812	0.11552	0.00134	4.31639	0.09519	0.271004	0.005086	0.851	-20.4	-17.1			1888	20	1696	18	1546	26

Table 25: Raw data of concordant and disconcordant U-Pb analysis of all samples.

	ppm			Ratios								Discordance		Ages					
Name	U	^{206}Pb	$^{206}Pb_c$(%)	206/204	$^{207}Pb/^{206}Pb^*$	1SE	$^{207}Pb/^{235}U^*$	1SE	$^{206}Pb/^{238}U^*$	1SE	Rho	Central (%)	Minimum rim (%)	207/206	1σ	207/235	1σ	206/238	1σ
MA2-4-20-001	487	35.7	0.00E+00	5649	0.05589	0.00017	0.52856	0.00924	0.068591	0.001181	0.985	-4.7	-1.3	448	6	431	6	428	7
MA2-4-20-002	220	55	2.50E-01	8145	0.10414	0.00039	3.20589	0.09089	0.22326	0.006275	0.991	-26	-25	1699	7	1459	22	1299	33
MA2-4-20-003	448	100.8	0.00E+00	15069	0.0832	0.00026	2.3719	0.05173	0.206775	0.004463	0.990	-5.4	-4	1274	6	1234	16	1212	24
MA2-4-20-004	292	70.5	2.70E-01	5141	0.10329	0.00038	3.05081	0.088	0.214217	0.00613	0.992	-28.2	-27.3	1684	6	1420	22	1251	33
MA2-4-20-005	434	11.4	0.00E+00	299	0.09006	0.00146	0.31656	0.00972	0.025494	0.000665	0.849	-89.7	-89	1427	30	279	7	162	4
MA2-4-20-006	98	27.9	0.00E+00	49499	0.1089	0.00041	3.92413	0.10172	0.26135	0.006703	0.989	-17.9	-16.7	1781	7	1619	21	1497	34
MA2-4-20-007	59	15.4	0.00E+00	102	0.23859	0.00952	8.14911	0.40898	0.247721	0.007546	0.607	-60.1	-56.8	3111	64	2248	45	1427	39
MA2-4-20-008	21	1.4	0.00E+00	132	0.0622	0.00088	0.55045	0.01664	0.064183	0.001715	0.884	-42.4	-35.7	681	30	445	11	401	10
MA2-4-20-009	280	39.5	3.20E-01	4858	0.09643	0.00035	1.8	0.05503	0.135026	0.00411	0.993	-50.5	-49.8	1556	7	1044	20	816	23
MA2-4-20-010	76	13.8	0.00E+00	3616	0.07394	0.00026	1.73012	0.03256	0.169706	0.003138	0.983	-3	-1.1	1040	7	1020	12	1010	17
MA2-4-20-011	79	20.4	0.00E+00	2014	0.1037	0.00049	3.43117	0.07091	0.239984	0.00483	0.974	-20	-18.5	1691	9	1512	16	1387	25
MA2-4-20-012	100	30.1	2.70E-01	6592	0.15919	0.00075	6.09637	0.13811	0.277744	0.006156	0.978	-39.8	-39	2447	8	1990	20	1580	31
MA2-4-20-014	403	42.9	1.60E-01	3713	0.0844	0.00034	1.16224	0.02499	0.099869	0.00211	0.983	-55.4	-54.5	1302	8	783	12	614	12
MA2-4-20-013	47	14.1	0.00E+00	2917	0.10173	0.00042	3.85841	0.08297	0.275081	0.005806	0.981	-6.1	-4.5	1656	7	1605	17	1567	29
MA2-4-20-015	616	54.2	5.70E-01	2553	0.07408	0.00028	0.82152	0.019	0.080431	0.001835	0.987	-54.2	-53.3	1044	7	609	11	499	11
MA2-4-20-016	126	37.9	6.00E-01	2466	0.10681	0.00062	3.99929	0.09937	0.271564	0.006561	0.972	-12.7	-10.7	1746	10	1634	20	1549	33
MA2-4-20-017	372	13.2	0.00E+00	497	0.06127	0.00138	0.3	0.0164	0.038318	0.001738	0.896	-63.8	-56.3	649	46	285	13	242	11
MA2-4-20-018	234	8	0.00E+00	34	0.50914	0.02291	2.21148	0.14329	0.031503	0.001468	0.719	-96.6	-96.3	4268	64	1185	45	200	9
MA2-4-20-019	90	25.2	0.00E+00	16149	0.10606	0.00046	3.70917	0.09923	0.253632	0.006694	0.987	-17.8	-16.4	1733	8	1573	21	1457	34
MA2-4-20-020	155	51.6	0.00E+00	8417	0.10972	0.00039	4.58025	0.11726	0.302753	0.007675	0.99	-5.7	-4.5	1795	6	1746	21	1705	38
MA2-4-20-021	179	60.3	0.00E+00	6286	0.10958	0.00054	4.32855	0.1795	0.286499	0.011796	0.993	-10.6	-9.1	1792	9	1699	34	1624	59
MA2-4-20-022	129	26.6	0.00E+00	15966	0.07818	0.00027	2.01875	0.0478	0.18727	0.004387	0.989	-4.2	-2.5	1152	7	1122	16	1107	24
MA2-4-20-023	104	34.9	0.00E+00	27202	0.11075	0.00045	4.59899	0.13223	0.301162	0.008573	0.990	-7.2	-5.8	1812	7	1749	24	1697	42
MA2-4-20-024	189	40.5	1.00E+00	1456	0.09158	0.00067	2.51536	0.06233	0.199202	0.004714	0.955	-21.6	-19	1459	14	1276	18	1171	25
MA2-4-20-025	228	37.6	2.00E+00	841	0.07719	0.00099	1.62081	0.04508	0.15228	0.003756	0.887	-20.2	-14.8	1126	24	978	17	914	21
MA2-4-20-026	691	57.7	1.70E-01	12628	0.07392	0.00036	0.79178	0.01614	0.077687	0.001537	0.97	-55.6	-54.3	1039	10	592	9	482	9
MA2-4-20-027	48	3.4	0.00E+00	1796	0.06004	0.00067	0.5465	0.01334	0.066013	0.001433	0.889	-32.9	-26.1	605	23	443	9	412	9
MA2-4-20-028	388	103.1	1.50E-01	9736	0.1044	0.00038	3.51945	0.07948	0.244492	0.005449	0.987	-19.2	-18.1	1704	6	1532	18	1410	28
MA2-4-20-029	569	40.6	9.50E-01	1532	0.08629	0.001	0.79246	0.02009	0.066609	0.001502	0.890	-71.3	-69.7	1345	21	593	11	416	9
MA2-4-20-030	256	62.9	2.10E-01	9673	0.10386	0.00043	3.22621	0.09417	0.225286	0.00651	0.99	-25.1	-23.9	1694	7	1463	23	1310	34
MA2-4-20-031	180	57.2	0.00E+00	15605	0.1092	0.0004	4.34597	0.11513	0.288636	0.007573	0.99	-9.6	-8.4	1786	7	1702	22	1635	38
MA2-4-20-032	339	76.2	1.60E-01	12056	0.10342	0.00057	3.08778	0.09319	0.216541	0.006424	0.983	-27.6	-26	1686	10	1430	23	1264	34
MA2-4-20-033	113	24	1.60E-01	6789	0.10179	0.00049	2.76364	0.06877	0.196918	0.004807	0.981	-32.8	-31.5	1657	9	1346	19	1159	26
MA2-4-20-034	234	57.1	2.10E-01	7373	0.10539	0.0004	3.19873	0.09624	0.220131	0.006571	0.992	-28.1	-27.1	1721	7	1457	23	1283	35
MA2-4-20-035	96	31.9	0.00E+00	13050	0.11059	0.00042	4.65107	0.11461	0.305034	0.007428	0.988	-5.8	-4.5	1809	6	1758	21	1716	37
MA2-4-20-036	115	18.5	0.00E+00	4334	0.06968	0.00028	1.44426	0.03318	0.150319	0.003398	0.984	-1.9		919	8	907	14	903	19
MA2-4-20-037	357	23.7	0.00E+00	3851	0.05742	0.00025	0.49801	0.00966	0.062902	0.001188	0.974	-23.3	-19.6	508	9	410	7	393	7
MA2-4-20-038	228	57.7	1.60E-01	14832	0.10551	0.00035	3.40313	0.07383	0.233924	0.005015	0.988	-23.7	-22.7	1723	6	1505	17	1355	26
MA2-4-20-039	154	46.1	0.00E+00	10932	0.10147	0.00033	3.85572	0.08981	0.275605	0.006357	0.990	-5.6	-4.4	1651	6	1604	19	1569	32
MA2-4-20-040	89	15.2	4.10E-01	6213	0.07107	0.0003	1.56776	0.03392	0.159996	0.003396	0.981	-0.3		959	8	958	13	957	19
MA2-4-20-041	411	33.1	2.50E+00	1432	0.0564	0.0004	0.53059	0.02043	0.068233	0.002582	0.983	-9.4	-1.7	468	15	432	14	426	16
MA2-4-20-042	384	27.7	4.30E-01	3116	0.05443	0.00022	0.51207	0.01003	0.068235	0.001307	0.978	9.8	3.2	389	9	420	7	426	8
MA2-4-20-043	44	6.1	0.00E+00	2075	0.07025	0.00043	1.26431	0.02684	0.130528	0.002651	0.957	-16.4	-13.2	936	12	830	12	791	15
MA2-4-20-044	27	8.2	0.00E+00	2032	0.10288	0.00044	3.90215	0.09559	0.2751	0.006636	0.985	-7.4	-5.8	1677	7	1614	20	1567	34
MA2-4-20-045	182	50.6	3.60E-01	6719	0.10513	0.00037	3.71607	0.08527	0.256352	0.005811	0.988	-16	-14.8	1717	6	1575	18	1471	30
MA2-4-20-046	22	6.7	0.00E+00	2589	0.10316	0.00054	3.9216	0.10014	0.275718	0.006889	0.978	-7.5	-5.5	1682	9	1618	21	1570	35
MA2-4-20-047	57	18.2	0.00E+00	4564	0.10567	0.00045	4.27477	0.10369	0.29339	0.007007	0.985	-4.4	-2.9	1726	8	1689	20	1658	35
MA2-4-20-048	99	31.8	4.90E-01	4626	0.10517	0.00047	4.0866	0.1456	0.281811	0.009962	0.992	-7.7	-6.2	1717	8	1652	29	1600	50
MA2-4-20-049	329	57.1	1.60E-01	10677	0.10315	0.0005	2.33245	0.0629	0.163992	0.004351	0.984	-45	-43.9	1682	9	1222	19	979	24
MA2-4-20-050	157	39	3.30E-01	6541	0.10499	0.00037	3.31551	0.07244	0.229039	0.00494	0.987	-24.8	-23.8	1714	6	1485	17	1329	26

Table 26: Raw data of concordant and disconcordant U-Pb analysis of all samples.

MA2-4-20-051	157	40.1	3.10E-01	5042	0.10327	0.00041	3.3451	0.08612	0.234917	0.005978	0.988	-21.3	-20.1			1684	7	1492	20	1360	31
MA2-4-20-052	205	63	2.10E-01	15987	0.10717	0.00041	4.15742	0.10947	0.281357	0.007331	0.990	-9.9	-8.6			1752	7	1666	22	1598	37
MA2-4-20-053	160	63.3	0.00E+00	54	0.31515	0.00815	15.62114	0.71269	0.359495	0.013512	0.824	-51	-47.8			3546	38	2854	44	1980	64
MA2-4-20-054	92	17.1	5.80E-01	2443	0.09173	0.00046	2.19305	0.06018	0.1734	0.004678	0.983	-31.9	-30.4			1462	9	1179	19	1031	26
MA2-4-20-055	478	35.2	0.00E+00	14603	0.05595	0.00021	0.53163	0.0117	0.068913	0.001495	0.985	-4.8	-0.5			450	8	433	8	430	9
MA2-4-20-056	136	25.4	0.00E+00	3292	0.07389	0.00031	1.75812	0.03852	0.172574	0.003712	0.982	-1.3				1038	8	1030	14	1026	20
MA2-4-20-057	260	56.1	0.00E+00	8414	0.07939	0.00027	2.18128	0.05157	0.199282	0.004661	0.989	-1				1182	7	1175	16	1171	25
MA2-4-20-058	229	26.8	7.30E-01	2149	0.06333	0.00023	0.9549	0.02184	0.109362	0.002469	0.987	-7.3	-4.7			719	7	681	11	669	14
MA2-4-20-059	97	9.9	1.30E+00	1358	0.05932	0.00039	0.79973	0.02773	0.097771	0.00333	0.982	4				579	14	597	16	601	20
MA2-4-20-060	501	63.1	3.00E-01	6483	0.0843	0.00034	1.36061	0.0323	0.117057	0.002738	0.985	-47.6	-46.6			1300	8	872	14	714	16
MA2-4-20-061	634	108	2.90E-01	6699	0.10612	0.00082	2.89256	0.06206	0.197696	0.003956	0.933	-35.9	-34			1734	13	1380	16	1163	21
MA2-4-20-062	153	41.4	4.40E-01	4725	0.10623	0.0029	4.2628	0.20699	0.291041	0.011679	0.826	-5.8				1736	47	1686	40	1647	58
MA2-4-20-063	229	64.4	0.00E+00	27033	0.10998	0.00306	4.60023	0.21871	0.303353	0.011692	0.811	-5.8				1799	48	1749	40	1708	58
MA2-4-20-064	666	168.1	4.70E-01	3812	0.10504	0.0029	3.73704	0.2027	0.258019	0.012045	0.861	-15.3	-6.2			1715	48	1579	43	1480	62
MA2-4-20-065	492	29.9	0.00E+00	7211	0.05525	0.00038	0.54783	0.01019	0.07191	0.001245	0.931	6.2				422	15	444	7	448	7
MA2-4-20-066	72	17.9	6.50E-01	2726	0.10288	0.00084	4.0137	0.09819	0.282944	0.006527	0.943	-4.8	-1.6			1677	15	1637	20	1606	33
MA2-4-20-067	516	63.6	3.50E-01	4264	0.09836	0.00078	1.99235	0.04793	0.146905	0.003335	0.944	-47.6	-45.8			1593	15	1113	16	884	19
MA2-4-20-068	360	78.5	5.70E-01	2831	0.09594	0.00079	3.256	0.07976	0.246146	0.00568	0.942	-9.2	-6			1547	15	1471	19	1419	29
MA2-4-20-069	314	47.6	0.00E+00	6399	0.07288	0.00054	1.7	0.03508	0.173158	0.003247	0.93	2				1011	14	1023	13	1029	18
MA2-4-20-070	423	25.5	0.00E+00	2463	0.05582	0.00041	0.53402	0.01292	0.069383	0.001599	0.952	-3				445	16	434	9	432	10
MA2-4-20-071	785	48.6	8.10E-01	1531	0.06629	0.0005	0.66203	0.01377	0.072437	0.001405	0.932	-46.3	-43.4			815	15	516	8	451	8
MA2-4-20-072	327	50.9	0.00E+00	5016	0.07374	0.00173	1.76421	0.06843	0.173519	0.005357	0.796	-0.3				1034	46	1032	25	1031	29
MA2-4-20-073	232	21.3	6.60E-01	2601	0.07178	0.00067	1.08112	0.02531	0.109239	0.002345	0.917	-33.4	-29.7			980	18	744	12	668	14
MA2-4-20-074	344	85.1	1.20E-01	12467	0.09934	0.00266	3.64751	0.17431	0.266304	0.010549	0.829	-6.2				1612	48	1560	38	1522	54
MA2-4-20-075	891	76.9	1.30E+00	1029	0.07562	0.00061	1.04405	0.02644	0.100135	0.002403	0.948	-45.4	-42.9			1085	16	726	13	615	14
MA2-4-20-076	391	91.5	0.00E+00	8975	0.10057	0.00081	3.75979	0.08601	0.271137	0.005808	0.936	-6.1	-2.9			1635	14	1584	18	1547	29
MA2-4-20-077	679	35.2	0.00E+00	3552	0.05568	0.0004	0.5	0.00846	0.061534	0.001012	0.918	-12.8	-5.2			439	15	393	6	385	6
MA2-4-20-078	294	31.8	1.20E+00	1463	0.06439	0.00152	1.05018	0.04312	0.118287	0.003979	0.819	-4.7				755	48	729	21	721	23
MA2-4-20-079	595	158.6	0.00E+00	34606	0.10874	0.00091	4.5963	0.10928	0.306563	0.006827	0.937	-3.5	-0.4			1778	15	1749	20	1724	34
MA2-4-20-080	823	95.8	4.70E-01	2934	0.08618	0.00218	1.57268	0.06155	0.132359	0.003948	0.762	-42.8	-36.7			1342	47	959	24	801	22
MA2-4-20-081	411	94.7	2.30E-01	6545	0.09751	0.00081	3.47512	0.07903	0.258485	0.005467	0.93	-6.7	-3.4			1577	15	1522	18	1482	28
MA2-4-20-082	30	7.7	5.20E-01	2463	0.10556	0.00095	4.3542	0.11272	0.299176	0.007258	0.937	-2.4				1724	16	1704	21	1687	36
MA2-4-20-083	301	75.7	2.00E-01	37821	0.10486	0.0012	3.97831	0.13461	0.275169	0.008762	0.941	-9.5	-5.3			1712	20	1630	27	1567	44
MA2-4-20-084	760	73.3	0.00E+00	749	0.0949	0.00249	1.41466	0.05599	0.10811	0.0032	0.748	-59.5	-55.5			1526	47	895	24	662	19
MA2-4-20-085	487	113.5	0.00E+00	25967	0.10806	0.00303	3.83395	0.17399	0.257329	0.009186	0.787	-18.4	-10.3			1767	48	1600	37	1476	47
MA2-4-20-086	582	149.9	0.00E+00	26263	0.09721	0.00259	3.79546	0.16982	0.283186	0.010187	0.804	2.6				1571	47	1592	36	1607	51
MA2-4-20-087	744	73	2.50E-01	8203	0.08265	0.00252	1.33834	0.07009	0.117441	0.005003	0.813	-45.6	-37.8			1261	58	863	30	716	29
MA2-4-20-088	528	100	2.30E-01	7519	0.10283	0.00083	3.14606	0.08104	0.22189	0.005426	0.949	-25.3	-22.8			1676	15	1444	20	1292	29
MA2-4-20-089	1014	161.7	1.10E-01	12933	0.10349	0.00285	2.53492	0.11019	0.177656	0.005972	0.773	-40.6	-34.7			1688	47	1282	32	1054	33
MA2-4-20-090	121	34.1	0.00E+00	4502	0.10815	0.00306	4.61703	0.21793	0.309614	0.011704	0.801	-1.9				1769	49	1752	39	1739	58
MA2-4-20-091	804	50.1	0.00E+00	6846	0.05696	0.00039	0.58901	0.01151	0.075	0.001373	0.937	-5				490	15	470	7	466	8
MA2-4-20-092	324	77.1	1.80E-01	10770	0.10471	0.00291	3.81932	0.16975	0.264548	0.00918	0.781	-12.9	-4.1			1709	52	1597	36	1513	47
MA2-4-20-093	407	115.9	1.90E-01	9895	0.10698	0.00308	4.47043	0.23591	0.303065	0.013407	0.838	-2.7				1749	52	1725	44	1706	66
MA2-4-20-094	505	82.7	2.90E-01	8108	0.10134	0.00078	2.72529	0.05856	0.195042	0.003916	0.934	-33.1	-31			1649	14	1335	16	1149	21
MA2-4-20-095	371	51	1.50E-01	14496	0.079	0.00057	1.78663	0.03964	0.164014	0.00344	0.945	-17.8	-14.6			1172	14	1041	14	979	19
MA2-4-20-096	424	25.5	0.00E+00	2738	0.05537	0.00044	0.52792	0.01175	0.069152	0.001438	0.934	0.9				427	17	430	8	431	9
MA2-4-20-097	386	45.3	0.00E+00	1077	0.09957	0.00279	1.74608	0.1037	0.127187	0.006657	0.881	-55.4	-50.1			1616	50	1026	38	772	38
MA2-4-20-098	572	100.1	4.00E-01	5347	0.09976	0.00276	2.72164	0.11593	0.197875	0.006417	0.761	-30.7	-23.7			1620	50	1334	32	1164	35
MA2-4-20-099	33	6.6	2.00E+00	1008	0.08777	0.00082	2.78531	0.06471	0.230148	0.004895	0.916	-3.4				1378	17	1352	17	1335	26
MA2-4-20-100	120	30.4	2.90E-01	7331	0.10639	0.00092	4.30704	0.10029	0.2936	0.006344	0.928	-5.2	-1.9			1739	15	1695	19	1659	32
MA2-4-20-101	50	13	0.00E+00	5037	0.11038	0.00103	4.65055	0.12637	0.305566	0.007801	0.939	-5.5	-2.1			1806	16	1758	23	1719	39
MA2-4-20-102	164	39	1.10E+00	1775	0.10425	0.00116	4.01831	0.11037	0.279543	0.007024	0.915	-7.4	-3.3			1701	20	1638	22	1589	35
MA2-4-20-103	365	54.6	5.60E-01	3198	0.10006	0.00279	2.32169	0.09846	0.168284	0.005376	0.753	-41.3	-35.4			1625	51	1219	30	1003	30
MA2-4-20-104	21	4.7	0.00E+00	1229	0.10182	0.00104	3.73445	0.1039	0.266018	0.00688	0.930	-9.3	-5.5			1657	18	1579	22	1521	35
MA2-4-20-105	176	28.7	4.10E-01	5338	0.09933	0.00277	2.51143	0.10722	0.183368	0.005926	0.757	-35.4	-28.9			1612	47	1275	31	1085	32
MA2-4-20-106	42	2.5	3.10E+00	428	0.02848	0.00071	0.27875	0.00893	0.07098	0.001427	0.628	-3.2				-351	32	250	7	442	9
MA2-4-20-107	154	8.8	0.00E+00	2789	0.05636	0.00049	0.54715	0.01174	0.070414	0.001382	0.914	-6.2				466	19	443	8	439	8
MA2-4-20-108	310	18.1	0.00E+00	5742	0.05548	0.00039	0.55228	0.01225	0.0722	0.001519	0.949	4.3				432	15	446	8	449	9
MA2-4-20-109	184	41.4	0.00E+00	14364	0.10476	0.00084	3.88599	0.10244	0.269036	0.006758	0.953	-11.4	-8.6			1710	14	1611	21	1536	34

Table 27: Raw data of concordant and disconcordant U-Pb analysis of all samples.

	ppm			Ratios								Discordance		Ages					
Name	U	^{206}Pb	$^{206}Pb_c$(%)	206/204	$^{207}Pb/^{206}Pb^*$	1SE	$^{207}Pb/^{235}U^*$	1SE	$^{206}Pb/^{238}U^*$	1SE	Rho	Central (%)	Minimum rim (%)	207/206	1σ	207/235	1σ	206/238	1σ
MA2-2-4-001	243	37.6	7.40E-02	9143	0.0725	0.00027	1.65802	0.07727	0.165865	0.007704	0.997	-1.2		1000	7	993	30	989	43
MA2-2-4-002	280	87.6	1.90E+00	480	0.17826	0.00172	7.5109	0.4536	0.30558	0.018218	0.987	-39.5	-37.8	2637	15	2174	54	1719	90
MA2-2-4-003	558	227.8	4.90E-01	3279	0.18149	0.00083	9.7	0.68575	0.386347	0.027347	0.998	-24.6	-23.9	2667	7	2404	65	2106	127
MA2-2-4-004	432	109.8	9.40E-01	1820	0.10473	0.00068	3.77128	0.20882	0.261163	0.014362	0.993	-14	-12	1710	12	1587	44	1496	73
MA2-2-4-005	43	20.1	8.10E-01	1662	0.16544	0.00129	10.05305	0.25016	0.44071	0.010416	0.95	-7.5	-5.2	2512	13	2440	23	2354	47
MA2-2-4-006	725	264.3	2.10E-02	45717	0.1178	0.00075	5.51293	0.1132	0.339428	0.006628	0.951	-2.3		1923	11	1903	18	1884	32
MA2-2-4-007	115	67.1	0.00E+00	19071	0.19927	0.00166	14.94535	0.39602	0.543949	0.013681	0.949	-0.9		2820	13	2812	25	2800	57
MA2-2-4-008	151	75.6	1.10E-01	11388	0.16421	0.0012	10.59156	0.25591	0.467795	0.010772	0.953	-1.2		2499	11	2488	22	2474	47
MA2-2-4-009	321	13.9	0.00E+00	2148	0.05251	0.00036	0.2915	0.00507	0.040262	0.000646	0.921	-17.6	-7.8	308	15	260	4	254	4
MA2-2-4-010	143	34.6	0.00E+00	8178	0.08499	0.00045	2.6353	0.04868	0.224889	0.003981	0.958	-0.6		1315	10	1311	14	1308	21
MA2-2-4-011	181	72.4	0.00E+00	11060	0.12416	0.00073	6.4	0.13556	0.371446	0.007612	0.961	1.1		2017	10	2027	19	2036	36
MA2-2-4-012	740	221.8	3.00E-02	30806	0.10519	0.00058	4.00142	0.08335	0.275883	0.005538	0.964	-9.6	-7.6	1718	10	1634	17	1571	28
MA2-2-4-013	167	53	0.00E+00	17103	0.10767	0.00064	4.36313	0.08582	0.293901	0.005506	0.953	-6.4	-4.2	1760	11	1705	16	1661	27
MA2-2-4-014	203	42.9	0.00E+00	10290	0.07787	0.00043	2.10196	0.03638	0.195785	0.003208	0.947	0.9		1143	11	1149	12	1153	17
MA2-2-4-015	855	253.5	9.70E-04	61919	0.11646	0.00075	4.41507	0.08798	0.274955	0.005186	0.946	-19.9	-18	1903	11	1715	16	1566	26
MA2-2-4-016	416	136.2	1.20E-01	15661	0.11341	0.00078	4.69559	0.11374	0.300299	0.006978	0.959	-9.9	-7.6	1855	12	1766	20	1693	35
MA2-2-4-017	184	58.4	0.00E+00	16202	0.11486	0.00074	4.68406	0.09847	0.295762	0.005917	0.952	-12.5	-10.4	1878	11	1764	18	1670	29
MA2-2-4-018	670	178.1	2.80E-01	5062	0.113	0.00079	3.78746	0.08132	0.243092	0.004937	0.946	-26.8	-24.8	1848	12	1590	17	1403	26
MA2-2-4-019	304	74.1	0.00E+00	28783	0.08982	0.00058	2.79765	0.05357	0.225908	0.004071	0.941	-8.4	-5.7	1422	12	1355	14	1313	21
MA2-2-4-020	97	56.8	0.00E+00	15160	0.19986	0.002	14.9846	0.44275	0.543774	0.01512	0.941	-1.1		2825	15	2814	28	2799	63
MA2-2-4-021	328	108.9	6.30E-02	16495	0.11476	0.00067	4.83254	0.09835	0.305403	0.005955	0.958	-9.6	-7.6	1876	10	1791	17	1718	29
MA2-2-4-022	329	116.4	0.00E+00	98604	0.11066	0.00078	4.9984	0.10785	0.327582	0.00668	0.945	1		1810	13	1819	18	1827	32
MA2-2-4-023	259	80.6	0.00E+00	14641	0.10177	0.00069	4.01716	0.08855	0.286296	0.006002	0.951	-2.3		1657	13	1638	18	1623	30
MA2-2-4-024	995	198.6	1.10E-01	19961	0.10511	0.00089	2.7206	0.07306	0.187721	0.004782	0.949	-38.5	-36.4	1716	16	1334	20	1109	26
MA2-2-4-025	481	7.2	0.00E+00	1455	0.04911	0.00051	0.09318	0.00186	0.013761	0.000234	0.855	-42.7	-15.3	153	24	90	2	88	1
MA2-2-4-026	484	165	0.00E+00	29601	0.11727	0.00074	5.06291	0.10737	0.313129	0.006339	0.955	-9.5	-7.3	1915	11	1830	18	1756	31
MA2-2-4-027	328	101.1	1.40E-02	30177	0.11652	0.00078	4.57771	0.09838	0.284938	0.005815	0.95	-17	-15	1903	12	1745	18	1616	29
MA2-2-4-028	238	82.1	0.00E+00	27175	0.11752	0.00081	5.14935	0.1129	0.317792	0.006613	0.949	-8.3	-6	1919	12	1844	19	1779	32
MA2-2-4-029	223	3.3	4.00E-01	1607	0.05299	0.00134	0.09957	0.00306	0.013629	0.000241	0.574	-73.9	-56.1	328	55	96	3	87	2
MA2-2-4-030	575	210.2	0.00E+00	33245	0.11461	0.00078	5.26257	0.12546	0.33303	0.007609	0.958	-1.3		1874	12	1863	20	1853	37
MA2-2-4-031	821	188.3	7.30E-02	244905	0.10625	0.0007	3.0618	0.06727	0.209009	0.004379	0.954	-32.4	-30.6	1736	12	1423	17	1224	23
MA2-2-4-032	1027	262.4	0.00E+00	35531	0.09162	0.00066	2.95391	0.09654	0.233838	0.007455	0.975	-8	-5	1459	13	1396	25	1355	39
MA2-2-4-033	546	81.6	2.20E+00	629	0.09867	0.00201	1.81146	0.05673	0.133156	0.003163	0.759	-52.7	-49.2	1599	35	1050	20	806	18
MA2-2-4-034	337	97.4	8.10E-02	13987	0.11395	0.00087	4.1602	0.11444	0.264793	0.006997	0.961	-21	-18.7	1863	13	1666	23	1514	36
MA2-2-4-035	583	201.6	0.00E+00	62981	0.11391	0.00072	4.96793	0.1115	0.316304	0.006816	0.960	-5.6	-3.3	1863	11	1814	19	1772	33
MA2-2-4-036	229	21.2	0.00E+00	410	0.10399	0.00742	1.23171	0.09343	0.085903	0.002212	0.339	-71.5	-63.4	1697	130	815	43	531	13
MA2-2-4-037	396	148.9	0.00E+00	59770	0.12054	0.00085	5.71007	0.1422	0.343574	0.00821	0.960	-3.5	-1.1	1964	12	1933	22	1904	39
MA2-2-4-038	578	117.3	0.00E+00	5389	0.07488	0.00052	1.915	0.04357	0.185473	0.004018	0.952	3.2		1065	13	1086	15	1097	22
MA2-2-4-039	395	107.4	1.70E-01	18794	0.11277	0.00141	4.80977	0.09187	0.309324	0.004472	0.757	-6.6	-2.8	1845	22	1787	16	1737	22
MA2-2-4-040	57	23.1	5.80E-01	4754	0.16252	0.00305	10.46279	0.41826	0.466906	0.016474	0.883	-0.6		2482	31	2477	37	2470	72
MA2-2-4-041	547	49.2	1.60E+00	2542	0.08356	0.00256	1.22306	0.04096	0.106152	0.001443	0.406	-51.8	-45.2	1282	59	811	19	650	8
MA2-2-4-042	333	41.8	0.00E+00	27340	0.06953	0.00069	1.43856	0.02166	0.150055	0.001697	0.751	-1.6		915	20	905	9	901	10
MA2-2-4-043	188	44.3	0.00E+00	23151	0.11556	0.00153	4.34355	0.09193	0.272617	0.004492	0.779	-19.9	-16.4	1889	23	1702	17	1554	23
MA2-2-4-044	138	39.7	1.80E-02	27215	0.11712	0.00179	5.43007	0.24308	0.336262	0.014153	0.940	-2.7		1913	27	1890	38	1869	68
MA2-2-4-045	483	211.9	0.00E+00	158045	0.1966	0.00385	13.2597	0.39632	0.489152	0.011047	0.756	-10	-5.4	2798	32	2698	28	2567	48
MA2-2-4-046	691	69.6	1.10E-01	19178	0.09803	0.00147	1.64569	0.05047	0.121751	0.003256	0.872	-56.4	-53.7	1587	27	988	19	741	19
MA2-2-4-047	179	27.6	0.00E+00	9928	0.07738	0.00088	2.0	0.03353	0.186715	0.002316	0.737	-2.6		1131	21	1113	11	1104	13
MA2-2-4-048	831	129.5	7.70E-02	29873	0.10108	0.00136	2.51175	0.04989	0.180221	0.002634	0.736	-38	-35.1	1644	24	1275	14	1068	14
MA2-2-4-049	281	54.7	0.00E+00	33508	0.10922	0.00146	3.46518	0.06969	0.230106	0.003461	0.748	-27.9	-24.8	1786	23	1519	16	1335	18
MA2-2-4-050	319	62.7	0.00E+00	20544	0.11239	0.00153	3.64224	0.07911	0.235049	0.003972	0.778	-28.8	-25.5	1838	24	1559	17	1361	21

Table 28: Raw data of concordant and disconcordant U-Pb analysis of all samples.

MA2-2-4-052	352	78.5	4.90E-02	96702	0.16889	0.00298	6.16906	0.16324	0.264921	0.005226	0.745	-45.3	-42.7			2547	27	2000	23	1515	27
MA2-2-4-053	700	57.5	9.80E-01	1777	0.10977	0.0015	1.51757	0.03592	0.100272	0.001935	0.815	-68.8	-67.3			1796	24	937	14	616	11
MA2-2-4-054	129	15.6	0.00E+00	20164	0.06966	0.00081	1.40809	0.02348	0.14661	0.001748	0.715	-4.2	.			918	23	892	10	882	10
MA2-2-4-056	358	55.5	0.00E+00	18757	0.07726	0.00088	1.99313	0.0375	0.187092	0.002801	0.796	-2.2	.			1128	22	1113	13	1106	15
MA2-2-4-055	179	47.7	9.80E-02	46530	0.11558	0.00161	5.0	0.11054	0.3164	0.005348	0.771	-7.1	-2.8			1889	24	1826	19	1772	26
MA2-2-4-057	336	39.2	0.00E+00	20958	0.06768	0.00075	1.32735	0.02185	0.142235	0.001728	0.738	-0.2	.			859	22	858	10	857	10
MA2-2-4-058	1054	265.2	2.70E-02	116565	0.11181	0.00153	4.60443	0.09324	0.29867	0.004446	0.735	-9	-5			1829	23	1750	17	1685	22
MA2-2-4-059	293	47.3	0.00E+00	16350	0.07904	0.00093	2.1383	0.04107	0.196203	0.002983	0.791	-1.7	.			1173	23	1161	13	1155	16
MA2-2-4-060	388	100.6	9.40E-02	32934	0.1102	0.00156	4.66131	0.10143	0.306791	0.005062	0.758	-4.9	-0.4			1803	24	1760	18	1725	25
MA2-2-4-061	264	48.6	0.00E+00	69	0.3402	0.02468	10.06516	0.83159	0.21458	0.008489	0.479	-72	-68.6			3664	111	2441	76	1253	45
MA2-2-4-062	274	72.4	5.50E-02	27497	0.11614	0.00163	5.07139	0.11132	0.316699	0.005353	0.770	-7.5	-3.2			1898	24	1831	19	1774	26
MA2-2-4-063	418	104.4	6.10E-02	51538	0.11215	0.00162	4.58702	0.09873	0.296647	0.00473	0.741	-9.9	-5.7			1835	25	1747	18	1675	24
MA2-2-4-64	334	104	0.00E+00	8806	0.11565	0.00096	5.30052	0.16042	0.33242	0.009671	0.961	-2.4	.			1890	14	1869	26	1850	47
MA2-2-4-65	953	111.3	4.60E-01	4937	0.09198	0.00069	1.59986	0.03623	0.126147	0.002697	0.944	-50.6	-49			1467	13	970	14	766	15
MA2-2-4-66	628	94.5	1.00E-01	20203	0.07815	0.00054	1.74461	0.04059	0.161914	0.003596	0.955	-17.1	-14.1			1151	13	1025	15	967	20
MA2-2-4-67	410	102.1	8.20E-02	14823	0.11137	0.00095	4.08973	0.12141	0.266331	0.007575	0.958	-18.5	-15.8			1822	15	1652	24	1522	39
MA2-2-4-68	216	62.9	0.00E+00	12345	0.11542	0.00096	4.9254	0.13881	0.3095	0.008335	0.956	-9	-6.1			1886	14	1807	24	1738	41
MA2-2-4-69	99	21.8	4.10E-01	3971	0.09879	0.00079	3.20273	0.08224	0.235121	0.005734	0.950	-16.6	-13.8			1601	14	1458	20	1361	30
MA2-2-4-70	273	3.8	0.00E+00	951	0.0526	0.0011	0.10929	0.00323	0.015068	0.000315	0.708	-69.6	-54.9			312	45	105	3	96	2
MA2-2-4-71	144	42.5	0.00E+00	7145	0.1172	0.001	5.09775	0.14967	0.315463	0.008859	0.956	-8.7	-5.8			1914	14	1836	25	1768	43
MA2-2-4-72	368	106.5	0.00E+00	24951	0.11427	0.00095	4.81439	0.14155	0.305562	0.008615	0.959	-9.1	-6.2			1868	15	1787	25	1719	43
MA2-2-4-73	734	251.4	0.00E+00	52261	0.11899	0.00101	5.9	0.18048	0.35966	0.01057	0.961	2.4	.			1941	14	1961	27	1981	50
MA2-2-4-75	197	41.7	4.20E-01	4191	0.11018	0.0009	3.42514	0.10047	0.225471	0.00635	0.960	-30.1	-27.9			1802	15	1510	23	1311	33
MA2-2-4-76	126	17	0.00E+00	4232	0.06776	0.00052	1.36273	0.03591	0.14585	0.003678	0.957	2	.			861	15	873	15	878	21
MA2-2-4-77	169	41.9	0.00E+00	10851	0.11352	0.00098	4.15917	0.11382	0.265717	0.006903	0.949	-20.4	-17.8			1857	15	1666	22	1519	35
MA2-2-4-78	179	41.6	0.00E+00	2252	0.11281	0.00096	3.85185	0.11294	0.247642	0.006946	0.957	-25.3	-22.8			1845	15	1604	24	1426	36
MA2-2-4-79	81	21.7	0.00E+00	4384	0.10365	0.00088	4.10182	0.11672	0.287025	0.007799	0.955	-4.3	-1			1690	15	1655	23	1627	39
MA2-2-4-80	140	2.1	0.00E+00	415	0.05101	0.00112	0.10462	0.00366	0.014875	0.000404	0.777	-61	-30.5			241	49	101	3	95	3
MA2-2-4-81	89	26.2	0.00E+00	68543	0.10697	0.00091	4.62506	0.13921	0.313574	0.009058	0.96	0.6	.			1748	15	1754	25	1758	44
MA2-2-4-82	439	89.8	0.00E+00	6433	0.11048	0.00091	3.4	0.0915	0.220183	0.005724	0.953	-32	-29.8			1807	15	1494	21	1283	30
MA2-2-4-83	209	53.6	0.00E+00	10292	0.11312	0.00094	4.31085	0.11953	0.276402	0.007311	0.954	-16.8	-14.2			1850	14	1695	23	1573	37
MA2-2-4-84	192	54.4	0.00E+00	8871	0.1034	0.00084	4.32339	0.12344	0.303255	0.008301	0.959	1.4	.			1686	15	1698	24	1707	41
MA2-2-4-85	33	19.1	0.00E+00	5213	0.24197	0.00358	20.13447	0.95117	0.603491	0.027073	0.95	-3.6	.			3133	23	3098	46	3044	109
MA2-2-4-086	242	51.8	8.10E-01	1898	0.09169	0.00071	2.90741	0.0795	0.229981	0.006033	0.959	-9.6	-6.4			1461	14	1384	21	1334	32
MA2-2-4-087	455	115.7	2.90E-01	5891	0.11089	0.00091	4.12514	0.11545	0.269808	0.007216	0.956	-17	-14.3			1814	14	1659	23	1540	37
MA2-2-4-088	15	2.2	0.00E+00	398	0.07293	0.002	1.64628	0.06833	0.163715	0.00511	0.752	-3.7	.			1012	52	988	26	977	28
MA2-2-4-089	74	23.5	0.00E+00	5956	0.12119	0.00109	5.66771	0.17349	0.339186	0.009925	0.956	-5.3	-2.2			1974	15	1926	26	1883	48
MA2-2-4-090	713	211.3	0.00E+00	26372	0.11151	0.00092	4.85158	0.14289	0.315552	0.00892	0.960	-3.5	-0.4			1824	14	1794	25	1768	44
MA2-2-4-091	147	45.5	0.00E+00	20868	0.11324	0.00096	5.14773	0.15193	0.329696	0.009321	0.958	-0.9	.			1852	15	1844	25	1837	45
MA2-2-4-092	472	132.5	9.00E-02	30538	0.11265	0.00095	4.65716	0.13637	0.299848	0.008405	0.957	-9.4	-6.4			1843	14	1760	24	1691	42
MA2-2-4-093	463	104	4.50E-02	24244	0.10872	0.0009	3.61242	0.0952	0.240978	0.006028	0.949	-24.1	-21.7			1778	15	1552	21	1392	31
MA2-2-4-094	559	7.1	1.30E+00	9751	0.03787	0.00041	0.07242	0.00177	0.013868	0.000304	0.897	-78.5	-76.5			-417	33	71	2	89	2
MA2-2-4-095	422	118.2	0.00E+00	25686	0.1055	0.00086	4.34976	0.12265	0.299029	0.008076	0.958	-2.4	.			1723	14	1703	23	1686	40
MA2-2-4-096	420	47.7	9.00E-01	2282	0.10827	0.00097	1.815	0.0433	0.121578	0.002689	0.927	-61.5	-60.2			1771	16	1051	16	740	15
MA2-2-4-097	373	112.1	9.90E-01	1808	0.11862	0.00122	5.16269	0.16148	0.315662	0.009326	0.945	-9.9	-6.4			1936	17	1846	27	1769	46
MA2-2-4-098	470	63.2	9.60E-01	1981	0.11103	0.00091	2.22228	0.07551	0.145166	0.004787	0.97	-55.4	-54			1816	14	1188	24	874	27
MA2-2-4-100	401	68.6	2.30E-01	9238	0.1033	0.00087	2.64808	0.06985	0.185925	0.00465	0.948	-37.7	-35.6			1684	15	1314	19	1099	25

Table 29: Raw data of concordant and disconcordant U-Pb analysis of all samples.

	ppm				Ratios								Discordance			Ages					
Name	U	^{206}Pb		$^{206}Pb_c$(%)	206/204	$^{207}Pb/^{206}Pb^*$	1SE	$^{207}Pb/^{235}U^*$	1SE	$^{206}Pb/^{238}U^*$	1SE	Rho	Central (%)	Minimum rim (%)		207/206	1σ	207/235	1σ	206/238	1σ
MA2-2-8-001	133	35		3.70E-01	4565	0.10394	0.00092	4.09355	0.16667	0.28563	0.011351	0.976	-5.1	-1.7		1696	16	1653	33	1620	57
MA2-2-8-002	122	22.1		1.60E+00	2053	0.09457	0.00232	2.58136	0.1126	0.197966	0.007141	0.827	-25.5	-18		1520	46	1295	32	1164	38
MA2-2-8-003	527	137.9		1.20E-01	18647	0.10622	0.00102	4.19131	0.1739	0.28618	0.011551	0.973	-7.4	-3.8		1736	17	1672	34	1622	58
MA2-2-8-004	493	131.3		2.00E-02	46357	0.10686	0.00116	4.13364	0.14215	0.280542	0.009156	0.949	-9.9	-5.9		1747	20	1661	28	1594	46
MA2-2-8-005	132	29.3		8.40E-02	13371	0.09738	0.00095	3.15391	0.10106	0.234889	0.007168	0.952	-15.1	-11.5		1575	18	1446	25	1360	37
MA2-2-8-006	275	74.9		9.20E-02	33677	0.10712	0.00098	4.41361	0.18319	0.298835	0.012099	0.975	-4.2	-0.8		1751	16	1715	34	1686	60
MA2-2-8-007	112	7		0.00E+00	2844	0.05641	0.00051	0.54717	0.01752	0.070349	0.002161	0.959	-6.7	.		469	20	443	11	438	13
MA2-2-8-008	257	25.5		2.70E-01	6787	0.0799	0.00071	1.24874	0.04745	0.11335	0.004187	0.972	-44.3	-41.7		1195	17	823	21	692	24
MA2-2-8-009	326	33.8		3.10E-01	6896	0.08602	0.00369	1.5	0.12486	0.126206	0.00903	0.858	-45.3	-33.9		1339	82	929	51	766	52
MA2-2-8-010	627	43.5		4.40E-01	3059	0.06924	0.0014	0.76604	0.03077	0.080242	0.002787	0.865	-46.8	-39.9		906	41	577	18	498	17
MA2-2-8-011	328	22.2		7.60E-02	9749	0.05634	0.00046	0.59327	0.01918	0.076373	0.00239	0.968	1.9	.		466	17	473	12	474	14
MA2-2-8-012	688	38.8		1.10E-01	25700	0.05658	0.00094	0.51304	0.01248	0.065764	0.001173	0.733	-14	.		475	36	420	8	411	7
MA2-2-8-015	150	37.9		7.90E-02	19204	0.11105	0.00233	4.4543	0.13353	0.290923	0.006239	0.715	-10.6	-4.7		1817	37	1723	25	1646	31
MA2-2-8-016	240	50.5		1.10E-01	9561	0.09504	0.00185	3.20534	0.09219	0.244604	0.005183	0.737	-8.6	-2.1		1529	35	1458	22	1411	27
MA2-2-8-017	260	59.8		0.00E+00	10792	0.10844	0.00134	4.34948	0.08699	0.29089	0.004577	0.787	-8.1	-4.2		1773	21	1703	17	1646	23
MA2-2-8-018	316	71.8		0.00E+00	10848	0.10884	0.00135	4.32439	0.08492	0.288169	0.004396	0.777	-9.4	-5.6		1780	22	1698	16	1632	22
MA2-2-8-019	816	35.3		2.10E-01	18492	0.05518	0.00054	0.4	0.00817	0.055763	0.000922	0.859	-17.1	-6.6		420	21	359	6	350	6
MA2-2-8-020	524	127.3		1.80E-01	9879	0.17622	0.0032	7.81881	0.30245	0.321805	0.010988	0.883	-35.8	-32.2		2618	29	2210	35	1799	54
MA2-2-8-021	194	47.1		0.00E+00	15429	0.10808	0.00135	4.56718	0.09603	0.306491	0.00518	0.804	-2.8	.		1767	22	1743	18	1723	26
MA2-2-8-022	297	68.7		0.00E+00	19937	0.10758	0.00131	4.35706	0.08726	0.293749	0.004668	0.793	-6.4	-2.4		1759	21	1704	17	1660	23
MA2-2-8-023	357	79.4		0.00E+00	10309	0.10326	0.00175	4.01594	0.09687	0.282059	0.004845	0.712	-5.5	-0.2		1684	32	1637	20	1602	24
MA2-2-8-024	234	52		0.00E+00	6839	0.10023	0.00118	3.88565	0.07686	0.281177	0.004473	0.804	-2.1	.		1628	22	1611	16	1597	23
MA2-2-8-025	626	92.2		7.90E-02	26901	0.10102	0.0012	2.60108	0.04856	0.186734	0.002686	0.771	-35.7	-32.9		1643	21	1301	14	1104	15
MA2-2-8-026	229	42.8		2.80E-01	8092	0.1015	0.00126	3.33564	0.06504	0.238347	0.003588	0.772	-18.4	-14.8		1652	21	1489	15	1378	19
MA2-2-8-028	130	30.4		0.00E+00	8488	0.10726	0.00136	4.3826	0.09115	0.296331	0.004883	0.792	-5.2	-1		1753	23	1709	17	1673	24
MA2-2-8-029	985	221.1		0.00E+00	75834	0.09881	0.0012	3.8578	0.08356	0.283153	0.005082	0.829	0.4	.		1602	22	1605	17	1607	26
MA2-2-8-027	38	2.1		0.00E+00	915	0.061	0.00097	0.5992	0.01345	0.071238	0.001128	0.705	-31.7	-22.6		639	33	477	9	444	7
MA2-2-8-030	347	65.5		0.00E+00	9496	0.09752	0.00115	3.15003	0.06308	0.234264	0.003795	0.809	-15.5	-11.7		1577	22	1445	15	1357	20
MA2-2-8-031	107	26.2		0.00E+00	8734	0.10792	0.00133	4.48865	0.09785	0.301656	0.005417	0.824	-4.2	.		1765	22	1729	18	1700	27
MA2-2-8-032	204	45.3		0.00E+00	19075	0.09864	0.00118	3.73955	0.08065	0.274965	0.004929	0.831	-2.3	.		1599	22	1580	17	1566	25
MA2-2-8-033	216	50.2		0.00E+00	12234	0.10612	0.0013	4.20535	0.09105	0.28741	0.005136	0.825	-6.9	-2.7		1734	22	1675	18	1629	26
MA2-2-8-034	423	96.7		7.20E-01	2138	0.10221	0.00122	3.59722	0.0717	0.255245	0.004074	0.801	-13.4	-9.6		1665	22	1549	16	1465	21
MA2-2-8-035	231	36.2		4.70E-01	3347	0.09607	0.00119	2.6584	0.06497	0.200694	0.00423	0.862	-26.1	-22.4		1549	23	1317	18	1179	23
MA2-2-8-036	1160	236.1		7.70E-02	28271	0.10602	0.00129	3.75602	0.08681	0.256942	0.005045	0.85	-16.6	-12.8		1732	22	1583	19	1474	26
MA2-2-8-037	525	70		0.00E+00	55146	0.07819	0.00084	1.82119	0.03485	0.168939	0.002677	0.828	-13.6	-9.1		1152	20	1053	13	1006	15
MA2-2-8-038	1064	48.3		3.30E-01	7095	0.05555	0.00066	0.44072	0.01031	0.057544	0.001161	0.862	-17.4	-5		434	25	371	7	361	7
MA2-2-8-039	396	48.7		0.00E+00	18526	0.07037	0.00077	1.53634	0.02843	0.158338	0.002367	0.808	1	.		939	21	945	11	948	13
MA2-2-8-040	700	144.5		0.00E+00	48490	0.10562	0.00133	3.82124	0.0796	0.262402	0.004348	0.795	-14.5	-10.6		1725	23	1597	17	1502	22
MA2-2-8-041	112	16.1		0.00E+00	4567	0.07644	0.00088	1.94185	0.03752	0.184253	0.002862	0.804	-1.6	.		1107	22	1096	13	1090	16
MA2-2-8-042	462	94.3		0.00E+00	9776	0.10566	0.00134	3.78619	0.07894	0.259885	0.004299	0.793	-15.3	-11.5		1726	22	1590	17	1489	22
MA2-2-8-043	93	18.4		1.40E+00	1636	0.09697	0.00162	3.31806	0.08295	0.248158	0.00461	0.743	-9.8	-4.4		1567	30	1485	20	1429	24
MA2-2-8-044	555	135		0.00E+00	10249	0.11218	0.00146	4.74713	0.1036	0.30691	0.005373	0.802	-6.8	-2.6		1835	23	1776	18	1725	27
MA2-2-8-045	119	26.2		0.00E+00	7515	0.10622	0.00136	4.08358	0.0862	0.278813	0.004684	0.796	-9.8	-5.7		1736	22	1651	17	1585	24
MA2-2-8-046	192	38.5		3.10E-01	5927	0.10434	0.00133	3.66503	0.08555	0.254753	0.004981	0.838	-15.7	-11.7		1703	22	1564	19	1463	26
MA2-2-8-049	336	52.8		1.80E-01	25348	0.10085	0.00132	2.85131	0.0807	0.205059	0.005148	0.887	-29.2	-25.5		1640	23	1369	21	1202	28
MA2-2-8-050	383	76.7		0.00E+00	25760	0.09109	0.00105	3.18327	0.06733	0.253446	0.004504	0.840	0.6	.		1449	21	1453	16	1456	23
MA2-2-8-051	265	63.1		0.00E+00	23305	0.10708	0.00132	4.41844	0.09326	0.29926	0.005128	0.812	-4.1	.		1750	22	1716	17	1688	25
MA2-2-8-052	106	25.4		0.00E+00	7150	0.10782	0.00134	4.46571	0.0962	0.300392	0.005281	0.816	-4.5	-0.2		1763	22	1725	18	1693	26
MA2-2-8-053	489	62		2.60E-01	5966	0.09646	0.00114	2.13905	0.0406	0.160828	0.002387	0.782	-41.1	-38.5		1557	22	1162	13	961	13
MA2-2-8-054	150	29.4		1.80E-01	19820	0.10325	0.00129	3.48174	0.08245	0.244566	0.00492	0.849	-18	-14.1		1683	23	1523	19	1410	25
MA2-2-8-055	255	58		0.00E+00	12254	0.10994	0.00141	4.25846	0.09775	0.280933	0.005353	0.830	-12.7	-8.7		1798	22	1685	19	1596	27
MA2-2-8-056	320	61.2		1.80E-01	12798	0.10057	0.00216	3.07947	0.0944	0.22208	0.00485	0.712	-23.1	-17.4		1635	39	1428	23	1293	26
MA2-2-8-057	556	144		9.00E-02	37115	0.10713	0.00264	4.1875	0.21059	0.283502	0.012431	0.872	-9.2	-0.5		1751	42	1672	41	1609	62
MA2-2-8-058	251	14		0.00E+00	5048	0.05621	0.00116	0.5191	0.01391	0.066977	0.001148	0.640	-9.6	.		461	45	425	9	418	7
MA2-2-8-059	248	67.2		0.00E+00	20123	0.10956	0.00245	4.73871	0.15236	0.313694	0.007252	0.719	-2.1	.		1792	38	1774	27	1759	36
MA2-2-8-060	215	57.9		0.00E+00	21869	0.10991	0.00247	4.72026	0.15174	0.311474	0.007163	0.715	-3.2	.		1798	41	1771	27	1748	35

Table 30: Raw data of concordant and disconcordant U-Pb analysis of all samples.

MA2-2-8-061	104	26.4	0.00E+00	17464	0.11088	0.00284	4.52216	0.16157	0.295804	0.007368	0.697	-9	-1.7			1814	45	1735	30	1670	37
MA2-2-8-062	687	184.8	9.60E-02	32794	0.11029	0.0028	4.38239	0.24734	0.288185	0.014533	0.894	-10.8	-2			1804	45	1709	47	1632	73
MA2-2-8-063	578	121.8	1.00E-01	15385	0.1061	0.00235	3.58419	0.11092	0.245012	0.005307	0.700	-20.6	-14.9			1733	39	1546	25	1413	27
MA2-2-8-064	1356	14.8	2.10E+00	754	0.05715	0.00105	0.10102	0.00331	0.01282	0.000347	0.827	-84	-80.6			497	40	98	3	82	2
MA2-2-8-065	187	45.3	0.00E+00	14400	0.10128	0.0022	3.94165	0.12253	0.282272	0.00629	0.717	-3.1				1648	40	1622	25	1603	32
MA2-2-8-066	70	18	8.20E-01	2415	0.1082	0.00277	4.45604	0.16006	0.298678	0.007534	0.702	-5.4				1769	46	1723	30	1685	37
MA2-2-8-067	54	14.2	0.00E+00	3939	0.11225	0.00293	4.757	0.17313	0.307363	0.007785	0.696	-6.7				1836	48	1777	31	1728	38
MA2-2-8-068	646	135.9	6.50E-02	30120	0.10518	0.00233	3.56792	0.10964	0.246037	0.005247	0.694	-19.4	-13.6			1717	38	1542	24	1418	27
MA2-2-8-069	95	25.2	0.00E+00	21794	0.11117	0.00254	4.71519	0.15175	0.307611	0.006976	0.705	-5.6				1819	41	1770	27	1729	34
MA2-2-8-070	207	32.4	1.30E-01	13965	0.0782	0.00177	2.00552	0.06005	0.186001	0.003642	0.654	-4.9				1152	43	1117	20	1100	20
MA2-2-8-071	273	17.1	0.00E+00	14350	0.05822	0.00122	0.6068	0.01651	0.07559	0.001311	0.637	-13.2				538	44	482	10	470	8
MA2-2-8-072	137	36	2.40E-01	11168	0.10737	0.00238	4.23967	0.1566	0.286393	0.008465	0.800	-8.5	-1.2			1755	39	1682	30	1623	42
MA2-2-8-073	536	96.2	9.70E-02	28497	0.10665	0.0024	3.05901	0.09747	0.208036	0.004688	0.707	-33	-28.1			1743	40	1422	24	1218	25
MA2-2-8-074	285	16.7	0.00E+00	19515	0.05667	0.00119	0.54962	0.01558	0.070335	0.001344	0.674	-8.8				479	46	445	10	438	8
MA2-2-8-075	138	35.7	3.20E-01	8689	0.10595	0.00234	4.13578	0.14544	0.283114	0.007744	0.778	-8.1	-0.9			1731	40	1661	29	1607	39
MA2-2-8-076	213	17.1	5.30E-01	4306	0.0734	0.00166	0.9909	0.03134	0.097908	0.002167	0.7	-43.2	-36.5			1025	44	699	16	602	13
MA2-2-8-077	60	26.8	2.80E-01	7383	0.19766	0.00671	13.76023	0.62999	0.504911	0.015519	0.671	-7.5	-0.1			2807	53	2733	43	2635	66
MA2-2-8-078	75	19.4	3.60E-01	5244	0.10817	0.00249	4.44473	0.14298	0.298002	0.006707	0.7	-5.6				1769	40	1721	27	1681	33
MA2-2-8-079	150	38.6	2.60E-01	5821	0.10729	0.00244	4.32239	0.14438	0.2922	0.007149	0.732	-6.5				1754	40	1698	28	1653	36
MA2-2-8-080	630	27.2	3.50E-01	5489	0.05608	0.00103	0.40031	0.01078	0.05177	0.00102	0.731	-29.3	-12.7			456	40	342	8	325	6
MA2-2-8-081	312	58.2	2.50E-01	7165	0.10429	0.00238	3.16121	0.09645	0.21984	0.004462	0.665	-27.2	-22			1702	41	1448	24	1281	24
MA2-2-8-082	742	202.7	0.00E+00	41688	0.11475	0.00275	5.01282	0.16426	0.316827	0.007076	0.682	-6.2				1876	40	1821	28	1774	35
MA2-2-8-083	185	48.3	0.00E+00	19978	0.11198	0.00265	4.70277	0.15472	0.304584	0.00697	0.696	-7.3	-0.5			1832	41	1768	28	1714	34
MA2-2-8-084	140	37.5	0.00E+00	6319	0.11179	0.00265	4.81671	0.15868	0.312489	0.007158	0.695	-4.7				1829	44	1788	28	1753	35
MA2-2-8-085	259	15.2	0.00E+00	3720	0.05641	0.00109	0.54463	0.0156	0.070026	0.001486	0.741	-7.1				468	40	441	10	436	9
MA2-2-8-086	24	6.5	7.50E+00	251	0.10216	0.00682	4.09168	0.29723	0.290488	0.008325	0.395	-1.3				1664	119	1653	59	1644	42
MA2-2-8-087	191	49.8	8.10E-02	21075	0.11046	0.00261	4.52572	0.1602	0.297165	0.007832	0.745	-8.1	-1			1807	42	1736	29	1677	39
MA2-2-8-088	285	51	1.40E+01	119	0.10108	0.00538	2.53002	0.15554	0.181531	0.005581	0.5	-37.5	-26			1644	93	1281	45	1075	30
MA2-2-8-089	194	52.4	0.00E+00	29223	0.11106	0.00264	4.81069	0.1612	0.314148	0.007429	0.706	-3.5				1817	42	1787	28	1761	36
MA2-2-8-090	40	8.9	1.10E+00	2637	0.10009	0.00255	3.3685	0.1686	0.244087	0.010513	0.861	-14.9	-6.1			1626	46	1497	39	1408	54
MA2-2-8-091	328	58.9	1.70E-01	11846	0.1059	0.00246	3.08083	0.09778	0.21099	0.004553	0.68	-31.5	-26.4			1730	41	1428	24	1234	24
MA2-2-8-093	214	57.6	1.60E-01	14744	0.1085	0.00292	4.3321	0.2598	0.289581	0.015526	0.894	-8.6				1774	47	1699	49	1639	78
MA2-2-8-094	89	5.3	0.00E+00	10156	0.05844	0.00118	0.57669	0.0159	0.071564	0.001348	0.683	-19.1	-2.1			546	44	462	10	446	8
MA2-2-8-095	563	105.7	0.00E+00	35489	0.08635	0.00185	2.63776	0.07973	0.221538	0.004729	0.706	-4.6				1346	39	1311	22	1290	25
MA2-2-8-096	185	40.2	3.10E-01	5769	0.09787	0.00225	3.42161	0.10932	0.253561	0.005634	0.696	-9	-1.7			1584	39	1509	25	1457	29
MA2-2-8-097	116	29.1	7.00E-01	3152	0.10378	0.00281	3.83297	0.23203	0.267865	0.014508	0.895	-10.8	-1			1693	48	1600	49	1530	74
MA2-2-8-098	231	56.9	9.10E-02	21410	0.10809	0.00259	4.28203	0.1428	0.287317	0.006661	0.695	-8.9	-2			1767	43	1690	27	1628	33
MA2-2-8-099	318	42.2	3.50E-01	3514	0.07212	0.00145	1.50118	0.04621	0.150965	0.003517	0.757	-9				989	40	931	19	906	20
MA2-2-8-100	145	27.4	3.60E-01	5302	0.10366	0.00245	3.20189	0.10239	0.224013	0.004831	0.674	-25.3	-19.6			1691	42	1458	25	1303	25
MA2-2-8-101	739	138.2	9.20E-02	19844	0.09734	0.00224	2.95366	0.09456	0.220073	0.004909	0.697	-20.4	-14.1			1574	44	1396	24	1282	26
MA2-2-8-102	232	49.5	2.10E+00	2605	0.09202	0.00203	2.96361	0.10572	0.233573	0.00654	0.785	-8.7	-0.6			1468	41	1398	27	1353	34
MA2-2-8-103	389	104.1	0.00E+00	22501	0.10934	0.00266	4.71595	0.16181	0.312824	0.007571	0.705	-2.2				1788	44	1770	29	1755	37
MA2-2-8-104	180	44.8	3.30E-01	5564	0.10736	0.00259	4.28214	0.14686	0.289267	0.00704	0.71	-7.6	-0.3			1755	42	1690	28	1638	35
MA2-2-8-105	203	52.9	0.00E+00	9330	0.10797	0.00257	4.23786	0.17109	0.284663	0.009277	0.807	-9.6	-1.9			1765	42	1681	33	1615	47
MA2-2-8-106	329	61.4	9.80E+00	176	0.06516	0.00237	1.79489	0.08316	0.199788	0.005747	0.621	55.4	31.8			779	72	1044	30	1174	31
MA2-2-8-107	142	35.3	0.00E+00	58750	0.10908	0.00313	4.45921	0.1771	0.296499	0.008151	0.692	-7				1784	51	1723	33	1674	41
MA2-2-8-108	282	17.3	0.00E+00	5040	0.05602	0.00111	0.57043	0.01595	0.073858	0.001451	0.703	1.5				453	44	458	10	459	9
MA2-2-8-109	220	54.6	0.00E+00	14570	0.10842	0.00265	4.33887	0.14634	0.290242	0.006733	0.688	-8.3	-1.3			1773	45	1701	28	1643	34
MA2-2-8-110	376	49.6	1.80E-01	14338	0.07497	0.00189	1.66209	0.05411	0.160802	0.003319	0.634	-10.7				1068	49	994	21	961	18
MA2-2-8-111	191	11.6	0.00E+00	1860	0.0567	0.00133	0.55722	0.02229	0.071277	0.002311	0.811	-7.8				480	49	450	15	444	14
MA2-2-8-112	192	48	3.30E-01	6196	0.10496	0.0025	4.00688	0.15165	0.276881	0.008152	0.778	-9.1	-1.4			1714	43	1636	31	1576	41
MA2-2-8-113	36	8.8	6.00E-01	4371	0.10453	0.00256	4.09722	0.14031	0.284282	0.006793	0.698	-6.2				1706	43	1654	28	1613	34
MA2-2-8-114	108	26.1	8.70E-01	1942	0.10578	0.00261	4.08562	0.14185	0.280119	0.006845	0.704	-8.9	-1.5			1728	43	1651	28	1592	34
MA2-2-8-115	286	72.1	0.00E+00	36932	0.10909	0.00318	4.50082	0.19436	0.299229	0.009544	0.739	-6.2				1784	54	1731	36	1687	47

Table 31: Raw data of concordant and disconcordant U-Pb analysis of all samples.

	ppm			Ratios								Discordance		Ages					
Name	U	^{206}Pb	$^{206}Pb_c$(%)	206/204	$^{207}Pb/^{206}Pb^*$	1SE	$^{207}Pb/^{235}U^*$	1SE	$^{206}Pb/^{238}U^*$	1SE	Rho	Central (%)	Minimum rim (%)	207/206	1σ	207/235	1σ	206/238	1σ
MA2-2-16-001	175	21.1	0.00E+00	499	0.09689	0.00082	1.76764	0.04465	0.132316	0.00315	0.942	-51.8	-50.1	1565	15	1034	16	801	18
MA2-2-16-002	133	19.2	0.00E+00	3122	0.07236	0.00056	1.5695	0.03829	0.157309	0.003637	0.948	-5.9	-1.4	996	15	958	15	942	20
MA2-2-16-003	337	83.5	3.70E-01	4022	0.10578	0.00095	3.79868	0.10871	0.260451	0.007078	0.950	-15.3	-12.2	1728	16	1592	23	1492	36
MA2-2-16-004	265	64.8	0.00E+00	12855	0.10032	0.00082	3.61909	0.09827	0.261646	0.006776	0.954	-9.1	-6	1630	14	1554	22	1498	35
MA2-2-16-005	341	89.4	0.00E+00	14088	0.10087	0.00082	3.90479	0.11011	0.280763	0.007581	0.957	-3.1		1640	15	1615	23	1595	38
MA2-2-16-006	96	97.1	5.40E+01	18	0.47487	0.01469	35.65153	2.7587	0.544501	0.038619	0.917	-40	-35.3	4165	45	3657	76	2802	161
MA2-2-16-007	159	10.2	0.00E+00	1824	0.05652	0.00055	0.53612	0.01265	0.068791	0.001476	0.910	-9.6		473	20	436	8	429	9
MA2-2-16-008	105	6.8	0.00E+00	960	0.05684	0.00051	0.55333	0.0131	0.070605	0.001549	0.927	-9.7	-0.6	485	20	447	9	440	9
MA2-2-16-009	70	17.4	0.00E+00	2207	0.1001	0.00089	3.71596	0.11082	0.269225	0.007664	0.955	-6.2	-2.7	1626	16	1575	24	1537	39
MA2-2-16-010	201	48.4	0.00E+00	9702	0.09868	0.00082	3.50208	0.10127	0.257402	0.007127	0.958	-8.6	-5.4	1599	15	1528	23	1477	37
MA2-2-16-011	53	11.3	1.80E+00	1141	0.08158	0.00069	2.56068	0.07574	0.227653	0.006456	0.959	7.8	0.6	1235	15	1289	22	1322	34
MA2-2-16-012	199	12.9	0.00E+00	1361	0.05598	0.00046	0.5465	0.0128	0.070807	0.001554	0.937	-2.4		451	17	443	8	441	9
MA2-2-16-013	456	44.1	3.40E-01	5855	0.08955	0.00075	1.30391	0.03379	0.1056	0.002588	0.946	-57	-55.3	1416	16	847	15	647	15
MA2-2-16-014	43	2.7	0.00E+00	521	0.05851	0.00078	0.55864	0.01553	0.069245	0.001688	0.876	-22.1	-11.6	549	29	451	10	432	10
MA2-2-16-015	95	27.1	0.00E+00	4784	0.10757	0.00093	4.51156	0.1316	0.304172	0.00847	0.955	-3		1759	15	1733	24	1712	42
MA2-2-16-016	66	17.3	0.00E+00	5560	0.10047	0.00088	3.89605	0.11438	0.281234	0.007881	0.955	-2.4		1633	16	1613	24	1598	40
MA2-2-16-017	385	100.7	8.20E-02	25817	0.10424	0.00097	3.91059	0.12157	0.272083	0.008071	0.954	-9.9	-6.5	1701	16	1616	25	1551	41
MA2-2-16-018	781	43.7	0.00E+00	4184	0.05698	0.00047	0.48726	0.01175	0.062021	0.001404	0.939	-21.6	-14.2	491	18	403	8	388	9
MA2-2-16-019	127	25.5	0.00E+00	4315	0.09665	0.00085	2.89767	0.07975	0.217434	0.005672	0.948	-20.6	-17.6	1561	16	1381	21	1268	30
MA2-2-16-020	45	5.2	4.10E+00	709	0.06227	0.00333	1.05621	0.06533	0.123012	0.003829	0.503	10		684	110	732	32	748	22
MA2-2-16-21	184	40.7	5.50E-01	6016	0.09505	0.00075	3.10721	0.09291	0.237085	0.006841	0.965	-11.4	-8.4	1529	14	1434	23	1372	36
MA2-2-16-22	74	19.3	0.00E+00	4323	0.10111	0.00091	3.89693	0.11387	0.279538	0.00777	0.951	-3.8	-0.2	1645	16	1613	24	1589	39
MA2-2-16-23	601	33.2	1.90E+00	844	0.06442	0.00444	0.53999	0.03998	0.060792	0.001649	0.366	-51.1	-0.4	756	139	438	26	380	10
MA2-2-16-24	131	28.2	6.80E-01	3965	0.09349	0.0008	2.97455	0.08041	0.230761	0.005914	0.948	-11.8	-8.4	1498	16	1401	21	1338	31
MA2-2-16-25	228	27.1	4.60E-01	4067	0.09667	0.00083	1.70902	0.04752	0.128224	0.003392	0.951	-53.2	-51.5	1561	15	1012	18	778	19
MA2-2-16-26	513	150.2	0.00E+00	37078	0.11215	0.001	4.85995	0.14571	0.314299	0.008993	0.954	-4.5	-1.2	1834	16	1795	25	1762	44
MA2-2-16-27	230	12.1	0.00E+00	938	0.06516	0.00106	0.52075	0.01427	0.057965	0.001277	0.804	-54.9	-49.8	779	32	426	10	363	8
MA2-2-16-28	448	112.9	0.00E+00	15405	0.10044	0.00086	3.74638	0.11036	0.270534	0.007624	0.957	-6.1	-2.7	1632	16	1581	24	1544	39
MA2-2-16-29	132	34.8	0.00E+00	7638	0.1046	0.00094	4.10121	0.11965	0.284374	0.007894	0.951	-6.2	-2.8	1707	16	1655	24	1613	40
MA2-2-16-30	334	19.1	0.00E+00	2170	0.05508	0.00048	0.45876	0.01257	0.060407	0.00157	0.948	-9.3		415	19	383	9	378	10
MA2-2-16-31	205	46.4	3.00E-01	6504	0.10325	0.00091	3.4689	0.10141	0.243667	0.006791	0.953	-18.3	-15.4	1683	16	1520	23	1406	35
MA2-2-16-32	70	12.2	0.00E+00	3826	0.08009	0.00076	2.04077	0.05719	0.184806	0.004873	0.941	-9.6	-5.1	1199	18	1129	19	1093	27
MA2-2-16-33	144	37.6	0.00E+00	7637	0.10088	0.0009	3.87794	0.11382	0.278802	0.007794	0.952	-3.8	-0.2	1640	16	1609	24	1585	39
MA2-2-16-34	401	26.5	0.00E+00	6797	0.05624	0.00045	0.55992	0.01337	0.072205	0.001624	0.942	-2.8		462	17	451	9	449	10
MA2-2-16-35	538	39.5	0.00E+00	10116	0.05692	0.00045	0.62955	0.01521	0.080214	0.001829	0.944	1.9		489	17	496	9	497	11
MA2-2-16-36	910	252.8	0.00E+00	189508	0.10876	0.00098	4.45792	0.13456	0.297267	0.008562	0.954	-6.5	-3.1	1779	16	1723	25	1678	43
MA2-2-16-37	148	25.7	0.00E+00	11391	0.07824	0.00065	2.03402	0.05463	0.188552	0.004819	0.951	-3.7		1153	15	1127	18	1114	26
MA2-2-16-38	318	44.2	3.40E-02	55611	0.09467	0.00083	1.96333	0.05287	0.150417	0.003828	0.945	-43.5	-41.3	1521	16	1103	18	903	21
MA2-2-16-39	127	27.6	3.00E+00	484	0.09722	0.00163	3.08843	0.10173	0.230387	0.006535	0.861	-16.5	-10.8	1572	30	1430	25	1337	34
MA2-2-16-40	36	5	0.00E+00	7551	0.07536	0.00083	1.58816	0.04795	0.152844	0.004295	0.931	-16	-10.8	1078	21	966	19	917	24
MA2-2-16-041	251	52.8	9.50E-02	16280	0.09668	0.00106	2.89519	0.04589	0.217197	0.002484	0.722	-20.7	-17.7	1561	20	1381	12	1267	13
MA2-2-16-042	143	38.9	0.00E+00	6965	0.10177	0.00105	3.89809	0.06166	0.277809	0.003337	0.759	-5.2	-1.8	1657	19	1613	13	1580	17
MA2-2-16-044	564	102.5	7.60E-02	18044	0.1015	0.00104	2.65177	0.04156	0.18949	0.00224	0.754	-35.1	-32.8	1652	18	1315	12	1119	12
MA2-2-16-045	428	69	7.50E-02	13720	0.09911	0.00108	2.33619	0.0594	0.170962	0.003926	0.903	-39.6	-36.9	1607	19	1223	18	1017	22
MA2-2-16-046	415	109.7	3.40E-01	5480	0.10737	0.00112	4.00441	0.06353	0.270502	0.003231	0.753	-13.6	-10.5	1755	19	1635	13	1543	16
MA2-2-16-047	109	15.4	1.40E-01	6761	0.09755	0.00109	2.00913	0.04259	0.149377	0.002695	0.851	-46.1	-43.7	1578	20	1119	14	897	15
MA2-2-16-048	388	65.4	1.70E-01	9250	0.10073	0.00095	2.47382	0.04059	0.17812	0.002387	0.817	-38.4	-36.2	1638	18	1264	12	1057	13
MA2-2-16-049	571	92.6	1.50E-01	16209	0.09791	0.001	2.2878	0.03406	0.169466	0.001842	0.73	-39.2	-37	1585	18	1209	11	1009	10
MA2-2-16-050	379	105	0.00E+00	13937	0.10787	0.00112	4.21636	0.07405	0.283498	0.004017	0.807	-9.9	-6.6	1764	19	1677	14	1609	20
MA2-2-16-051	344	86.1	0.00E+00	20268	0.10083	0.0011	3.59765	0.05666	0.258778	0.002934	0.72	-10.6	-7.4	1639	20	1549	13	1484	15
MA2-2-16-052	320	70.2	2.80E-02	20974	0.10467	0.0011	3.26778	0.05179	0.226425	0.002687	0.749	-25.4	-22.7	1709	19	1473	12	1316	14
MA2-2-16-053	25	6.7	0.00E+00	1133	0.10369	0.00135	3.87687	0.08577	0.271167	0.004857	0.81	-9.6	-5.3	1691	24	1609	18	1547	25
MA2-2-16-054	40	10.8	0.00E+00	3803	0.10226	0.00118	3.91332	0.07202	0.277546	0.003977	0.778	-5.9	-2	1666	20	1616	15	1579	20
MA2-2-16-055	26	4.7	0.00E+00	869	0.07864	0.00086	2.03764	0.04657	0.187914	0.00377	0.878	-5		1163	21	1128	16	1110	20

Table 32: Raw data of concordant and disconcordant U-Pb analysis of all samples.

MA2-2-16-056	132	31.7	1.30E-01	13068	0.10092	0.00113	3.44313	0.05487	0.247436	0.0028	0.71	-14.7	-11.5			1641	20	1514	13	1425	14
MA2-2-16-057	105	19.5	3.60E-01	4314	0.09755	0.00122	2.66649	0.06697	0.198258	0.004318	0.867	-28.5	-24.9			1578	23	1319	19	1166	23
MA2-2-16-058	642	41.3	1.30E-01	8091	0.05638	0.0005	0.52675	0.00781	0.067764	0.000803	0.799	-9.9	-0.9			467	19	430	5	423	5
MA2-2-16-059	261	63.5	0.00E+00	7051	0.09389	0.001	3.24318	0.05642	0.250522	0.003447	0.791	-4.8	-0.9			1506	19	1468	14	1441	18
MA2-2-16-060	223	15	0.00E+00	2773	0.05688	0.00054	0.55843	0.00779	0.071204	0.000724	0.729	-9.3				487	20	451	5	443	4
MA2-2-16-061	40	4.4	0.00E+00	1849	0.08713	0.00111	1.41753	0.03187	0.117997	0.002185	0.823	-49.9	-47.1			1363	24	896	13	719	13
MA2-2-16-062	216	33.9	0.00E+00	10672	0.07452	0.00074	1.68421	0.02802	0.163908	0.00219	0.803	-7.9	-3.2			1056	19	1003	11	978	12
MA2-2-16-063	559	121.2	1.30E-01	21055	0.10104	0.00112	3.11674	0.0579	0.223728	0.003336	0.802	-22.9	-19.8			1643	20	1437	14	1302	18
MA2-2-16-064	1227	173.2	0.00E+00	40092	0.07119	0.00063	1.45899	0.02436	0.148637	0.002102	0.847	-7.7	-3.1			963	17	914	10	893	12
MA2-2-16-065	57	14.6	0.00E+00	2845	0.10367	0.0011	3.7625	0.07077	0.263226	0.004083	0.825	-12.2	-8.8			1691	19	1585	15	1506	21
MA2-2-16-066	422	69.9	2.10E-01	8004	0.10169	0.00119	2.49607	0.05449	0.178032	0.003286	0.845	-39.2	-36.5			1655	21	1271	16	1056	18
MA2-2-16-067	230	53.5	2.30E-01	8051	0.10432	0.00121	3.47055	0.06685	0.241274	0.003717	0.8	-20.2	-16.9			1702	21	1521	15	1393	19
MA2-2-16-068	356	107.6	0.00E+00	24038	0.1107	0.00128	4.7147	0.08222	0.30889	0.004027	0.748	-4.8	-1.2			1811	20	1770	15	1735	20
MA2-2-16-069	58	16	0.00E+00	2615	0.10301	0.0011	4.02822	0.07673	0.283611	0.00447	0.827	-4.7	-0.9			1679	20	1640	15	1610	22
MA2-2-16-070	49	3.2	0.00E+00	1083	0.06218	0.00141	0.59786	0.01629	0.069729	0.001047	0.551	-37.4	-24.8			680	49	476	10	435	6
MA2-2-16-071	487	31.5	0.00E+00	8042	0.05665	0.00055	0.53358	0.00821	0.068307	0.000816	0.777	-11.3	-1.9			478	21	434	5	426	5
MA2-2-16-072	86	19	3.20E-01	5210	0.09894	0.00115	3.13275	0.0602	0.229634	0.003518	0.797	-18.7	-15.2			1604	21	1441	15	1333	18
MA2-2-16-073	149	8.9	0.00E+00	2292	0.0561	0.00061	0.48974	0.00917	0.063311	0.000962	0.811	-13.7	-2.6			456	23	405	6	396	6
MA2-2-16-074	328	75.4	3.50E-01	5166	0.10782	0.00125	3.51405	0.06219	0.236376	0.003161	0.756	-24.8	-21.9			1763	20	1530	14	1368	16
MA2-2-16-075	153	34.8	0.00E+00	7068	0.09304	0.00103	3.02962	0.05011	0.236169	0.002904	0.743	-9.1	-5.4			1489	20	1415	13	1367	15
MA2-2-16-076	83	14	0.00E+00	977	0.0779	0.00084	1.92335	0.04923	0.179059	0.004161	0.908	-7.8	-2.6			1144	21	1089	17	1062	23
MA2-2-16-077	338	64.4	3.80E-01	5787	0.10042	0.00104	2.74081	0.04343	0.197952	0.002373	0.756	-31.3	-28.8			1632	18	1340	12	1164	13
MA2-2-16-078	198	39.9	4.90E-02	18854	0.10781	0.00116	3.14852	0.0608	0.211804	0.003401	0.832	-32.7	-30			1763	18	1445	15	1238	18
MA2-2-16-079	230	60.5	0.00E+00	11712	0.10255	0.00106	3.8326	0.07534	0.271066	0.004526	0.849	-8.4	-4.7			1671	18	1600	16	1546	23
MA2-2-16-080	122	34.2	0.00E+00	6185	0.11002	0.00136	4.3449	0.07884	0.286431	0.003796	0.73	-11.1	-7.5			1800	22	1702	15	1624	19
MA2-2-16-081	101	18.8	0.00E+00	6421	0.08051	0.0008	2.17195	0.03978	0.195647	0.003017	0.842	-5.2	-0.7			1210	18	1172	13	1152	16
MA2-2-16-082	86	5.8	0.00E+00	1265	0.05943	0.00084	0.59585	0.01122	0.072717	0.000912	0.666	-23.2	-13.4			583	30	475	7	453	5
MA2-2-16-083	93	24.8	0.00E+00	4302	0.10103	0.00116	3.82967	0.06846	0.274927	0.003756	0.764	-5.3	-1.4			1643	21	1599	14	1566	19
MA2-2-16-084	114	25.8	0.00E+00	4802	0.11088	0.00123	3.60763	0.06221	0.235977	0.003106	0.763	-27.4	-24.7			1814	19	1551	14	1366	16
MA2-2-16-085	65	18.7	0.00E+00	5428	0.10973	0.00124	4.50641	0.0854	0.297843	0.004541	0.804	-7.2	-3.6			1795	20	1732	16	1681	23
MA2-2-16-086	89	5.8	0.00E+00	823	0.05663	0.00059	0.54698	0.00852	0.070047	0.000807	0.74	-8.9				477	23	443	6	436	5
MA2-2-16-087	172	24.8	1.40E+00	1735	0.07394	0.00224	1.53279	0.0504	0.150353	0.00193	0.39	-14.1				1040	59	944	20	903	11
MA2-2-16-088	785	213.3	0.00E+00	45479	0.10864	0.0013	4.18899	0.07879	0.279661	0.004056	0.771	-11.9	-8.3			1777	22	1672	15	1590	20
MA2-2-16-089	448	89.8	1.30E-01	20891	0.10278	0.0011	2.97071	0.05038	0.20962	0.002754	0.775	-29.4	-26.7			1675	19	1400	13	1227	15
MA2-2-16-090	543	37.7	0.00E+00	6578	0.05541	0.00052	0.56328	0.00863	0.073724	0.000892	0.79	7.2				429	20	454	6	459	5
MA2-2-16-091	190	57.4	0.00E+00	14004	0.1097	0.00119	4.69673	0.08648	0.310516	0.004615	0.807	-3.3				1794	19	1767	15	1743	23
MA2-2-16-092	94	21	6.80E-01	2004	0.0949	0.00092	3.06839	0.05402	0.234495	0.003442	0.834	-12.2	-8.8			1526	18	1425	13	1358	18
MA2-2-16-093	143	8.9	0.00E+00	694	0.07772	0.00345	0.70573	0.03431	0.065861	0.001308	0.408	-65.9	-57.3			1140	80	542	20	411	8
MA2-2-16-094	443	52.9	2.50E-01	10011	0.09248	0.00097	1.61326	0.02871	0.126514	0.001816	0.807	-50.9	-48.8			1477	20	975	11	768	10
MA2-2-16-095	177	45.7	0.00E+00	10947	0.10734	0.00116	3.96467	0.07159	0.26787	0.003874	0.801	-14.4	-11.1			1755	20	1627	15	1530	20
MA2-2-16-096	111	15.2	4.80E+00	359	0.08944	0.00416	1.70852	0.08358	0.138543	0.002102	0.31	-43.5	-31.9			1414	89	1012	31	836	12
MA2-2-16-097	83	22.2	0.00E+00	2700	0.10057	0.00118	3.86971	0.08804	0.279065	0.005437	0.856	-3.3				1635	21	1607	18	1587	27
MA2-2-16-098	148	26.7	5.30E-01	5086	0.09735	0.00104	2.54282	0.05035	0.189437	0.003162	0.843	-31.5	-28.6			1574	19	1284	14	1118	17
MA2-2-16-099	20	3.3	0.00E+00	625	0.0855	0.00164	2.02579	0.06196	0.171833	0.004099	0.78	-24.8	-18.7			1327	36	1124	21	1022	23
MA2-2-16-100	413	53.6	3.00E-01	4708	0.09051	0.00103	1.71441	0.02977	0.137372	0.0018	0.755	-45	-42.6			1436	21	1014	11	830	10
MA2-2-16-101	43	11.5	0.00E+00	2925	0.09829	0.00108	3.74391	0.07584	0.276267	0.004703	0.841	-1.4				1592	19	1581	16	1573	24
MA2-2-16-102	555	138.7	0.00E+00	12897	0.10466	0.00113	3.74953	0.07229	0.259826	0.00415	0.828	-14.4	-11			1708	19	1582	15	1489	21
MA2-2-16-103	282	18.1	0.00E+00	1543	0.05615	0.00056	0.53407	0.00934	0.068978	0.000992	0.822	-6.4				458	21	435	6	430	6
MA2-2-16-104	441	80.1	4.80E-02	13809	0.10136	0.00108	2.67628	0.0451	0.1915	0.002494	0.773	-34.3	-31.8			1649	19	1322	12	1129	13
MA2-2-16-105	24	11.9	0.00E+00	1582	0.21019	0.00358	14.21328	0.38465	0.490442	0.010312	0.777	-13.9	-10.1			2907	27	2764	26	2573	45
MA2-2-16-106	128	14.6	7.50E-01	1993	0.06704	0.00079	1.1266	0.02471	0.121885	0.002257	0.844	-12.3	-5.6			839	23	766	12	741	13
MA2-2-16-107	85	22.7	0.00E+00	5162	0.10036	0.0012	3.81998	0.07393	0.27607	0.004203	0.787	-4.1				1631	22	1597	16	1572	21
MA2-2-16-108	101	27	0.00E+00	3959	0.10181	0.00122	3.92791	0.07555	0.279823	0.004214	0.783	-4.6	-0.4			1657	22	1619	16	1590	21
MA2-2-16-109	573	40.4	1.20E+00	1814	0.07235	0.00098	0.73776	0.0145	0.073954	0.001051	0.723	-55.7	-52.6			996	27	561	8	460	6
MA2-2-16-110	169	7.5	0.00E+00	603	0.10809	0.00858	0.72062	0.05836	0.048353	0.000784	0.2	-84.7	-79.9			1767	148	551	34	304	5

Table 33: Raw data of concordant and disconcordant U-Pb analysis of all samples.

	ppm				Ratios							Discordance		Ages					
Name	U	^{206}Pb	$^{206}Pb_c$(%)	206/204	$^{207}Pb/^{206}Pb^*$	1SE	$^{207}Pb/^{235}U^*$	1SE	$^{206}Pb/^{238}U^*$	1SE	Rho	Central (%)	Minimum rim (%)	207/206	1σ	207/235	1σ	206/238	1σ
SK5-A-2-001	380	31.6	0.00E+00	4550	0.0554	0.00022	0.66571	0.01049	0.087156	0.00133	0.969	26.9	20.5	428	8	518	6	539	8
SK5-A-2-002	167	15.9	0.00E+00	4075	0.06082	0.00026	0.83079	0.00967	0.099066	0.00107	0.928	-4	-0.4	633	9	614	5	609	6
SK5-A-2-003	622	49.4	2.90E-01	7022	0.06936	0.00044	0.78931	0.01156	0.082539	0.001091	0.903	-45.5	-43.4	909	13	591	7	511	6
SK5-A-2-004	296	75.1	3.10E-02	33840	0.10762	0.00037	4.05281	0.09095	0.273126	0.006057	0.988	-13	-11.9	1759	6	1645	18	1557	31
SK5-A-2-005	652	114.9	0.00E+00	38119	0.07426	0.00024	1.84443	0.02614	0.18015	0.002485	0.973	2	.	1048	6	1061	9	1068	14
SK5-A-2-006	612	72.9	6.40E-01	2458	0.08542	0.00041	1.43674	0.02156	0.121984	0.001733	0.947	-46.5	-45.3	1325	9	904	9	742	10
SK5-A-2-007	308	20.5	0.00E+00	8836	0.05539	0.00021	0.53214	0.00601	0.069676	0.00074	0.941	1.5	.	428	8	433	4	434	4
SK5-A-2-008	432	26.5	5.10E-01	6780	0.05463	0.00048	0.44007	0.00654	0.058425	0.000699	0.805	-8	.	397	19	370	5	366	4
SK5-A-2-009	400	114.8	0.00E+00	48987	0.10823	0.0004	4.36633	0.06018	0.292589	0.003883	0.963	-7.4	-6	1770	6	1706	11	1654	19
SK5-A-2-010	318	65	9.30E-02	40381	0.10184	0.00045	2.97676	0.04815	0.211986	0.003296	0.961	-27.7	-26.4	1658	8	1402	12	1239	18
SK5-A-2-011	640	112.2	1.30E-01	107172	0.10383	0.00044	2.58528	0.03145	0.180589	0.002058	0.937	-39.9	-38.9	1694	7	1296	9	1070	11
SK5-A-2-012	439	87.3	8.40E-02	41567	0.10323	0.0016	3.18222	0.16609	0.223565	0.011141	0.955	-25.1	-20.2	1683	28	1453	40	1301	59
SK5-A-2-013	591	120	2.90E-01	7769	0.09881	0.0005	2.78614	0.05685	0.204506	0.004043	0.969	-27.5	-26	1602	9	1352	15	1199	22
SK5-A-2-014	25	4.9	2.40E-01	2882	0.08355	0.0008	2.28827	0.04548	0.198644	0.003459	0.876	-9.7	-5.6	1282	18	1209	14	1168	19
SK5-A-2-015	209	59.8	1.80E-01	10274	0.10577	0.00054	4.03371	0.04767	0.276587	0.002952	0.903	-10	-8.2	1728	9	1641	10	1574	15
SK5-A-2-016	211	61.9	0.00E+00	19685	0.10904	0.00043	4.51415	0.06348	0.300263	0.004057	0.961	-5.8	-4.4	1783	7	1734	12	1693	20
SK5-A-2-017	34	6.8	0.00E+00	2178	0.08425	0.00047	2.37499	0.0347	0.204454	0.002759	0.924	-8.4	-5.9	1298	11	1235	10	1199	15
SK5-A-2-018	193	23.2	4.00E-01	4524	0.06608	0.00034	1.15266	0.01718	0.126513	0.001768	0.937	-5.4	-1.9	809	11	778	8	768	10
SK5-A-2-019	152	42.4	0.00E+00	12354	0.10924	0.00042	4.31566	0.06089	0.286521	0.003886	0.961	-10.3	-8.9	1787	7	1696	12	1624	19
SK5-A-2-020	112	7.3	2.40E-01	4099	0.05463	0.00032	0.51259	0.00678	0.068057	0.000806	0.895	7.2	.	397	13	420	5	424	5
SK5-A-2-021	338	39	4.00E-01	5404	0.08009	0.00054	1.31088	0.02448	0.118715	0.002067	0.932	-41.9	-39.9	1199	13	851	11	723	12

Table 34: Raw data of concordant and disconcordant U-Pb analysis of all samples.

	ppm				Ratios							Discordance		Ages					
Name	U	^{206}Pb	$^{206}Pb_c$(%)	206/204	$^{207}Pb/^{206}Pb^*$	1SE	$^{207}Pb/^{235}U^*$	1SE	$^{206}Pb/^{238}U^*$	1SE	Rho	Central (%)	Minimum rim (%)	207/206	1σ	207/235	1σ	206/238	1σ
SK5-A-8-001	273	101.3	1.30E-01	30149	0.10676	0.00071	4.54733	0.13227	0.308912	0.008745	0.973	-0.6	.	1745	11	1740	24	1735	43
SK5-A-8-002	393	38.5	0.00E+00	5580	0.05687	0.00031	0.65439	0.01384	0.083457	0.001706	0.966	6.5	.	486	12	511	8	517	10
SK5-A-8-003	240	50.4	2.10E-03	24144	0.07478	0.00041	1.83859	0.04392	0.178315	0.004144	0.973	-0.5	.	1063	11	1059	16	1058	23
SK5-A-8-005	283	23.3	2.30E-01	6859	0.05326	0.00031	0.51279	0.01137	0.069834	0.001492	0.964	29.1	17.9	340	13	420	8	435	9
SK5-A-8-006	363	132.5	0.00E+00	27211	0.1083	0.00073	4.51423	0.13431	0.302304	0.008759	0.974	-4.4	-1.9	1771	11	1734	25	1703	43
SK5-A-8-007	351	86.2	6.50E-02	21018	0.08414	0.00053	2.38336	0.06134	0.205451	0.005129	0.970	-7.7	-4.9	1296	12	1238	18	1205	27
SK5-A-8-009	409	84.9	5.80E-02	25808	0.08765	0.00063	2.15022	0.05746	0.177923	0.004582	0.964	-25.2	-22.6	1375	13	1165	19	1056	25
SK5-A-8-010	435	146.2	1.60E-01	14533	0.10677	0.00067	4.2	0.1163	0.282122	0.007697	0.974	-9.3	-7	1745	11	1665	23	1602	39
SK5-A-8-011	853	86.4	0.00E+00	3564	0.0761	0.00066	0.90437	0.02311	0.08619	0.002073	0.941	-53.6	-51.3	1098	17	654	12	533	12
SK5-A-8-013	396	100.2	4.10E-01	3177	0.10293	0.00066	2.99279	0.08	0.210882	0.005472	0.971	-29.1	-27.2	1678	12	1406	20	1234	29
SK5-A-8-014	686	63.5	1.60E-01	11932	0.0726	0.00133	0.81753	0.02711	0.081673	0.002257	0.833	-51.5	-46.5	1003	35	607	15	506	13
SK5-A-8-015	202	56.2	7.90E-02	14194	0.09293	0.00068	2.99828	0.08651	0.233996	0.006533	0.968	-9.8	-6.9	1486	13	1407	22	1355	34
SK5-A-8-016	118	25.5	1.80E-01	7330	0.07537	0.00051	1.89882	0.04727	0.182722	0.00438	0.963	0.3	.	1078	13	1081	17	1082	24
SK5-A-8-017	458	146.1	1.80E-01	9963	0.10697	0.00072	3.94442	0.11442	0.267429	0.007548	0.973	-14.2	-11.9	1748	12	1623	23	1528	38
SK5-A-8-018	136	18.7	3.70E-01	4498	0.08806	0.00061	1.4	0.03771	0.117835	0.002996	0.965	-50.8	-49.2	1384	13	902	16	718	17
SK5-A-8-019	175	43.9	3.10E-01	5178	0.08022	0.00048	2.33515	0.05997	0.211116	0.005273	0.973	3	.	1202	12	1223	18	1235	28
SK5-A-8-020	234	85.4	3.50E-02	33630	0.10883	0.00073	4.57973	0.13666	0.30521	0.008873	0.974	-4	-1.5	1780	11	1746	25	1717	44
SK5-A-8-022	554	89.8	1.80E-01	7723	0.0967	0.00071	2.23555	0.09698	0.167662	0.007167	0.985	-38.8	-37	1562	14	1192	30	999	40
SK5-A-8-023	1	.	0.00E+00	2	1.01575	0.30198	85.98885	75.7001	0.613981	0.508762	0.941	-51.3	.	5259	567	4534	884	3086	2032
SK5-A-8-024	390	25.9	5.10E-01	3304	0.05141	0.0002	0.51365	0.01972	0.072464	0.002768	0.995	76.6	58.2	259	9	421	13	451	17
SK5-A-8-025	283	82.8	3.20E-02	25426	0.10827	0.00037	4.28633	0.23278	0.287136	0.015562	0.998	-9.2	-8.3	1770	6	1691	45	1627	78
SK5-A-8-026	76	12.8	2.60E-01	3308	0.0807	0.00038	1.9624	0.08753	0.176373	0.007824	0.994	-14.9	-13	1214	9	1103	30	1047	43
SK5-A-8-027	335	57.6	4.20E-01	2921	0.09886	0.00032	2.47067	0.11323	0.181251	0.008287	0.998	-35.8	-35.1	1603	6	1263	33	1074	45

Table 35: Raw data of concordant and disconcordant U-Pb analysis of all samples.

	ppm				Ratios								Discordance			Ages					
Name	U	^{206}Pb	$^{206}Pb_c$(%)	206/204	$^{207}Pb/^{206}Pb^*$	1SE	$^{207}Pb/^{235}U^*$	1SE	$^{206}Pb/^{238}U^*$	1SE	Rho	Central (%)	Minimum rim (%)		207/206	1σ	207/235	1σ	206/238	1σ
HR5-8-9-001	890	258.5	5.60E-01	2500	0.18001	0.00229	6.17484	0.18565	0.248787	0.006776	0.906	-51.1	-49.2		2653	21	2001	26	1432	35
HR5-8-9-002	50	10.3	0.00E+00	1449	0.07582	0.00064	1.86446	0.04562	0.178341	0.004093	0.938	-3.2			1090	17	1069	16	1058	22
HR5-8-9-003	110	3.4	0.00E+00	342	0.06359	0.00149	0.23394	0.0072	0.026683	0.000533	0.648	-77.7	-73.7		728	49	213	6	170	3
HR5-8-9-004	1	0.1	0.00E+00	26	0.84185	0.04296	2626.365	2325.883	22.62659	20.00459	0.998	1833.9			4994	71	7995	899	20386	5458
HR5-8-9-005	694	47.7	0.00E+00	8042	0.05416	0.00041	0.44164	0.00973	0.05914	0.001223	0.939	-2			378	17	371	7	370	7
HR5-8-9-006	1282	55.2	0.00E+00	7180	0.05193	0.00041	0.26591	0.00585	0.037139	0.000763	0.934	-17	-4.1		282	17	239	5	235	5
HR5-8-9-007	169	40.8	0.00E+00	9391	0.08146	0.00068	2.31016	0.05946	0.205686	0.005006	0.946	-2.4			1233	16	1215	18	1206	27
HR5-8-9-008	540	25.2	0.00E+00	3006	0.05179	0.00041	0.28277	0.00721	0.039598	0.00096	0.951	-9.5			276	17	253	6	250	6
HR5-8-9-009	203	68.4	0.00E+00	71429	0.10012	0.0009	3.96617	0.11273	0.287307	0.007745	0.948	0.1			1626	16	1627	23	1628	39
HR5-8-9-011	509	291.6	0.00E+00	11817	0.1803	0.00407	12.5007	0.47766	0.502853	0.015495	0.806	-1.4			2656	36	2643	36	2626	66
HR5-8-9-012	442	35.5	1.00E-01	10504	0.0603	0.00085	0.54906	0.01214	0.066041	0.001121	0.768	-33.9	-25.9		614	29	444	8	412	7
HR5-8-9-013	187	38.1	3.10E-01	8279	0.07112	0.00099	1.66524	0.03695	0.169815	0.002931	0.778	5.6			961	27	995	14	1011	16
HR5-8-9-014	648	11	0.00E+00	3504	0.04781	0.0006	0.09269	0.00165	0.014062	0.00018	0.716	0.3			90	28	90	2	90	1
HR5-8-9-015	177	37.9	4.40E-03	14954	0.07465	0.00108	1.81915	0.03977	0.176739	0.002896	0.750	-1			1059	28	1052	14	1049	16
HR5-8-9-016	395	157.2	6.20E-02	42533	0.119	0.00211	5.5614	0.16571	0.338941	0.008107	0.803	-3.5			1941	30	1910	26	1882	39
HR5-8-9-017	438	185.3	9.30E-02	32377	0.16954	0.00389	8.2756	0.28833	0.35402	0.00929	0.753	-27.1	-22.6		2553	38	2262	32	1954	44
HR5-8-9-018	559	136.1	3.10E-01	8979	0.10543	0.00179	2.93798	0.0786	0.202102	0.004183	0.774	-34	-30.1		1722	31	1392	20	1187	22
HR5-8-9-019	177	18.7	0.00E+00	919	0.07429	0.00175	0.9	0.02969	0.087035	0.002049	0.707	-50.8	-44.9		1049	47	647	16	538	12
HR5-8-9-020	130	32.7	4.20E-02	12383	0.08213	0.00125	2.38141	0.06033	0.210308	0.004267	0.801	-1.6			1249	29	1237	18	1230	23
HR5-8-9-021	443	106.2	1.40E-01	57821	0.07732	0.00115	2.11751	0.053	0.198631	0.004007	0.806	3.7			1129	30	1155	17	1168	22
HR5-8-9-022	83	14.2	0.00E+00	726	0.08118	0.00148	1.58721	0.04607	0.141808	0.0032	0.777	-32.3	-26.7		1226	36	965	18	855	18
HR5-8-9-023	1334	66.4	2.60E-01	7491	0.05223	0.00032	0.34486	0.00475	0.047886	0.000591	0.896	2.1			296	14	301	4	302	4
HR5-8-9-024	709	138.4	1.10E-01	92123	0.13882	0.00114	3.53824	0.05581	0.184858	0.002488	0.853	-54.9	-53.7		2213	14	1536	12	1093	14
HR5-8-9-025	770	71.6	0.00E+00	33436	0.05792	0.00021	0.70657	0.01109	0.088474	0.001352	0.973	3.9			527	8	543	7	547	8
HR5-8-9-026	614	26.9	0.00E+00	5637	0.05206	0.00029	0.29563	0.00472	0.041186	0.000615	0.936	-9.8	-0.4		288	12	263	4	260	4
HR5-8-9-027	272	86.9	0.00E+00	28343	0.10515	0.00044	4.35133	0.06531	0.300131	0.004326	0.960	-1.7			1717	7	1703	12	1692	21
HR5-8-9-028	115	41.4	0.00E+00	9117	0.1229	0.00058	5.70877	0.08714	0.33689	0.004888	0.951	-7.3	-5.7		1999	8	1933	13	1872	24
HR5-8-9-029	176	65.8	0.00E+00	29554	0.11662	0.00053	5.61676	0.08996	0.349301	0.005363	0.959	1.6			1905	8	1919	14	1931	26
HR5-8-9-030	1002	298.1	2.90E-02	78755	0.11073	0.00047	4.2458	0.06827	0.278095	0.00431	0.964	-14.3	-12.9		1811	7	1683	13	1582	22
HR5-8-9-031	425	19.6	2.10E-01	3566	0.05085	0.0003	0.30788	0.00389	0.043915	0.00049	0.883	18.8	6.5		234	13	273	3	277	3
HR5-8-9-032	64	6.4	0.00E+00	1810	0.06073	0.00053	0.80941	0.01256	0.096672	0.001236	0.823	-5.8			630	18	602	7	595	7
HR5-8-9-033	20	3.8	0.00E+00	797	0.07681	0.00065	1.9	0.03877	0.175841	0.003349	0.915	-7	-2.8		1116	17	1068	14	1044	18
HR5-8-9-034	236	12.7	0.00E+00	3505	0.05357	0.00039	0.37903	0.00521	0.051314	0.000595	0.844	-8.9			353	16	326	4	323	4
HR5-8-9-035	564	44.8	1.80E-01	6630	0.14581	0.00095	1.54189	0.03399	0.076697	0.001615	0.955	-82.1	-81.7		2297	11	947	14	476	10
HR5-8-9-036	436	19.3	0.00E+00	1365	0.05211	0.0003	0.30331	0.00466	0.042217	0.000601	0.928	-8.3			290	13	269	4	267	4
HR5-8-9-037	164	2.3	0.00E+00	500	0.05393	0.00075	0.10072	0.00175	0.013547	0.000143	0.606	-76.9	-71.5		368	31	97	2	87	1
HR5-8-9-038	115	55.7	2.90E-02	13200	0.19326	0.00117	11.91557	0.22577	0.447176	0.008026	0.947	-16.7	-15.2		2770	9	2598	18	2383	36
HR5-8-9-039	154	7.7	0.00E+00	1800	0.05298	0.00041	0.34774	0.00459	0.047608	0.000505	0.805	-8.7			328	17	303	3	300	3
HR5-8-9-040	83	26.4	0.00E+00	6577	0.1071	0.0005	4.41385	0.06685	0.298909	0.004308	0.952	-4.2	-2.4		1751	8	1715	13	1686	21
HR5-8-9-041	348	102.9	7.60E-03	70823	0.11215	0.00052	4.3	0.06248	0.279445	0.003829	0.948	-15.1	-13.6		1835	8	1697	12	1589	19
HR5-8-9-042	592	28	0.00E+00	6668	0.05221	0.00024	0.32497	0.00427	0.045142	0.000556	0.938	-3.5			295	10	286	3	285	3
HR5-8-9-043	347	185.1	0.00E+00	48482	0.19651	0.00124	13.34988	0.27096	0.492711	0.009502	0.950	-9.3	-7.6		2797	10	2705	19	2582	41
HR5-8-9-044	436	59.3	1.70E-01	11805	0.07122	0.00029	1.27405	0.01532	0.129743	0.001466	0.94	-19.5	-17.5		964	8	834	7	786	8
HR5-8-9-045	156	12.9	0.00E+00	3050	0.0572	0.00037	0.62519	0.0086	0.079274	0.000964	0.884	-1.5			499	14	493	5	492	6
HR5-8-9-046	934	53.5	2.10E-01	6836	0.05615	0.00032	0.424	0.00655	0.054771	0.000786	0.929	-25.6	-20.7		458	13	359	5	344	5
HR5-8-9-047	77	7.6	0.00E+00	1385	0.06143	0.0006	0.77823	0.01432	0.091877	0.001435	0.849	-14	-7.3		654	21	584	8	567	8
HR5-8-9-048	42	11.2	0.00E+00	4279	0.09376	0.00054	3.26116	0.04949	0.252262	0.00354	0.925	-3.9	-1.5		1503	11	1472	12	1450	18
HR5-8-9-049			0.00E+00	2	0.84434	2.54093	265.4389	800.4576	2.280048	0.442146	0.064	94.6	13		4998	23329	5671	3050	7657	869
HR5-8-9-050	914	245.4	0.00E+00	50660	0.09836	0.0004	3.43447	0.04883	0.253248	0.003453	0.959	-9.7	-8.1		1593	7	1512	11	1455	18
HR5-8-9-051	136	42.8	0.00E+00	11175	0.10641	0.00047	4.37359	0.06151	0.298105	0.003979	0.949	-3.7	-2		1739	8	1707	12	1682	20
HR5-8-9-052	972	181.9	4.50E-02	31749	0.08338	0.00035	2.02159	0.03636	0.175838	0.003073	0.972	-19.8	-18.2		1278	8	1123	12	1044	17
HR5-8-9-053	390	122.4	0.00E+00	21262	0.10553	0.00063	4.30179	0.07517	0.295647	0.004858	0.940	-3.5	-1.3		1724	10	1694	14	1670	24
HR5-8-9-054	109	33.2	0.00E+00	10811	0.10065	0.00041	3.97586	0.05984	0.286496	0.004154	0.963	-0.8			1636	7	1629	12	1624	21
HR5-8-9-055	114	12.1	0.00E+00	6506	0.06189	0.00039	0.86413	0.0116	0.101272	0.001201	0.883	-7.6	-2.9		670	13	632	6	622	7

Table 36: Raw data of concordant and disconcordant U-Pb analysis of all samples.

HR5-8-9-056	321	95.3	0.00E+00	30763	0.11706	0.00049	4.51173	0.06807	0.279522	0.004052	0.961	-19	-17.8			1912	7	1733	13	1589	20
HR5-8-9-057	669	48.7	0.00E+00	10223	0.05624	0.00023	0.54127	0.00666	0.069802	0.000808	0.941	-6	-1.5			462	9	439	4	435	5
HR5-8-9-058	367	8.5	0.00E+00	2408	0.05112	0.00035	0.15849	0.00205	0.022488	0.000247	0.85	-42.2	-33.4			246	15	149	2	143	2
HR5-8-9-059	133	35.5	0.00E+00	7680	0.0944	0.00044	3.29109	0.04525	0.25286	0.003274	0.942	-4.6	-2.7			1516	8	1479	11	1453	17
HR5-8-9-060	1254	31.8	0.00E+00	405	0.09181	0.00076	0.30754	0.00543	0.024295	0.000379	0.883	-90.5	-90.1			1463	15	272	4	155	2
HR5-8-9-061	334	61.1	7.00E-02	4306	0.10163	0.00095	2.39762	0.06707	0.171098	0.004514	0.943	-41.5	-39.3			1654	17	1242	20	1018	25
HR5-8-9-062	203	2.9	0.00E+00	1102	0.05288	0.00072	0.1012	0.00179	0.013879	0.000159	0.647	-73.1	-66			324	30	98	2	89	1
HR5-8-9-063	505	26.4	2.80E-02	15533	0.05334	0.00024	0.36266	0.00527	0.049315	0.000683	0.953	-9.8	-3.6			343	10	314	4	310	4
HR5-8-9-064	112	6.8	0.00E+00	1574	0.06129	0.0007	0.48351	0.0091	0.057211	0.000855	0.794	-46	-41.1			650	23	400	6	359	5
HR5-8-9-065	295	96	6.60E-02	16260	0.12166	0.00056	5.14125	0.07935	0.306489	0.004515	0.954	-14.8	-13.4			1981	8	1843	13	1723	22
HR5-8-9-066	236	80.7	0.00E+00	35184	0.11742	0.0005	5.20308	0.07963	0.321371	0.004726	0.961	-7.2	-5.8			1917	8	1853	13	1796	23
HR5-8-9-067	622	173.7	6.40E-02	108520	0.10982	0.0005	4.00502	0.05476	0.264499	0.003409	0.943	-17.7	-16.2			1796	8	1635	11	1513	17
HR5-8-9-068	133	30.6	0.00E+00	11766	0.08537	0.00042	2.55846	0.03457	0.21736	0.002734	0.931	-4.7	-2.4			1324	9	1289	10	1268	14
HR5-8-9-069	69	23	0.00E+00	5780	0.1172	0.00052	5.0449	0.08207	0.312203	0.004884	0.962	-9.7	-8.2			1914	8	1827	14	1752	24
HR5-8-9-070	534	22	0.00E+00	5507	0.05164	0.00025	0.28058	0.00429	0.03941	0.000572	0.950	-7.6				269	11	251	3	249	4
HR5-8-9-071	475	151.7	0.00E+00	144484	0.10853	0.00042	4.49611	0.06961	0.300448	0.004505	0.968	-5.2	-3.8			1775	7	1730	13	1694	22
HR5-8-9-072	251	48.8	0.00E+00	11421	0.08002	0.00029	2.02848	0.02614	0.183848	0.002275	0.960	-9.9	-8.3			1198	7	1125	9	1088	12
HR5-8-9-073	490	175.2	0.00E+00	48439	0.11909	0.00049	5.48848	0.09081	0.33424	0.005357	0.969	-5	-3.5			1943	7	1899	14	1859	26
HR5-8-9-074	288	40	4.40E-01	6225	0.09871	0.00091	1.82936	0.05601	0.134408	0.003926	0.954	-52.3	-50.4			1600	16	1056	20	813	22
HR5-8-9-075	323	14	0.00E+00	2540	0.05254	0.00036	0.30364	0.00393	0.041914	0.000462	0.851	-14.6	-4.6			309	15	269	3	265	3
HR5-8-9-076	806	107	6.30E-02	19716	0.07007	0.00029	1.22789	0.01489	0.127092	0.00145	0.941	-18.1	-16.1			930	8	813	7	771	8
HR5-8-9-077	546	65.4	2.30E+00	631	0.07797	0.00036	1.18775	0.01741	0.110489	0.001538	0.950	-43.2	-41.8			1146	9	795	8	676	9
HR5-8-9-078	94	15.5	0.00E+00	6518	0.07274	0.00037	1.57474	0.02097	0.157007	0.001928	0.922	-7.1	-4.3			1007	10	960	8	940	11
HR5-8-9-079	716	180.3	4.50E-02	31293	0.09992	0.00044	3.30769	0.04875	0.240091	0.003375	0.954	-16.1	-14.6			1623	8	1483	11	1387	18
HR5-8-9-080	192	2.8	0.00E+00	753	0.06118	0.00178	0.11965	0.00379	0.014184	0.000178	0.395	-86.5	-82.3			646	61	115	3	91	1
HR5-8-9-081	547	253.4	0.00E+00	51766	0.17424	0.00097	10.36174	0.19201	0.431295	0.00762	0.953	-13.1	-11.6			2599	9	2468	17	2312	34
HR5-8-9-082	87	46.2	0.00E+00	12781	0.17906	0.00106	12.1921	0.24018	0.493833	0.00928	0.954	-2.6	-0.8			2644	10	2619	18	2587	40
HR5-8-9-083	329	54.5	0.00E+00	18330	0.07112	0.00028	1.54435	0.0196	0.157482	0.001901	0.951	-2				961	8	948	8	943	11
HR5-8-9-084	658	131.1	0.00E+00	24020	0.08105	0.00058	2.10611	0.03512	0.188455	0.00284	0.904	-9.8	-6.6			1223	13	1151	11	1113	15
HR5-8-9-085	70	8.3	0.00E+00	3213	0.06658	0.00043	1.04489	0.01597	0.113819	0.001576	0.906	-16.6	-12.9			825	13	726	8	695	9
HR5-8-9-086	229	16.3	0.00E+00	4224	0.05575	0.00028	0.52161	0.00673	0.067855	0.000809	0.924	-4.5				443	11	426	4	423	5
HR5-8-9-087	379	15	0.00E+00	3470	0.05155	0.00026	0.26959	0.00363	0.037926	0.000472	0.926	-9.9	-0.7			266	11	242	3	240	3
HR5-8-9-088	426	155.6	0.00E+00	123698	0.11923	0.00053	5.64539	0.08981	0.343407	0.005244	0.960	-2.5	-0.9			1945	7	1923	14	1903	25
HR5-8-9-089	437	30.9	3.00E-01	6309	0.0545	0.00029	0.50917	0.00653	0.067763	0.000794	0.913	8.2	1.4			392	11	418	4	423	5
HR5-8-9-090	358	18.3	0.00E+00	3097	0.05384	0.00027	0.36668	0.00675	0.04939	0.000874	0.961	-15.1	-8.7			365	11	317	5	311	5
HR5-8-9-091	478	24.6	0.00E+00	3631	0.05315	0.00024	0.3629	0.00483	0.049516	0.000619	0.940	-7.3	-0.6			335	10	314	4	312	4
HR5-8-9-092	172	36.9	0.00E+00	7505	0.08072	0.00034	2.27054	0.03265	0.203996	0.002805	0.956	-1.6				1215	8	1203	10	1197	15
HR5-8-9-093	194	3.3	0.00E+00	448	0.06472	0.00194	0.14461	0.00466	0.016206	0.000194	0.372	-87.1	-83.8			765	61	137	4	104	1
HR5-8-9-094	162	59.9	6.40E-01	3631	0.12018	0.00059	5.73588	0.0945	0.346163	0.005444	0.955	-2.5	-0.8			1959	8	1937	14	1916	26
HR5-8-9-095	83	1	0.00E+00	356	0.06222	0.00323	0.10605	0.00596	0.012361	0.000264	0.38	-88.9	-80.9			682	108	102	5	79	2
HR5-8-9-096	258	12.3	4.00E-01	2758	0.05195	0.00073	0.32857	0.00606	0.045868	0.000543	0.642	2.1				283	31	288	5	289	3
HR5-8-9-097	766	118.9	5.20E-01	3320	0.09303	0.00071	1.85914	0.0507	0.144939	0.003796	0.96	-44.2	-42.3			1489	14	1067	18	873	21
HR5-8-9-098	218	67	1.90E-01	8463	0.11424	0.00054	4.57992	0.07367	0.290764	0.004471	0.956	-13.5	-11.9			1868	8	1746	13	1645	22
HR5-8-9-099	414	31.5	0.00E+00	1070	0.0665	0.00087	0.66772	0.01317	0.072819	0.001077	0.75	-46.5	-42.1			822	26	519	8	453	6
HR5-8-9-100	1030	331.1	0.00E+00	59295	0.11336	0.00045	4.70947	0.07632	0.301313	0.004732	0.969	-9.6	-8.2			1854	7	1769	14	1698	23
HR5-8-9-101	604	149.4	4.20E-01	2871	0.0923	0.00045	2.97098	0.04467	0.233448	0.003318	0.945	-9.1	-7.1			1474	9	1400	11	1353	17
HR5-8-9-102	191	15.1	0.00E+00	2262	0.05645	0.00029	0.59092	0.00878	0.075926	0.00106	0.94	0.4				470	11	471	6	472	6
HR5-8-9-103	94	19.6	5.40E-01	4390	0.10106	0.00066	2.72988	0.07728	0.19592	0.005397	0.973	-32.5	-30.7			1644	11	1337	21	1153	29
HR5-8-9-104	73	1.1	0.00E+00	246	0.0505	0.00092	0.09924	0.00231	0.014252	0.000205	0.619	-58.6	-26.4			218	42	96	2	91	1
HR5-8-9-106	827	260.9	1.10E+00	1496	0.11092	0.00092	4.48194	0.07841	0.293056	0.00452	0.882	-9.9	-7.1			1815	14	1728	15	1657	23
HR5-8-9-107	228	36.9	0.00E+00	6366	0.07027	0.00029	1.49956	0.01893	0.154771	0.001848	0.946	-1				936	8	930	8	928	10
HR5-8-9-108	328	65	7.90E-02	16125	0.08397	0.00036	2.19443	0.0287	0.189538	0.002345	0.946	-14.6	-12.8			1292	8	1179	9	1119	13
HR5-8-9-109	173	20.6	2.90E-01	19423	0.06604	0.00035	1.04755	0.01669	0.115042	0.001732	0.945	-13.8	-10.6			808	11	728	8	702	10
HR5-8-9-110	256	103.4	2.00E-02	31437	0.18497	0.00115	9.74981	0.17865	0.382286	0.006587	0.94	-26.4	-25			2698	10	2411	17	2087	31
HR5-8-9-111	501	27.6	0.00E+00	4362	0.05309	0.00025	0.3873	0.00621	0.052913	0.000809	0.955					333	10	332	5	332	5

Table 37: Raw data of concordant and disconcordant U-Pb analysis of all samples.

	ppm			Ratios								Discordance		Ages					
Name	U	^{206}Pb	$^{206}Pb_c$(%)	206/204	$^{207}Pb/^{206}Pb^*$	1SE	$^{207}Pb/^{235}U^*$	1SE	$^{206}Pb/^{238}U^*$	1SE	Rho	Central (%)	Minimum rim (%)	207/206	1σ	207/235	1σ	206/238	1σ
DE1-2-01	154	48	0.00E+00	6524	0.1091	0.00124	4.39521	0.08211	0.292193	0.00434	0.795	-8.4	-4.8	1784	20	1711	15	1652	22
DE1-2-02	469	71.7	7.50E-01	2425	0.07496	0.001	1.51951	0.02908	0.14702	0.002021	0.718	-18.4	-13.1	1067	26	938	12	884	11
DE1-2-03	255	66.5	2.60E-01	4481	0.10444	0.00119	3.63362	0.05791	0.252328	0.002817	0.700	-16.6	-13.6	1704	21	1557	13	1450	15
DE1-2-04	299	70	1.00E-01	17977	0.10497	0.00131	3.33518	0.05796	0.230426	0.002797	0.699	-24.3	-21.3	1714	22	1489	14	1337	15
DE1-2-05	291	64.4	9.40E-02	17087	0.09925	0.00123	2.88624	0.08398	0.210916	0.005551	0.904	-25.7	-21.8	1610	22	1378	22	1234	30
DE1-2-06	649	37.6	3.20E-01	10824	0.05316	0.00053	0.43984	0.00761	0.060004	0.000852	0.820	12.2		336	22	370	5	376	5
DE1-2-07	91	24.8	0.00E+00	5088	0.10079	0.0012	3.83413	0.07016	0.275907	0.003825	0.758	-4.7	-0.7	1639	20	1600	15	1571	19
DE1-2-08	284	35	1.90E-01	9258	0.08744	0.00099	1.54987	0.02929	0.128555	0.001948	0.802	-45.7	-43.2	1370	20	950	12	780	11
DE1-2-09	407	33.8	1.80E-01	7094	0.072	0.00079	0.9	0.0137	0.086903	0.000997	0.722	-47.4	-44.4	986	21	632	7	537	6
DE1-2-10	358	95.6	2.10E-01	6805	0.10689	0.00145	4.00687	0.0734	0.271871	0.003339	0.671	-12.7	-9	1747	24	1636	15	1550	17
DE1-2-11	297	39.3	2.90E-01	3526	0.0684	0.00068	1.32275	0.02028	0.140257	0.001638	0.762	-4.2		881	19	856	9	846	9
DE1-2-12	506	32	0.00E+00	9025	0.05531	0.00053	0.52173	0.00711	0.068413	0.000664	0.712	0.4		425	20	426	5	427	4
DE1-2-13	1057	66.2	0.00E+00	290	0.13615	0.00412	1.27716	0.0494	0.068035	0.001639	0.623	-83.1	-81.8	2179	48	836	22	424	10
DE1-2-14	341	65.6	3.70E-01	7295	0.09969	0.00125	2.82929	0.05377	0.205845	0.002942	0.752	-27.9	-24.7	1618	21	1363	14	1207	16
DE1-2-15	845	209.9	5.20E-02	29917	0.10665	0.00134	3.92234	0.07111	0.266729	0.003496	0.723	-14.1	-10.6	1743	22	1618	15	1524	18
DE1-2-16	181	39.7	9.20E-02	13717	0.09642	0.00114	3.16511	0.05172	0.238082	0.002686	0.69	-12.8	-9.3	1556	21	1449	13	1377	14
DE1-2-17	564	144.4	1.10E-01	10947	0.10509	0.00073	3.68646	0.05885	0.254408	0.003661	0.901	-16.6	-14.3	1716	12	1568	13	1461	19
DE1-2-18	251	33.5	0.00E+00	11793	0.08979	0.00067	1.65294	0.03215	0.133518	0.002399	0.924	-45.9	-44	1421	14	991	12	808	14
DE1-2-19	432	108.3	1.20E-01	29755	0.10448	0.00069	3.56001	0.04808	0.247129	0.002905	0.87	-18.4	-16.3	1705	12	1541	11	1424	15
DE1-2-20	224	63.5	0.00E+00	8706	0.10787	0.00083	4.14822	0.07093	0.278906	0.004254	0.892	-11.4	-8.8	1764	14	1664	14	1586	21
DE1-2-21	310	61.1	2.50E-01	3901	0.10381	0.00075	2.81802	0.05332	0.196889	0.003445	0.925	-34.5	-32.6	1693	13	1360	14	1159	19
DE1-2-22	775	59.6	9.60E-02	18397	0.07103	0.00045	0.76423	0.01367	0.078039	0.001304	0.934	-51.3	-49.4	958	13	576	8	484	8
DE1-2-23	284	67.7	4.80E-01	4286	0.10543	0.00073	3.45975	0.04862	0.237998	0.002915	0.872	-22.3	-20.2	1722	12	1518	11	1376	15
DE1-2-24	159	23.6	1.70E-01	3692	0.10765	0.00076	2.21309	0.03168	0.1491	0.001855	0.869	-52.5	-51.2	1760	13	1185	10	896	10
DE1-2-25	759	169.3	7.50E-02	19917	0.10442	0.00071	3.19748	0.04754	0.222097	0.00294	0.89	-26.6	-24.7	1704	12	1457	11	1293	16
DE1-2-26	45	13.5	0.00E+00	3839	0.10865	0.00078	4.52413	0.07456	0.302001	0.004482	0.901	-4.8	-2.2	1777	13	1735	14	1701	22
DE1-2-27	171	50.4	0.00E+00	6355	0.10811	0.00076	4.40018	0.06749	0.29519	0.004023	0.889	-6.4	-3.9	1768	13	1712	13	1667	20
DE1-2-28	81	15.9	3.70E-01	3815	0.08604	0.00081	2.38848	0.04713	0.201347	0.003496	0.880	-12.8	-9	1339	18	1239	14	1183	19
DE1-2-29	141	38.5	0.00E+00	6323	0.10807	0.00082	4.11143	0.06411	0.275928	0.003755	0.873	-12.5	-10	1767	14	1657	13	1571	19
DE1-2-30	309	75.7	0.00E+00	4498	0.10732	0.00064	3.91866	0.07745	0.264821	0.004992	0.954	-15.3	-13.3	1754	10	1618	16	1514	25
DE1-2-31	113	26.5	8.00E-01	41534	0.10011	0.00081	3.34681	0.0856	0.242478	0.005884	0.949	-15.5	-12.6	1626	14	1492	20	1400	31
DE1-2-32	310	76	2.70E-01	6364	0.10502	0.00086	3.71235	0.09796	0.256379	0.006435	0.951	-15.9	-13.1	1715	14	1574	21	1471	33
DE1-2-34	366	64.7	0.00E+00	36980	0.10413	0.00051	2.90575	0.04253	0.202393	0.002794	0.943	-32.9	-31.6	1699	9	1383	11	1188	15
DE1-2-35	106	6.3	0.00E+00	2070	0.05632	0.00031	0.5	0.00869	0.068861	0.001055	0.943	-7.9	-2.1	465	12	435	6	429	6
DE1-2-36	377	21.9	0.00E+00	2133	0.0561	0.00024	0.52349	0.00754	0.067675	0.000931	0.955	-7.8	-3.1	456	9	427	5	422	6
DE1-2-37	104	24.5	2.50E+00	880	0.08785	0.00195	2.57343	0.18504	0.212462	0.014528	0.951	-10.9	-1.3	1379	41	1293	53	1242	77
DE1-2-38	565	104.5	2.10E-01	5588	0.1028	0.00052	2.98014	0.05001	0.210244	0.003363	0.953	-29.2	-27.7	1675	9	1403	13	1230	18
DE1-2-39	190	54.3	0.00E+00	4188	0.10843	0.00053	4.80706	0.10083	0.321549	0.00656	0.973	1.6		1773	8	1786	18	1797	32
DE1-2-40	265	63.5	3.50E-01	3704	0.10532	0.00079	3.73861	0.09191	0.257453	0.006026	0.952	-15.8	-13.3	1720	13	1580	20	1477	31
DE1-2-41	599	34.4	0.00E+00	420	0.12016	0.00492	1.36765	0.13581	0.082547	0.007469	0.911	-76.8	-73.1	1959	72	875	58	511	44
DE1-2-42	202	48.4	1.70E-01	18223	0.10524	0.00122	3.67053	0.1669	0.252949	0.011118	0.967	-17.2	-13.3	1719	21	1565	36	1454	57
DE1-2-43	308	39.4	0.00E+00	7133	0.07016	0.0003	1.44762	0.02183	0.14964	0.002166	0.960	-3.9	-1.4	933	9	909	9	899	12
DE1-2-44	308	17.9	0.00E+00	6810	0.05565	0.00025	0.52586	0.00664	0.068528	0.000808	0.934	-2.7		439	10	429	4	427	5
DE1-2-45	252	61.2	0.00E+00	29079	0.10861	0.00056	4.18373	0.06597	0.279391	0.004166	0.946	-11.9	-10.2	1776	9	1671	13	1588	21
DE1-2-46	233	59.7	0.00E+00	14542	0.10828	0.00068	4.3078	0.08146	0.288532	0.005146	0.943	-8.7	-6.5	1771	11	1695	16	1634	26
DE1-2-47	110	28.5	0.00E+00	6362	0.10856	0.00062	4.41449	0.08999	0.294927	0.005771	0.96	-7	-4.9	1775	10	1715	17	1666	29
DE1-2-48	106	18.1	0.00E+00	22806	0.08346	0.00044	2.29585	0.03726	0.19951	0.003062	0.946	-9.2	-6.8	1280	10	1211	11	1173	16
DE1-2-49	61	25.9	0.00E+00	5094	0.18333	0.00137	12.1	0.2986	0.478963	0.011256	0.953	-7.2	-5.1	2683	12	2613	23	2523	49
DE1-2-50	287	60.1	0.00E+00	5342	0.09912	0.0006	3.28222	0.0652	0.240171	0.004546	0.953	-15.2	-13.1	1608	11	1477	15	1388	24

Table 38: Raw data of concordant and disconcordant U-Pb analysis of all samples.

DE1-2-51	237	64.3	0.00E+00	6840	0.09201	0.00136	2.99806	0.0927	0.236335	0.006421	0.879	-7.6	-1.6			1467	27	1407	24	1368	33
DE1-2-52	92	29.9	0.00E+00	11321	0.1095	0.00189	4.26871	0.14843	0.282728	0.008529	0.868	-11.7	-6			1791	30	1687	29	1605	43
DE1-2-54	114	32.5	2.60E-01	8058	0.10508	0.00181	3.71272	0.13135	0.256242	0.007912	0.873	-16	-10.3			1716	30	1574	28	1471	41
DE1-2-56	384	118.4	1.90E-02	38466	0.10889	0.00192	4.19314	0.15145	0.279294	0.008803	0.873	-12.2	-6.3			1781	32	1673	30	1588	44
DE1-2-57	350	73.2	1.90E-01	8274	0.10302	0.00183	2.75018	0.09707	0.19361	0.005909	0.865	-34.9	-30.4			1679	32	1342	26	1141	32
DE1-2-58	695	50.6	9.20E-02	11540	0.05382	0.00081	0.51349	0.01689	0.069193	0.002025	0.89	19.2				364	32	421	11	431	12
DE1-2-59	60	19.1	5.50E-01	2257	0.10511	0.00176	4.22195	0.15624	0.291322	0.009615	0.892	-4.5				1716	30	1678	30	1648	48
DE1-2-60	132	41.5	3.00E-01	5204	0.10754	0.00176	4.2	0.1521	0.281118	0.009173	0.894	-10.3	-4.6			1758	28	1668	30	1597	46
DE1-2-61	345	126.6	1.70E-01	6601	0.10725	0.00081	4.50225	0.15107	0.304466	0.009952	0.974	-2.6				1753	14	1731	28	1713	49
DE1-2-62	406	12.5	0.00E+00	108	0.15632	0.00468	0.70221	0.06207	0.032581	0.002709	0.941	-92.8	-92.1			2416	50	540	37	207	17
DE1-2-63	107	32.1	9.00E-01	1482	0.09897	0.00132	3.49561	0.07538	0.256169	0.004342	0.786	-9.4	-4.9			1605	24	1526	17	1470	22
DE1-2-64	155	56.3	2.60E-01	9046	0.10648	0.00072	4.45066	0.11674	0.303145	0.007683	0.966	-2.2				1740	12	1722	22	1707	38
DE1-2-65	432	36.4	5.70E-01	2555	0.0588	0.00059	0.54914	0.01368	0.067737	0.001545	0.915	-25.3	-17.9			560	21	444	9	423	9
DE1-2-66	151	20.8	7.10E-01	1541	0.06331	0.00042	1.01507	0.02654	0.116277	0.002939	0.967	-1.4				719	14	711	13	709	17
DE1-2-67	291	77.3	7.80E-01	2852	0.10505	0.00121	3.19561	0.1197	0.220623	0.007863	0.951	-27.6	-24.2			1715	20	1456	29	1285	42
DE1-2-68	114	26.3	0.00E+00	3055	0.0783	0.00056	2.1	0.08325	0.192746	0.007586	0.984	-1.7				1155	14	1143	27	1136	41
DE1-2-69	1154	128.3	0.00E+00	5429	0.09333	0.00063	1.1693	0.02756	0.090867	0.002051	0.958	-65.2	-64.1			1495	12	786	13	561	12
DE1-2-71	491	119.6	9.30E-01	1885	0.10334	0.00098	2.85895	0.11495	0.200652	0.007842	0.972	-32.8	-30.2			1685	17	1371	30	1179	42
DE1-2-70	244	60.3	3.50E-02	36854	0.1092	0.0008	3.40956	0.15857	0.226441	0.010401	0.988	-29.1	-27.1			1786	13	1507	37	1316	55
DE1-2-72	120	44.3	0.00E+00	13406	0.10959	0.0008	4.80066	0.12976	0.317704	0.008269	0.963	-0.9				1793	13	1785	23	1779	40
DE1-2-73			0.00E+00	3	0.64499	0.05616	311.2588	104.7216	3.499998	1.137447	0.966	234.8				4613	123	5832	341	9696	1629
DE1-2-74	541	117.1	9.70E-02	10716	0.09886	0.00076	2.50576	0.06216	0.183829	0.004333	0.950	-34.9	-32.8			1603	14	1274	18	1088	24
DE1-2-75	235	77	8.80E-02	18308	0.10852	0.00155	4.36766	0.12499	0.291892	0.007245	0.867	-7.9	-3			1775	25	1706	24	1651	36
DE1-2-76	454	116.7	4.60E-01	3066	0.10344	0.00063	3.37826	0.1666	0.236867	0.011593	0.992	-20.8	-19			1687	10	1499	39	1370	60
DE1-2-77	332	75.9	0.00E+00	16374	0.08838	0.00045	2.54296	0.08576	0.20867	0.006957	0.989	-13.3	-11.4			1391	9	1284	25	1222	37
DE1-2-78	558	71.5	3.70E-01	4726	0.09286	0.00066	1.50484	0.06317	0.117534	0.004862	0.986	-54.6	-53.2			1485	13	932	26	716	28
DE1-2-80	193	57.5	0.00E+00	68376	0.10842	0.0006	4.10963	0.14996	0.274906	0.009915	0.988	-13.2	-11.4			1773	10	1656	30	1566	50
DE1-2-81	295	60.6	0.00E+00	11437	0.07403	0.00042	1.9138	0.07423	0.187494	0.007196	0.989	6.8				1042	11	1086	26	1108	39
DE1-2-82	679	90.9	2.20E-01	7344	0.0937	0.00054	1.5656	0.07136	0.121179	0.005479	0.992	-53.8	-52.7			1502	11	957	28	737	32
DE1-2-83	970	72.7	0.00E+00	13974	0.05502	0.00028	0.51046	0.01886	0.067284	0.002463	0.991	1.6				413	11	419	13	420	15
DE1-2-84	1087	189.3	9.60E-02	28283	0.09725	0.00075	2.14429	0.08456	0.159916	0.006183	0.98	-42.1	-40.2			1572	14	1163	27	956	34
DE1-2-85	575	126.9	7.90E-02	20624	0.10326	0.00049	2.8986	0.14259	0.203594	0.009969	0.995	-31.8	-30.7			1683	8	1382	37	1195	53
DE1-2-86	616	83.8	1.00E-01	70066	0.09091	0.00065	1.56434	0.07391	0.124801	0.005829	0.989	-50.3	-48.8			1445	13	956	29	758	33
DE1-2-87	424	98.1	9.30E-02	15951	0.10497	0.00068	3.07508	0.14745	0.212475	0.010096	0.991	-30.2	-28.5			1714	12	1427	37	1242	54
DE1-2-88	304	81.1	8.00E-02	14883	0.10516	0.00061	3.52225	0.14335	0.24292	0.009787	0.990	-20.4	-18.7			1717	11	1532	32	1402	51
DE1-2-89	357	115.1	0.00E+00	7569	0.10904	0.00061	4.39548	0.1912	0.292357	0.012611	0.992	-8.3	-6.4			1783	10	1711	36	1653	63
DE1-2-90	380	76.6	1.10E-01	14992	0.10002	0.00065	2.52502	0.10054	0.183089	0.007193	0.987	-36.1	-34.5			1625	12	1279	29	1084	39
DE1-2-91	198	37.5	1.90E-01	13776	0.09659	0.00087	2.19258	0.07301	0.164643	0.00528	0.963	-39.8	-37.5			1559	16	1179	23	983	29
DE1-2-92	363	30.7	0.00E+00	5414	0.0562	0.0004	0.55312	0.01143	0.071386	0.001383	0.938	-3.5				460	15	447	7	445	8
DE1-2-93	259	90.7	3.30E-02	24472	0.10877	0.00099	4.42422	0.11988	0.295013	0.007533	0.942	-7.2	-3.9			1779	16	1717	22	1667	37
DE1-2-94	264	21	6.10E-01	4296	0.05527	0.00129	0.50266	0.01993	0.065964	0.002112	0.807	-2.7				423	50	414	13	412	13
DE1-2-95	649	225.3	2.20E-01	11710	0.10918	0.00103	4.40274	0.12493	0.292456	0.007827	0.943	-8.4	-5			1786	17	1713	23	1654	39
DE1-2-96	269	90.9	1.30E-01	11071	0.10718	0.001	4.19648	0.11915	0.283958	0.007613	0.944	-9.1	-5.7			1752	16	1673	23	1611	38
DE1-2-97	593	182.3	1.80E-01	15037	0.10624	0.00096	3.80041	0.09776	0.259449	0.006251	0.937	-16	-13			1736	16	1593	21	1487	32
DE1-2-98	1026	221.1	3.60E-02	34208	0.07776	0.00061	1.93699	0.04698	0.180662	0.004146	0.946	-6.7	-2.7			1141	15	1094	16	1071	23
DE1-2-99	166	42.3	1.60E-01	7739	0.0871	0.00077	2.6	0.0652	0.214008	0.005092	0.938	-9.1	-5.3			1363	17	1292	19	1250	27
DE1-2-100	1543	131.7	0.00E+00	23885	0.05514	0.0004	0.5356	0.01328	0.070449	0.00167	0.956	5.2				418	16	436	9	439	10
DE1-2-101	516	37.4	3.60E-01	10641	0.05411	0.00057	0.44691	0.01712	0.0599	0.002205	0.961	-0.2				376	23	375	12	375	13
DE1-2-102	320	102.5	1.00E-01	19792	0.10704	0.00099	3.99032	0.11246	0.270368	0.007195	0.944	-13.3	-10.1			1750	16	1632	23	1543	37
DE1-2-103	397	143.5	5.70E-02	24976	0.1077	0.001	4.53067	0.12976	0.305093	0.008268	0.946	-2.9				1761	17	1737	24	1717	41
DE1-2-104	567	50.1	0.00E+00	18058	0.05694	0.00043	0.5842	0.01345	0.074417	0.001619	0.945	-5.6				489	16	467	9	463	10
DE1-2-105	566	192.4	3.50E-02	28473	0.10573	0.00093	4.2356	0.11389	0.290538	0.00738	0.945	-5.4	-2.1			1727	17	1681	22	1644	37
DE1-2-106	624	192.4	1.90E-01	7978	0.10531	0.00095	3.77644	0.10223	0.260088	0.006638	0.943	-14.9	-11.8			1720	17	1588	22	1490	34
DE1-2-107	1311	86.9	3.00E-01	5344	0.05353	0.0004	0.4	0.01201	0.054856	0.001574	0.967	-2.1				352	17	345	9	344	10
DE1-2-108	485	185	0.00E+00	47155	0.10911	0.00101	4.85785	0.1447	0.322905	0.009138	0.95	1.2				1785	16	1795	25	1804	45
DE1-2-109	308	114.5	0.00E+00	17717	0.10864	0.00104	4.75406	0.13973	0.317363	0.00882	0.946					1777	17	1777	25	1777	43
DE1-2-110	352	125.7	0.00E+00	30435	0.10847	0.00102	4.5519	0.13215	0.304368	0.008361	0.946	-3.9	-0.3			1774	16	1741	24	1713	41

10.5 Appendix 4

Table 39: Raw data of concordant and disconcordant hafnium analysis of all samples.

Sample	$^{175}Hf/^{177}Hf$	1SE	$^{178}Hf/^{177}Hf$	1SE	$^{176}Lu/^{177}Hf$	1SE	$^{176}Yb/^{177}Hf$	1SE	Fract	1SE	Yb Fract	1SE	Hf tot	1SE	Yb tot	1SE	Lu tot	1SE	$^{175}Hf/^{177}Hf(HfFract)$	1SE
ER3-9S-2-003G	0.281934	0.000012	1.46723	0.000017	0.00169	0.00004	0.0843	0.0026	-1.46	0.00	-1.42	0.00	8.31	0.150	0.980	0.046	0.10	0.00	0.28	0.00
ER3-9S-2-010G	0.281776	0.000011	1.46720	0.000019	0.00124	0.00004	0.0611	0.0011	-1.45	0.00	-1.43	0.01	5.39	0.110	0.444	0.004	0.05	0.00	0.28	0.00
ER3-9S-2-020G	0.281532	0.000012	1.46724	0.000019	0.00072	0.00002	0.0380	0.0014	-1.46	0.00	-1.42	0.01	7.91	0.130	0.418	0.019	0.04	0.00	0.28	0.00
ER3-9S-2-029G	0.281885	0.000010	1.46721	0.000024	0.00083	0.00002	0.0409	0.0012	-1.44	0.00	-1.42	0.01	6.43	0.210	0.366	0.023	0.04	0.00	0.28	0.00
ER3-9S-2-031G	0.281895	0.000012	1.46724	0.000016	0.00165	0.00001	0.0806	0.0006	-1.44	0.00	-1.43	0.01	6.97	0.130	0.777	0.018	0.08	0.00	0.28	0.00
ER3-9S-2-036G	0.281831	0.000011	1.46725	0.000021	0.00091	0.00008	0.0400	0.0031	-1.45	0.00	-1.40	0.01	7.84	0.270	0.443	0.051	0.05	0.01	0.28	0.00
ER3-9S-2-039G	0.281894	0.000010	1.46722	0.000014	0.00069	0.00001	0.0337	0.0009	-1.45	0.00	-1.40	0.01	8.37	0.120	0.390	0.014	0.04	0.00	0.28	0.00
ER3-9S-2-040C	0.282437	0.000010	1.46725	0.000026	0.00037	0.00000	0.0184	0.0000	-1.46	0.00	-1.43	0.02	6.11	0.097	0.155	0.003	0.02	0.00	0.28	0.00
ER3-9S-2-049G	0.281840	0.000010	1.46719	0.000020	0.00042	0.00000	0.0214	0.0003	-1.45	0.00	-1.41	0.01	7.50	0.120	0.223	0.006	0.02	0.00	0.28	0.00
ER3-9S-2-078G	0.281746	0.000013	1.46721	0.000023	0.00192	0.00001	0.0915	0.0013	-1.45	0.00	-1.43	0.00	5.16	0.077	0.659	0.020	0.07	0.00	0.28	0.00
ER3-9S-2-080G	0.281749	0.000010	1.46722	0.000022	0.00057	0.00001	0.0277	0.0006	-1.45	0.00	-1.39	0.01	7.97	0.300	0.312	0.019	0.03	0.00	0.28	0.00
ER3-9S-2-081G	0.281818	0.000010	1.46722	0.000025	0.00141	0.00006	0.0657	0.0024	-1.46	0.00	-1.43	0.01	6.51	0.140	0.586	0.008	0.06	0.00	0.28	0.00
ER3-9S-2-088G	0.281566	0.000011	1.46723	0.000018	0.00062	0.00000	0.0325	0.0003	-1.46	0.00	-1.41	0.01	7.25	0.110	0.325	0.007	0.03	0.00	0.28	0.00
ER3-9S-2-091G	0.281873	0.000012	1.46721	0.000024	0.00210	0.00002	0.1202	0.0014	-1.45	0.00	-1.44	0.00	5.16	0.068	0.870	0.018	0.08	0.00	0.28	0.00
ER3-9S-2-092G	0.281809	0.000013	1.46722	0.000018	0.00111	0.00002	0.0501	0.0012	-1.45	0.00	-1.45	0.01	7.02	0.160	0.490	0.022	0.05	0.00	0.28	0.00
ER3-9S-2-094G	0.281854	0.000011	1.46724	0.000021	0.00132	0.00001	0.0642	0.0008	-1.45	0.00	-1.43	0.00	7.90	0.160	0.683	0.004	0.07	0.00	0.28	0.00
ER3-9S-2-097G	0.281725	0.000011	1.46725	0.000020	0.00060	0.00001	0.0286	0.0008	-1.46	0.00	-1.45	0.01	7.22	0.100	0.288	0.013	0.03	0.00	0.28	0.00
ER3-9S-14-012C	0.282416	0.000010	1.46721	0.000024	0.00090	0.00005	0.0481	0.0023	-1.47	0.00	-1.43	0.01	6.28	0.190	0.408	0.008	0.04	0.00	0.28	0.00
ER3-9S-14-013C	0.282364	0.000012	1.46717	0.000022	0.00187	0.00006	0.1059	0.0019	-1.46	0.00	-1.42	0.00	7.35	0.110	1.046	0.023	0.10	0.00	0.28	0.00
ER3-9S-14-016G	0.281835	0.000014	1.46723	0.000032	0.00144	0.00002	0.0783	0.0015	-1.47	0.00	-1.44	0.01	5.00	0.091	0.544	0.020	0.05	0.00	0.28	0.00
ER3-9S-14-022C	0.282176	0.000011	1.46728	0.000020	0.00012	0.00000	0.0059	0.0002	-1.46	0.00	-1.47	0.03	7.69	0.110	0.063	0.002	0.01	0.00	0.28	0.00
ER3-9S-14-023G	0.281790	0.000011	1.46719	0.000024	0.00072	0.00000	0.0362	0.0003	-1.47	0.00	-1.43	0.01	6.71	0.090	0.334	0.008	0.03	0.00	0.28	0.00
ER3-9S-14-024C	0.281942	0.000034	1.46720	0.000022	0.00062	0.00003	0.0341	0.0013	-1.46	0.00	-1.43	0.01	5.80	0.086	0.270	0.008	0.02	0.00	0.28	0.00
ER3-9S-14-058C	0.282247	0.000014	1.46721	0.000031	0.00157	0.00010	0.0791	0.0062	-1.46	0.00	-1.44	0.01	4.41	0.150	0.459	0.012	0.05	0.00	0.28	0.00
ER3-9S-14-059G	0.281599	0.000015	1.46724	0.000028	0.00080	0.00001	0.0417	0.0009	-1.44	0.00	-1.43	0.01	5.33	0.091	0.312	0.012	0.03	0.00	0.28	0.00
ER3-9S-14-069G	0.281839	0.000010	1.46725	0.000018	0.00074	0.00001	0.0400	0.0010	-1.46	0.00	-1.43	0.01	6.40	0.120	0.361	0.016	0.03	0.00	0.28	0.00
ER3-9S-14-091G	0.281753	0.000013	1.46727	0.000024	0.00188	0.00002	0.0931	0.0006	-1.46	0.00	-1.44	0.01	4.82	0.077	0.620	0.009	0.06	0.00	0.28	0.00
ER3-9S-14-093G	0.281476	0.000012	1.46722	0.000013	0.00089	0.00003	0.0488	0.0021	-1.46	0.00	-1.43	0.01	5.85	0.150	0.397	0.027	0.04	0.00	0.28	0.00
MA2-4-4-008G	0.281576	0.000010	1.46725	0.000020	0.00212	0.00003	0.0922	0.0012	-1.42	0.00	-1.41	0.00	8.68	0.280	1.107	0.029	0.13	0.00	0.28	0.00
MA2-4-4-024G	0.281498	0.000010	1.46719	0.000016	0.00134	0.00001	0.0751	0.0004	-1.45	0.00	-1.43	0.00	7.35	0.160	0.752	0.018	0.07	0.00	0.28	0.00
MA2-4-4-037C	0.282743	0.000010	1.46726	0.000018	0.00162	0.00007	0.0765	0.0047	-1.45	0.00	-1.43	0.00	7.46	0.150	0.772	0.036	0.08	0.00	0.28	0.00
MA2-4-4-038G	0.281832	0.000008	1.46723	0.000014	0.00047	0.00001	0.0197	0.0003	-1.45	0.00	-1.40	0.01	10.02	0.240	0.278	0.007	0.03	0.00	0.28	0.00
MA2-4-4-051G	0.281968	0.000011	1.46717	0.000020	0.00088	0.00002	0.0432	0.0006	-1.44	0.00	-1.42	0.01	8.62	0.170	0.504	0.008	0.05	0.00	0.28	0.00
MA2-4-4-059C	0.282361	0.000010	1.46724	0.000028	0.00197	0.00007	0.0780	0.0021	-1.41	0.00	-1.39	0.01	8.05	0.220	0.842	0.025	0.11	0.00	0.28	0.00
MA2-4-4-070C	0.282349	0.000018	1.46717	0.000022	0.00235	0.00005	0.1066	0.0021	-1.47	0.00	-1.42	0.01	4.20	0.130	0.632	0.028	0.07	0.00	0.28	0.00
MA2-4-4-075C	0.282230	0.000012	1.46721	0.000025	0.00095	0.00002	0.0496	0.0020	-1.44	0.00	-1.41	0.01	8.17	0.170	0.570	0.034	0.05	0.00	0.28	0.00
MA2-4-4-076C	0.282233	0.000013	1.46720	0.000033	0.00219	0.00003	0.0945	0.0015	-1.49	0.00	-1.40	0.01	4.70	0.190	0.588	0.021	0.07	0.00	0.28	0.00
MA2-4-4-087G	0.281955	0.000013	1.46720	0.000024	0.00095	0.00002	0.0478	0.0009	-1.44	0.00	-1.42	0.01	6.64	0.240	0.434	0.012	0.04	0.00	0.28	0.00
MA2-4-4-092C	0.282445	0.000010	1.46723	0.000022	0.00121	0.00012	0.0705	0.0070	-1.45	0.00	-1.41	0.01	7.17	0.130	0.668	0.059	0.06	0.00	0.28	0.00
MA2-2-4-012G	0.281706	0.000012	1.46725	0.000016	0.00168	0.00007	0.0806	0.0041	-1.46	0.00	-1.41	0.00	7.04	0.160	0.805	0.056	0.08	0.01	0.28	0.00
MA2-2-4-079G	0.281459	0.000012	1.46723	0.000033	0.00047	0.00000	0.0247	0.0003	-1.46	0.00	-1.40	0.01	5.29	0.082	0.181	0.005	0.02	0.00	0.28	0.00
MA2-2-4-081G	0.281434	0.000013	1.46727	0.000021	0.00197	0.00010	0.0830	0.0050	-1.45	0.00	-1.42	0.01	5.29	0.045	0.608	0.041	0.07	0.00	0.28	0.00
MA2-2-4-084G	0.281822	0.000013	1.46716	0.000022	0.00197	0.00003	0.1038	0.0015	-1.45	0.00	-1.43	0.01	4.94	0.065	0.706	0.009	0.07	0.00	0.28	0.00
MA2-2-4-095G	0.281488	0.000013	1.46722	0.000028	0.00104	0.00004	0.0557	0.0024	-1.44	0.00	-1.42	0.01	5.88	0.110	0.440	0.011	0.04	0.00	0.28	0.00

Table 40: Raw data of concordant and disconcordant hafnium analysis of all samples.

MA2-2-8-001G	0.281625	0.000011	1.46725	0.000026	0.00066	0.00001	0.0307	0.0002	-1.45	0.00	-1.40	0.01	7.12	0.210	0.305	0.009	0.03	0.00	0.28	0.00
MA2-2-8-003G	0.281610	0.000012	1.46722	0.000026	0.00137	0.00002	0.0772	0.0018	-1.45	0.00	-1.43	0.01	6.23	0.078	0.666	0.021	0.06	0.00	0.28	0.00
MA2-2-8-004G	0.281796	0.000010	1.46720	0.000018	0.00061	0.00001	0.0278	0.0005	-1.46	0.00	-1.40	0.01	6.76	0.160	0.254	0.006	0.03	0.00	0.28	0.00
MA2-2-8-006G	0.281674	0.000012	1.46724	0.000025	0.00162	0.00003	0.0878	0.0019	-1.45	0.00	-1.43	0.00	5.54	0.140	0.671	0.029	0.06	0.00	0.28	0.00
MA2-2-8-007C	0.282697	0.000010	1.46727	0.000024	0.00083	0.00003	0.0435	0.0022	-1.45	0.00	-1.43	0.01	6.32	0.055	0.380	0.021	0.04	0.00	0.28	0.00
MA2-2-8-011C	0.282465	0.000014	1.46718	0.000022	0.00250	0.00010	0.1156	0.0030	-1.45	0.00	-1.44	0.00	5.40	0.190	0.842	0.009	0.09	0.00	0.28	0.00
MA2-2-8-012C	0.282283	0.000010	1.46722	0.000017	0.00151	0.00004	0.0803	0.0022	-1.46	0.00	-1.42	0.00	7.66	0.089	0.849	0.027	0.08	0.00	0.28	0.00
MA2-2-8-016G	0.282017	0.000011	1.46723	0.000023	0.00146	0.00010	0.0706	0.0023	-1.43	0.00	-1.41	0.01	6.35	0.160	0.616	0.009	0.06	0.00	0.28	0.00
MA2-2-8-023G	0.281874	0.000013	1.46723	0.000032	0.00209	0.00002	0.1106	0.0022	-1.46	0.00	-1.44	0.01	5.29	0.220	0.813	0.048	0.08	0.00	0.28	0.00
~~MA2-2-8-024G~~	~~0.277383~~	~~0.000120~~	~~1.47052~~	~~0.000085~~	~~0.00155~~	~~0.00002~~	~~0.0837~~	~~0.0009~~	~~-1.22~~	~~0.01~~	~~-3.42~~	~~0.03~~	~~5.61~~	~~0.150~~	~~0.613~~	~~0.009~~	~~0.06~~	~~0.00~~	~~0.28~~	~~0.00~~
MA2-2-8-029G	0.281873	0.000014	1.46716	0.000016	0.00267	0.00004	0.1291	0.0024	-1.44	0.00	-1.43	0.00	7.56	0.110	1.348	0.033	0.14	0.00	0.28	0.00
MA2-2-8-032G	0.282001	0.000015	1.46725	0.000022	0.00139	0.00004	0.0700	0.0016	-1.45	0.00	-1.43	0.00	5.99	0.170	0.574	0.004	0.06	0.00	0.28	0.00
MA2-2-8-033G	0.281622	0.000012	1.46723	0.000018	0.00127	0.00009	0.0671	0.0054	-1.46	0.00	-1.43	0.01	5.97	0.074	0.543	0.040	0.05	0.00	0.28	0.00
~~MA2-2-8-043G~~	~~0.277460~~	~~0.000020~~	~~1.47047~~	~~0.000035~~	~~0.00096~~	~~0.00002~~	~~0.0570~~	~~0.0007~~	~~-1.22~~	~~0.00~~	~~-4.32~~	~~0.03~~	~~5.66~~	~~0.025~~	~~0.414~~	~~0.004~~	~~0.04~~	~~0.00~~	~~0.28~~	~~0.00~~
MA2-2-8-045G	0.281525	0.000009	1.46721	0.000028	0.00050	0.00002	0.0259	0.0008	-1.46	0.00	-1.45	0.01	5.91	0.100	0.209	0.003	0.02	0.00	0.28	0.00
MA2-2-8-051G	0.281556	0.000012	1.46720	0.000020	0.00082	0.00003	0.0421	0.0018	-1.46	0.00	-1.43	0.01	6.49	0.097	0.377	0.019	0.04	0.00	0.28	0.00
MA2-2-8-057G	0.281663	0.000012	1.46718	0.000028	0.00163	0.00002	0.0686	0.0010	-1.47	0.00	-1.43	0.01	5.68	0.200	0.538	0.028	0.06	0.00	0.28	0.00
MA2-2-8-058C	0.282450	0.000010	1.46716	0.000021	0.00034	0.00000	0.0171	0.0002	-1.46	0.00	-1.37	0.02	5.74	0.110	0.135	0.005	0.01	0.00	0.28	0.00
MA2-2-8-065G	0.281926	0.000016	1.46720	0.000022	0.00177	0.00003	0.0891	0.0010	-1.46	0.00	-1.43	0.00	5.82	0.100	0.713	0.005	0.07	0.00	0.28	0.00
MA2-2-8-074C	0.282475	0.000011	1.46721	0.000022	0.00101	0.00003	0.0528	0.0016	-1.46	0.00	-1.42	0.01	6.20	0.079	0.454	0.011	0.04	0.00	0.28	0.00
~~MA2-2-8-075G~~	~~0.277828~~	~~0.000075~~	~~1.47000~~	~~0.000046~~	~~0.00090~~	~~0.00001~~	~~0.0543~~	~~0.0012~~	~~-1.26~~	~~0.00~~	~~-4.14~~	~~0.10~~	~~6.52~~	~~0.110~~	~~0.459~~	~~0.017~~	~~0.04~~	~~0.00~~	~~0.28~~	~~0.00~~
MA2-2-8-085C	0.282526	0.000016	1.46720	0.000035	0.00225	0.00005	0.1117	0.0018	-1.45	0.00	-1.44	0.01	4.80	0.140	0.732	0.011	0.07	0.00	0.28	0.00
MA2-2-8-086G	0.281645	0.000020	1.46728	0.000018	0.00049	0.00001	0.0247	0.0004	-1.46	0.00	-1.43	0.01	5.10	0.095	0.177	0.005	0.02	0.00	0.28	0.00
MA2-2-8-096G	0.281881	0.000014	1.46722	0.000017	0.00100	0.00004	0.0523	0.0026	-1.46	0.00	-1.44	0.01	5.94	0.081	0.435	0.026	0.04	0.00	0.28	0.00
MA2-2-8-108C	0.282321	0.000042	1.46724	0.000021	0.00100	0.00004	0.0508	0.0016	-1.47	0.00	-1.43	0.01	7.23	0.049	0.504	0.015	0.05	0.00	0.28	0.00
MA2-2-8-111C	0.282487	0.000010	1.46719	0.000019	0.00108	0.00004	0.0529	0.0018	-1.46	0.00	-1.43	0.01	6.31	0.200	0.453	0.002	0.05	0.00	0.28	0.00
MA2-2-8-112G	0.281590	0.000011	1.46724	0.000029	0.00135	0.00004	0.0633	0.0012	-1.46	0.00	-1.43	0.01	5.47	0.090	0.478	0.003	0.05	0.00	0.28	0.00
MA2-2-8-113G	0.281484	0.000011	1.46729	0.000025	0.00087	0.00000	0.0466	0.0005	-1.45	0.00	-1.44	0.01	4.99	0.071	0.322	0.007	0.03	0.00	0.28	0.00
~~MA2-2-8-114G~~	~~0.275677~~	~~0.000025~~	~~1.47142~~	~~0.000046~~	~~0.00076~~	~~0.00000~~	~~0.0515~~	~~0.0003~~	~~-1.17~~	~~0.00~~	~~-5.71~~	~~0.04~~	~~4.31~~	~~0.016~~	~~0.278~~	~~0.003~~	~~0.02~~	~~0.00~~	~~0.28~~	~~0.00~~
MA2-2-16-004G	0.282001	0.000018	1.46721	0.000023	0.00124	0.00003	0.0570	0.0017	-1.46	0.00	-1.42	0.00	8.15	0.150	0.631	0.009	0.07	0.00	0.28	0.00
MA2-2-16-005G	0.281884	0.000010	1.46721	0.000022	0.00135	0.00001	0.0715	0.0011	-1.45	0.00	-1.42	0.00	7.15	0.140	0.722	0.025	0.07	0.00	0.28	0.00
MA2-2-16-007C	0.282599	0.000011	1.46723	0.000018	0.00048	0.00001	0.0259	0.0005	-1.43	0.00	-1.43	0.01	6.74	0.200	0.240	0.011	0.02	0.00	0.28	0.00
MA2-2-16-008C	0.282695	0.000012	1.46720	0.000019	0.00090	0.00002	0.0469	0.0006	-1.46	0.00	-1.44	0.01	5.88	0.120	0.374	0.005	0.04	0.00	0.28	0.00
MA2-2-16-009G	0.281875	0.000013	1.46728	0.000018	0.00127	0.00002	0.0621	0.0006	-1.45	0.00	-1.44	0.00	5.88	0.150	0.502	0.010	0.05	0.00	0.28	0.00
MA2-2-16-009G	0.281875	0.000013	1.46728	0.000018	0.00127	0.00002	0.0621	0.0006	-1.45	0.00	-1.44	0.00	5.88	0.150	0.502	0.010	0.05	0.00	0.28	0.00
MA2-2-16-010G	0.281893	0.000014	1.46719	0.000019	0.00136	0.00003	0.0603	0.0011	-1.45	0.00	-1.43	0.01	6.55	0.170	0.545	0.011	0.06	0.00	0.28	0.00
MA2-2-16-012C	0.282683	0.000014	1.46719	0.000023	0.00084	0.00001	0.0355	0.0008	-1.46	0.00	-1.46	0.01	5.02	0.091	0.247	0.009	0.03	0.00	0.28	0.00
MA2-2-16-016G	0.281850	0.000011	1.46720	0.000023	0.00065	0.00001	0.0308	0.0005	-1.46	0.00	-1.44	0.01	6.32	0.120	0.272	0.010	0.03	0.00	0.28	0.00
MA2-2-16-017G	0.281667	0.000010	1.46717	0.000019	0.00117	0.00009	0.0571	0.0042	-1.46	0.00	-1.42	0.01	7.43	0.300	0.551	0.028	0.06	0.00	0.28	0.00
ER5-8-9-005C	0.282578	0.000023	1.46720	0.000033	0.00321	0.00005	0.1470	0.0018	-1.52	0.00	-1.44	0.01	3.48	0.099	0.710	0.028	0.08	0.00	0.28	0.00
ER5-8-9-027G	0.281709	0.000011	1.46724	0.000023	0.00184	0.00006	0.0890	0.0025	-1.43	0.00	-1.45	0.00	7.12	0.061	0.874	0.018	0.09	0.00	0.28	0.00
ER5-8-9-040G	0.281619	0.000013	1.46723	0.000027	0.00053	0.00000	0.0285	0.0004	-1.48	0.00	-1.45	0.01	5.77	0.100	0.229	0.007	0.02	0.00	0.28	0.00
ER5-8-9-045C	0.282534	0.000017	1.46720	0.000021	0.00406	0.00008	0.2746	0.0057	-1.46	0.00	-1.43	0.00	7.70	0.045	2.906	0.049	0.22	0.00	0.28	0.00
ER5-8-9-048G	0.281621	0.000012	1.46728	0.000017	0.00055	0.00000	0.0285	0.0002	-1.47	0.00	-1.47	0.01	5.93	0.110	0.234	0.006	0.02	0.00	0.28	0.00
ER5-8-9-050G	0.281791	0.000011	1.46720	0.000016	0.00142	0.00002	0.0736	0.0007	-1.47	0.00	-1.43	0.00	9.04	0.170	0.906	0.018	0.09	0.00	0.28	0.00
ER5-8-9-051G	0.281670	0.000015	1.46724	0.000024	0.00130	0.00008	0.0676	0.0036	-1.46	0.00	-1.46	0.01	6.35	0.130	0.580	0.025	0.06	0.00	0.28	0.00
ER5-8-9-053G	0.281840	0.000016	1.46723	0.000023	0.00246	0.00019	0.1170	0.0089	-1.43	0.00	-1.43	0.00	7.13	0.046	1.143	0.083	0.12	0.01	0.28	0.00
ER5-8-9-054G	0.281831	0.000011	1.46726	0.000020	0.00225	0.00003	0.1212	0.0008	-1.45	0.00	-1.42	0.00	7.82	0.037	1.311	0.010	0.12	0.00	0.28	0.00
ER5-8-9-057C	0.282472	0.000016	1.46724	0.000030	0.00237	0.00012	0.1188	0.0037	-1.45	0.00	-1.42	0.00	6.65	0.240	1.053	0.033	0.11	0.00	0.28	0.00
ER5-8-9-059G	0.281954	0.000015	1.46717	0.000019	0.00119	0.00002	0.0643	0.0012	-1.47	0.00	-1.44	0.00	5.93	0.084	0.524	0.017	0.05	0.00	0.28	0.00
ER5-8-9-086C	0.282623	0.000012	1.46725	0.000016	0.00101	0.00001	0.0523	0.0004	-1.46	0.00	-1.45	0.01	6.78	0.120	0.495	0.012	0.05	0.00	0.28	0.00
ER5-8-9-089C	0.282832	0.000014	1.46725	0.000023	0.00233	0.00004	0.1188	0.0024	-1.43	0.00	-1.42	0.00	7.96	0.055	1.299	0.026	0.13	0.00	0.28	0.00
ER5-8-9-102C	0.282624	0.000012	1.46725	0.000021	0.00095	0.00001	0.0441	0.0004	-1.46	0.00	-1.44	0.01	6.16	0.140	0.375	0.011	0.04	0.00	0.28	0.00